A Systems Approach to Understanding Mechanisms of Drug Induced Mitochondrial Toxicity

Thesis Submitted for the Degree of Doctor of Philosophy (PhD)

By

Ashley John Broom B.Sc. (Hons)
(CID:00725856)

Supervision

Professor Alan R Boobis OBE - Imperial College London

Professor Timothy W Gant - Public Health England

Doctor Jonathan Lyon - GlaxoSmithKline

Imperial College London
Department of Medicine

August 2015

Declaration of Originality

I (Ashley John Broom), hereby declare that the data and information contained within this thesis is, to the best of my knowledge, original and all work of others is adequately referenced.

Copyright Declaration

The copyright of this thesis rests with the author and is made available under a Creative Commons Attribution Non-Commercial No Derivatives licence. Researchers are free to copy, distribute or transmit the thesis on the condition that they attribute it, that they do not use it for commercial purposes and that they do not alter, transform or build upon it. For any reuse or redistribution, researchers must make clear to others the licence terms of this work.

Acknowledgements

I am truly indebted to a vast number of people for their help, support and motivation over the past four years. Please bear with me!

First of all I would like to thank my funding bodies (the Medical Research Council CASE award programme and GlaxoSmithKline) for providing the opportunity to complete this PhD project.

Secondly, I would like to acknowledge the tremendous support I have received from my industrial manager, Jon Lyon and colleagues in GlaxoSmithKline's Safety Assessment (SA) facility in Ware. Jon has had to calm me down, pick me up and coach me through, for which I will always remain very thankful and appreciative for his patience and his trust in me. A massive thank you must also go to the other SA "Mito-Team" (Gino, Jimbo, Dave and Angie) who were all such fantastic company and a pleasure to work with (often until the early-hours of the morning)! I especially thank Gino for his company on the infamous trip to Philadelphia where work had to be suspended due to Hurricane Sandy in October 2012. On the other side of the pond, I would also like to thank Jimmy Mangum, Catherine Hu and Kevin French for their support. I would also like to acknowledge other members of the Investigative Preclinical Toxicology group. The CPT team (Anita, Graeme and Chloe) for their guidance with cell culture and Dave Baker for drinking beer and playing snooker with me! Elsewhere at GlaxoSmithKline, I must thank Paul McGill and Ian Francis for their excellent electron microscopy support, the Laboratory Animal Sciences and Histopathology team for their diligent animal experimentation, Mitul Gandhi for his help with lactate/pyruvate analyses and the Drug-Metabolism and Pharmacokinetics groups for performing the drug-concentration toxicokinetic analyses.

I also owe a debt of gratitude to my academic supervisor Alan Boobis, whose intellect and unwavering support have been both admired and appreciated respectively. Furthermore, I would like to thank Tim Gant who originally gave me this opportunity and who was so welcoming and supportive during my 18 month stint in his laboratories in Oxfordshire. This project would not have been possible without you both.

Away from science, I would like to say a massive thank you to my Mum, Dad and sister, Kathryn for their love and encouragement. I am forever indebted to you for kindly letting me move home during the process of writing this thesis. The Channel Islands (Jersey) was certainly an atmosphere conducive to writing, despite the draw of Beauport Bay, The Watersplash Bar and El-Tico ribs! I would also like to apologise to my friends who I have somewhat neglected over the past four years… I hope I can make up for this soon.

Finally a big thank you to my girlfriend Laura for her love and support throughout thesis complications, gene-chip malfunctions, cell-culture contaminations etc... But most of all just for being there. I promise to be there for you too.

Abstract

A Systems Approach to Understanding Mechanisms of Drug Induced Mitochondrial Toxicity

Ashley J Broom, Imperial College London, Department of Medicine

Mitochondria are important to the pharmaceutical industry. Mitochondrial perturbation is central to the aetiology of many poorly treated human diseases (e.g. neurodegenerative diseases, diabetes and cancer) and hence mitochondria are increasingly becoming therapeutic targets. However, drug-induced mitochondrial toxicity (DIMT) has also gained recognition as a significant cause of safety related attrition (including multiple post-market withdrawals). The present work ultimately aimed to discern the mechanisms downstream of DIMT *in vitro* and *in vivo* with two tool compounds which act via inhibition of the mitochondrial electron transport chain (ETC) (GSK932121A) or via uncoupling of mitochondrial oxidative phosphorylation (GSK2617971A).

The first objective was to compare mitochondrial functional responses between *in vitro* (treatment of mitochondria isolated from control animals or *in vitro* cell lines) and *in vivo* scenarios using oxygen consumption rate (OCR) and calcium retention capacity (CRC) assays. The direction of change in these assays was often different between the *in vitro* and *in vivo* situation. Whilst seemingly contradictory, these differences reflect an adapted state *in vivo* which results from the initial insult in combination with compensatory changes made by the tissue to maintain energy production. In contrast, only the initial, unconfounded, response to treatment is observable *in vitro*. Integration of both is key to the future risk assessment of mitochondrially-active drug candidates.

The second objective was to use a systems approach to build candidate adverse outcome pathways (AOP)/modes of action (MOA) for both tool compounds. AOP/MOAs were constructed based on key events observed *in vivo*. With both compounds, effect on body temperature, increased lactate/pyruvate ratio, gene expression changes indicative of a fasted state (induction of gluconeogenic genes) and mitochondrial ultrastructure effects were key events observed in the adverse outcome. Future work using additional compounds with mitochondrial activities would help validate the proposed AOP/MOAs.

The third objective was to highlight markers of underlying mitochondrial perturbation with utility for future pre-clinical monitoring in the absence of overt DIMT. A number of mitochondrial functional changes (e.g. effect on CRC) were observed prior to the onset of overt toxicity *in vivo,* with both compounds and these endpoints have potential use in tailored future studies with mitochondrially-active drug candidates.

These findings add to the knowledgebase on DIMT, particularly with regard to the candidate AOP/MOAs which have been postulated. This will facilitate the selection of more sensitive and functional endpoints for use in future toxicology studies with drugs where mitochondrial impairment is suspected.

Table of Contents

Acknowledgements iii

List of Tables xi

List of Figures xiii

List of Abbreviations xvii

1.0. General Introduction 1

1.1. The Importance of Drug-Induced Mitochondrial Toxicity 2

1.2. Introduction to Mitochondria 3

1.3. Mitochondrial Structure and Genome 4

1.4. Mitochondrial Function 7

1.4.1. Mitochondria: Energy Production 7

1.4.2. Mitochondria: ROS 10

1.4.3. Mitochondria: Cell Death 11

1.5. Mechanisms of DIMT 12

1.5.1. Direct inhibitors of OXPHOS: 14

1.5.2. Inhibitors of mitochondrial substrate oxidation: 20

1.5.3. ROS generation: 21

1.5.4. Inducing mitochondrial permeability transition: 21

1.5.5. Oxidation and Mutations of mtDNA, or Inhibition of mtDNA Synthesis: 23

1.5.6. Multiple Mechanisms 24

1.6. Methods of Detecting DIMT 24

1.7. Challenges and Complexities 30

1.8. The use of a Systems Approach 33

1.9. Tool Compounds Studied 34

1.9.1. GSK932121A (Complex III Inhibitor) 35

1.9.2. GSK2617971A (OXPHOS Uncoupler) 37

1.10. Thesis Rationale and Aims 38

2.0. Materials and Methods 41

2.1. Animals 42

2.1.1. GSK932121A Studies – GlaxoSmithKline, Ware, Hertfordshire UK 42

2.1.2. GSK2617971A Study – GlaxoSmithKline, Upper Merion, Pennsylvania, USA 42

2.2. In Life Clinical Observations 43

2.3. Preparation of Dosing Solutions 43

2.3.1. GSK932121A Studies – GlaxoSmithKline, Ware, Hertfordshire UK 43

2.3.2. GSK2617971A Study – GlaxoSmithKline Upper Merion, PA, USA 43

2.3.3. Formulation of compounds for *in vitro* experiments 44

2.4. Measurement of Blood Gasses and Bicarbonate 44

2.5. Blood Sampling 45

2.5.1. Preparation of plasma from whole blood samples 45

2.6. Measurement of GSK932121A and GSK261971A Concentration in Plasma 46

2.7. Body Temperature Measurements 46

2.8. Isolated Mitochondrial Methods 47

2.8.1. Isolation of Mitochondria 47

2.8.2. Assessment of Protein Concentration 49

2.8.3. Assessment of Mitochondrial Bioenergetics using the Seahorse XF24 Analyser 49

2.8.4. Calcium Retention Capacity Assay 51

2.8.5. Mitochondrial Membrane Potential Assay 53

2.8.6. Complex III Activity Assay 53

2.9. Cell Culture Techniques 54

2.9.1. HepG2 Cell Culture and Media Composition 54

2.9.2. Assessment of Cytotoxicity 56

2.9.3. Analysis of Whole Cell Bioenergetics in HepG2 Cells 56

2.9.4. *In vitro* Compound Wash out Experiment 58

2.10. Imaging and Histology 59

2.10.1. TEM Analysis of Isolated Mitochondrial Pellets 59

2.10.2. TEM Analysis of HepG2 Cells 59

2.10.3. TEM Analysis of Liver 60

2.10.4. Light Microscopy of Liver 60

2.11. Western Blot 60

2.12. Reduced / Oxidised Glutathione Assay 61

2.13. Measurement of Lactate / Pyruvate in Plasma 62

2.14. Measurement of Lactate in Cell Culture Media 62

2.15. Total RNA Extraction 63

2.15.1. HepG2 Lysate Preparation 63

2.15.2. Rat Liver Tissue Homogenate Preparation 64

2.15.3. Total RNA Extraction 64

2.16. RNA Quantification and Assessment of Integrity 65

2.16.1. Quantification Using the NanoDrop Spectrophotometer 65

2.16.2. Assessment of RNA Integrity 65

2.17. Transcriptional Profiling using Affymetrix Genechip Microarrays 66

2.17.1. Generation of Sense Strand cDNA 66

2.17.2. Fragmentation and Labelling of cDNA Template 67

2.17.3. Hybridisation, Wash and Staining of Affymetrix Genechips 68

2.17.4. Scanning of Genechips and Statistical Analysis of Microarray Data 68

2.17.5. Pathway Analysis 69

2.17.6. Compound Connectivity Mapping 69

2.18. TaqMan RT-PCR Analysis from *In vitro* Samples 70

2.18.1. Gene Panel 71

2.18.2. First Strand cDNA Synthesis 72

2.18.3. TaqMan RT-PCR 72

2.18.4. RT-PCR Statistical Analysis 73

2.19. Global Metabolomics Profiling 73

3.0. Mechanisms of DIMT – GSK932121A Induced Complex III Inhibition 75

3.1. Introduction 76

3.1.1. Chapter Aims 76

3.2. Results 77

3.2.1. Confirmation of Respiratory Chain Inhibition 77

3.2.2. Acute Dose In Vivo Study (Non Mitochondrial Endpoints) 80

3.2.3. Acute Dose In Vivo Study (Mitochondrial Endpoints) 86

3.2.4. Transcriptomics 90

3.3. Discussion 92

3.3.1. Summary 96

4.0. A Metabolomics Approach to Understanding Mechanisms of Drug-Inudced Respiratory Chain Inhibition 98

4.1. Introduction 99

4.1.1. Chapter Aims 100

4.1.2. Study Design 100

4.1.3. Metabolomics Data Visualisation 101

4.2. Results and Discussion 102

4.2.1. In Life Effects and Comparison of Endpoints to Chapter 3 Study 102

4.2.2. Effect of GSK932121A on Total Metabolites in the Liver and Plasma 105

4.2.3. Metabolomics: Complex III inhibition has a prominent impact on plasma TCA cycle intermediates 106

4.2.4. Metabolomics: Complex III Inhibition causes an increase in glycogenolysis and glycolysis 108

4.2.5. Metabolomics: Complex III inhibition has an effect on mitochondrial FA oxidation 111

4.2.6. Metabolomics: Complex III Inhibition has an effect on amino acid catabolism 115

4.2.7. Metabolomics: Inhibition of Complex III Causes Increased Levels of Hepatic Oxidative Stress 118

4.3. Further Discussion 121

4.3.1. Metabolomics 121

4.4. Summary…. 121

5.0. Integration of GSK932121A Data into an AOP/MOA 123

5.1. Introduction – AOP/MOA of GSK932121A Toxicity 124

5.2. Key Events: Complex III Inhibition 126

5.3. Possible Key Events: Complex III Inhibition 128

5.4. Associated Events 131

5.5. Modifying Factors 135

5.6. AOP/MOA of Respiratory Chain Inhibitors 135

5.7. Summary 136

6.0. Mechanism of DIMT– GSK2617971A Induced Uncoupling of OXPHOS..... 138

6.1. Introduction 139

6.1.1. Chapter Aims 140

6.2. Results 140

6.2.1. Confirmation of the Uncoupling Activity of GSK2617971A 140

6.2.2. Acute Dose *In vivo* Study With GSK2617971A – Non Mitochondrial Endpoints . 144

6.2.3. Acute Dose *in vivo* Study with GSK2617971A – Mitochondrial Endpoints 147

6.2.4. Identifying Mechanisms of Toxicity following OXPHOS Uncoupling *in vivo* using Transcriptomics..... 154

6.3. Discussion..... 159

6.4. Summary..... 165

7.0. The Effect of Sub-Cytotoxic Concentrations of GSK932121A and GSK2617971A in vitro and Comparison with a Bioinformatically Selected 'Similar' Chemical 166

7.1. Introduction 167

7.1.1. Experimental Aims 168

7.2. Results 169

7.2.1. Identifying Effectual Sub-Cytotoxic Concentrations 169

7.2.2. In Vitro Lactate Generation 174

7.2.3. RT-PCR – Metabolic Switch Gene Panel 179

7.2.4. In vitro Electron Microscopy 188

7.2.5. Compound Connectivity Mapping 190

7.3. Discussion..... 198

7.3.1. Mitochondrial Toxicity, Cytotoxicity and Lactate Generation 198

7.3.2. Gene Panel Discussion..... 200

7.3.3. The Link Between Azacyclonol and GSK932121A and GSK2617971A 202

7.3.4. Summary..... 204

8.0. Thesis Discussion 206

8.1. Manifestation of Mitochondrial Toxicity *in vitro* versus *in vivo* 207

8.2. The Use of a Systems Approach to Generate AOP's 209

8.3. Markers of DIMT in the Absence of Overt Toxicity 212

8.4. Future Work..... 215

8.5. Summary..... 216

REFERENCES 218

APPENDIX I – STRUCTURAL ASSESSMENT OF ISOLATED MITOCHONDRIAL FRACTIONS 237

APPENDIX 1.1: Transmission Electron Microscopy 237

APPENDIX 1.2: Western Blot 240

APPENDIX II – FUNTIONAL ASSESSMENT OF ISOLATED MITOCHONDRIAL FRACTIONS 243

APPENDIX III – CONCENTRATION OF GSK932121A IN ISOLATED LIVER MITOCHONDRIA OF RATS TREATED WITH A 50MG/KG DOSE (CHAPTER 3) 246

APPENDIX IV: METABOLOMICS RAW DATA 247

APPENDIX V: METABOLON PLASMA LACTATE ANALYSIS 251

List of Tables

TABLE 1.1: Examples of assays used in the pharmaceutical industry for the analysis of DIMT.. 29

TABLE 2.1: Overview of blood sampling methodologies. 45

TABLE 2.2: Media constituents for HepG2 cell culture. 54

TABLE 2.3: HepG2 cell seeding density and flask/plate details. 55

TABLE 2.4: Serum free Seahorse assay media constituents 57

TABLE 2.5: Concentration of BOFA reagents loaded into the drug injection ports and final concentration in the well.. 57

TABLE 2.6: Details of the five antibodies comprising the mitochondrial membrane integrity western blot antibody cocktail (ab220414). 61

TABLE 2.7: Details of the primers and probes used for *in vitro* RT-PCR experiments 71

TABLE 4.1: Statistical summary of a plasma and liver metabolite changes. 106

TABLE 4.2: Impact of GSK932121A (50mg/kg) on plasma TCAi 107

TABLE 5.1: Experimental and literature evidence of key events in the complex III AOP/MOA including the plausibility of the relationships between the key events and remaining uncertainties at each stage. 127

TABLE 5.2: Evidence for, and remaining uncertainty surrounding PKE's in the AOP/MOA of complex III inhibition. 130

TABLE 6.1: Direction of change in protein coding gene expression in GSK2617971A treated rat livers. 154

TABLE 6.2: IPA network analysis (biological theme analysis) of top 32 protein coding genes differentially altered in response to GSK2617971A (30 and 60mg/kg). 156

TABLE 6.3: IPA-Tox analysis of top 32 protein coding genes differentially altered in response to GSK2617971A. 158

TABLE 7.1: Genes selected for use in TaqMan gene-panel. 181

TABLE 7.2: Effect of GSK932121A and GSK2617971A on the intracellular levels of HepG2 cell glycogen and lipid. 189

TABLE 7.3: Genes submitted for connectivity mapping analysis. 191

TABLE 8.1: Representation of the relationships between Toxicity Pathways, Mode of Action Pathways, Adverse Outcome Pathways, and Source to Outcome Pathways. 211

APPENDIX TABLE 1.1: TEM Analysis of crude mitochondrial pellets isolated from five tissues of high metabolic load. 239

APPENDIX TABLE 2.1: Non-quantitative comparison between obtained RCR values for mitochondria isolated from five tissues of high metabolic load and published RCR values..... 245

APPENDIX TABLE 3.1: Levels of GSK932121A in the mitochondrial fraction. 246

APPENDIX TABLE 4.1: Liver metabolomics raw data. 247

APPENDIX TABLE 4.2: Plasma metabolomics raw data. 250

List of Figures

FIGURE 1.1: Structure of a eukaryotic mitochondrion. 5

FIGURE 1.2: The mitochondrial respiratory chain. 9

FIGURE 1.3: Graphical representation of mitochondria as a mediator of drug-induced toxicity....13

FIGURE 1.4: Schematic representation of drugs which have been implicated in inhibition of OXPHOS either via direct inhibition of respiratory chain complexes I-IV or via chemical uncoupling. 17

FIGURE 1.5: Putative mPTP proteins in the OMM and IMM in normal physiological and pathophysiological conditions. 22

FIGURE 1.6: Chemical structure of GSK932121A. 35

FIGURE 1.7: Schematic of the approach taken to manufacture a GSK932121A pro-drug 37

FIGURE 1.8: Chemical structure of GSK2617971A. 38

FIGURE 2.1: The Seahorse Bioscience BOFA assay 50

FIGURE 2.2: Graphical representation of the CRC assay. 52

FIGURE 2.3: Graphical representation of the whole cell OCR assay for determination of bioenergetic parameters. 58

FIGURE 2.4: A typical lactate assay standard curve. 63

FIGURE 2.5: Gel image and electropherogram output from Agilent 2100 Bioanalyser – Assessment of RNA integrity. 66

FIGURE 3.1: Complex III activity assay with GSK932121A. 78

FIGURE 3.2: Analysis of liver mitochondrial OCR following in vitro treatment of control liver mitochondria with GSK932121A (measured using Seahorse XF24 analyser). 79

FIGURE 3.3: Assessment of the mitochondrial CRC. 80

FIGURE 3.4: Relationship between core body temperature and plasma GSK932121A concentration. 81

FIGURE 3.5: Analysis of arterial blood gasses ($p0_2$ and $pC0_2$) and bicarbonate (HCO_3) in whole blood of animals treated with GSK932121A (50mg/kg). 82

FIGURE 3.6: Effect of 50mg/kg GSK932121A on liver LM and TEM compared to VC. 84

FIGURE 3.7: Effect of 50mg/kg GSK932121A on whole blood lactate:pyruvate ratio compared with blood taken from VC animals 85

FIGURE 3.8: Analysis of liver GSH, GSSG and ratio of GSH:GSSG following treatment of rats with 50mg/kg GSK932121A compared to vehicle control. 86

FIGURE 3.9: Analysis of liver mitochondrial CRC following treatment of rats with GSK932121A *in vivo*. 87

FIGURE 3.10: Analysis of liver mitochondrial bioenergetics using the Seahorse XF24 analyser following treatment of rats with GSK932121A *in vivo* 89

FIGURE 3.11: PCA of Affymetrix transcriptomics data (from liver of GSK932121A and VC animals) highlighting relationship between degree of experimental data separation and plasma drug concentration. 91

FIGURE 3.12: Correlative analysis of gene copy number for 4 significantly altered genes and GSK932121A plasma concentration. 92

FIGURE 4.1: Metabolomics data visualisation. 102

FIGURE 4.2: Effect of 12.5mg/kg and 50mg/kg GSK932121A on body temperature, blood lactate:pyruvate ratio and isolated liver mitochondria CRC and OCR 104

FIGURE 4.3: Schematic representation of the glycogenolysis, glycolysis and PPP. 108

FIGURE 4.4: GSK932121A causes a dose dependent reduction in liver starch/glycogen intermediates at a 4 hour time point. 109

FIGURE 4.5: Effect of GSK932121A treatment on key glycolysis metabolites in the liver of GSK932121A and VC treated animals 110

FIGURE 4.6: Schemiatic representation of the carnitine shuttle and ketogenesis. 112

FIGURE 4.7: Effect of GSK932121A on plasma free carnitine. 113

FIGURE 4.8: Effect of GSK932121A on plasma and liver BHBA and plasma FA-acylcarnitine levels 114

FIGURE 4.9: Schematic representation of α-ketobutyrate and α-hydroxybutyrate involvement in the supply of carbon sources to the TCA cycle. 115

FIGURE 4.10: Effect of GSK932121A on plasma and liver BCAA's 117

FIGURE 4.11: Effect of GSK932121A on plasma AKB and its downstream metabolite AHB over a 4 hour time course 118

FIGURE 4.12: Effect of GSK932121A on oxidative stress and anti-oxidant stress response in the liver. 120

FIGURE 5.1.: Key events in the AOP/MOA for complex III inhibition. 126

FIGURE 5.2: PKE's in the AOP for complex III inhibition 129

FIGURE 5.3: Hybrid AOP/MOA including key events, possible key events and associated events in the toxicological progression of complex III inhibition related toxicity..... 132

FIGURE 6.1: Comparison of the OXPHOS uncoupling activity of GSK2617971A to 2,4-DNP in control isolated liver mitochondria. 142

FIGURE 6.2: Assessment of the mitochondrial CRC following *in vitro* treatment of control liver mitochondria with GSK2617971A and 2,4-DNP. 143

FIGURE 6.3: Relationship between core body temperature and plasma GSK2617971A concentration) 145

FIGURE 6.4: Effect of GSK2617971A treatment on blood lactate: pyruvate ratio. 146

FIGURE 6.5: TEM analysis of kidney sections of rats treated with 60mg/kg GSK2617971A and VC. 147

FIGURE 6.6: Analysis of kidney and liver mitochondrial bioenergetics using the Seahorse XF24 analyser following treatment of rats with GSK2617971A *in vivo* 149

FIGURE 6.7: Reversibility of the uncoupling effect of GSK2617971A demonstrated *in vitro* in HepG2 cells..... 150

FIGURE 6.8: Analysis of mitochondrial ΔΨ (JC-1) in liver and kidney mitochondria from animals treated with GSK2617971A compared to VC…….151

FIGURE 6.9: Analysis of mitochondrial CRC in kidney and liver mitochondria isolated from GSK2617971A treated rats and VC 153

FIGURE 6.10: PCA analysis of global hepatic transcriptional data pre and post statistical refinement. 155

FIGURE 6.11: Proposed AOP/MOA for mitochondrial OXPHOS uncoupling *in vivo*. 164

FIGURE 7.1: Analysis of HepG2 mitochondrial OCR following acute *in vitro* treatment with GSK932121A (measured using Seahorse XF_e96 analyser). 170

FIGURE 7.2: The effect of GSK932121A on HepG2 cytotoxicity (LDH) 171

FIGURE 7.3: Effect of GSK2617971A (OXPHOS uncoupling) on HepG2 cell metabolism (OCR and ECAR). 172

FIGURE 7.4: Effect of GSK2617971A on HepG2 cell cytotoxicity..... 173

FIGURE 7.5: Effect of glucose concentration on the generation of lactate in HepG2 cell supernatant following treatment with Oligomycin and Antimycin A 176

FIGURE 7.6: Effect of sub-cytotoxic concentrations of GSK932121A and GSK2617971A on HepG2 cell lactate generation up to 8 hours. 178

FIGURE 7.7: Heat map showing the effect in HepG2 cells of GSK932121A on a selection of pertinent genes involved in the response to DIMT. 184

FIGURE 7.8: Heat map showing the effect in HepG2 cells of GSK2617971A on a selection of pertinent genes involved in the response to DIMT. 187

FIGURE 7.9: Exemplar volcano plot for GSK2617971A / GSK932121A connectivity map and top ten connected compounds. 193

FIGURE 7.10: Effect of azacyclonol on mitochondrial OCR in both HepG2 cells and isolated control liver mitochondria. 194

FIGURE 7.11: Effect of azacyclonol on both HepG2 cell lactate generation and on the intracellular level of glycogen clusters and lipid droplets. 196

FIGURE 7.12: Heat map showing the effect in HepG2 cells of azacyclonol on a selection of pertinent genes involved in the response to DIMT. 197

FIGURE 8.1: Graphical representation of the relative metabolic states of potential target patient populations and the commonly used preclinical animal species. 214

APPENDIX FIGURE 1.1: Assessment of mitochondria isolated from 5 rodent tissues via Western blot. 241

APPENDIX FIGURE 2.1: RCR values obtained for mitochondria isolated from liver, kidney, heart, skeletal muscle and brain rat tissues. 244

APPENDIX FIG.5.1: Plasma lactate measured by Metabolon following treatment of rats with 12.5mg/kg and 50mg/kg GSK932121A. 251

List of Abbreviations

ΔΨ	-	Membrane potential
2-DG	-	2-deoxyglucose
2,4-DNP	-	2,4-dinitrophenol
AHB	-	α-hydroxybutyrate
AKB	-	α-ketobutyrate
ADP	-	Adenosine diphosphate
AOP	-	Adverse outcome pathway
ATP	-	Adenosine triphosphate
BHBA	-	3-hydroxybutyrate
BOFA	-	Basal, oligomycin, FCCP, antimycin A
CCCP	-	Carbonyl cyanide m-chlorophenyl-hydrazone
cDNA	-	Complementary deoxyribonucleic acid
CoA	-	Coenzyme A
CRC	-	Calcium retention capacity
cRNA	-	Complementary ribonucleic acid
Ct	-	Cycle threshold
DIMT	-	Drug-induced mitochondrial toxicity
DMSO	-	Dimethyl sulfoxide
DNA	-	Deoxyribonucleic acid
dNTP	-	Deoxynucleotide triphosphates
ECAR	-	Extracellular acidification rate
EDTA	-	Ethylenediaminetetraacetic acid
EGTA	-	Ethylene glycol-bis (2-aminoethylether)-*N,N,N',N*-tetraacetic acid
ETC	-	Electron transport chain
FA	-	Fatty acid
FAD	-	Flavin adenine nucleotide
FCCP	-	Carbonyl cyanide-*4*-(trifluoromethoxy)phenylhydrazon
FDA	-	Food and drug administration
FTIH	-	First time in human
gDNA	-	Genomic deoxyribonucleic acid
GSH	-	Reduced glutathione
GSSG	-	Oxidised glutathione

HEPES		N-2.hydroxyethylpiperazine-N'-2-ethanesulfonic acid
IMS	-	Inter-membrane space
IRS	-	Insulin receptor substrate
LDH	-	Lactate dehydrogenase
IP	-	Intraperitoneal
IPA	-	Ingenuity pathway analysis
IVT	-	In vitro transcription
LD_{50}	-	50% lethal dose
Me^2	-	Divalent metal ion
MOA	-	Mode of action
mPTP	-	Mitochondrial permeability transition pore
mRNA	-	Messenger ribonucleic acid
NAD^+/NADH	-	Nicotinamide adenine dinucleotide oxidised / reduced
NRTI	-	Nucleotide reverse transcriptase inhibitors
NSAID	-	Non-steroidal anti-inflammatory drug
mw	-	Molecular weight
OCR	-	Oxygen consumption rate
OD	-	Optical density
OXPHOS	-	Oxidative phosphorylation
PBS	-	Phosphate buffered saline
PCA	-	Principle component analysis
PDK	-	Pyruvate dehydrogenase kinase
PKE	-	Possible key event
PPP	-	Pentose phosphate pathway
RCR	-	Respiratory control ratio
RMA	-	Robust multichip average
RNA	-	Ribonucleic acid
ROS	-	Reactive oxygen species
rRNA	-	Ribosomal ribonucleic acid
RT-PCR	-	Real time – polymerase chain reaction
SARM	-	Selective androgen receptor modulator
Sod2	-	Superoxide dismutase 2
TBST	-	Tris buffered saline with Tween 20
TCA/TCAi	-	The citric acid cycle / intermediates
VC	-	Vehicle control

1.0. GENERAL INTRODUCTION

1.1. The Importance of Drug-Induced Mitochondrial Toxicity

"Failures to predict adverse drug reactions have immense financial implications, result in adverse human suffering and erode in trust of regulatory and pharmaceutical processes" [1].

The importance of drug-induced mitochondrial toxicity (DIMT) was realised when a number of nucleoside reverse transcriptase inhibitors (NRTIs, used for the treatment of HIV) were withdrawn from the market, due in part to deleterious effects on mitochondrial function [2]. Since then, a number of drugs have been reported to affect mitochondrial function with consequent adverse clinical reactions, necessitating Food and Drug Administration (FDA) black box warnings and drug withdrawals. An example is the first-in-class 2,4-thiazolidinedione anti-diabetic drug troglitazone, which had to be withdrawn from the market in 2000 due to delayed onset idiosyncratic hepatotoxicity which was later linked to adverse effects on mitochondrial function [3].

Mitochondria are important to the pharmaceutical industry. Mitochondrial toxicity is increasingly implicated in the aetiology of adverse drug reactions. Drugs from diverse chemical and therapeutic classes are known to undermine mitochondrial function and despite multiple clinical examples of mitochondrial toxicity, there remains no regulatory requirement to discharge the risk of mitochondrial effects as part of the pre-first time in human (FTIH) toxicology package [4]. This is not necessarily surprising as any regulatory requirement to discharge mitochondrial liability would represent a dynamic shift in drug safety assessment away from where the International Conference on Harmonisation of Technical Requirements for Registration of Pharmaceuticals for Human Use (ICH) is at present (i.e. assessing and identifying apical endpoints) and towards identifying key molecular events. Efforts have been made in industry in terms of *in vitro* preclinical screening for mitochondrial activity but there have been few rigorous efforts to correlate *in vitro* findings with *in vivo* functional endpoints or with conventional measures of toxicity. Improved *in vivo* assessment of mitochondrial function could facilitate the development of safer medicines but methods are currently underdeveloped and invalidated for practical application in preclinical studies [5]. The overall goal remains to identify and manage mitochondrial toxicity from the earliest possible point in drug development and support the safe progression of molecules, which may interact with mitochondria, to the market.

Despite the potentially potent effect of drugs which cause DIMT, mitochondria are increasingly seen as attractive targets for pharmacological intervention (i.e. therapeutic targeting of sub-optimal mitochondria) due to their central role in the mechanism of many common human diseases; e.g. as treatments for metabolic disorders (e.g. diabetes), neurodegenerative disorders, COPD and cancer. Given the diversity of metabolic pathways potentially affected by altering mitochondrial function, development of mitochondrial-targeting medicines clearly requires judicious safety assessment and risk management [5, 6]. Methods to assess drug-induced modulation of mitochondrial processes *in vivo* require particular attention. It is however important to acknowledge that, whilst a change in direction of a mitochondrial endpoint may be desirable (e.g. inhibition of the mitochondrial permeability transition pore, mPTP), a change in the other direction (i.e. potentiation of the mPTP) might be undesirable. The availability of quantitative measures of this activity are particularly useful in both situations.

This thesis focusses on the assessment of DIMT and correlates results obtained from *in vivo* studies to those obtained from *in vitro* studies. *In vivo* studies were performed using a systems toxicology approach in order to identify biochemical mechanisms downstream of DIMT and to generate adverse outcome pathways (AOP).

1.2. Introduction to Mitochondria

Mitochondria, from the Greek *mito* (thread) and *chondros* (grains) are energy producing organelles that exist in the cytoplasm of eukaryotic cells. Mitochondria perform a variety of important functions including adenosine triphosphate (ATP) synthesis, calcium signalling/homeostasis, fatty acid (FA) metabolism, apoptosis initiation, regulation of cellular proliferation and biosynthesis of heme, pyrimidine and steroid structures [7].

Mitochondria were discovered in the late 19th century by Robert Alttman. They were originally called “bio-blasts” and described as "elementary organisms" living inside cells and carrying out vital functions [8]. Upon visualisation by electron microscopy in 1952, they were described as a collection of cytosolic free-floating individual vesicles forming thread-like structures inside cells [9, 10]. Just a year later in 1953, the oxidation capacity of mitochondria was revealed by discovering that specific staining of mitochondria by Janus Green B was due to the capacity of cytochrome oxidase to reoxidise the dye [11]. The following two decades saw a spate of discoveries relating to the role of mitochondria in cellular

respiration and oxidative phosphorylation (OXPHOS). Key discoveries included demonstration of the membranous localisation of the respiratory chain [12], demonstration of energy coupling between electron transport and ATP synthesis [13] and reconstitution of OXPHOS and related reactions [14].

Mitochondria are now widely acknowledged to be dynamic, pleomorphic structures constantly undergoing fission and fusion, with these processes tightly regulated by cellular stimuli and bioenergetic need [15]. Fission and fusion events allow the exchange of organelle content such as proteins, solutes, lipids and deoxyribonucleic acid (DNA) [16]. A wide body of evidence now suggests that impairment of the mitochondrial capacity is implicated in a number of human diseases and neuropathies [17].

The numbers of mitochondria in a cell vary widely depending on the cell type, owing to the differing degrees of reliance on cell sustainability and metabolic load [18]. Within a cell, the distribution of mitochondria is unequal, depending on the cellular energetic or metabolic demands; for example, in cardiac cells, mitochondria are localised to the contractile apparatus, whilst in a sperm cell they are wrapped tightly around the motile flagellum [19].

1.3. Mitochondrial Structure and Genome

Mitochondria are highly compartmentalised organelles with two membranes, an outer mitochondrial membrane (OMM) rich in cholesterol / porin molecules and an inner mitochondrial membrane (IMM) rich in cardiolipin. These membranes functionally separate two distinct regions, the intermembrane space (IMS) and the water-containing matrix (shown in Fig.1.1). Mitochondria can only be visualised in detail using an electron microscope and are usually roughly ovoid but they may assume a filamentous shape or a vesicular form.

The OMM comprises two lipid bilayer membranes and contains many aqueous pores permeable to all ions and molecules up to 14 kDa [20]. This makes the IMS chemically equivalent to the cytosol with respect to the small molecules it contains. In contrast to the OMM, the IMM is impermeable to ions and polar molecules but contains many protein transporters spanning the membrane. Furthermore, the IMM is virtually devoid of cholesterol and is rich in cardiolipin (which binds the proteins of the ETC) [21]. The content of the matrix is dependent upon the availability of the transport proteins in the IMM to facilitate the import/export of molecules such as ATP/ADP which are transported via the adenosine nucleoside

translocator (ANT). The impermeability of the IMM allows an electrochemical gradient to be maintained and this gradient provides the proton motive force for ATP generation. Maintaining the integrity of the IMM is critical for mitochondrial function. The IMM is the most common target for mitochondrial toxicants. Many xenobiotics damage mitochondria either by increasing the permeability of the IMM or by inhibiting transport proteins within it. Furthermore, many drugs have a very high affinity for cardiolipin and thereby preferentially bind to the IMM and affect important organelle processes.

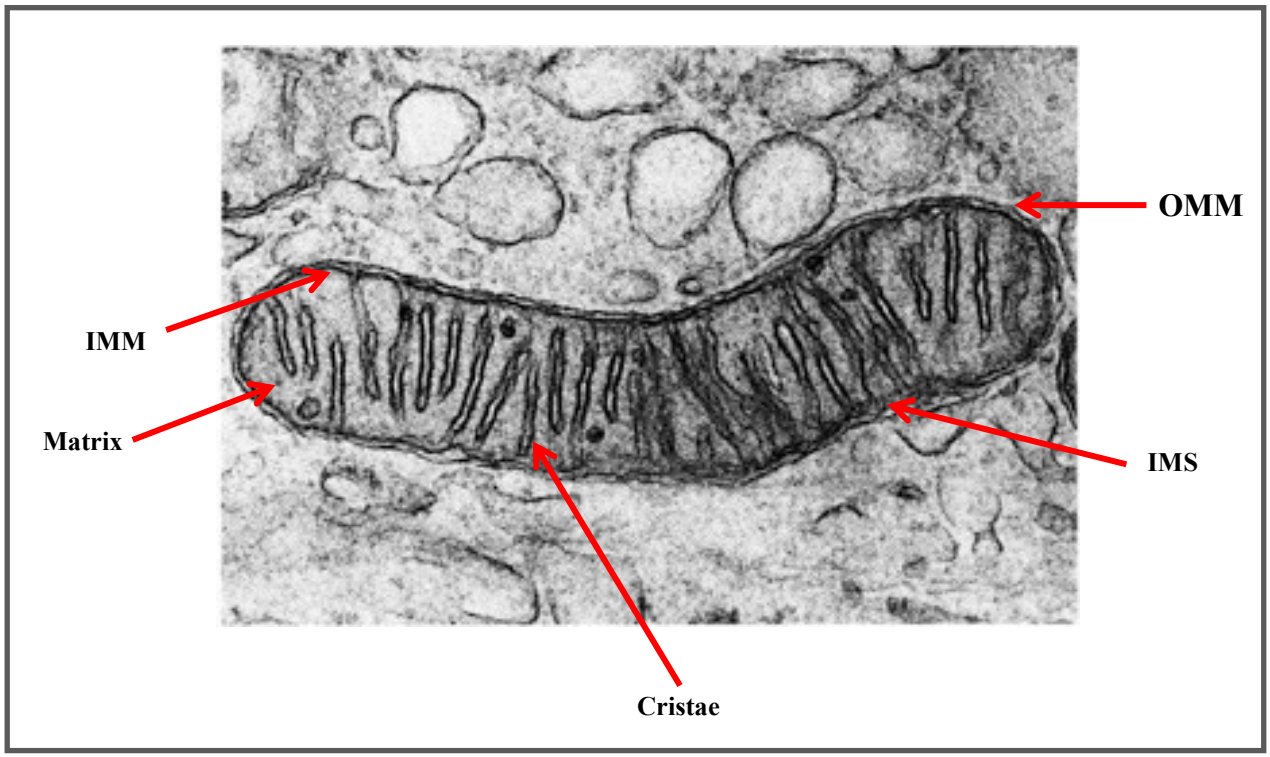


FIGURE 1.1: Structure of a eukaryotic mitochondrion: Electron microscopy image of a mitochondrion. Arrows show the key structural regions of the mitochondria, the outer mitochondrial membrane (OMM), the inner mitochondrial membrane (IMM), the intermembrane space (IMS), the matrix and the cristae. Image taken from [http://imgbuddy.com/mitochondria-microscope.asp] – Accessed 09 June 2015.

The IMM is invaginated forming structures known as cristae which greatly increase its total surface area for maximal ATP production. These cristae contain clusters of five protein complexes (complex I, II, III, IV and V) which are involved in a process known as oxidative phosphorylation (OXPHOS) where electron transport is tightly coupled to ATP synthesis [22].

The mitochondrial matrix contains the vast majority of mitochondrial proteins, including those involved in fatty acid (FA) β-oxidation, haem/steroid synthesis and the tricarboxylic acid (TCA) cycle. The mitochondrial matrix also contains several copies of mitochondrial DNA (mtDNA) with the number of copies varying according to cell-type [6].

Mitochondria are the only organelles outside the nucleus that contain their own genome. A single DNA polymerase (polymerase-gamma, pol-γ) with base excision repair activity ensures the replication of mtDNA. Although pol-γ is a nuclear derived protein, its only known function is the replication of mtDNA and therefore any mutation or inhibition of this enzyme will manifest only in effects on mtDNA. The mtDNA shows substantial similarity to bacterial genomes (e.g. circular, unenclosed and lacking histones) leading to the theory that mitochondria were originally free-living aerobic bacteria that were then engulfed by eukaryotic cells more than a billion years ago [23]. The bacterial origin of mitochondria has implications for the drug discovery process as drugs designed to impair bacterial protein synthesis may have the potential to cause an adverse effect in the host's mitochondrial ribosomes [24]. Mammalian mitochondrial ribosomes (55S) differ from bacterial (70S) and cytoplasmic ribosomes (80S) in terms of weight and molecular structure. Mitochondrial ribosomes are encoded in nuclear genes and imported into mitochondria where they assemble with mitochondrially transcribed rRNAs into ribosomes responsible for the translation of the 13 mitochondrial mRNAs encoding essential OXPHOS proteins [25].

mtDNA is maternally inherited and is present as several copies within the mitochondrial matrix. The mitochondrial genome consists of a small circular chromosome and each copy of mtDNA encodes 13 proteins, as well as 22 tRNA's and 2 rRNA's [26]. Whilst the proteins encoded by mtDNA are essential for OXPHOS, the majority of mitochondrial proteins are encoded by the nuclear genome and transported into the organelle by the means of protein localisation signalling and transporter molecules [27].

Mutations in mtDNA can cause serious disorders (mitochondrial-diseases) such as neuropathy, ataxia and retinitis pigmentosa (NARP), Leber hereditary optic neuropathy (LHON) and myoclonic epilepsy with ragged red fibres (MERRF) [28]. Not all mitochondrial diseases are due to mutations in mtDNA with some arising as a result of mutation in the nuclear genome. Moreover, polymorphic variations can give rise to a situation known as heteroplasmy, where each cell can have copies of both mutated mtDNA and wild-type DNA [29]. Unlike nuclear DNA, mtDNA is not protected by histone proteins and is located in close proximity to sites where reactive oxygen species (ROS) are routinely generated. This increases the

susceptibility of mtDNA to ROS-related oxidative damage. Also, some DNA repair processes are less efficient for mtDNA compared with nuclear DNA and as such the mutation rate is estimated to be at least 10-20 times higher [30].

1.4. Mitochondrial Function

1.4.1. MITOCHONDRIA: ENERGY PRODUCTION

Mitochondrial energy production is achieved by electron transfer in the respiratory chain, using a process known as OXPHOS. Approximately 95% of ATP is generated during aerobic (i.e. consuming oxygen) respiration by mitochondria. Mitochondria are also the site for other metabolic pathways, most notably the β-oxidation of FA's and the TCA cycle.

Glucose is broken down in the cytosol during glycolysis (shown in Fig.4.3 in chapter 4), yielding a net gain of 2ATP molecules, 2 nicotinamide adenine dinucleotide (NADH) molecules and pyruvate. Under aerobic conditions, pyruvate is transferred to the mitochondrial matrix where it is converted to acetyl coenzyme A (acetyl CoA) by pyruvate dehydrogenase [31]. In the mitochondrial matrix the TCA cycle occurs whereby a series of enzyme-mediated chemical reactions occur with the objective of oxidising acetyl CoA to produce molecules capable of supplying electrons to the mitochondrial respiratory chain or replenishing molecular intermediates for other pathways. In brief, the output of the TCA cycle is the formation of $2CO_2$, 3NADH, 1GTP and $1FADH_2$. Additionally succinate formed in the cycle can be oxidised by complex II of the mitochondrial respiratory chain (see Fig.1.2).

An alternative way of generating energy via OXPHOS is by using lipids which are stored in the form of FA's in triglycerides. FA's are degraded via catabolism in the mitochondrial matrix via a process known as β-oxidation. The process involves the extraction of several units of acetyl CoA by oxidation. The triglycerides are hydrolysed by lipases resulting in glycerol and FA. Glycerol can follow the glycolytic pathway while FA's are processed via β-oxidation, wherein dehydration, hydration and oxidation occur to convert FA's into several products used in mitochondrial metabolism including succinyl-CoA, which enters the TCA cycle.

In addition, the mitochondrion is the site at which the terminal steps of amino acid catabolism occur resulting in the production of acetyl CoA. Acetyl-CoA is therefore a convergence point for many catabolic pathways and enters the TCA cycle where energy rich electrons, abstracted from the oxidation of substrates, are used to reduce nicotinamide adenine dinucleotide (NAD^+ to NADH) and flavin adenine dinucleotide (FAD^+ to $FADH_2$). These high energy electrons (reducing equivalents) are then transferred to the IMM where they enter the electron transport chain (ETC)[32].

NADH is oxidised by complex I (NADH:ubiquinone reductase) and the released energy is used to reduce ubiquinone and produce an electrochemical proton gradient. The majority of substrates produced via the TCA cycle (i.e. resulting from dietary fats, glucose and amino acids) are oxidised by this route meaning that this is the main entry point for channelling electrons into the ETC. Meanwhile the reduced form of FAD ($FADH_2$), a prosthetic group within complex II (succinate dehydrogenase), also donates electrons to ubiquinone [33]. This means that the second entry point of the respiratory chain is complex II-III (cytochrome bc1 complex) wherein complex III oxidises the reduced ubiquinol, promotes the generation of an electrochemical proton gradient by pumping protons across the IMM and reducing the water soluble carrier protein cytochrome c. Cytochrome c is attached to the cytosolic side of the IMM and serves as an electron carrier between complex III and IV. Complex IV (cytochrome oxidase) directly reduces molecular oxygen to water and further contributes protons to the electrochemical proton gradient.

As described above the transfer of electrons down an energy gradient is concomitant with the process of proton pumping from the matrix to the IMS by complexes I, III and IV resulting in the generation of an electrochemical (proton-motive) gradient i.e. the mitochondrial membrane potential ($\Delta\Psi$) [34] . The energy contained in the electrochemical gradient is utilised by complex V (ATP synthase) to make ATP from adenosine diphosphate (ADP) and inorganic phosphate. The overall rate of electron transport in the respiratory chain of mitochondria is regulated by the amplitude of the electrochemical potential (known as respiratory control). This is beneficial as under physiological conditions the decrease in proton gradient is due to the metabolic demand of the mitochondrion, and as a result an immediate stimulation of oxygen consumption (increased ETC activity) is observable. This means that the rate of respiration is therefore intrinsically coupled to the rate of metabolism. An overview of the ETC and OXPHOS system is shown in Fig.1.2 below.

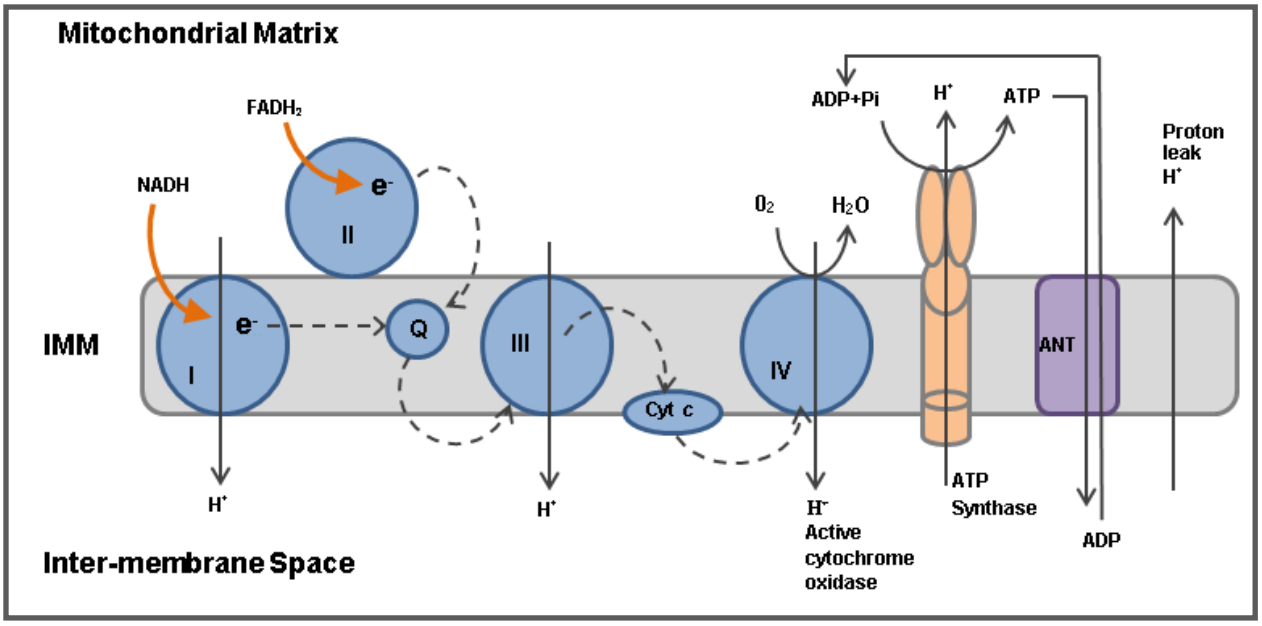


FIGURE 1.2: The mitochondrial respiratory chain: High-energy electrons derived from reduced substrates are transferred through several multi-protein complexes to molecular oxygen. This provides the energy to move protons across the inner mitochondrial membrane with ATP synthase utilising this energy to generate ATP. [H^+- protons, Q-ubiquinone]. Image not scaled.

Mitochondria are unique among cellular organelles, in that they can build up a $\Delta\Psi$ of -180 to -220 mV. On particular occasions (e.g. when the IMM becomes permeable or in the presence of a proton/ion-ophore) the $\Delta\Psi$ can be completely dissipated resulting in ATP depletion and an increase level of mitochondrial oxygen consumption (i.e. increased ETC output). A futile proton cycle then ensues, as protons bypass the F_0F_1 subunit of ATP synthase causing production heat [35]. This process is known as mitochondrial uncoupling and can be protein dependent (e.g. in the presence of an uncoupling protein or UCP) or protein independent (requiring the presence of an ionophore or cationic lipid). ATP synthesis is therefore tightly coupled to electron transport with ATP synthase capable of converting energy from the electrochemical gradient into chemical bond energy in either direction [36].

Mitochondria are able to respond to a certain level of direct or indirect stress by utilisation of an innate respiratory reserve capacity. Reserve capacity is used to describe the amount of extra ATP that can be produced via OXPHOS at times of sudden increases in energy demand [37]. There are likely to be differing sensitivities to drug treatment in individuals based on age/genetics/co-medication etc. that alters the reserve mitochondrial capacity. Furthermore, the reserve capacity can often mask potential drug/mitochondrial interactions until the cell has a requirement to utilise that reserve capacity (e.g. under

conditions of stress) [38]. Effects may therefore not be seen until much later after exposure, a phenomenon recognised with cardiotoxicity. The mechanisms, by which the mitochondrial reserve capacities become compromised, are not well elucidated or understood [39].

1.4.2. MITOCHONDRIA: ROS

The normal process of electron transport is associated with some low level leakage of electrons which are directly donated to molecular oxygen. This results in the formation of reactive oxygen species such as superoxide which can react with, and damage, phospholipids, proteins and mtDNA [40]. Although the superoxide anion has limited chemical reactivity, it can be converted into more highly reactive species for example hydrogen peroxide (H_20_2) and more particularly the hydroxide radical via Fenton chemistry [41]. Approximately 2-4% of the total oxygen consumed by mitochondria is not totally reduced to water and results in the formation of ROS. Under normal physiological conditions cells are able to counteract the harmful effects of ROS by several anti-oxidant defence systems including mitochondrial superoxide dismutase, glutathione peroxidase, peroxiredoxin (which utilises thioredoxin to counteract the effect of hydrogen peroxide) glutathione reductase, α-tocopherol and cytochrome c [42]. Furthermore, the methionine residues of mitochondrial proteins are able to prevent the oxidation of protein cysteine residues, inducing the formation of methionine sulphoxide and thus maintain protein functionality [43]. However when production of ROS exceeds the capacity of the anti-oxidant defence systems, oxidative stress ensues.

The main sources of ROS are complex I (primary source due to having the most reducing capacity) with complex III, monoamine oxidase and complex IV also contributing to burden. Mitochondrial proteins which are localised around the ETC (located primarily in the matrix or acting as IMM transporters) are constantly in danger of being impaired by oxidative stress [44]. Furthermore, impairment of complex I and complex III by oxidative stress can result in increased ROS generation from these sites and then a vicious cycle ensues [45]. In addition, chemical inhibition of the respiratory chain at multiple sites further increases the production of superoxide anions and as such drug-induced ROS generation may be a key player in the AOP of mitochondrial targeting compounds [46].

Loss of regulation of cellular calcium concentrations can also increase the production of superoxide anions by the mitochondrial respiratory chain. Calcium is able to bind to the phospholipid/cardiolipin rich

IMM which induces both a conformational and functional alteration in membrane function in turn facilitating electron leak from the respiratory chain [47].

1.4.3. MITOCHONDRIA: CELL DEATH

Mitochondria have been demonstrated to play a crucial role in the cell death pathways, apoptosis and necrosis.

Necrosis describes the processes whereby cells suffer damage that results in increased cellular volume, aggregation of chromatin, disorganisation of the cytoplasmic contents, loss of plasma membrane integrity and loss of cellular functionality. During the progression of necrosis, most of the cell contents are released, causing damage to neighbouring cells, an increase in localised inflammation and irreversible damage to the surrounding tissue. Necrosis was always believed to be caused by passive disturbance; however, recent studies have suggested it can be regulated although in both scenarios, mitochondria have been heavily implicated in the control of necrosis. Cell death by necrosis can occur due to activation of the mitochondrial permeability transition (MPT) which comprises collapse of the proton motive force, a decrease in ATP production and an increase in ATP hydrolysis via F_0F_1-ATP synthase running in reverse (i.e. hydrolysing ATP in order to maintain the $\Delta\Psi$, resulting in ATP depletion) [48]. Furthermore, it has been described that cell swelling during necrosis, due to alterations in the cytoskeleton and inhibition of the Na^+/K^+ pump) is caused by impaired cellular respiration and loss of $\Delta\Psi$ [49].

Apoptosis, a form of programmed cell death, is a process by which cells are eliminated from the body during embryonic development, tissue homeostasis, normal cell turnover and following cell injury. In brief, apoptosis can result from two independent routes (intrinsic and extrinsic). During the extrinsic pathway, apoptosis is triggered by ligand-induced activation of death receptors at the cell surface, such as TNFR, CD95/Fas and TRAIL-R1/R2. The intrinsic apoptotic pathway heavily involves the mitochondria, either as initiators or propagators of the apoptotic signal.

An early event during intrinsic apoptosis is the release of cytochrome c from the IMM of the mitochondria into the cytosol. Cytochrome c then binds apoptotic protease activating factor (Apaf-1) and procaspase-9 promoting the formation of the heptameric apoptosome and the resultant activation of a group of cysteine proteases called “caspases”[50]. Caspases are categorised into initiators (caspase-2,-8,-

9, 10), effectors (caspase-3,-6,-7) and inflammatory (caspase-1,-4,-5) and they function to coordinate programmed cell death via chromatin condensation, DNA fragmentation and membrane blebbing [51].

Furthermore under certain apoptotic conditions (e.g. mitochondrial swelling) mitochondria release proteins such as cytochrome c (release mentioned above), Smac/DIABLO and the apoptosis inducing factor (AIF). AIF is then targeted to the nucleus where it binds to DNA, stimulating chromatin condensation and DNA breakdown [52]. Protein release from the mitochondria is a complex process and includes the oligomerisation on the OMM of the pro-apoptotic proteins Bax and Bak (pro-apoptotic Bcl2 proteins), which form a cytochrome c permeable channel. It is also now known the MPT pore (mPTP) can regulate calcium induced apoptosis and as such, the alteration in the calcium signal reaching mitochondria and/or the combined impact of apoptotic agents or pathological conditions (i.e. oxidative stress) can induce a profound alteration of mitochondrial structure, function and downstream cell death. This is highlighted by the work of Zamzami and colleagues who demonstrated that mitochondrial fragmentation during apoptosis was closely related to the collapse in $\Delta\Psi$, with this collapse being considered the point of no return in the apoptosis cascade [53].

1.5. Mechanisms of DIMT

Drugs can interfere with mitochondrial function in many different ways. Given the structural and functional complexities of mitochondria it is unsurprising that many of these interactions can lead to DIMT. The mechanisms involved are reviewed below (Fig.1.3).

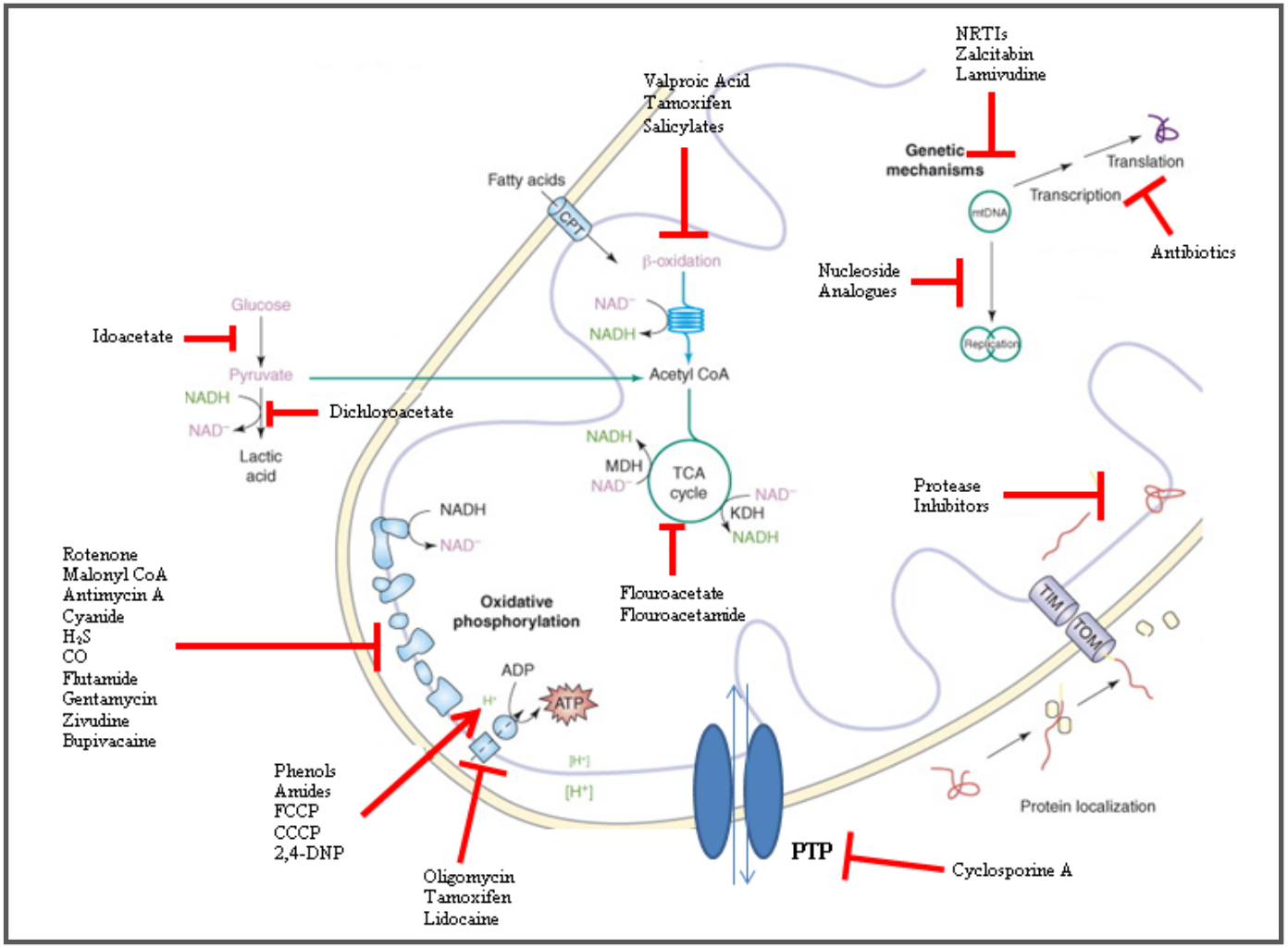


FIGURE 1.3: Graphical representation of mitochondria as a mediator of drug-induced toxicity: Mechanisms include not only direct inhibition or uncoupling of ETC and OXPHOS but also inhibition of transport or oxidation of substrates, of the mPTP as well as molecular targets of mitochondrial biogenesis (i.e. inhibition of mtDNA replication, transcription and translation, and import or post-translational processing of proteins). The result is either inhibition/uncoupling of the respiratory chain directly, an indirect failure to generate and assemble functional substrate for the ETC or induction of cell death pathways. All of which lead to ATP depletion and cellular bioenergetic deficit. Image taken and adapted from [27].

1.5.1. DIRECT INHIBITORS OF OXPHOS:

Drugs that interfere with OXPHOS include both inhibitors of the distinct complexes of the ETC and uncoupling agents. Acute poisoning of the respiratory chain classically presents signs and symptoms such as muscle weakness, fatigue, hypotension, confusion and nausea. The inhibition of the ETC and consequential inability to utilise oxygen at cytochrome oxidase causes cytotoxic hypoxia despite normal or above average blood oxygen. In contrast, uncouplers of OXPHOS from ETC function (caused by dissipation of the electrochemical proton gradient) induce disproportionate oxygen consumption. Uncouplers also cause ATP depletion and metabolic acidosis, but classically, little or no effect on blood oxygen is observed; The free energy of substrate oxidation is liberated as heat resulting in fever [20].

Complex I is the most susceptible of the ETC complexes to drug-induced malfunction. More than 60 different types of natural and synthetic compounds can perturb mitochondrial complex I activity including pesticides, neurotoxins, and antibiotics. It has been suggested, following rigorous structure activity relationship (SAR) studies that, generally compounds with complex I inhibitory activity have modular similarity to ubiquinone [54, 55]. Inhibitors of complex I can be broadly classified into one of three categories, namely, compounds that inhibit at the level of the NADH-flavin interface (such as rhein), complex I and III non-specific quinolone antagonists (such as myxothiazol) and finally, specific and potent inhibitors of complex I such as rotenone.

Complex II (succinate dehydrogenase) is less commonly studied in terms of its role in pharmacotoxicology. This is unexpected considering that recent research has revealed a role for complex II in many roles independent to cell metabolism, such as succinate signalling, ischaemic preconditioning, ROS generation and ageing [56]. Complex II is experimentally inhibited using malonate or 3-nitroproprionic acid, but is also inhibited by a number of foloruoquinilones, fungicides, diazoxide and chloramphenicol (although many are not specific to complex II). Other compounds which affect mitochondrial complex II include the anticancer-drug etoposide, arsenic trioxide, cisplatin and menadione [57].

Complex III is the second membrane spanning protein complex of the ETC. The sensitivity of various species to complex III inhibition varies significantly and as such, complex III inhibitors have been explored for use as anti-malarials, fungicides and anti-cancer drugs. Importantly the inhibition of complex

III of the mitochondrial chain (leading to ATP-depletion) is not the only harmful effect of these molecules. The generation of ROS following chemical inhibition of complex III likely contributes to the subsequent cellular and tissue toxicity. Inhibitors of complex III are generally categorised according to the site of action and these are outlined below.

- Group I – Quinol antagonists encompassing a β-methoxyacrylate group that block the process of ubiquinol oxidation (e.g. myxothiazol, strobilurines and oudemasins).
- Group II – Contain a 6-hydroxyquinone fragment and block electron transfer to cytochrome c1 and thus inhibit the reduction of cytochrome b1 (e.g. undecylhydroxydioxobenzothiazole, UHDBT).
- Group III – Impede electron transfer from heme to a quinone or semiquinone molecule at the Q_i site of complex III (e.g. antimycin A and funiculosin).

Inhibitors of the Q_i site of complex III such as antimycin are specific for the cytochrome-bc1 complex whereas naturally occurring Q_o site inhibitors are less specific and possess a ubiquinone-like structure which often causes co-inhibition of complex I (albeit with significantly lower potency than the inhibitory effect they exert on complex III). Zinc ions are also acknowledged to inhibit the mitochondrial respiratory chain via complex III. Zinc binds reversibly and with high affinity to the Q_o site of the cytochrome-bc1 complex and is able to inhibit oxygen consumption with high potency. Other mono- and di-valent metal cations, such as, Hg^{2+}, Ag^{+}, Cu^{2+} and Cd^{2+} have been shown to inhibit mitochondrial complex III although with lower efficiency [20].

Complex IV is a heme/copper terminal oxidase that exploits cytochrome c as an electron donor. Complex IV inhibitors have also been categorised into four distinct groups: (A) heme-binding inhibitors that are non-competitive with both oxygen and cytochrome c (e.g. azide, cyanide and sulphide), (B) inhibitors competitive with oxygen (e.g. carbon monoxide and nitric oxide) that are reversible, (C) inhibitors which are competitive with cytochrome c (e.g. polycations) and (D) non-competitive inhibitors which do not affect the heme-groups (e.g. phosphate ions and alkaline pH) [20].

Complex V (ATP-synthase) uses the electrochemical proton gradient to synthesise ATP from ADP and inorganic phosphate. The enzyme is able to operate in either direction, for example under some conditions it can work as an ATPase to hydrolyse ATP and generate the proton gradient. ATP synthase is well conserved evolutionarily and as such many of its known inhibitors are of natural origin (mostly fungal).

Many antibiotics/mycotoxins were isolated because of their selective and potent toxicity against other fungi (e.g. aurovertins A, leucionstatins A+B and the classical inhibitors of mitochondrial ATP-synthase, oligomycin A-D). Injection of the ATP-synthase inhibitor oligomycin into rats causes inhibition of oxygen consumption, and severe lactic acidosis with little to no change in arterial blood oxygen levels. These mycotoxins all bind to either the F_1 or the F_0 subunit of the enzyme to block proton conduction. The acute 50% lethal dose (LD_{50}) values from both IP and subcutaneous injection are in the region of 1-10mg/kg in rats and mice [58, 59]. Other compounds and classes of compounds have shown acute inhibitory activity against mitochondrial ATP-synthase, though with less potency than the mycotoxins described above. These include, local anaesthetics [60], paraquat [61], the β-adrenergic receptor antagonist propranolol [62] and organotin composites [63].

Examples of drugs that inhibit the mitochondrial respiratory chain (either via direct ETC complex inhibition or mitochondrial uncoupling) are shown in Fig.1.4 below.

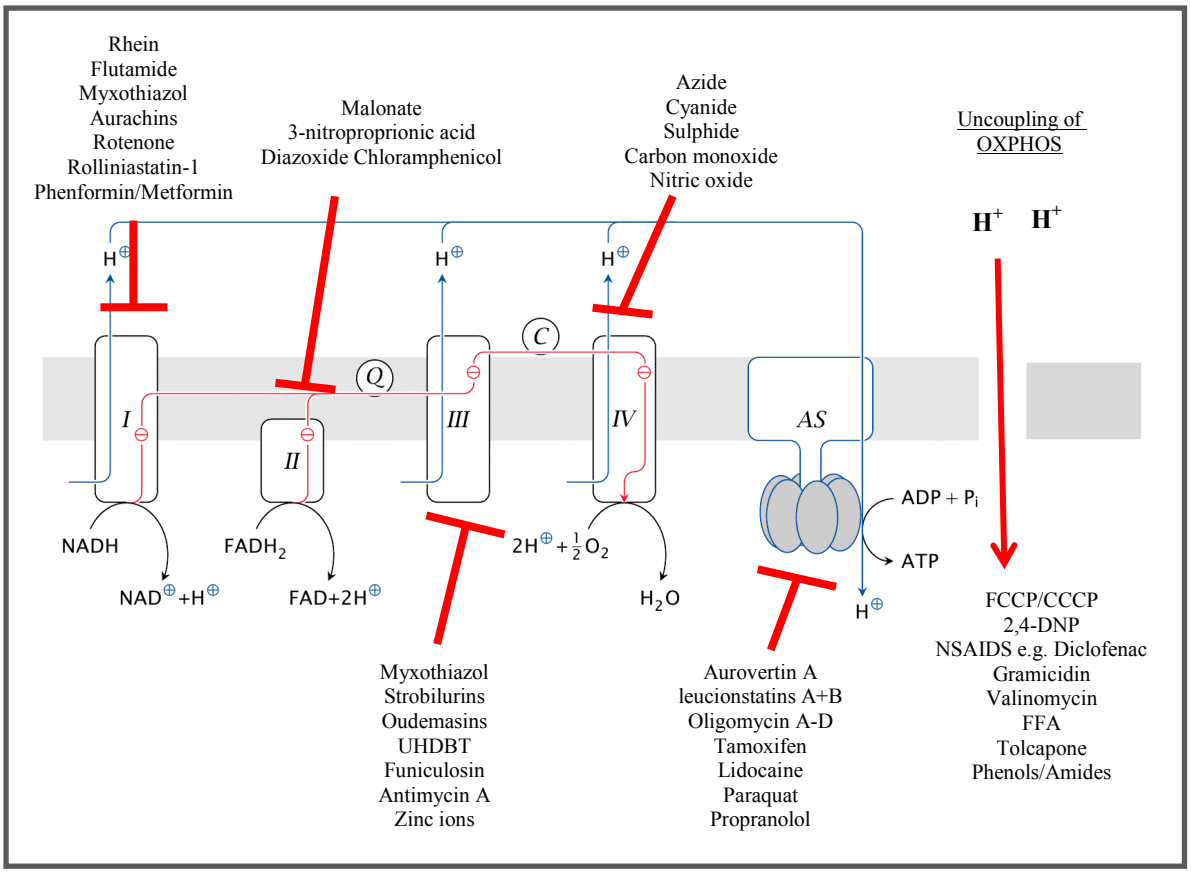


FIGURE 1.4: Schematic representation of drugs which have been implicated in inhibition of OXPHOS either via direct inhibition of respiratory chain complexes I-IV or via chemical uncoupling. Image taken and modified from [http://watcut.uwaterloo.ca/webnotes/Metabolism/rchainOverview.html] – Accessed 29th May 2015.

Uncoupling of OXPHOS is considered to be a common characteristic of anti-inflammatory agents with an ionisable group such as the non-steroidal anti-inflammatory drugs (NSAIDs) diclofenac, aspirin, nimesulide and indomethancin. All of these drugs, despite being taken routinely across the world, exert an uncoupling effect at concentrations corresponding to their pharmacological doses [64, 65]. In their review written in 2000, Wallace & Starkov suggest that the term uncoupling should encompass any energy-dissipating process which competes for energy with routine mitochondrial functions, and thus induces a metabolically futile wasting of energy. They explain that this description encompasses any drug-induced enhancement of any energy-consuming mitochondrial function (such as ion, metabolite or protein transport) as well as the classic idea of uncouplers (the dissipation of the proton gradient and impact on ATP production) [20]. Typically uncouplers of OXPHOS provoke a loss of mitochondrial $\Delta\Psi$, a

reduction in mitochondrial ATP production, increased levels of substrate oxidation and increased heat production. Uncouplers can be broadly categorised into the following:

- *Lipophilic weak acids* – The majority of compounds processing protonophoric activity are lipophilic weak acids with an acid-dissociable group and strong electron withdrawing moieties. Examples of uncouplers in this group include carbonyl cyanide phenylhydrazones and salicylanilides. Compounds such as carbonyl cyanide p-triflouromethoxy-phenyl-hydrazone (FCCP) and cyanide meta-chlorophenylhydrazone (CCCP) are possibly the most frequently used uncouplers in the laboratory. In mice, FCCP and CCP induce rapid rigor mortis and death after IP injection with LD_{50} values of 32 and 40μmol/kg respectively.

- *Substituted phenols* – The best represented and most studied class of uncouplers are the substituted phenols, including the highly toxic 2,4-dinitrophenol (2,4-DNP). Used in the 1930's as a weight loss drug, numerous 2,4-DNP-associated side effects were recognised and it was eventually withdrawn from the market [5]. Although not licensed as a drug, 2,4-DNP is still occasionally used as a fat burning agent to this day, and numerous fatalities per year are still attributed to dinitrophenol poisoning [66], with signs and symptoms including hyperthermia, malaise, dyspnea, respiratory failure and ultimately death. Its potency is highlighted by an LD_{50} of just 141μmol/kg in mice [67]. SAR studies have confirmed that substituted phenols uncouple via the protonophoric mode of action (MOA), and revealed important correlations between the uncoupling activity and physicochemical properties such as hydrophobicity, acidity and lipid membrane stability [68].

- *Salicylanilide (2-hydroxy-N-phenylbenamide) derivatives* – The salicylanilides have been widely used as anticestodal, antinematodal and antihelminithic drugs despite being protonophoric uncouplers of mitochondrial OXPHOS. The mechanism of uncoupling is similar to that of other A^- protonophores. SAR relationships with 28 salicylanilide derivatives revealed that both hydrophobicity and electron-withdrawing potential were required for uncoupling to take place [67].

- *Free fatty acids* (FFAs, both endogenous and exogenous) – FFAs have long been known to be efficient uncouplers of mitochondrial OXHOS. Studies have shown that the adenine nucleotide translocator (ANT) is involved in the uncoupling action of FFAs. Many pathologies are associated with the accumulation of free long-chain FA's in affected tissues and the effect of this accumulation

on mitochondrial function can be devastating, rapidly increasing local temperature generation and oxygen consumption at the expense of substrates for oxidation.

- *Ionophores* – Ionophores are compounds of various chemical structures that are capable of transporting small ions across a lipid membrane. Ionophores have been reviewed in [69, 70] and generally are sub-categorised based on their physicochemical properties or their mechanism of ion transport. Channel-type ionophores (e.g. gramicidin A, D and S) are generally short amphiphilic peptides that form channels in lipid membranes. These channels can be selective toward small ions such as protons or K^+ depending on the peptide, the membrane structure and conditions. The resulting increase in permeability toward protons and K^+ effectively collapses the $\Delta\Psi$ in mitochondria, due either to proton cycling or electrophoretic K^+ transport. Carrier type ionophores (e.g. valinomycin and nigericin) are able to form neutral or charged lipid soluble complexes with an ion to facilitate its electrophoretic transport or electroneutral exchange with protons across the IMM. Furthermore, calcimycin can form a lipid-soluble complex with Me^{2+} to transport divalent cations across lipid membranes by means of electroneural $Me^{2+/}2H^+$ exchange. Dissipation of the calcium gradient establishes a futile energy-dissipating cyclic flux of calcium.

- *Cationic uncouplers* (e.g. the cyanine dye triS-C4(5)) – This category of OXPHOS uncouplers comprises compounds that uncouple mitochondria by increasing membrane permeability to ions [71]. The mechanism of toxicity requires the presence of inorganic phosphate and it is likely that the Pi-dependent compounds affect the physical integrity of the mitochondrial membranes.

- *Alternate electron acceptors* – These compounds greatly diminish the efficiency of energy conversion by disrupting the prescribed pathway of electrons down the ETC and as a result increase the oxidation of substrates and divert excess energy to wasteful heat production. Terminal electron acceptors (those which are capable of being reduced by an electron carrier of the ETC) intercept electrons from the ETC and participate in futile redox cycling, whereby the compound is reduced at the expense of energy derived from substrates. Alternate electron acceptors (or electron-shunts), such as adriamycin, paraquat and a number of naphthoquinones, accept electrons and then feed them back to the respiratory chain at higher redox potential. This allows electrons to bypass a portion of the ETC excluding it from energy generation. Typically the secondary electron acceptor that completes the redox cycle is a terminal complex of the ETC and not molecular oxygen. A classic example of an

alternate electron acceptor is the antineoplastic agent doxorubicin (adriamycin). With a redox potential of -320mV doxorubicin is a good alternate electron acceptor from mitochondrial complex I, which then forms the reduced semiquinone free radical intermediate. The oxidation of mitochondrial glutathione, induction of the mPTP and the oxidation of cardiac mtDNA highlight the importance of mitochondrial redox cycling as a critical pathway in the mechanism of doxorubicin induced cardiotoxicity. Furthermore, naphthoquinones represent another important class of alternate electron acceptors that redox cycle on the mitochondrial respiratory chain. This area of research has been extensively studied in the laboratories of Tim Gant with SAR studies indicating that a univalent redox potential of approximately -180mV being the primary determinant of whether naphthoquinones are good redox cyclers [72]. Furthermore, the rates of free radical generation correlate with the degree of mitochondrial toxicity and the extent of cytotoxicity [73]. Despite the detrimental toxicity associated with alternate electron acceptors, electron shunts have been used therapeutically to bypass respiratory chain dysfunction (i.e. shunting electrons from complex I to complex IV). A key example of this is the use of menadione to treat mitochondrial encephelomyopathies, which are frequently characterised by cytochrome bc-1 deficiency. Menadione enables electrons to bypass the dysfunctional portion of the chain and significantly improves the bioenergetic deficiency caused by these disorders leading to significant improvement in neurological and muscular performance [74].

1.5.2. INHIBITORS OF MITOCHONDRIAL SUBSTRATE OXIDATION:

Compounds causing inhibition of substrate oxidation are, for the most part, structural mimics of the natural substrate and thus act via competitive inhibition of the respective reaction [75]. Inhibition of substrate oxidation interferes with the generation and delivery of reducing equivalents to the respiratory chain. As a result, inhibitors of mitochondrial substrate utilisation ultimately cause metabolic deficit similar to that of direct ETC inhibitors and therefore tissues with high metabolic rates are most sensitive to inhibitors of substrate oxidation. An example includes the inhibition of FA oxidation by valproic acid and salicylic acid [76]. Likewise, fluoroacetate and fluoroacetamide represent structural analogues which condense with oxaloacetate to form fluorocitrate, a potent inhibitor of the TCA cycle enzyme aconitase [77]. It is important to acknowledge that inhibitors of mitochondrial substrate oxidation include inhibitors of both enzymes within the metabolic pathways and transport proteins required for substrate delivery to the mitochondrial matrix [78]. For example, etomoxir (a potent inhibitor of carnitine palmitoyl-transferase 1) was withdrawn from late stage clinical trials due to cardiac toxicity and heart failure [79, 80].

1.5.3. ROS GENERATION:

In the IMM, ROS, particularly superoxide radicals, can be generated by complex I, iron sulphur protein, complex II, complex III, cytochrome oxidase and monoamine oxidase. As described in the previous section, generation of ROS such as superoxide, H_2O_2 and hydroxyl radicals (that escape the antioxidant defence mechanisms of the cell) act via the peroxidation of phospholipids in the biological membranes and cause oxidative damage to DNA and proteins, as a result, spreading damage beyond the confounds of the organelle. The damaging action of ROS in the central nervous system has been implicated in Alzheimer's and Parkinson's diseases [81]. A plethora of drugs can induce mitochondrial toxicity via direct ROS production (by interfering with complex I/III etc.) or indirectly via inducing mPTP induction, disrupting the respiratory chain, uncoupling OXPHOS, damaging mtDNA and subsequent protein synthesis or by impeding/depleting the cellular antioxidant pool [82]. Likewise many drugs have been developed as antioxidants (e.g. coenzyme Q_{10}). Deliberately targeted to mitochondria, these molecules have been applied therapeutically in different congenital OXPHOS disorders.

1.5.4. INDUCING MITOCHONDRIAL PERMEABILITY TRANSITION:

The mitochondrial permeability transition pore (mPTP) resides in the IMM which (under normal physiological conditions) is impermeable to all, but a few, selected metabolites and ions. Under conditions of stress mitochondria can undergo permeability transition (i.e. pore opening) which in general terms encompasses a sudden, non-selective increase in IMM permeability to all solute of a molecular mass less than 1500 KDa (see Fig.1.5 below). Upon opening of the mPTP, low molecular weight substrates and water can freely penetrate the mitochondrial matrix resulting in mitochondrial swelling, loss of $\Delta\Psi$, outer membrane rupture and the release of cytochrome c into the cytosol (leading to the initiation of cell-death pathways). It is this triggering of cell death which underlies the toxicity of t-butyl-hydroperoxide, valproic acid and the hepatotoxicity of diclofenac. Further examples of xenobiotics or endogenous factors which can induce permeability transition include the steroid hormone dehydroepiandrosterone, naproxen, salicylic acid and the neurotoxin MPP^+ [53]. Importantly, modulation of the mPTP tends to occur via binding to a particular component of the pore such as ionidamine binding to the adenine nucleotide transloacse (ANT) [6].

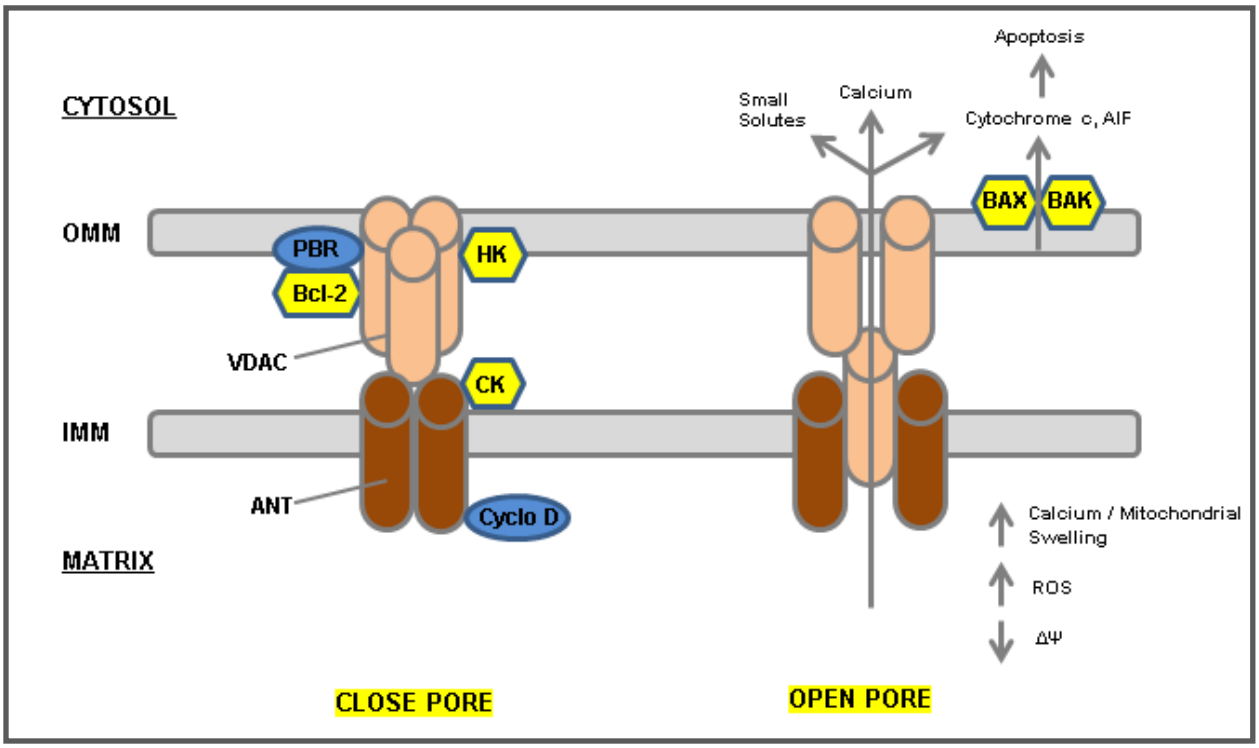


FIGURE 1.5: Putative mPTP proteins in the OMM and IMM in normal physiological and pathophysiological conditions. [CK – creatine kinase, HK - hexokinase, Bcl-2 – BAX – BCL2-associated X protein, PBR - peripheral benzodiazepine receptor (since renamed Translocator Protein), AIF – apoptosis inducing factor, BAK – BCL2 antagonist/killer, Cyclo D – cyclophillin D]. Image drawn based on figure published in [83]. Image not scaled.

ANT is one of the principle components of the mPTP. Further examples of drugs which inhibit this protein include agaric acid and atractyloside and these agents lead to substrate depletion, decreased ATP output and generation of ROS. Importantly, other drugs such as cyclosporine and Ro 68-3400 have the opposite effect by inhibiting the mPTP. As well as its use as an immunosuppressant, cyclosporine has become a pivotal tool compound for experimental studies into the function and control of the mPTP [84]. Furthermore therapeutic groups are investigating the utility of inhibiting the mPTP for the treatment of neurodegenerative disorders [85] and ischemia reperfusion injury [86] / myocardial preconditioning [87].

1.5.5. OXIDATION AND MUTATIONS OF MTDNA, OR INHIBITION OF MTDNA SYNTHESIS:

The disruption of nuclear genes important for mitochondrial homeostasis can lead to autosomal inherited disease. Over 110 specific mutations of mtDNA have been described [88]. Further, inhibition of mtDNA synthesis and/or DNA oxidation is a key characteristic of the toxicity of many antiretroviral drugs.

The thymine analogues zidovudine and stavudine, the adenosine analogue didanosine, the cytosine analogues zalcitabine and lamivudine and the guanine analogue abcavir are nucleoside reverse transcriptase inhibitors (NRTI) used to prevent the replication of the human immunodeficiency virus (HIV). These analogues are recognised by the host DNA polymerases before binding and preventing elongation of the replicating strand (resulting in truncated and unstable replicons). Toxicity is associated with the fact that mitochondria contain just a single DNA polymerase (Pol-γ) which has a high affinity nature for these nucleoside analogues [89]. The resulting truncated and unstable mtDNA is responsible for mtDNA depletion observed post-NRTI therapy and this not only leads to a decrease in mitochondrial abundance but mitochondria which do survive lack many of the mtDNA-encoded protein subunits essential to the ETC complexes [90].

A small number of acquired immunodeficiency disorder (AIDS) patients have suffered adverse outcomes as a result of mitochondrial toxicity, caused by long term anti-retroviral therapy that includes hyperlactaemia, sensory neuropathy and liver steatosis. In rare cases, NRTI-induced lactic acidosis, liver failure or pancreatitis has been fatal. Furthermore, mtDNA depletion has been demonstrated in the liver of HIV patients with both stavudine and zalcitabin NRTI's inducing time/concentration-dependent mtDNA depletion [91].

Crucially, if a large proportion of the mtDNA present is mutated the mitochondria will become dysfunctional, although retain the ability to replicate via biogenesis. This results in the spreading of the mutation and may be behind the persistent and cumulative nature of mitochondrial toxicity [92]. As mammalian cells contain between 2000-5000 copies of the mitochondrial genome, toxicity from mtDNA damage or depletion only becomes apparent gradually with chronic treatment. As a result of the problems with the HIV drugs however, the FDA now require all antiviral submissions in this therapeutic class to include assessment of the effect on mtDNA [93].

ROS generated during OXPHOS has been shown to induce oxidative DNA damage including single- and double-strand breaks, abasic sites and base damages. Due to the close proximity of mtDNA to the respiratory chain, mtDNA has demonstrated a higher susceptibility (than nuclear DNA) to damage such as 8-oxoguanine [94].

In addition to effects directly to mtDNA, another well-established mode of toxicity is via drug-interference with mitochondrial protein synthesis (i.e. the translation of mtRNA). Mitochondria contain their own enzymatic machinery required to translate protein from mtDNA encoded RNA molecules with the ribosomal proteins distinctly different to those in the cytosol which decode the nuclear genome. Inhibition of protein synthesis is believed to result from binding to mitochondrial ribosomes with higher affinity than ribosome-RNA binding. Examples include linezolid [95], chloramphenicol [96] and some of the tetracycline antibacterial medicines [97].

1.5.6. MULTIPLE MECHANISMS

A major problem relating to the assessment of DIMT is the fact that many drugs likely induce mitochondrial dysfunction via a number of different mechanisms. A classic example is the anti-epilepsy medication valproic acid that inhibits mitochondrial FA β-oxidation (by both sequestering coenzyme A and inactivating β-oxidation enzymes via electrophilic metabolites) and induces mitochondrial permeability transition [98, 99]. A second example is the anti-anginal drug, amiodarone which has been shown to inhibit mitochondrial complexes I, IV and V, uncouple OXPHOS and inhibit FA oxidation [100]. Furthermore both the anti-psychotic drug chlorpromazine, and the anti-cancer drug flutamide, both uncouple OXPHOS and inhibit mitochondrial ETC complex I. It is therefore clear that to identify and assess DIMT pre-clinically, a battery of endpoints should be analysed which encompasses the array of potential mechanisms of mitochondrial toxicity. Furthermore, a wide dose range should always be assessed.

1.6. Methods of Detecting DIMT

No single assay can identify all mechanisms of DIMT. A range of assays, spanning multiple mitochondrial endpoints, is therefore required. It is important that attempts to assess DIMT are

multifaceted in scope and take into account the distinct mechanisms by which drugs can interfere with the coordinated regulation of intermediary metabolism and energy production by the cell [101].

Model systems for studying mitochondrial toxicity include whole cells maintained in culture, isolated mitochondria, tissue sections (for histopathological markers) and sub-mitochondrial particles. The system used is largely dependent upon the assay being performed however is of pivotal importance when relating findings to potential events *in vivo*. It is essential to understand the limitations of the systems being used and take due consideration of these limitations when interpreting the findings. For example, whilst used widely in the study of mitochondrial function/dysfunction the following limitations are associated with the use of isolated mitochondrial fractions:

- Reports in the literature suggest that only around 30% of the total mitochondrial pool can be isolated by differential centrifugation [102].
- Compromised structural integrity following manual homogenisation of tissue and presence of cellular debris in the mitochondrial fraction.
- Disintegration of mitochondrial-cytoskeletal networks and heterogeneous branching of organelles [21].
- *Ex vivo* dosing of mitochondria with compounds, provokes an exaggerated response as the drug is not subjected to metabolism and does not have to penetrate the cell thus having unrestricted access to the mitochondria.
- It was recently discovered that many subunits of the OXPHOS system are phosphoproteins. Furthermore it was suggested that these and other mitochondrial phosphoproteins could be the substrates of protein kinase A and protein kinase C amongst others [103]. If a compound has an effect on a kinase which regulates the activity of the OXPHOS complexes, this effect may not be observed in isolated mitochondria if the affected kinase is not of mitochondrial localisation.

Furthermore it is important to determine the quality of mitochondrial preparations being used. This can be achieved by determination of the respiratory control ratio (RCR), calculated as the rate of respiration in the presence of ADP divided by the rate obtained after the expenditure of ADP. Typical RCR values can range from 3-12.5 depending upon the age of the donor, species, substrate choice and organ [104] (see appendix 2).

Many of the *in vitro* experiments described below (table 1.1), such as the oxygen consumption and ATP assays, are performed in immortalised cell lines, grown in glucose-containing medium. For ease of culturing, it is routine practice to use immortalised cells lines for pre-clinical screening activities however these have a preference for synthesising ATP via glycolysis when grown in glucose-conditioned media [105]. This phenomenon is named the Crabtree effect and, due to reduced reliance on OXPHOS for energy production, makes identification of mitochondrial toxicants challenging [106]. In order to overcome this, cells can be grown in a medium containing galactose as opposed to glucose which forces the cells to rely on mitochondria for their ATP synthesis and are therefore more susceptible to DIMT with compounds which either inhibit the ETC or uncouple mitochondrial OXPHOS [107].

High throughput methods (e.g. oxygen sensitive probes) have been developed with the ultimate objective of allowing company and research laboratories to perform large-scale screening of compounds which interfere with mitochondrial processes (Table 1.1 below describes assays regularly used in the detection of mitochondrial dysfunction in the drug-safety arena). This table is by no means exhaustive as mitochondria affect such a wide variety of cellular events. For example analysis of proteins involved in cell signalling pathways may provide information about mitochondrial function but is not a regularly used assay.

In vitro techniques using cell culture or isolated mitochondria are commonly used to evaluate the effects of drugs on mitochondria. These methods will remain crucial for target elucidation, for example, distinguishing effects on the ETC (oxidation) from effects on phosphorylation efficiency (uncoupling) [108]. It seems unlikely however, that *in vitro* assessment can adequately define the relevance of mitochondrial dysfunction *in vivo*, especially with enough confidence to adequately monitor safety or assess risk. Furthermore, traditional drug safety methodologies may be insufficient. Standard endpoints used for safety testing in preclinical and clinical development, such as clinical signs, histopathology, haematology and clinical chemistry are very important for detecting compounds with unintended effects, but they are relatively imprecise and insensitive for detecting alterations in mitochondrial function. For drugs that have some level of *in vitro* mitochondrial activity, it is anticipated that safety studies may need to be augmented with more specialised or targeted evaluations

Specific *in vivo* endpoints are likely required in the future in order to improve understanding of DIMT *in vivo*. This may include the analysis of isolated mitochondrial fractions from treated animals [109],

specialist imaging techniques such as positron emission tomography (PET) [110] or enhanced nuclear magnetic resonance (NMR) techniques, such as magnetic resonance spectroscopy (MRS) [111]. The ideal assessments for use in drug development would be non-invasive and demonstrate a good degree of target organ specificity, predictivity and clinical translatability [5]. At present however, these assessments are only implemented when mitochondrial toxicity is a limiting factor in the development of a candidate drug and are not routine. Further work is therefore required in order to validate and develop such endpoints and to understand their capability and limitations.

Assay or Endpoint	Model System(s)	Technology / Methodology	Comments
Morphological analysis	Fixed tissue/isolated mitochondrial pellet /protein isolate.	Electron microscopy	Glutaraldehyde fixation and subsequent steps to sectioning and uranyl acetate/lead-citrate staining.
		Western blot	Separation of protein via SDS-PAGE and transfer to nitrocellulose membrane. Probing with antibodies against various mitochondrial structural/bioenergetic proteins followed by secondary antibody detection and chemoluminescent visualisation.
Respiration (oxygen consumption)	Cells or isolated mitochondria	Clarke type electrode	Polarographic procedure using mitochondria suspended in sucrose EDTA/EGTA solution with substrates and specific ETC inhibitors at 25-30°C (stirring). ADP/0 ratio can be calculated (mol ADP phosphorylated per mol oxygen atom consumed)
		Oxygen sensitive probes (Luxcel / Seahorse Biosciences)	O_2 quenchable fluorophores measure oxygen consumption in a multi-well microplate. Seahorse technology produces a transient micro-chamber within which oxygen is measured following sequential injections of mitochondrial compounds. BOFA analysis (Basal, ADP, Oligomycin, FCCP, Antimycin A) facilitates calculation of multiple respiratory parameters such as RCR, respiratory reserve capacity, proton leak, non-mitochondrial respiration, basal respiration and respiration at an uncoupled state.
Calcium retention capacity (CRC)	Isolated mitochondria	Calcium green 5-N, Arsenazo III specific ion electrode/ fluorescent spectrophotometer.	Changes in absorbance spectrum at wavelength pair 675-685nm (ASZ III) or calcium Green fluorescence (505nm/531nm) denote calcium fluxes following substrate stimulation.
Mitochondrial $\Delta\Psi$	Cells or isolated mitochondria	JC-1, TMRM, TMRE, NAO, RH-123. Fluorescent spectrometric reader.	Fluorescent markers which accumulate in the matrix and are released when the $\Delta\Psi$ is decreased. A number of fluorescent dyes are commercially available (e.g. JC-1, TMRM etc.)
mPTP/mitochondrial Swelling	Isolated mitochondria	Spectrophotometer (JC-1 / TMRM) $+KH_2P0_4$ to induce swelling	Swelling is recorded spectrophotometrically at 540nm using succinate energised mitochondria.
ATP levels	Cells and fresh frozen tissue	High energy phosphate analysis (AMP, ADP + ATP)	Determination of high energy phosphate content in immediately snap frozen tissue / cells (scraped into perchloric acid) by HPLC.
		ATP quantification, cell ATP luminescent titre.	Inorganic phosphate determination / Firefly luciferin/luciferase system. Determination of ATP using cell-based luminescence system. Measurement of "glow-type" luminescent signal.
ROS	Cells in culture, isolated mitochondria, frozen tissue.	DCFDA luminol probe	Hydrolysed from CM-H2-DCFDA inside cell and reacts with ROS to form fluorescent DCF (503-529nm).
		GSSH/GSSG ratio. Determination of antioxidant status.	Determination of glutathione in its reduced (GSH) and oxidised state (GSSG) can be analysed by mass spectrometry or via absorbance in many different biological samples (cells, mitochondria, blood)
		Superoxide dismutase assay (SOD)	Catalyses conversion of superoxide radicals to hydrogen peroxide via redox cycling. Analysis of SOD activity using a 96 well colorimetric assay.

		Flow cytometry techniques. Multiple tags (Thiolite Green/ Cell Tracker Orange, Mitosox Red, Rhodamine 123, CM-H2DCFDA, H2DCFDA, Xfect)	Thiolite Green / Cell Tracker Orange – GSH + ROS = GSSG. Thiolite Green is a sensor for measuring thiol compounds. (GSH depletion) MitoSox Red – Oxidation of MitoSox Red reagent by superoxide produces red fluorescence. Rhodamine 123 – binds to mitochondrial membranes and inhibits transport processes such as the ETC. Fluorescence proportional to the dissipation of mitochondrial ΔΨ. CM-H2DCFDA / H2DCFDA – ROS generation. DCFH-DA hydrolysed by esterases to DCFH, DCFH + ROS->DCF (fluorescent product measured). Xfect protein transfectant - DNA damage (γ H2AX, DNA double strand break response biomarker)
		Gene Expression – RT-PCR (Taqman/Cybr green analysis)	Panel of oxidative stress biomarkers on a low density gene-array or TaqMan gene card. RNA-cDNA from cells or tissues.
Gene expression/mtDNA content and deletion	Fresh frozen tissue	RT-PCR, Microarray technology	RNA isolation from snap frozen tissue or cells. Reverse transcription of RNA to cDNA prior to analysis of mitochondrial gene expression using real time quencher/fluorescent TaqMan technology. Alternatively to measure mtDNA depletion determine the copy number of a mitochondrial gene (e.g. cytochrome c oxidase) relative to a nuclear-DNA housekeeper (e.g. β-actin)
Mitochondrial complex activity (I-V)	Isolated mitochondria	Mitochondria energised with appropriate substrates and product dependent changes in absorbance are monitored.	Complex I activity measured as a rotenone-sensitive decrease in NADH concentration at 340nm Complex II-III activity is measured by a succinate-dependent antimycin-A sensitive reduction of cytochrome c at 550 nm The rate at which cytochrome c is oxidised, represents the Vmax of the reaction performed by complex IV.
Citrate synthase activity	Cells / snap frozen tissue.	Spectrophotometry.	Citrate synthase is involved in the TCA cycle and widely used as a measure of mitochondrial mass. Citrate synthase drives the reaction of acetyl CoA and oxaloacetate to form CoA. The production of CoA was monitored by the reaction with DTNB and the increase in absorbance at 412nm. The Vmax rates, when linear are normalized to the protein concentration of samples.
Lactate/Pyruvate Assay	Cells (E.g. HepG2)	Mass spectrometry	[NADH]/[NAD+] is in equilibrium with [lactate]/[pyruvate] in the cytoplasm and extracellular space. Methods are available to measure [NAD+] accurately; however quantifying NADH accurately is a challenge. Quantifying [pyruvate] and [lactate] in culture media is a surrogate for measurement of [NAD+] and [NADH]. Measurement of lactate:pyruvate also provides a measure of cellular glycolytic activity.
	Blood (serum)	Clinical pathology analyser	
Intracellular triglyceride accumulation/	Cells	Colorimetric assay – biochemical analyser.	A change in the intracellular triglyceride content of cells provides an indication of potential changes in the mitochondrial bioenergetic function or βoxidation. Triglyceride reagent (Randox) determines intracellular triglyceride levels through a colorimetric method based on enzymatic degradation of triglycerides.
Metabolites	Cells, tissue, blood, biological fluids etc.	NMR, mass spectrometry	Global metabolomics has allowed for a systems level analysis of mitochondrial toxicity. Permits the identification of a chemical fingerprint allowing the identification of metabolic toxicological pathways or to identify biomarkers of mitochondrial dysfunction.

TABLE 1.1: Examples of assays used in the pharmaceutical industry for the analysis of DIMT.

1.7. Challenges and Complexities

Despite the wide range of assays regularly being used to detect mitochondrial perturbation *in vitro,* many challenges remain.

1. **Lack of robust *in vivo* methods for detecting DIMT –** As described above, reliance upon traditional drug development methods may be insufficient in detecting mitochondrial perturbation *in vivo*. It is important to distinguish between the detection of an adverse effect due to mitochondrial toxicity (apical effect) and effects on mitochondria that will lead to toxicity (i.e. an AOP). Current methods were designed preferentially to identify and assess apical endpoints (e.g. increased blood lactate concentration due to DIMT) whereas the move is now to develop an AOP strategy (i.e. identification of reduction in respiratory reserve capacity which may cause toxicity due to mitochondrial dysfunction, i.e. an upstream event in AOP). This move will enhance the predictive ability of drug safety scientists in R&D.

   Meanwhile however, standard endpoints used for safety testing (e.g. clinical signs, histopathology, haematology, serum biochemistry etc.) are relatively imprecise and insensitive for detecting alterations in mitochondrial function. For drugs that perturb mitochondrial function, development studies may need to be supplemented with more specialised or targeted evaluations; however, these novel approaches are under-developed and un-validated for use in preclinical toxicology studies. Furthermore there have been no rigorous efforts to correlate *in vitro* and *in vivo* functional endpoints with conventional measures of efficacy and toxicity. As a result, drug safety scientists are currently unable to answer difficult questions from drug discovery groups such as;

   - Which changes or what magnitude of mitochondrial perturbation *in vitro* is required to cause adverse in-life toxicity and thus prompt potential candidate-termination?
   - By how much do I need to reduce the *in vitro* effects on mitochondria to justify replacing the lead molecule with a new candidate?
   - Which endpoints from the *in vitro* or *in vivo* battery of assays are most relevant to assess the safety of drug candidates?

   Ultimately, the complexity of DIMT *in vivo* makes performing risk assessments a major challenge. Progress is required to enable the design of more efficient pre-clinical studies with more sensitive and specific measures of mitochondrial function, especially when *in vitro* activity has been noted.

2. **Lack of suitable animal models to detect mitochondrial dysfunction:** Routine pathology and clinical chemistry performed post drug administration in rodent models have so far proved relatively insensitive to DIMT. Mitochondrial capacity decreases with age or lack of exercise, suggesting that aged, sedentary rodents may be more appropriate and representative models for studying DIMT rather than young, active animals. Research has demonstrated that rodents which were selected to be low capacity runners, had reduced mitochondrial content, reduced oxidative capacity and were more prone to hepatic injury than their control counterparts [112]. Although various mouse models are available which exhibit impaired mitochondrial function, few have been used in the pharmaceutical industry for toxicology studies. One exception that has seen modest use however is the phenotypically normal superoxide dismutase 2 ($Sod2^{+/-}$) mouse. Heterozygous for the mitochondrial antioxidant manganese Sod2, this model shows increased levels of oxidative stress. An example of its utility was demonstrated when $Sod2^{+/-}$ mice showed signs of hepatotoxicity post-treatment with troglitazone with no marked changes observed in the wild-type group [113]. The effect of oxidative stress has also been explored in a study of mutant Drosophila melanogaster with reduced Sod2 expression, where the authors describe reduced mitochondrial aconitase activity and shorter life spans than wild type flies [114]. Toxicological investigations in Drosophila are rarely used however, in drug development due to translatability issues. Other mouse models which have been shown to have impaired mitochondrial function include, the mtDNA deletion mito-mouse [115], the $ANT^{-/-}$ mouse [116], the mutant pol-γ mouse [117] and the $Tim23^{+/-}$ mouse which lacks a translocase for the IMM [118]. These models remain largely untested and un-validated for use as tools in the assessment of DIMT.

3. **Persistence of mitochondrial aberration**: While many assays exist to characterise the effect of a drug on mitochondrial function they do not address why the effect is latent (e.g. the delayed-onset liver and heart toxicity after treatment with troglitazone). As mitochondria undergo continuous replacement through division the most rational hypothesis for persistent perturbation is via compound-associated/ROS-dependent damage to the mtDNA which is then passed onto daughter mitochondria during replication. Whilst next generation sequencing approaches have vastly improved our understanding of mitochondrial diseases few data have been generated on drug-mtDNA interaction and DNA damage accumulation.

4. **Lack of *in silico* methods to predict DIMT:** *In silico* methods to predict DIMT are still in their infancy, largely due to the large number of mechanisms by which a compound could impair

mitochondrial function. However some progress around classification of compounds based on physicochemical properties is emerging. For example, studies have identified that many protonophoric uncouplers contain characteristic acidic dissociable groups, electron withdrawing moieties and large hydrophobic groups (e.g. 2,4-DNP, FCCP, benzimidazoles and even some non-steroidal anti-inflammatory drugs (NSAID)) [119]. Furthermore, Zhang *et al* in 2009 discussed the potential to predict DIMT *in silico* and whilst promising prediction accuracies (~77%) were reported, the compound test set used was relatively small and to date no comprehensive analysis downstream of a high throughput screen has been published [120]. Further work is clearly required in order to identify whether compounds which target mitochondria or impart a particular effect on mitochondrial function, share a common set of physicochemical properties.

5. **Lack of validated biomarkers for identifying DIMT in patients and/or preclinical species:** In 2006, the FDA along with other organisations set up a biomarkers consortium to search-for and validate new pathological markers (critical path initiative). To date there are no validated biomarkers of DIMT and in fact, the CPI has resulted in very few validated/qualified biomarkers of any type. Recent attempts have however included the use of mtDNA encoded proteins in peripheral fat and peripheral blood mononuclear cells (PBMC's) from HIV-positive individuals on anti-retroviral therapy [121] and the use of blood transcriptomic markers (genes involved in OXPHOS) of drug induced liver injury [122]. Furthermore, circulating acylcarnitine metabolites have been suggested as good biomarkers of hepatotoxicity related to mitochondrial dysfunction *in vivo* [123]. Blood lactate has also been suggested as a good circulating biomarker of mitochondrial dysfunction however its presence in the systemic circulation is likely a secondary adaptation to perturbed energy production, takes time to manifest and is largely unspecific (i.e. can be due to generalised liver injury, steatosis, diabetes etc.). All of these candidates have shown proof-of-concept; however, they require stringent validation prior to use in preclinical safety-studies.

6. **Conclusively attributing mitochondrial dysfunction to particular drugs:** Demonstrating that *in vitro* observations predict *in vivo* outcomes pre-clinically and then conclusively predict clinical outcomes in humans (taking into account cross-species concordance) is inherently challenging. Hallmarks of mitochondrial toxicity are not easily translatable into the patient population. Additionally the hypothesised biomarkers of mitochondrial dysfunction are relatively non-specific, i.e. there is no certainty that observations are attributable to an adverse drug reaction as opposed to

other influences (e.g. the condition itself, inflammation, poor tissue perfusion etc). Despite this caveat, easily translatable endpoints between pre-clinical and clinical studies should be sought. For example, whilst isolated mitochondria are still a valuable tool in the understanding of particular mechanisms of DIMT perhaps the routine use of isolated tissue mitochondria to assess preclinical toxicity is not be a progressive approach (i.e. due to the inherent lack of tissue availability in human trials)? It is however important to acknowledge that the era of searching for single protein biomarkers which are specific, translatable and measurable may potentially be over or at least in decline. It is likely that a tailored selection of specific investigations is required. Alternatively, there is great interest in certain types of novel biomarkers such as miRNA species and these will continue to be evaluated.

1.8. The use of a Systems Approach

Where limited understanding exists in terms of the mechanisms downstream of a toxicological event a principle method of investigating the response is the use of a systems approach. Whilst the job of a toxicologist is to understand and ultimately predict the adverse effect of chemicals in a biological system, this task is incredibly complicated due to the inherent complexity of biological systems. Furthermore, observational toxicology has certain limitations such as the difficulty in developing effective *in vitro* assays, in developing informative biomarkers and the problems involved in designing out structural liabilities based on SAR. The true value of a systems approach is therefore the ability to build an AOP/MOA which focuses on the identification of the key events, their quantitative inter-relationships and human relevance.

The field of systems toxicology (i.e. a systems approach) is relatively new, with the term coined for the first time in 2003 [124]. The definition of what encompasses systems toxicology does however vary greatly in the literature. The concept of a "systems approach" is still often confused with the field of systems biology, where computational and mathematical modelling is a central aspect. A systems approach is more reliant on the integration of data from multiple disciplines/endpoints (including both targeted and non-targeted investigations) to improve mechanistic understanding, search for biomarkers and identify the most sensitive endpoints for different types of toxicological event. In contrast, systems biology/toxicology relies on the modelling of global 'omics' data and using mathematical algorithms to drive predictions. The use of both approaches have been integral to the shift in emphasis in both drug-

safety science and in biomedical research away from investigating single cells in isolation and towards studying the true complexity of biological systems [125].

A systems approach encompasses the integration of classical toxicology (e.g. pathology, clinical chemistry etc.) with both novel methods of evaluation and the quantitative analysis of molecular changes occurring across multiple layers of biological organisation. Tailored approaches therefore need to be combined with global analyses in order to gain an understanding of both the local effects of xenobiotics on hypothesised outcomes and the emergent/systems level effects [126].

The selected endpoints for analysis should be dictated by the aims of the experiment or as a result of any known understanding of the molecule's AOP, and as a result, be tailor-made to the specific adverse reaction observed. Whether the effect is observed within a single cell, organ, or at the level of the whole organism dictates the depth of the system and thus the approach to be taken (i.e. this drives how complex or niche the system needs to be). In toxicology, the effect being studied is often at the organism level (i.e. an adverse in life effect) and although targeted evaluations remain pivotal to improve mechanistic understanding at a particular target site/organ, these need to be anchored to the adverse effect. Alternatively, the toxicological event may be a histopathological lesion in a single tissue and therefore the system reduces considerably in size, although one must be cautious that this is not an over-simplification (inter-organ/tissue effects may be important). Either way, due to the extent of biochemical cellular responses following drug-induced perturbation of cellular processes, a systems approach will likely always entail the use of global methods. As a result and key to identifying the fundamental mechanisms of dysfunction is careful analysis of these data using interaction networking and biological theme analyses.

1.9. Tool Compounds Studied

Two molecules (no longer in active development within GlaxoSmithKline) were chosen to study mechanisms of DIMT, based on their potent and selective effect on mitochondrial function. Furthermore, the mechanisms by which they affect mitochondrial function (respiratory chain inhibition and uncoupling) are commonly observed in preclinical assessment of drugs for mitochondrial activity. These compounds are introduced in section 1.9.1 and 1.9.2 below.

1.9.1. GSK932121A (COMPLEX III INHIBITOR)

GSK932121A (shown in Fig.1.6 below) is a 4(1H)-pyridone molecule that was in development as an anti-malarial medicine. In FTIH trials, GSK932121A was well tolerated however adverse toxicity was observed in pre-clinical studies with a pro-drug of GSK932121A, designed to increase oral bioavailability. This toxicity profile was later observed using GSK932121A itself when dosed IP (to provide similar systemic exposure levels to those achieved with pro-drug). These data resulted in GSK932121A's termination from development due to a potentially narrow therapeutic index [127].

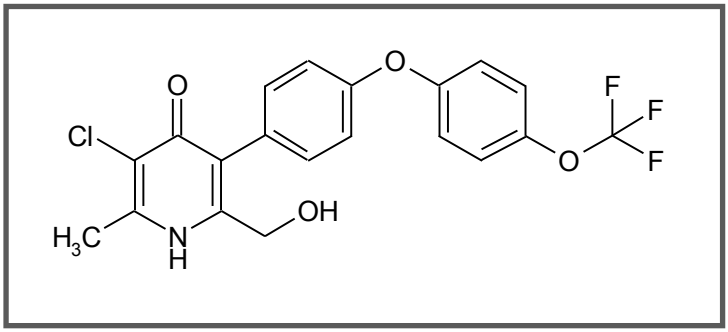


FIGURE 1.6: Chemical structure of GSK932121A (mw: 425.786). This pyridone molecule was designed for the treatment of the *Plasmodium falciparum* malaria infection.

Mitochondria are seen as an attractive target for anti-infective medicines. Due to the integral function mitochondria play in cellular biochemistry a sound therapeutic approach is to induce mitochondrial dysfunction in the infectious species (e.g. parasite), whilst avoiding crossover to the mammalian target. This approach has shown proof of principle by the atovaquone/proguanil (GlaxoSmithKline's Malarone) combination therapy, used today as a treatment of multi-drug-resistant malaria. The drug works via inhibition of the Q_o site of the cytochrome bc1 complex thus inhibiting mitochondrial electron transport. As the ETC is located in the plasma membrane in prokaryotes as opposed to within the mitochondria in eukaryotes it is hypothesised that drugs will effect mitochondrial processes with much higher potency in prokaryotic systems and thus provide a wide therapeutic window.

Similar to atovaquone, GSK932121A is a selective inhibitor of the mitochondrial ETC. As described by Bueno and colleagues in 2012, GSK932121A inhibits the plasmodial cytochrome bc1 complex in the low nanomolar range (IC_{50}= 0.007μM). GSK932121A is significantly more potent against the *P.falciparum*

target compared to mammalian cytochrome bc1 isolated from either human HEK293 cells (IC_{50}= 0.4μM, 57x less potent) or rat H9C2 cells (IC_{50}= 0.6μM, 86x less potent). In whole cells the trend continued, wherein, cytotoxicity was observed at significantly higher doses in mammalian derived HepG2 cells (IC_{50}=10μM) and H9C2 cells (IC_{50}=14μM) compared to plasmodium derived cultures (3D7A and FCR3A) which both showed an IC_{50} for cytotoxicity of 0.006μM. This represents between a 1600-2400x higher potency against plasmodium cells compared to mammalian cells, suggesting a potentially wide therapeutic margin, based on *in vitro* data.

FTIH study with GSK932121A: There was no evidence of dose-limiting toxicity in oral pre-clinical studies and therefore GSK932121A was progressed to a FTIH study. The purpose of the FTIH study was to evaluate the safety and tolerability of the parent drug GSK932121A in comparison with placebo and to investigate the pharmacokinetics of the compound in man. Eight healthy adult male subjects received single doses of GSK932121A parent (3mg, n=4 or 30mg, n=4) with four separate subjects receiving placebo alone. GSK932121A was well tolerated.

The pro-drug approach: Improved bioavailability causes an adverse toxicological profile: Despite excellent solubility, GSK932121A demonstrated non-linear pharmacokinetics in preclinical species with decreased oral bioavailability at high doses of the solid dosage form. In attempts to improve the oral bioavailability of GSK932121A a pro-drug approach was investigated. A water soluble phosphate ester pro-moiety was attached to the C_6-CH_2-OH hydroxyl as shown in Fig.1.7 below. Water soluble phosphate esters increase solubility and stability and undergo rapid bio-conversion (by endogenous membrane bound alkaline phosphatases) causing the release of high concentrations of the parent drug. Early indications in rats showed an approximately 10-fold greater oral bioavailability of the pro-drug at high dose compared with the parent alone. Due to this outstanding physiochemical and pharmacokinetic profile, the pro-drug of GSK932121A was progressed into full pre-clinical testing as a backup for the parent GSK932121A candidate.

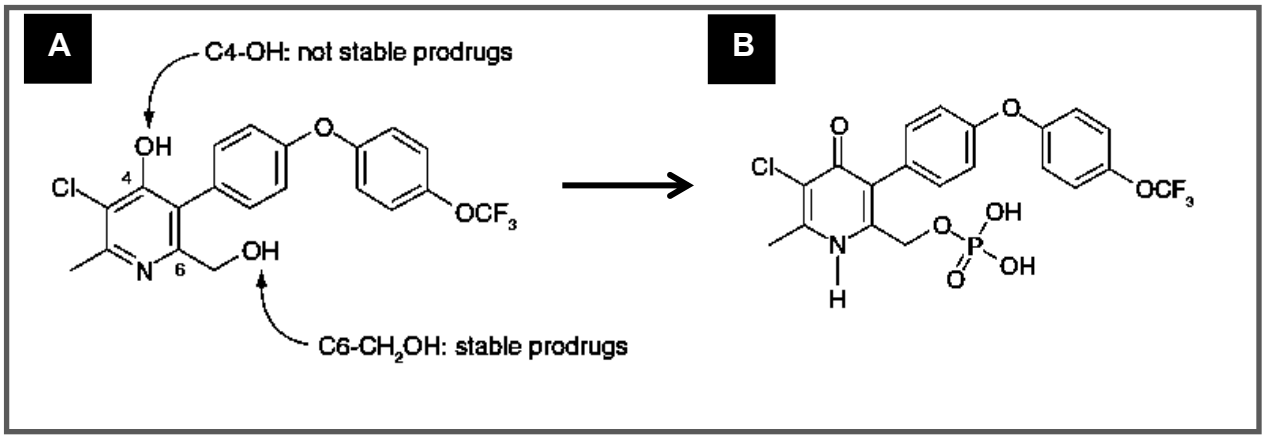


FIGURE 1.7: Schematic of the approach taken to manufacture a GSK932121A pro-drug. (A) A water soluble phosphate ester was added to the C_6-CH_2OH group of GSK932121A in order to improve both stability and solubility for the purposes of increasing oral bioavailability. (B) The resulting pro-drug showed increased bioavailability and improved PK profile but the increased systemic exposure levels resulted in acute toxicity consistent with mitochondrial impairment, which led to GSK932121A's termination due to a potentially narrow therapeutic index. Diagram adapted from [127].

During these pre-clinical studies unexpected, acute toxicity was observed in rats after oral administration of the pro-drug. The toxicity was characterized by hypothermia, cardiovascular abnormalities and at high-doses, sudden death. Upon further investigation, the severe, acute toxicity exhibited by the pro-drug could be replicated by the parent compound alone following IP administration, which induced similar exposure levels to those achieved with the pro-drug given orally. One hypothesis was that the toxicity observed in rats was due to inhibition of the mammalian bc1 mitochondrial complex by GSK932121A. FTIH studies with GSK932121A were put on hold and the compound later terminated despite its good tolerability profile at the two dose levels tested. A package of investigative work was initiated to explore the acute toxicity caused by GSK932121A within which the present work (chapters 3-5) forms an integral first stage.

1.9.2. GSK2617971A (OXPHOS UNCOUPLER)

Unlike GSK932121A (described above), GSK2617971A was withdrawn from active development early, during the preclinical stage. GSK2617971A is a pyrazole compound which was designed as a selective androgen receptor modulator (SARM) for the treatment of cachexia (muscle wastage). GSK2617971A

(Fig.1.8) has shown potent uncoupling activity *in vitro* and is acutely toxic *in vivo* in rats, when dosed at 60mg/kg–100mg/kg. GSK2617971A was terminated early in development following observations of toxicity in oral dose range finding (DRF) tolerability studies.

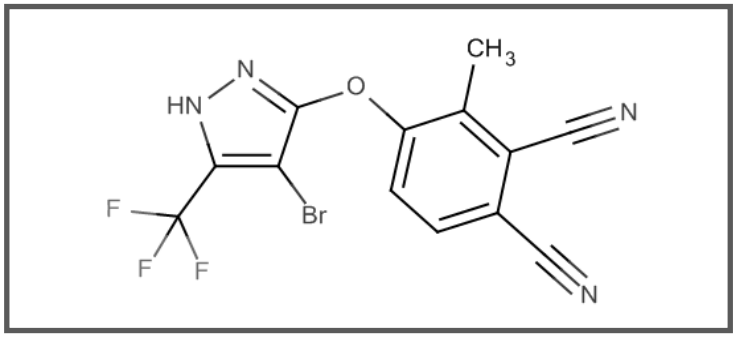


FIGURE 1.8: Chemical structure of GSK2617971A (mw: 371.118). This pyrazole molecule was designed as a selective androgen receptor modulator (SARM) intended for the treatment of cachexia.

Since GSK2617971A's termination from development, it has been used as a tool molecule for the study of DIMT. As compounds with some degree of OXPHOS uncoupling activity are regularly identified in preclinical screening, it was imperative to gain further understanding of its mechanism of toxicity *in vivo,* in order to better inform discovery groups of the potential safety liability of this class of mitochondrial toxicant (chapter 6). Furthermore, adverse effects caused by uncoupling of OXPHOS have been observed in the clinical situation following administration of medicines such as doxorubicin and therefore improved mechanistic understanding of this class of mitochondrial toxicant is translatable to effects observed in patients.

1.10. Thesis Rationale and Aims

Mitochondria are increasingly seen as attractive targets for pharmacological intervention due to their central role in the mechanism of many common human disorders (e.g. as treatments for metabolic disorders, neurodegenerative diseases and cancer). On the flipside, DIMT is gaining recognition in the pharmaceutical industry as a major cause of safety related attrition and a number of high profile drug withdrawals have been linked to deleterious effects on mitochondrial function (e.g. troglitazone, nefazodone and cervistatin). The potent effects of many of these compounds underscore the potential

risks associated with drugs causing mitochondrial toxicity. Improved methods to assess mitochondrial function would therefore aid both risk assessment of mitochondrially acting compounds but also assess the impact of drugs deliberately targeted to mitochondria for therapeutic purposes with the direction of change in a number of mitochondrial assays potentially being pivotal to assessing either pharmacological potential (e.g. inhibition of the mPTP to prevent aberrant cell death) or toxicity (e.g. potentiation of the mPTP).

The inherently complex nature of mitochondrial pathophysiology (notably the array of different mechanisms by which a compound can effect mitochondrial function) means there is currently a lack of understanding on how best to foresee, understand or accurately assess the risk of compounds which effect mitochondrial function. The major challenge is in relation to understanding DIMT *in vivo* and whilst the past decade has witnessed advances in the development and integration of *in vitro* assays to aid pre-clinical screening of mitochondrial agents, efforts to correlate the resultant data with *in vivo* outcomes are limited [1]. What is clear is that improved knowledge of the downstream toxicities associated with mitochondrial dysfunction would better enable toxicologists to provide informed advice to discovery groups, that are facing the prospect of potentially developing a drug which has some level of mitochondrial activity *in vitro* or de-selecting a molecule based on adverse mitochondrial effects. Furthermore, to date, few comprehensive AOP's exist where the molecular initiating event (MIE) is a drug-interaction with a major mitochondrial process. The benefits of AOP's to drug safety assessment scientists includes (but is not limited to), the ability to predict potential toxicological effects of other candidates showing similar *in vitro* activity, the ability to monitor the progress of an adverse drug reaction, the potential to identify early biomarkers and the ability to design more intelligent investigative safety studies which are tailored for mitochondrially-active therapeutics in development (i.e. both those targeted to mitochondria or those which may produce toxicity by affecting mitochondria).

The overall aim of this project was to use a systems approach to better understand mechanisms of mitochondrial toxicity both *in vitro* and *in vivo*. The overall hypothesis being that mitochondrial toxicity leads to a specific and quantifiable AOP that can be used in drug development to better understand and assess the risk caused by DIMT in the pre-clinical setting. Two GlaxoSmithKline compounds with known mitochondrial activity (GSK932121A and GSK2617971A) were used in order to develop AOPs for toxicity due to drug-induced respiratory chain inhibition and OXPHOS uncoupling respectively. These compounds, which are no longer in active development, were chosen as a), the drugs are potent and

selective mitochondrial toxicants and b) respiratory chain inhibition and OXPHOS uncoupling are frequently observed molecular initiating events in the preclinical analysis of drugs for mitochondrial activity. The overall aim of the thesis was broken down into a series of objectives.

1. To test the hypothesis that *in vitro* assessment of mitochondrial function (i.e. *in vitro* cell lines or *in vitro* testing of drugs on naïve isolated mitochondria) provides information on key events relevant to the *in vivo* effects and therefore is useful in detecting mitochondrial toxicity for preclinical hazard identification. The rationale was to show that *in vitro* testing is a suitable means of assessing key events for DIMT.

2. To assess the utility of using a systems toxicology approach in order to understand the underlying AOPs downstream of mitochondrial perturbation *in vivo*. Systems toxicology encompasses the integration of classical toxicology (e.g. pathology, clinical chemistry etc.) with, a) novel methods of evaluation, in this case functional mitochondrial changes and b) with the quantitative analysis of large networks of molecular changes occurring across multiple layers of biological organisation (in this case transcriptomic and metabolomic assessments). It was hypothesised that this systems approach would enable the development of AOP's for two mechanisms of DIMT (respiratory chain inhibition and OXPHOS uncoupling).

3. To identify markers of DIMT at sub-toxic doses (or prior to the onset of overt toxicity) based on the AOPs developed and to help in AOP development. The literature describes a number of examples whereby a drug is withdrawn from the market due to toxicity which was not evident throughout pre-clinical and clinical trials (e.g. troglitazone). It has been hypothesised that this is due to underlying damage to mitochondria which was not detected at the preclinical stage as mitochondrial functional changes have historically not been assessed. Mitochondria are able to respond to a certain level of direct or indirect stress (due to a reserve capacity) and this mitochondrial-resilience prevents the immediate onset of toxicity early in drug development. Markers of mitochondrial perturbation occurring at sub-toxic doses would be of immense value to monitoring the potential long term safety of molecules with some degree of mitochondrial activity *in vitro* but which are generally well tolerated. Furthermore, markers of mitochondrial effects at sub-toxic dose-levels helps in the development of AOP's (as described in objective 2) by enabling primary effects to be distinguished from consequential effects.

2.0. MATERIALS AND METHODS

2.1. Animals

All *in vivo* studies in rats were ethically reviewed and carried out in accordance with the Animals (Scientific Procedures) Act 1986 and the GSK Policy on the Care, Welfare and Treatment of Animals. All regulated procedures (i.e. dosing, implanting of microchip, and taking blood samples) were performed by personal license holders in GlaxoSmithKline's Safety Assessment and Laboratory Animal Sciences departments.

2.1.1. GSK932121A STUDIES – GLAXOSMITHKLINE, WARE, HERTFORDSHIRE UK

Female Crl:CD(SD) rats were obtained from Charles River Laboratories UK (Margate, Kent) and were housed under controlled environmental conditions (19-23°C, 55% ± 10% relative humidity, 12h dark-light cycles), with free access to both water and 5LF2 EURodent Diet (Purina Mills International, St Louis, MO, USA). All animals were implanted with an intrascapular Plexx microchip (Plexx B.V., Elst, The Netherlands) on arrival for the purposes of identification and body temperature measurement. Animals were acclimatised for at least 12 days prior to dose administration, and were 10 to 14 weeks old on the day of dosing (~270-350g).

2.1.2. GSK2617971A STUDY – GLAXOSMITHKLINE, UPPER MERION, PENNSYLVANIA, USA

Male Crl:Wi (Han) rats were obtained from Charles River Laboratories (Charles River Laboratories Inc., Stone Ridge, NY, USA) and were housed under controlled environmental conditions (64-79°F, 30-70% humidity and 12h dark-light cycles). Rats were offered 5002 Certified Rodent Diet (PMI Nutrition International, Richmond, IN, USA) and filtered tap water *ad libitum*. All animals were implanted with an intrascapular Plexx microchip (Plexx B.V., Elst, The Netherlands) on arrival for the purposes of identification and body temperature measurement. Animals were acclimatised for one week and were 10-12 weeks old on the day of dosing (~200-350g).

2.2. In Life Clinical Observations

In all studies that included the dosing of rodents with test substances, strict in-life monitoring was performed to both ensure animal wellbeing (by reducing suffering) and closely monitor the effect of drug treatment. Animals were checked for adverse effects immediately post-dose and then at approximate 15 minute intervals (in line with body temperature measurement). Animals were checked in accordance with GlaxoSmithKline Safety Assessment's project license and adverse effects were recorded directly onto Provantis V9.0 data management system (Instem, Staffordshire UK). A scoring metric of slight, moderate and severe was recorded alongside notification of the adverse event. Animals were killed immediately for ethical reasons if any adverse event was graded severe. Grading of the severity of clinical signs was performed by experienced animal technicians alongside the facilities named animal care and welfare officer (NACWO), with the in-house veterinary surgeon on standby.

2.3. Preparation of Dosing Solutions

All doses and concentrations are expressed in terms of the parent compound.

2.3.1. GSK932121A Studies – GlaxoSmithKline, Ware, Hertfordshire UK

A nanomilled, spray-dried formulation of GSK932121A (49.5% w/w), containing mannitol (44.5% w/w), hydroxypropylmethylcellulose Pharmacoat 603 (5% w/w) and sodium lauryl sulphate (1% w/w) was suspended in sterile water for IP administration. A dose of either 12.5mg/kg or 50mg/kg was selected based on data generated in previous GSK932121A single-dose tolerability studies. A single dose of either 12mg/kg GSK932121A, 50mg/kg GSK932121A or vehicle (described above, minus test article) was administered IP to female rats at a dose volume of 10 mL/kg.

2.3.2. GSK2617971A Study – GlaxoSmithKline, Upper Merion, PA, USA

Animals were separated into three groups (vehicle control (VC), low dose and high dose). Groups comprised n=6 with the exception of the low dose which had n=2 due to extenuating study circumstances. GSK2617971A was suspended in 30% koliphor/70% water vehicle. Vehicle control (VC) animals received koliphor/water alone. Doses of 30mg/kg and 60mg/kg were selected for this study based on

findings from earlier studies in rats that demonstrated that both doses provoked adverse signs with the 30mg/kg dose being well tolerated up to 24 hours. A dose of 100mg/kg has been shown to be lethal by 8 hours. A single dose of 30 mg/kg, 60mg/kg or VC was administered by gavage via the oral route to male rats at a dose volume of 10mL/kg.

2.3.3. FORMULATION OF COMPOUNDS FOR *IN VITRO* EXPERIMENTS

All compounds were formulated in dimethyl sulfoxide (DMSO) either within advised solubility ranges (as obtained from MSDS data sheets) or at a standard top concentration of 10mM. DMSO was used at a final concentration of 0.1% for cell culture experiments (to prevent cytotoxicity) or 0.5% for experiments using isolated mitochondria (shown to have no direct effect on mitochondrial function). Stocks in DMSO were stored at room temperature and out of direct sunlight for up to one year.

2.4. Measurement of Blood Gasses and Bicarbonate

Blood gas analysis was performed by Dr Jeffrey Ambroso (GlaxoSmithKline, Safety Assessment, RTP, NC, USA). For blood gas analysis (pO_2, pCO_2 and HCO_3) separate groups of animals underwent surgery to place vascular access ports at the site of blood collection. The jugular artery was isolated, cannulated (catheter entered approximately 2 cm into the jugular artery) and the catheter secured in place with ligatures of non-absorbable suture material (Ti-cron, Medline Industries Inc., IL, USA). A 2ml saline flush was given at the jugular surgical site prior to wound closure using absorbable suture material (PDS, Ethicon Ltd, NJ, USA). After surgery a one week recovery period was permitted prior to administration of test substance or VC as previously described (section 2.3.1 and 2.3.2). Whole blood samples (0.3mL volume) were collected via vascular access ports into heparinized syringes. Blood was sampled at 5 to 6 hours post dose (dependent on the observed clinical signs). All blood samples were analysed using a Roche OPTI CCA Blood Gas Analyser (Opti Medical System Inc., GA, USA), according to manufacturer's recommendations, within 2 hours of collection for pCO_2, pO_2 and HCO_3. Data are expressed as a percentage of baseline (pre-dose) measurement values.

2.5. Blood Sampling

Blood samples were taken in all of the *in vivo* studies for analysis of multiple parameters. Details of the blood sampling methodologies are described in table 2.1 below.

***In vivo* study and chapter**	**Site and details of blood collection**	**Volume of blood collected (mL)**	**Anti-coagulant and storage**	**Endpoint**
All studies (chapters 3, 4, 5 and 6)	Puncture of abdominal aorta under isoflurane anaesthesia.	0.3	EDTA microtainer, centrifuged to prepare plasma (see section 2.5.1 below) and frozen on solid carbon dioxide. Samples were stored at -20°C prior to analysis	Toxicokinetics
All studies (chapters 3, 4, 5 and 6)	Puncture of abdominal aorta under isoflurane anaesthesia.	0.1	0.1mL of blood added directly to 0.4mL of 0.4M perchloric acid and vortexed to ensure thorough mixing of blood/acid. Samples frozen on solid carbon dioxide and then stored at -80°C prior to analysis.	Lactate/ Pyruvate
GSK932121A metabolomics study	Jugular venepunture for in-life samples and puncture of abdominal aorta under isoflurane anaesthesia for terminal samples.	0.4	EDTA microtainer, centrifuged to prepare plasma (see section 2.5.1 below) and flash frozen in liquid nitrogen. Samples stored at -80°C prior to analysis.	Global Metabolomics Profiling

TABLE 2.1: Overview of blood sampling methodologies. Detail of blood sampling methodologies, employed on all *in vivo* studies described herein including the site of collection, the volume collected, the nature of the anti-coagulant, the storage conditions of the blood and the endpoint for which the blood was used for.

2.5.1. PREPARATION OF PLASMA FROM WHOLE BLOOD SAMPLES

Plasma forms the liquid component of whole blood and makes up ~55% of total blood volume [128]. Within a whole blood suspension, the plasma compartment normally contains the blood cells and is regularly used for biochemical analyses. Plasma was prepared from whole blood samples using the method described below.

Whole blood (typically between 0.2mL and 0.4mL) was collected into ethylenediaminetetraacetic acid [EDTA] microtainers (#365974, Becton Dickinson and Co, New Jersey, USA) and stored on ice until the end of autopsy procedure. All blood samples were then centrifuged for 3 minutes at 6000g following which the plasma supernatant compartment was removed and placed into pre-labelled polypropylene

tubes using a graduated pipette. Plasma samples were then immediately frozen on solid carbon dioxide and stored at -20°C prior to analysis.

2.6. Measurement of GSK932121A and GSK261971A Concentration in Plasma

GSK932121A and GSK2617971A levels were assessed in rat plasma (EDTA anticoagulant) by LC-MS/MS following protein precipitation. Levels of both drugs were quantified against a standard curve and normalised to a GSK932121/GSK2617971 [^{13}C6] internal standard. The lower limit of quantification (LLQ) was 10ng/mL using a 25µL aliquot of rat plasma. Briefly, protein was precipitated by adding 25µL of rat plasma to 200µL acetonitrile (plus internal standard working solution) with subsequent vortex mixing. Samples were then centrifuged for 10 minutes at 3000g and the supernatant transferred to a fresh Eppendorf tube. A sample volume of 2µl was then injected onto a Waters Aquity UPLC (Waters, Elstree, Hertfordshire, UK) connected to a SCIEX API4000 mass spectrometer (SCIEX, MA, USA) running in positive-ion mode employing the Turbo-Ionspray source. A 50 x 2.1mm BEH C18 1.7µm, (Waters) column was maintained at 50°C (solvent A: HPLC grade water 0.1% v/v formic acid, solvent B: Acetonitrile) with a flow rate of 0.8mL/min. A gradient from 10% to 80% solvent B was employed over 1.30min followed by a re-equilibration time of 0.7mins yielding a total run time of 2 minutes.

2.7. Body Temperature Measurements

All animals were implanted with a Plexx (Plexx B.V., Elst, The Netherlands) microchip for the purposes of identification and body temperature measurement. IPTT-300 programmable temperature transponders (#11059, Plexx) were implanted subcutaneously and without anaesthetic. Body temperature or ID readings were taken using a DAS-7007 S IPT/IPTT straight reader (#11087, Plexx) and DAS Host Software (#11064, Plexx) was used to link animal ID with temperature readings. Data were recorded telemetrically.

2.8. Isolated Mitochondrial Methods

2.8.1. ISOLATION OF MITOCHONDRIA

Mitochondria were isolated from selected rat tissues as described below.

Liver and Kidney Mitochondria: Mitochondria were prepared using the Qproteome Mitochondria Isolation kit (Qiagen, Limburg, Netherlands) according to the manufacturer's instructions. Briefly, 1.3g of liver or 1 whole kidney was homogenised in ice cold lysis buffer using a Qiagen Tissue Ruptor. The homogenate was incubated on an end-over-end shaker for 10 minutes at 4°C prior to centrifugation at 1300g for 13 minutes. The resulting pellet was resuspended in disruption buffer firstly by gentle pipetting and secondly using a Dounce homogenizer (4 strokes at 200rpm). The resulting lysate was centrifuged at 1000g for 13 minutes with the resulting supernatant washed and pelleted twice at 6000g for 13 minutes. The crude mitochondrial pellet was finally resuspended in Incubation Buffer B (130mM sucrose, 50mM KCl, 2.5mM KH_2P0_4 and 5mM N-2.Hydroxyethylpiperazine-N'-2-Ethanesulfonic Acid [HEPES], pH7.4 with KOH).

Skeletal Muscle Mitochondria: Mitochondria were prepared as described in [129] with minor modifications. Briefly, the gastrocnemius muscle block was removed from one hind limb of the animal. Visible tendons and ligaments were removed before the tissue was minced finely using dissection scissors. The tissue was washed using phosphate buffered saline (PBS) supplemented with 10mM ethylenediaminetetraacetic acid [EDTA], before suspending in PBS+10mM EDTA +0.05% trypsin for 30 minutes. The tissue was pelleted at 200g for 5 minutes to remove trypsin from solution and resuspended in Isolation Buffer 1 (67mM sucrose, 50mM Tris/HCl, 50mM KCl, 10mM EDTA, and 0.2% w/v FA-free BSA, pH 7.4). The tissue was homogenised using a Dounce homogeniser powered by an overhead motor (7 strokes at 1200rpm) before first filtering through a wide pored mesh (200μm) to remove connective tissue and secondly centrifuging at 900g for 10 minutes. The resulting supernatant was centrifuged at 8500g for 10 minutes and the pellet resuspended in Isolation Buffer 2 (250mM sucrose, 5mM ethylene glycol-bis (2-aminoethylether)-*N,N,N',N*-tetraacetic acid [EGTA], and 10mM Tris/HCl; pH 7.4). A final centrifugation at 8500g for 10 minutes produced the mitochondrial-enriched pellet which was resuspended in 0.25ml of Incubation Buffer B.

Brain Mitochondria: Mitochondria were prepared as described in [130] with minor modifications. Briefly, the whole brain was excised fresh, weighed and homogenised directly in a Dounce homogenizer powered by an overhead motor (9 strokes at 300rpm) in isolation medium (IM) (225mM sucrose, 74mM mannitol, 1mM EGTA and 5mM HEPES, pH7.4 with KOH). The homogenate was split into two and centrifuged twice (separately) at 1,300g for 3 min before re-centrifuging the pooled supernatants at 21,000g for 12 minutes. The resulting pellet was resuspended in 15% Percoll (GE Healthcare, UK) diluted in IM and layered slowly above a pre-prepared secondary gradient of 40% and 24% Percoll. The Percoll density gradients were centrifuged for 8 minutes at 30,750g with no braking to prevent disruption of the Percoll bandings. All material banding at the interface of the 24% and 40% gradient was removed and re-centrifuged in IM (minus EGTA) at 55,000g. Mitochondria were located at the bottom of the centrifuge tube as a liquid mass with approximately 1mL of mitochondria removed for downstream processing.

Heart Mitochondria: Mitochondria were prepared as described in [131]. Briefly, the heart was excised fresh and weighed before being finely minced using dissection scissors to ~1mm^3 sections. Aortic tissue, fat and clotted blood were removed from the suspension and the tissue rinsed thoroughly in ice cold Washing Medium (0.3M Sucrose, 10mM HEPES, 0.2mM EDTA, pH 7.2 with KOH) to remove remaining blood. The tissue was then washed a further three times in washing medium on a filter before being placed into 2.5mg/mL trypsin (Sigma #T8003) solution for 6 minutes prior to homogenisation using a Dounce homogeniser powered by an overhead motor (6 strokes at 400rpm). The homogenate was then left for a further 6 minutes in trypsin before undergoing a second homogenisation (4 strokes at 400rpm). The trypsin was then deactivated using trypsin inhibitor from soy bean (Sigma #T9128). The suspension was filtered through a nylon filter (25µm pore size) to remove remaining connective tissue. The filtrate was then centrifuged first at 600g for 15 minutes and second the supernatant was centrifuged at 8500g for 15 minutes. The pellet was then washed three times with 1mL washing buffer before resuspension and re-centrifugation at 8500g for 15 minutes. The resulting pellet was then resuspended in 20mL of isolation medium (0.3M sucrose, 10mM HEPES, 0.2mM EDTA + 1mg/ml fatty acid free BSA, pH 7.2. with KOH) and centrifuged at 9000g for 15 minutes. The final crude mitochondrial pellet was suspended in 0.5mL of Incubation Buffer B and stored on ice for immediate use.

2.8.2. ASSESSMENT OF PROTEIN CONCENTRATION

Protein content was measured using a bicinchoninic acid (BCA) protein assay kit (Pierce, Rockford, IL, USA) according to manufacturer's recommendations. Briefly, a 1:20 dilution of mitochondrial isolate was prepared in CHAPS hydrate. The protein suspension was vortexed before centrifuging at 12000g for 2 minutes. A volume of 25µL of sample or bovine serum albumin (BSA) standard (0µg/mL - 2000µg/mL) was pipetted into a clear bottomed 96 well plate in triplicate. 200µL of working reagent was added to each well and the plate was incubated for 15 minutes at 37°C prior to reading. Absorbance was measured at 562nm on a FlexStation3 microplate reader (Molecular Devices, Sunnyvale, CA, USA). A standard curve was prepared and used to determine the protein concentration of each unknown sample.

2.8.3. ASSESSMENT OF MITOCHONDRIAL BIOENERGETICS USING THE SEAHORSE XF24 ANALYSER

To assess bioenergetic parameters, i.e. ETC function and OXPHOS coupling, in isolated mitochondria, the Seahorse XF24 Extracellular Flux Analyser (Seahorse Biosciences, Billerica, MA) was utilised. The XF24 Seahorse platform utilises a disposable sensor cartridge that has 24 fluorescent sensors which measure the oxygen concentration in the well containing isolated mitochondria in a 24 well plate. The sensor cartridge also contains 24 pH probes for measurement of glycolytic function (extracellular acidification rate, ECAR), however as mitochondria in isolation do not contain a cytoplasmic compartment (and as such the capacity for glycolysis), ECAR measurements were only made in whole cells in culture. Oxygen consumption rate (OCR) is measured in a transient 2-7µL "micro-chamber" formed immediately above the mitochondrial layer enabling small changes in oxygen to be detected. The fluorescence sensors are connected to a fibre-optic wave guide that delivers light which excites the oxygen sensors at 530nm. The resulting florescence signal is emitted at 650nm and is detected by photo-sensitive detectors in the XF24 instrument [132]. Within the disposable sensor cartridge are four drug-injection ports which enable the user to inject substrates, inhibitors etc. throughout the course of the experiment and visualise, in real-time, the effect on cellular bioenergetics (Fig.2.1). With isolated mitochondria the principle assay used is a basal, oligomycin, FCCP, antimycin A (BOFA) assay which enables the user to determine drug-related effects on a number of respiratory parameters such as ATP-linked OCR, maximal uncoupled respiration and proton leak.

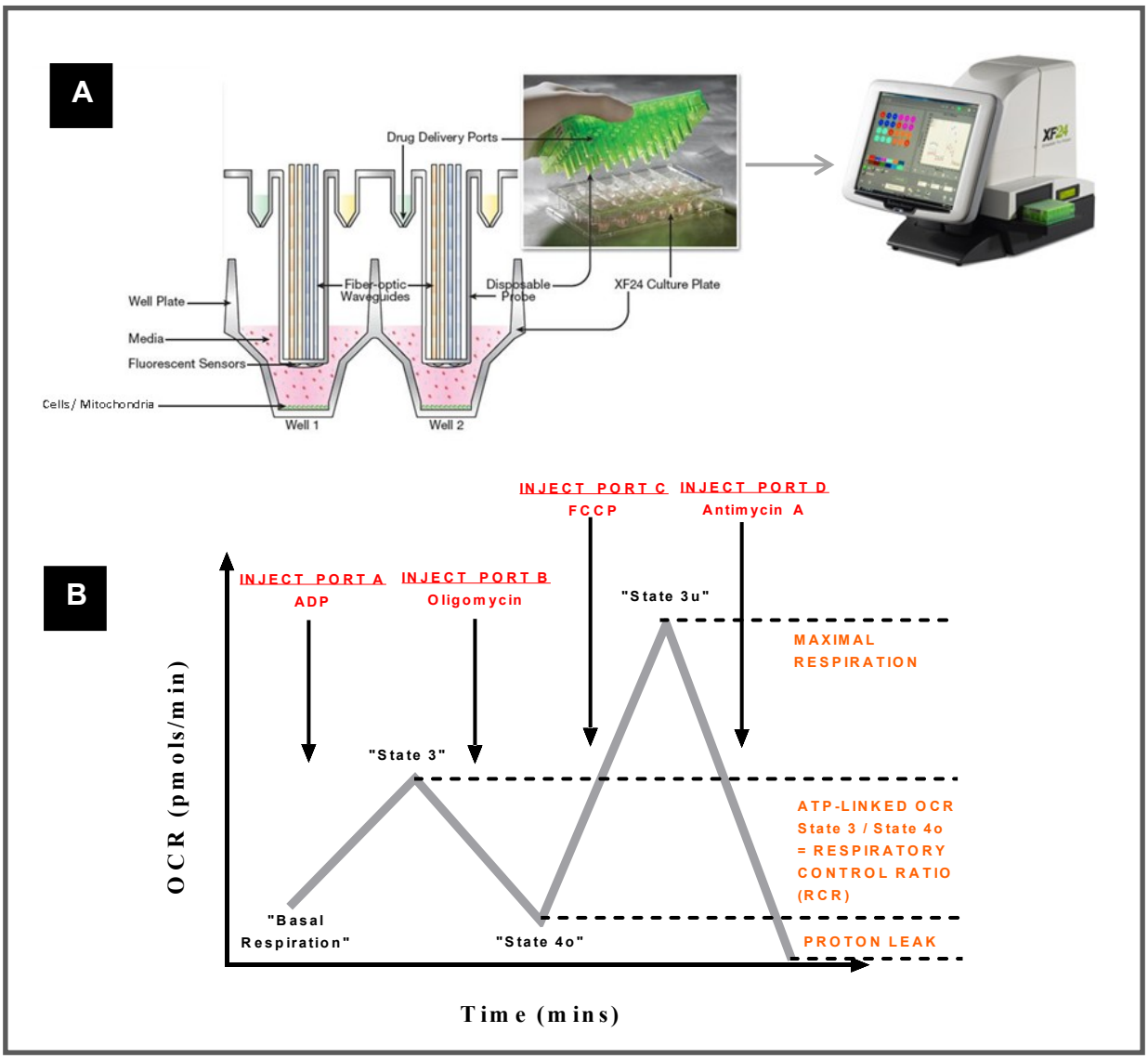


FIGURE 2.1: The Seahorse Bioscience BOFA assay: The Seahorse Bioscience BOFA assay analyses the effect of drug treatment on ETC function. (A) Mitochondria are seeded into a 24 well plate and centrifuged to ensure adherence. The mitochondrial monolayer is energised with substrate (and exposed to drug if performing an in vitro treatment of control mitochondria). The plate is then inserted into the XF24 analyser and subjected to pneumatic and sequential injections of tool-compounds from the assay ports A-D (previously loaded into the XF assay cartridge at optimised concentrations) which modulate ETC function. (B) The effect of drug treatment can be determined on a number of respiratory states (black text), or on calculated respiratory parameters (orange text), e.g. proton leak, respiratory control ratio (RCR, gold standard measure of mitochondrial health) and maximal uncoupled respiration.

A significant proportion of time was devoted to the optimisation of BOFA assay parameters from mitochondria isolated from five rodent tissues. OCR was monitored in the 24 well plate format as previously described [133]. Briefly, sequential measurements of basal respiration, state 3, state 4 and

uncoupled driven respiration were made through real-time additions of reagents through the drug-injection ports. Accordingly, (concentrations expressed as final concentrations and optimised as recommended by manufacturers) ADP (5mM for all mitochondria except for 10mM with heart mitochondria), oligomycin (2µM), FCCP (4µM) and antimycin A (4µM) were loaded into the 4 injection ports of the XF Assay Cartridge and sequentially injected into each well throughout the assay.

Mitochondria were diluted to a concentration of either 10µg protein/well (liver and skeletal muscle mitochondria), 7.5µg protein/well (brain mitochondria) or 2µg protein/well (heart and kidney mitochondria), in MAS-1 buffer (220mM mannitol, 70mM sucrose, 10mM KH_2PO_4, 5mM $MgCl_2$, 2mM HEPES, 1mM EGTA and 0.2% BSA in sterile water, pH 7.2 adjusted with KOH) supplemented with either 10mM succinate (liver, kidney and skeletal muscle mitochondria) or 10mM malate/glutamate (heart and brain mitochondria). Mitochondria were seeded at a volume of 50µL into each well of an XF24 V7 microplate and centrifuged for 20 minutes at 2000g (4°C). Following centrifugation, 450µL of MAS-1 buffer, supplemented with 10mM succinate and 2µM rotenone (liver, kidney and skeletal muscle mitochondria) or 10mM malate / glutamate (heart and brain mitochondria), were added to each well. The mitochondria were viewed briefly under a microscope to ensure consistent seeding/adhesion and then placed at 37°C for 8 minutes prior to loading into the XF24 analyser. Following a 12 minute equilibration, two baseline measurements were made using a 30 second mix, 4 minute measure cycle. Reagents were then sequentially injected into each well with a further 30 second mix, 1 minute wait, 4 minute measure cycle between each injection.

The direct effect on OCR of compounds was also examined by treating freshly isolated mitochondria *in vitro* following the above procedure with the following modification. A six point concentration range of the drug to be evaluated, or 0.5% DMSO control, was added to the mitochondria following centrifugation thereby constituting a 20 minute pre-measurement incubation period at 37°C.

2.8.4. CALCIUM RETENTION CAPACITY ASSAY

The calcium retention capacity (CRC) assay analyses the effect of drugs on the triggering of the mPTP. Mitochondria play a key role in regulating intracellular calcium concentrations during both normal and pathological states [134]. However, excess calcium is able to trigger the mPTP, characterised by a non-selective increase in the permeability of the inner mitochondrial membrane [135, 136]. mPTP activity is

affected by compounds that interfere with mitochondrial function and this can be monitored by measurement of CRC in mitochondrial isolates. Mitochondria from all five tissues were optimised for use in this assay both in the presence of drug (i.e. for *in vitro* examination of the direct effect of drugs on potentiation of calcium-induced mPTP) and in the absence of drug (i.e. analysis of mitochondria isolated from treated and control rats *in vivo*). The CRC assay is summarised in Fig.2.2 below.

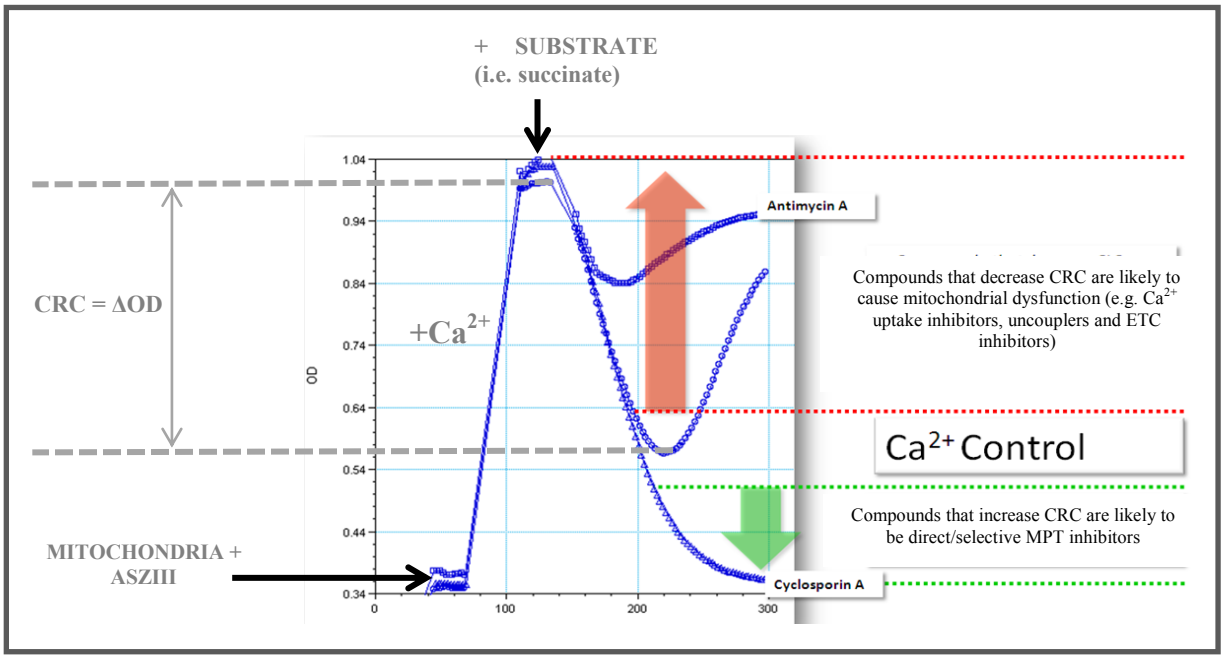


FIGURE 2.2: Graphical representation of the CRC assay. The CRC assay analyses the effects of drug treatment on the triggering of the mPTP. Mitochondria are mixed with a calcium sensitive dye (Arsenazo III, ASZIII) which upon the addition of a bolus dose of calcium binds and increases optical density (OD). When mitochondria are energised by a substrate (either succinate, in the presence of rotenone to prevent electron backflow or a complex I substrate i.e. pyruvate) they begin to uptake calcium (reduction in OD) until reaching permeability transition. The pore is then triggered and calcium is re-released.

Incubation Buffer B was used as the main CRC assay buffer for mitochondria isolated from all tissues. Buffer B was used both to dilute mitochondria to the appropriate concentration and to prepare the Arsenazo III dye mixture (calcium-sensing dye). Buffer B contains 130mM sucrose, 50mM KCl, 2.5mM KH_2P0_4 and 5mM HEPES, pH7.4 with KOH.

The CRC of freshly isolated mitochondria was determined as previously described [137] with minor modifications. Briefly, mitochondria were suspended at 0.2mg/ml (liver, heart, skeletal muscle and brain mitochondria) or 0.6mg/ml (kidney mitochondria) in Incubation Buffer B, supplemented either with

100μM Arsenazo III, 2.5μM rotenone and 1μg/mL oligomycin (liver, kidney and brain mitochondria) or in Incubation Buffer B with Arsenzo III alone (heart and skeletal muscle mitochondria) in each well of a 96 well microplate. Absorbance was measured every 2 seconds at 650nm in a FlexStation3 microplate reader (Molecular Devices, Sunnyvale, CA, USA). After approximately 1 minute of reading, calcium was added (1μmol/mg mitochondrial protein) shortly followed by the addition of 10mM succinate (liver, kidney and skeletal muscle mitochondria), 10mM malate/glutamate (brain mitochondria) or 2mM pyruvate (heart mitochondria) as the mitochondrial substrate. The CRC was calculated as the difference in optical density (ΔOD) between the point at which mitochondria were energised and undergoing MPT (highlighted in Fig.2.2 above).

The direct effect on CRC of compounds was also examined by treating freshly isolated mitochondria from a control rat *in vitro* following the above procedure with the following modification. Drugs were added over a concentration range, alongside a 0.5% DMSO VC and 1μM cyclosporine A (mPTP inhibitor) to the mitochondrial suspension prior to reading. The cyclosporine A control was used to ensure drug-induced modulation of CRC was detectable in the system used.

2.8.5. MITOCHONDRIAL MEMBRANE POTENTIAL ASSAY

Mitochondrial membrane potential (ΔΨ) was analysed in freshly isolated mitochondria using the Sigma Aldrich isolated mitochondria staining kit (CS0760) according to manufacturer's recommendations. The kit is based on mitochondrial staining using the 5,5′,6,6′-tetrachloro-1,1′,3,3′-tetraethylbenzimidazolocarbo-cyanine iodide (JC-1) dye. In normal cells, the JC-1 dye concentrates in the mitochondrial matrix where it forms red fluorescent aggregates. Any event that dissipates the ΔΨ prevents accumulation of JC-1 dye in the mitochondria. The dye is detected fluorometrically at 490nm (excitation) and emission wavelengths of 590nm (JC-1 aggregate) and 532nm (JC-1 monomer) using a FlexStation3 microplate reader (Molecular Devices, Sunnyvale, CA, USA).

2.8.6. COMPLEX III ACTIVITY ASSAY

The effect of GSK932121A on mitochondrial complex III was assessed in bovine heart mitochondria using the Mitosciences Complex III Activity Assay Kit (Abcam, Cambridge, UK #ab109905) and

following manufacturer's guidelines. Measurement of the conversion of cytochrome c from its oxidised to reduced form was made at 550nm using a Spectramax plus 384 spectrophotometer (Molecular Devices, Sunnyvale, CA, USA). Data were expressed in mOD/min.

2.9. Cell Culture Techniques

2.9.1. HepG2 Cell Culture and Media Composition

The human hepatocellular liver carcinoma cell line (HepG2) was originally purchased from BIOCAT and originated from a 15 year old adolescent Caucasian male. Cells were adapted to long term culture in modified DMEM medium as described below. Cells were cultured in galactose-conditioned modified DMEM according to table 2.2 below.

Constituent	Cat Number	Final Concentration
DMEM (with glutamine, without pyruvate and glucose)	Invitrogen #11966	N/A
Heat Inactivated FBS, EU Approved Origin: South America	Invitrogen #10500-064	10%
Galactose*	Sigma #G075	10mM
HEPES	Invitrogen #15630	5mM
Glutamax	Invitrogen #35050	2mM
Sodium Pyruvate	Sigma #S8636	100µM
Gentamicin	Gibco #15750-045	5µg/mL

TABLE 2.2: Media constituents for HepG2 cell culture - * A stock of 0.5M galactose was prepared in DMEM media, passed through a sterile filter and aliquots frozen at -20°C for up to 6 months.

Cell culture work was performed in a class II microbiological safety cabinet using sterile plastic ware. Cells were maintained/incubated at 37°C within a humidified atmosphere with 95% air and 5% CO2

Cell Revival: Upon resuscitation, one vial of cells (frozen at $1x10^6$ cells/mL) was flash thawed in a water bath at 37°C (for approximately 2 minutes or until no ice crystals were visible) before cells were transferred into a T80cm^2 flask containing 25mL of pre-warmed culture media and placed into an incubator to adhere for 24 hours. The following day the media was changed to remove residual DMSO

(used as a cryoprotectant to prevent cell ablation) from the freezing medium. Subsequently the media was changed every 3 days and cells were passaged once per week according to the method outlined below.

Cell Passaging: To passage cells, medium was removed and cells were washed with 20mL of PBS (at room temperature). Three-mL of 0.05% Trypsin-EDTA (Life Technologies #25300062) was added to the cells and the flask returned to the incubator for 5 minutes. The flask was then gently tapped to detach remaining cells before 10mL of culture medium was added to the flask to deactivate the trypsin. Cells were centrifuged at room temperature for 5 minutes at 1200 rpm and the supernatant was discarded. The pellet of cells was resuspended in 10mL of fresh complete media and passed through an 18G blunt-ended needle 5 times to disperse aggregated cells and generate a single celled population. Cells were counted using a haemocytometer (a 1:5 dilution of cells in culture media was routinely used to reduce the number of cells and improve counting efficiency) and seeded as described below. Cells were routinely maintained in T175cm^2 flasks with morphology and growth rate regularly assessed by light microscopy. The seeding densities used throughout this thesis were optimised stringently using cell-density titrations. Table 2.3 below details the seeding densities used both in routine cell maintenance (i.e. in T80 and T175 flasks) and in both 96 and 12 well plates.

Flask / Plate	Well size	Supplier	Seeding Density	Time until 70-80% Confluent
T80cm^2 Flask	80cm^2	Nunc (Thermo Scientific # 178905)	1x10^6	7 Days
T175cm^2 Flask	175cm^2	Nunc (Thermo Scientific # 178883)	3x10^6	6-7 Days
96 Well Plate	0.32cm^2	Corning (Sigma # CLS3596) / Seahorse Bioscience # 101085-004	2x10^4	24 hours
12 Well Plate	3.8cm^2	Corning (Sigma # CLS3513)	2.5x10^5	48 hours

TABLE 2.3: HepG2 cell seeding density and flask/plate details. Seeding densities were optimised throughout the project. Cell density titration experiments aimed to identify the best condition for the assay in question in relation to cell density and confluency and therefore densities are not reflective of the size of the well/flask.

Cryopreservation of HepG2 Cells for maintaining Stocks: Over time it was important to maintain a batch of frozen cells. During a passage cycle and immediately following trypsinisation, cells were resuspended in freezing medium containing 90% FBS (Invitrogen #10500-064) and 10% DMSO. Cells were then counted and 1mL aliquots (at a density of 1x10^6 cells/mL) were transferred to labelled cryovials (alternatively, 4 x 1ml aliquots from a 175cm^2 flask or 1 x 1ml aliquot from a 80cm^2 flask were cryopreserved). Vials were then placed in a Mr Frosty (controlled temperature freezing container filled with iso-propanol, Sigma Alrdich, #C1562) which was placed at -80°C for 24h. The frozen vials were

then transferred to a liquid nitrogen freezer for long-term storage. When freezing a batch of cells, one vial of cells was revived after several days to ensure the freezing process had been successful and the cells remained viable.

2.9.2. ASSESSMENT OF CYTOTOXICITY

The LDH Cytotoxicity Detection Kit (Roche Diagnostics, Basel, Switzerland #11644793001) was used to assess LDH leakage into cell culture medium following treatment with compounds and respective DMSO controls (as recommended by the manufacturer) on a SpectraMax Plus 384 plate reader (Molecular Devices, Sunnyvale, CA, USA). Data were expressed as a percentage of leaked LDH against total LDH (leaked values + Cell Lytic lysed samples) with 1% v/v Triton X-100 used as a positive control inducer of cytotoxicity.

2.9.3. ANALYSIS OF WHOLE CELL BIOENERGETICS IN HEPG2 CELLS

Whole cell bioenergetics/cell metabolism was assessed using the Seahorse XF_e96 Analyser (Seahorse Bioscience, Billerica, USA) essentially as described by [138] and [139] with minor modifications. The method described below is similar to that described in section 2.8.3 above although for cell culture analysis the XF_e96 analyser was utilised as oppose to the XF24. Additionally, with whole cells the Seahorse Analyser permits the analysis of both OCR (measure of ETC/OXPHOS) and ECAR (measure of glycolysis) providing an indication of the metabolic state of cells in culture. Again, drug injection ports allow the effect of compounds/inhibitors/substrates on whole cell bioenergetics to be assessed.

Briefly, HepG2 cells grown in galactose-conditioned DMEM media (as described in section 2.9.1) were plated into an XF96 cell culture plate (Seahorse Bioscience # 101085-004) at $2x10^4$ cells per well and incubated at 37°C (5% CO_2) for 24 hours. Following incubation, cells were removed from the incubator and the media was replaced with 175µL of serum-free assay media (table 2.4 below). Assay media was prepared fresh on the day of the assay and warmed to 37°C prior to the pH being adjusted to pH 7.4 with KOH.

Constituent	Concentration	Supplier #Part Number
XF Base Media	N/A	Seahorse Bioscience # 102353-100
L-Glutamine	2mM	Life Technologies #25030-081
Sodium Pyruvate	1mM	Sigma #P2256
Glucose	10mM	Sigma #G8270

TABLE 2.4: Serum free Seahorse assay media constituents

Following media replacement, cells were placed into a 37°C incubator (no CO_2 supplementation) for one hour. During this incubation a dose response of the compound of interest was prepared in serum free assay media. Oligomycin, FCCP and antimycin A/rotenone were also prepared at the concentrations below (table 2.5) in serum free media, enabling the analysis of multiple bioenergetic parameters. Compounds were added into the injection ports at increasing concentrations as additions are sequential (therefore to maintain a consistent volume of 25µL in each port, the working concentration of compound increased by 1X following each injection).

Compound	Concentration in Well	Final Concentration	Volume in Well Following Addition (µL)
Compound X	8X (dependent on dose response)	Dependent on dose response chosen	200
Oligomycin	9X (18µM)	2µM	225
FCCP	10X (2.5µM)	0.25µM	250
Antimycin A / Rotenone	11X (11µM)	1µM	275

TABLE 2.5: Concentration of BOFA reagents loaded into the drug injection ports and final concentration in the well. Concentrations of oligomycin, FCCP and antimycin A/rotenone were optimised as recommended by the manufacturer.

Using a multichannel pipette and the supplied XF_e96 cartridge loading guide, 25µL of compound X (port A), Oligomycin (port B), FCCP (port C) and antimycin A/rotenone (port D) were loaded into the assay cartridge which was then loaded into the XF_e96 analyser for calibration. After the cells had been incubated for one hour and the cartridge calibration was complete, the cells were loaded into the XF_e96 analyser to undergo a 12 minute equilibration period. Following equilibration, three 3 minute basal measurements were made prior to injection of the compound of interest through port A. The protocol then ensued with three 1 minute mix, 3 minute measure, 1 minute mix cycles between each respective injection. For whole cells in culture, bioenergetic parameters were calculated as shown in Fig.2.3 below.

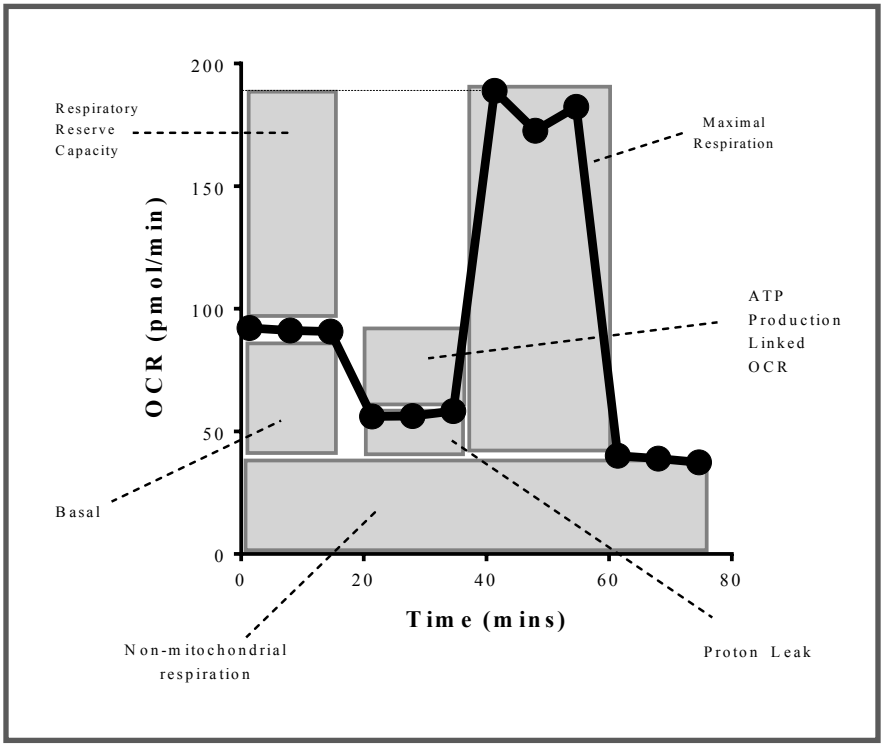


FIGURE 2.3: Graphical representation of the whole cell OCR assay for determination of bioenergetic parameters. Respective bioenergetic parameters were calculated in pmol/min as shown.

2.9.4. *IN VITRO* COMPOUND WASH OUT EXPERIMENT

In order to assess the reversibility of drug effects on mitochondrial OCR, the experiment described above (section 2.9.3.) was performed with the following modification. Following injection of the compound of interest from port A of the XF_e96 assay cartridge and subsequent capture of compound related effect on basal OCR, the cell plate was removed from the analyser. Cells were immediately washed 3 times with fresh XF assay media (37°C, pH7.4) with a final volume of 200µL left in the well. Cells were placed for approximately 30 minutes into a 37°C incubator (no CO_2 supplementation) whilst the XF_e96 analyser was re-calibrated. Basal OCR was immediately re-analysed in the XFe96 analyser to assess whether the effect of the drug was persistent. Data were expressed as a percentage of the 0.1% DMSO control for both pre and post-compound wash out.

2.10. Imaging and Histology

2.10.1. TEM Analysis of Isolated Mitochondrial Pellets

TEM analysis of isolated mitochondria is shown in Appendix 1.1. Isolated mitochondria were resuspended at a concentration of 1mg/ml in 4% formaldehyde/1% glutaraldehyde and transferred to 1.5mL Eppendorf tubes. Mitochondria were centrifuged at 12000 rpm for 5 minutes in a bench-top micro-centrifuge to form a solid pellet and left at room temperature for 48 hours. Pellets were processed into Agar 100 resin (Agar Scientific, Essex, UK). Ultra-thin sections (approximately 90 nm thick) were then prepared, stained with uranyl acetate and lead citrate and examined in a Hitachi H7500 transmission electron microscope (one grid section per mitochondrial preparation). An AMT XR41 Digital Camera System v 600.202 was used to capture TEM images. Micrographs were observed for mitochondrial ultrastructure as well as the presence of other cellular debris/organelles. No scoring metric was used. Data are shown in Appendix I. Electron microscopy analysis was performed by Ian Francis and Paul McGill (GlaxoSmithKline, Safety Assessment Histopathology, Ware, UK).

2.10.2. TEM Analysis of HepG2 Cells

HepG2 cells were fixed in 4% Formaldehyde/1% Glutaraldehyde. Cell culture media (plus compound / DMSO) was removed and replaced with 1mL of fixative per well (in a 12 well plate format). Cells were then gently scraped and analysed using a bench top light microscope to ensure detachment of cells from the cell-culture plate. Fixed cells from 3 replicate wells were subsequently pooled and transferred into a 15mL falcon tube where a further 3mL of fixative was added. Samples were then centrifuged at 1300g for 5 minutes to create a loose cell pellet. Following centrifugation, excess fixative was removed and the loose cell pellet (~1.5mL) was left at 2-8°C for 48 hours.

Following incubation, HepG2 samples were post-fixed using reduced osmium thiocarbohydrazide osmium (R-OTO method), and processed manually into Agar 100 epoxy resin (Agar Scientific, Essex, UK) [140]. Ultra-thin sections were taken that were subsequently blinded and 100 cells/experimental group were examined for any ultra-structural changes (including an assessment of lipid and glycogen content and any mitochondrial changes), using a Hitachi H7500 transmission electron microscope, operating at 80kV.

2.10.3. TEM ANALYSIS OF LIVER

Small blocks of the right lateral lobe of the liver were fixed in 4% formaldehyde/1% glutaraldehyde. These were post-fixed in 1% aqueous osmium tetroxide and processed into Agar 100 resin (Agar Scientific, Essex, UK). One μm toluidine blue stained survey sections were prepared and examined by LM to locate the areas of interest (such as the periportal region). Ultra-thin sections (approximately 90nm thick) were then prepared, stained with uranyl acetate and lead citrate and examined in a Hitachi H7500 transmission electron microscope (one grid section per animal). The AMT XR41 Digital Camera System v 600.202 was used to capture TEM digital images. No scoring system or blinding was implemented in the analysis of TEM samples.

2.10.4. LIGHT MICROSCOPY OF LIVER

Formalin fixed samples of liver (≤ 4 mm in thickness) were post-fixed in a final working solution of 2.5% potassium dichromate and 1% osmium tetroxide in distilled water for 8 hours at room temperature. The osmicated tissue samples were rinsed in running water for 2 hours, processed to paraffin block and sectioned at 5 microns. Tissue sections were stained with the routine hematoxylin and eosin (H&E) method and evaluated using a routine severity scoring system (mild, moderate and marked). Two sections per liver were initially analysed by group and then blind to confirm observations.

2.11. Western Blot

Western blot data is shown in Appendix 1.2. Mitochondrial protein was loaded onto NuPAGE Bis-Tris mini gels (# NP3015, Invitrogen) at 10μg in 1X LDS Sample Buffer and 1X NuPAGE Sample Reducing Agent and separated by SDS-PAGE at 200V for 35 minutes. Following electrophoresis, protein was transferred to a nitrocellulose membrane using the iBlot Dry Blotting System (#IB1001, Invitrogen). Following transfer, the membrane was blocked for 1 hour at room temperature in 5% FA-Free milk and 1X Tris buffered saline with Tween 20 [TBST] (#9997, Cell Signalling Technology, MA, USA). The membrane was washed three times in TBST (agitated for 5 minutes between each rinse) prior to a 1 hour

incubation at room temperature with the primary antibody cocktail (shown below) at a dilution of 1/230 in TBST (as recommended).

- Mitochondrial Membrane Integrity WB Antibody Cocktail (#ab110414, Abcam, Cambridge, UK). Contains the five mAbs shown in table 2.6 below targeting each of the primary structural units of the mitochondrion

Protein Name	**Structural Unit**	**Working Concentration (µg/ml)**	**Individual Catalogue Numbers**	**Molecular Weight (KDa)**
VDAC1/Porin	OMM	2	#ab14734	39
Cyclophillin D	Matrix	2	#ab110324	21
Ubiquinol-Cytochrome C Reductase Core Protein I (Complex III)	IMM	2	#ab110252	49
ATP5a (Complex Va)	IMM	4	#ab110273	53
Cytochrome C	IMS	0.1	#ab110325	12

TABLE 2.6: Details of the five antibodies comprising the mitochondrial membrane integrity western blot antibody cocktail (ab220414).

The membrane was then washed as described above, before a further 1 hour incubation in Goat-Anti-Mouse IgG Horseradish Peroxidase (HRP) linked secondary antibody (#ab6789, Abcam) at a dilution of 1/50000 in TBST. Following incubation the membrane was again washed as described above before visualisation of protein banding using the Supersignal West Dura Chemiluminsecent Kit (Thermo Scientific #34076) in a Bio-Rad Versa-Doc Imaging System (Bio-Rad, Hertfordshire, UK) according to manufacturer's recommendations.

2.12. Reduced / Oxidised Glutathione Assay

Measurement of total glutathione, GSH (reduced), GSSG (oxidised) and GSH: GSSG ratio was made using the NWLSS Glutathione Assay Kit (Northwest Life Science Specialties, LLC) according to the manufacturer's protocol. Briefly, 25µL of whole blood was resuspended in 1mL of assay buffer. Protein was pelleted by centrifugation following the addition of 100µL of metaphosphoric acid with collection of

the supernatant. Subsequent to further dilution (1:50-1:100 fold) the supernatant was used to measure total glutathione. Following addition of the thiol reagent 5-5'-dithiobis[2-nitrobenzoic acid] (DTNB), glutathione reductase and NADPH the plates were read at an absorbance of 405nm at 12 second time intervals for 3 minutes (reduced glutathione, GSH) or 15 minutes (oxidised glutathione, GSSG), using a Spectramax plus 384 spectrophotometer (Molecular Devices, Sunnyvale, CA, USA). GSSG levels were assessed by removing an aliquot of the same supernatant and subsequently depleting the sample of GSH via the addition of 10µL of 4N Sodium Hydroxide and 10µl of 500mM vinyl pyridine followed by a 1 hour incubation. Reduced levels of glutathione were calculated by subtracting the oxidised glutathione value from the total glutathione value obtained from the original supernatant.

2.13. Measurement of Lactate / Pyruvate in Plasma

Blood was collected into perchloric acid as detailed above. Lactate was measured on a Siemens Advia 1650 clinical chemistry analyser (Siemens Healthcare Diagnostics, Surrey, UK) using a Lactate assay kit (Randox Life Sciences, Crumlin, Northern Ireland) according to the manufacturer's instructions. Pyruvate was also measured on this analyser using reagents from Sigma-Aldrich. Pyruvate estimation was made by measuring the reduction in absorbance at 340nm due to oxidation of NADH to NAD as previously described [141]. Pyruvate concentration was established according to a standard curve of between 0 and 0.45mmol/L pyruvate. All data were recorded in mmol/L and presented as a ratio between lactate and pyruvate.

2.14. Measurement of Lactate in Cell Culture Media

Lactate was measured in supernatant medium using a colorimetric assay originally described by [142] and further used by [143]. The assay is based on the conversion of lactate to pyruvate by lactate dehydrogenase (LDH) activity reducing nicotinamide adenine dinucleotide (NAD^+) to its reduced form NADH. In detail, NADH reduces N-methylphenazonium methyl sulphate (PMS) to PMSH which reduces p-iodonitrotetrazolium violet (INT) to INTH. Briefly, 20µl of supernatant medium was incubated with 180µl of assay solution consisting of 86mM triethanolamine HCl, 8.6 M EDTA.Na, 3 mM MgCl2.6H20, 326nM PMS, 790nM INT, 7% ethanol, 0.4% Triton-X-100, 3.3mM β-NAD and 4U/mL LDH. After incubating for 7 minutes in dark conditions, the absorption of the colour product (INTH) was measured at

490 nm in a Biotek Synergy HT microtitre plate reader (Biotek,Winooski, VT, USA). A lactate standard curve (0-25mM) with a non-linear regression fit was used to determine lactate concentrations from treated cells (see Fig.2.4 below). Data were expressed as a percentage of control.

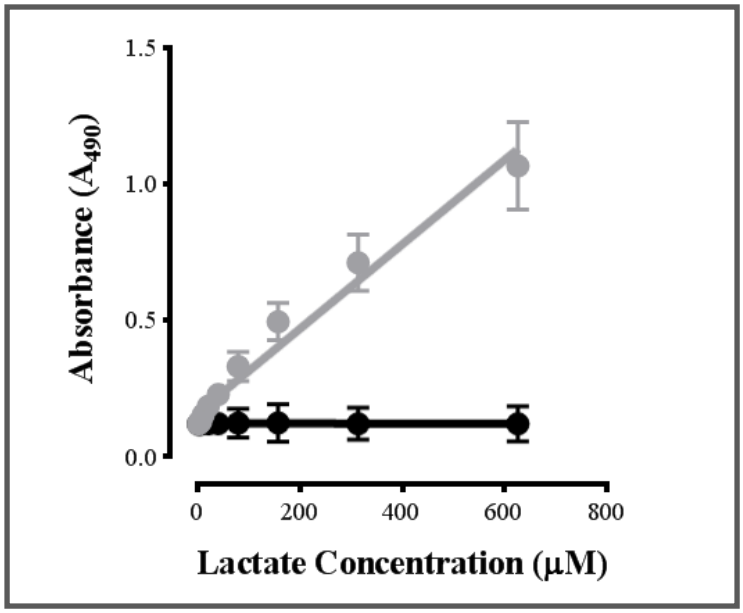


FIGURE 2.4: A typical lactate assay standard curve. Data points marked with a light grey line of best fit included LDH to initiate the assay whereas data marked with a black line lacked LDH (used as a negative control).

2.15. Total RNA Extraction

Total RNA extraction from rat liver tissue and HepG2 cell lysates was performed using the Promega SV RNA Isolation System (#Z3105, Promega, Madison, WI, USA). HepG2 cell lysate and rat liver tissue homogenates were prepared as described in section 2.15.1 and 2.15.2 below. RNA was then extracted in the same way and as described in section 2.15.3.

2.15.1. HepG2 Lysate Preparation

Remaining culture media was removed using an aspirator and the cell monolayer was washed with PBS (1mL/well in 12 well plate format). PBS was then removed and 175μL of SV Lysis Buffer was added to

each well prior to freezing the plate at -80°C. Upon thawing, the bottom of each well was scraped thoroughly using a sterile cell culture scraper and triplicate wells were pooled into an RNAse/DNAse free 1.2mL Eppendorf tube. Genomic DNA (gDNA) was sheared by passing the lysate through a sterile 19G blunt-ended needle (#300149, BD Biosciences, San Jose, CA, USA) five times and placed on ice. Lysates were immediately processed to RNA extraction.

2.15.2. RAT LIVER TISSUE HOMOGENATE PREPARATION

Approximately 90mg of snap frozen liver tissue was added to 525µL of SV RNA Lysis buffer in a Precellys Homogenisation Vial (#CK28, Precellys, Derbyshire, UK) and homogenised twice using the Precellys 24 at 6500rpm for 60 seconds. The homogenates were placed on ice for 5 minutes to allow the froth to settle before passing through a 19G blunt-ended needle to sheer gDNA. Tissue homogenates were immediately processed to RNA extraction.

2.15.3. TOTAL RNA EXTRACTION

Total RNA was extracted according to manufacturer's recommendations (Promega SV RNA Lysis System). Briefly, 175µL of hepatocyte lysate or liver homogenate was added to 350µL of SV Dilution Buffer and mixed by inversion 3 times. The mixture was heated for 3 minutes at 70°C and centrifuged for 10 minutes at 14,000g. The supernatant was transferred to a fresh RNase/DNase free 1.2mL Eppendorf tube containing 200µL 95% v/v ethanol, loaded onto an SV RNA Isolation spin column assembly and centrifuged at 14,000g for 1 minute. Liquid in the collection tube was discarded and 600µL of SV Wash solution added to each spin column prior to centrifuging at 14,000g for 1 minute. The collection tubes were again emptied and 50µL of SV DNase Incubation Mixture (prepared with 40µL of SV Yellow Core Buffer, 5µL 0.09M $MnCl_2$ and 5µL SV DNase I enzyme) was applied to the surface of each column membrane and incubated at room temperature for 15 minutes to allow DNA digestion to proceed. Following incubation, 200µL of SV DNase Stop Solution was added to each column and the spin column assemblies were again centrifuged at 14,000g for 1 minute prior to washing with 600µL SV RNA Wash solution and re-centrifuging at 14,000g for 1 minute. The collection tubes were again emptied, and a final wash step was performed to remove ethanol carry-over by adding 250µL of SV RNA wash solution to each spin column assembly and centrifuging at 14,000g for 2 minutes. The column within each SV RNA Isolation Tube Assembly was transferred to a fresh 1.2mL RNase/DNase free Eppendorf tube and 100µL

of SV Nuclease Free Water applied to the membrane. Total RNA was then eluted by centrifuging the column/tube assemblies at 14,000*g* for 1 minute. The columns were discarded and eluted total RNA stored at -80°C until required.

2.16. RNA Quantification and Assessment of Integrity

2.16.1. Quantification Using the NanoDrop Spectrophotometer

RNA concentration and yield were determined by UV absorbance using the Nanodrop ND-1000 Spectrophotmeter (Wilmington, DE, USA) according to manufacturer's recommendations. Briefly, the absorbance of each total RNA sample was determined (in 2µL volume) at 260nm (peak nucleic acid wavelength) and 280nm (protein wavelength) and normalised against an elution blank negative control. The A_{260}:A_{280} ratio was used to determine the level of protein contamination and a ratio of 1.8-2.2 was considered acceptable for downstream analysis. RNA concentration was calculated using the 260nm reading and a conversion factor based on the extinction coefficient for RNA (A_{260} of 1.0 = 40µg/ml for RNA). RNA concentration was expressed as ng/µL.

2.16.2. Assessment of RNA Integrity

Quality assurance of RNA samples was performed using the Agilent 2100 Bioanalyser (Santa Clara, CA, USA) and RNA 6000 Nano Chips (#5067-1511, Agilent) according to manufacturer's recommendations. Briefly, 550µL of RNA 6000 Nano Gel Matrix was passed through a spin column at 1500g for 10 minutes and 65µL aliquots made. To one 65µL aliquot, 1µL of RNA 600 Nano Dye Concentrate was added and thoroughly vortexed before centrifuging at 13,000g for 10 minutes. RNA samples (~4µL) were degraded at 70°C for 3 minutes. Gel-dye mix (9µl), Agilent RNA 6000 Nano Marker (5µl), ladder (1µl) and denatured samples (1µl) were pipetted into specific marked wells on the chip according to manufacturer's recommendations. Fully prepared chips were vortexed on an IKA vortexer at 2400rpm for 1 minute. The chip was run using the Bioanalyser 2100 within 5 minutes. During the analysis, negatively charged RNA molecules are separated according to size by migration towards an anode. Fluorescent dye molecules make RNA detectable by laser scanning with size and concentration of RNA determined by fluorescence detected. The Agilent 2100 software filters the data and presents the results as electropherograms or densitometry plots (Fig.2.5). Assessment of RNA integrity is made by evaluation of the

separation/definition of the 18S and 28S ribosomal peaks (rRNA). RNA integrity is quantified by an automatically generated RNA integrity number (RIN) which is scaled between 1-10 (with 10 being considered an RNA sample of exceptional quality). RIN numbers are generated using Agilent (Santa Clara, CA, USA) proprietary algorithms which base quantification on the entire electrophoretic trace of the RNA samples as opposed to simply the ratio of the ribosomal bands. This includes the presence or absence of degradation products. Samples not reaching the required RIN of ≥7.5 were re-processed (as per the manufacturer's guidelines).

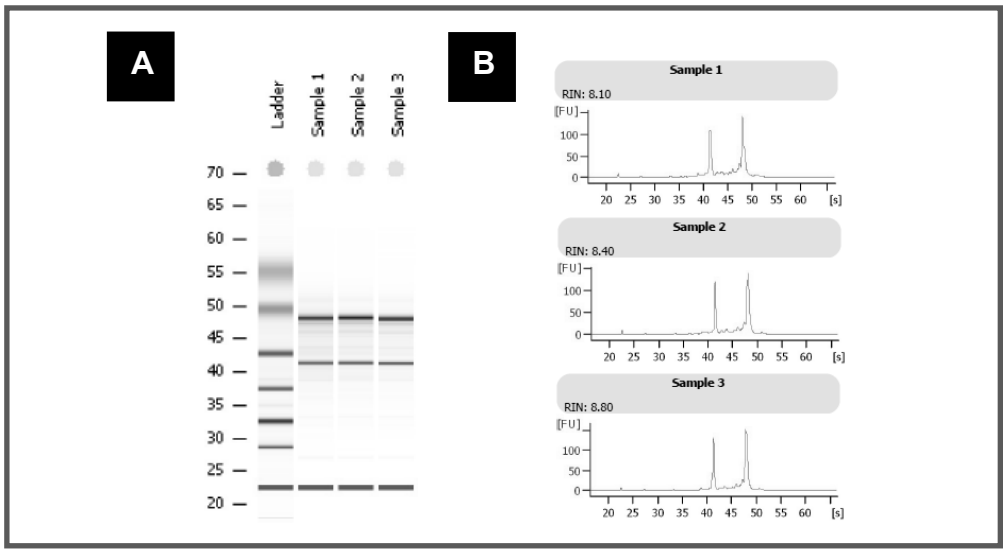


FIGURE 2.5: Gel image and electropherogram output from Agilent 2100 Bioanalyser – Assessment of RNA integrity. (A) Agarose gel image - Negatively charged RNA molecules are separated according to size using "lab on a chip" technology and are resolved on agarose gels. The two bands relate to the 18S and 28S ribosomal subunits. (B) Data can also be visualized on electropherograms where an RNA integrity number (RIN) is assigned based on the separation and definition of the 18S and 28S peaks. Samples 1-3 correspond to RNA isolated from snap frozen control rat liver.

2.17. Transcriptional Profiling using Affymetrix Genechip Microarrays

2.17.1. Generation of Sense Strand cDNA

Sense strand complementary deoxyribonucleic acid (cDNA) was generated from total RNA using the Ambion Whole Transcript (WT) Expression Kit (#4411974, Life Technologies, Paisley, UK) according to manufacturer's recommendations. Briefly, 200ng of RNA was used to generate first-strand cDNA using

primers containing a T7 promoter sequence before the resulting single stranded cDNA was converted to double stranded cDNA which acts as a template for transcription. This reaction uses DNA polymerase and RNase H to simultaneously degrade the RNA and synthesize first-cycle second-strand cDNA. Antisense complementary ribonucleic acid (cRNA) is then synthesised and amplified by *in vitro* transcription (IVT) using an RNA Polymerase which binds to the T7 promoter sequence which was previously engineered into the template strand based on the procedure outlined in [144]. cRNA was purified by removing enzymes, salts, inorganic phosphates and unincorporated nucleotides by magnetic bead capturing (using isopropanol), washing and elution. cRNA yield was then determined using the Nanodrop ND-1000 spectrophotometer as described above (2.16.1) before second-cycle sense-strand cDNA was prepared by random primer reverse transcription of 10µg cRNA. This process also incorporated dUTP at a fixed concentration which is required for DNA fragmentation described below (section 2.14.2). RNase H was then used to degrade the remaining cRNA template before second cycle sense-strand cDNA was purified using magnetic bead capturing (using ethanol), washing and elution. Purified sense strand cDNA yield was then determined using the Nanodrop ND-1000 spectrophotometer as described above (2.16.1).

2.17.2. FRAGMENTATION AND LABELLING OF CDNA TEMPLATE

Sense-strand cDNA was fragmented and labelled ready for Affymetrix genechip analysis using the Affymetrix WT Terminal Labelling and Hybridization Kit (#901524, Affymetrix, Santa Clara, CA, USA) according to manufacturer's recommendations. Briefly, 5.5µg of sense-strand cDNA generated using the Ambion WT Expression Kit (section 2.17.1) was fragmented using uracil DNA glycosylase (UDG) and apurinic-apyrimidinic endonuclease 1 (APE 1) enzymes in order to remove dUTP residues from ssDNA molecules and cleave phosphodiester backbones, thus leaving 3'-hydroxyl and 5'-deoxyribose phosphate terminus fragments. The length of the fragmented DNA was assessed using the Agilent 2100 bioanalyser (as described in section 2.16.2) with fragments ranging from 20-200 bases. Fragmented single-stranded DNA was labelled by terminal deoxynucleotidyl transferase (TdT) with biotin allonamide triphosphate as recommended.

2.17.3. HYBRIDISATION, WASH AND STAINING OF AFFYMETRIX GENECHIPS

The following procedure utilises the Affymetrix Hybridisation, Wash and Stain Kit (#900720, Affymetrix) according to manufacturer's recommendations. Briefly, fragmented and labelled DNA (from section 2.17.2) was added to a hybridisation cocktail containing, 20X eukaryotic hyb-controls, 2X hybridisation mix, control oligonucleotide B2, DMSO and nuclease free water (at concentrations defined by Affymetrix). The hybridisation cocktail was heated at 99°C for 5 minutes and then 45°C for a further 5 minutes in a heat block before centrifuging at 14,000g for 1 minute. Affymetrix Rat Gene 2.0 Sense Target (ST) Genechips (Format 100 #902125) were equilibrated to room temperature immediately before use and 130µL of hybridisation cocktail was injected into the array though the septa on the reverse of the chip. The arrays were then placed in a hybridization oven (with rotating arm) at 45°C (60rpm) for 17 hours.

Following hybridization, the array was vented and the hybridization cocktail removed. The probe array was then refilled with 160µL (for format 100 arrays) of Wash Buffer A. The Affymetrix Fluidics Station 450 was primed using fluidics script PRIME_450 to expose the lines to all wash buffers and to rinse with dH_20. Stain cocktail 1 and 2 and array holding buffer were pipetted into 1.5mL eppendorf vials and centrifuged at 14,000g for 30 seconds to remove air bubbles before being placed into positions 1-3 on the Affymetrix Fluidics Station 450. Wash buffer A, Wash buffer B and dH_20 were placed into reservoirs with the respective fluidics lines inserted. Arrays were clamped into place and the fluidics script FS450_0002 was run. When the wash/stain protocol was complete, arrays were ejected from the Fluidics Station and inspected to ensure no bubbles were present (arrays were re-filled with wash buffer A if bubbles required removing).

2.17.4. SCANNING OF GENECHIPS AND STATISTICAL ANALYSIS OF MICROARRAY DATA

The Affymetrix Genechip Scanner 3000 is controlled by the Affymetrix Genechip Command Console (AGCC). The scanner was turned on ~10 minutes prior to scanning to warm the laser. In the AGCC, autoloader function was selected. Arrays were firstly wiped clean using a non-abrasive tissue before loading onto the scanner carousel (up to 30 at a time). Scanning was started by clicking "start scan" in the AGCC. Once scanning was complete the hybridisation/scan image was inspected to ensure no gross scan-errors could be detected. CEL.files were then transferred from the PC and differential gene expression

analysis was performed using Array Studio version 7.0 (www.omicsoft.com). Affymetrix data were normalised using the robust multichip average (RMA) method [145] and differentially expressed genes were defined as those with greater than 1.5 fold change in expression, at $p<0.05$.

2.17.5. PATHWAY ANALYSIS

In order to infer biological meaning from transcriptomic data, biological theme analysis was undertaken. This analysis provides a functional view of the classes of genes and pathways significantly presented within a data-set. Ingenuity Pathway Analysis (IPA, Ingenuity, Redwood City, CA, USA) was utilised which is a proprietary analysis system that must be subscribed to (GlaxoSmithKline, Investigative Preclinical Toxicology Access, 2013-2015). IPA segregates gene groups according to a level of significance defined by the user. In the present study all network associations were defined by experimentally-supported literature evidence. All genes with a fold change of ± 1.5x and $p<0.05$ were submitted for pathway analysis. Alternatively, genes identified as being highly statistically significant with regard to separating experimental variables (using a principle component analysis, PCA) were inputted to IPA for more refined analyses. IPA generates a list of canonical pathways from the genes significantly affected alongside toxicological pathways altered. IPA also contains an interaction networking capability which enables visualisation of gene-connections within a given biological response. This permits visualisation of particular biochemical networks with the effected genes highlighted. Furthermore IPA provides an annotation of each mapped gene which vastly supports inference of biological meaning from the computationally generated network without repeated interfacing with the literature.

2.17.6. COMPOUND CONNECTIVITY MAPPING

Connectivity mapping is a process whereby novel pharmacological and toxicological properties can be identified in small molecules by comparing their gene expression signatures with others in a database. The technique also facilitates the identification of novel tool compounds which may mimic the biological action of the user's compound based on the genes which are differentially altered [146]. Compound connectivity mapping was used to compare the gene signatures generated from Affymetrix microarray analysis of GSK932121A and GSK2617971A treated animals (the query gene signature) to over 1000 compounds located in the Broad Institute expanded data set (reference dataset). This reference database

contains 6100 reference profiles characterised by different treatment conditions of each compound (applied to 5 human cell lines). A pattern matching algorithm/similarity metric was used to quantify the closeness of connection between the two biological states as a result of small molecule treatment. The query gene signature was composed of a short list of differentially altered genes most relevant and important to characterise the biological state arising following compound treatment (selection criteria of genes used for connectivity mapping analysis described in section 7.2.5). The sscMap (Java Application) was used essentially as described in [147]. Data were expressed as connection scores and p-values ($-Log_{10}p$).

2.18. TaqMan RT-PCR Analysis from *In vitro* Samples

Real-time quantitative PCR (RT-PCR) is a routinely used technique to measure gene expression. RT-PCR is usually performed on a small subset of gene transcripts and is a relatively low cost and sensitive profiling technique. In the case of TaqMan RT-PCR, the real time monitoring of PCR amplification of an amplicon is monitored by the incorporation of a probe consisting of two fluorophores. When the probe is either tethered or untethered to the template DNA and prior to polymerisation, the quencher fluorophore (usually long wavelength coloured dye) reduces the fluorescence from the reported fluorophore (usually short wavelength coloured dye) via fluorescence resonance energy transfer (FRET). The reporter dye is located on the 5' end of the probe and the quencher at the 3' end. Once the TaqMan probe has bound to its specific target piece of template DNA (and following denaturation at high temperatures), the primers anneal to the DNA and *Taq* polymerase incorporates nucleotides which removes the TaqMan probe from the template DNA. This polymerization separates the quencher from the reporter and allows the reporter to emit its fluorescence which is then quantified internally. RT-PCR allows the time at which the level of fluorescence passes a threshold level (known as the Cycle Threshold or Ct) to be determined. The higher the copy number of the target gene, the faster the fluorescence passes the Ct, and thus, by comparing Ct values for different reactions, it is possible to determine the relative gene expression between samples

2.18.1. GENE PANEL

Gene Symbol	Gene Name	Assay ID	Lot Number	RefSeq Accession No.	Context Sequence
Pck1	phosphoenolpyruvate carboxykinase 1 (soluble)	Hs01572978_g1	1312055	NM_002591	TGACAACTGCTGGTTGGCTCTCACT
Chac1	ChaC, cation transport regulator homolog 1 (E. coli)	Hs00225520_m1	1294249	NM_001142776	TGAAGATCATGAGGGCTGCACTTGG
Gapdh	glyceraldehyde-3-phosphate dehydrogenase	Hs02758991_g1	1317397	NM_001256799	GACTCATGACCACAGTCCATGCCAT
Ppargc1a	peroxisome proliferator-activated receptor gamma, coactivator 1 alpha	Hs01016719_m1	1308701	NM_013261	AAGGCAATTGAAGAGCGCCGTGTGA
Lpin1	lipin 1	Hs00299515_m1	1169040	NM_001261427	AGAGAAAGTGGTTGACATAGAAATC
Foxo1	forkhead box O1	Hs01054576_m1	1301006	NM_002015	GGCTGGAAGAATTCAATTCGTCATA
Hmox1	heme oxygenase (decycling) 1	Hs01110250_m1	1305084	NM_002133	TGCTCAACATCCAGCTCTTTGAGGA
Pdk4	pyruvate dehydrogenase kinase, isozyme 4	Hs01037712_m1	1316401	NM_002612	TTTAAGAATGCAATGCGGGCAACAG
Nr4a1	nuclear receptor subfamily 4, group A, member 1	Hs00374226_m1	1259635	NM_001202233	GGCTTCTTCAAGCGCACAGTGCAGA
G6pd	glucose-6-phosphate dehydrogenase	Hs00166169_m1	1295896	NM_000402	GGGTGCATCGGGTGACCTGGCCAAG
Nr4a2	nuclear receptor subfamily 4, group A, member 2	Hs00428691_m1	1290694	NM_006186	CTGGACTATTCCAGGTTCCAGGCGA
Irs2	insulin receptor substrate 2	Hs00275843_s1	1289193	NM_003749	CACGACGGTCACCCCCGTGTCCCCG
Nr4a3	nuclear receptor subfamily 4, group A, member 3	Hs00545009_g1	1241861	NM_006981	AAAGAAGTTGTCCGTACAGATAGTC
Ppara	peroxisome proliferator-activated receptor alpha	Hs00947536_m1	1302244	NM_001001928	GCTGCAAGGGCTTCTTTCGGCGAAC
Atf3	activating transcription factor 3	Hs00231069_m1	1310874	NM_001030287	CACAAAAGCCGAGGTAGCCCCTGAA

TABLE 2.7: Details of the primers and probes used for *in vitro* RT-PCR experiments. Table shows the details for the 15 genes selected for RT-PCR analysis (G6pd used as the housekeeper/normaliser gene). All genes had a FAM-NFQ reporter/quencher. The context sequence describes the nucleotides to which the assay was targeted.

2.18.2. FIRST STRAND cDNA SYNTHESIS

Total RNA samples were reverse transcribed into first strand cDNA prior to RT-PCR analysis. 1µg of total RNA was used to generate cDNA using the BioScript Reverse Transcriptase kit (Bioline #BIO-27036) according to manufacturer's recommendations. cDNA synthesis was carried out with (RT^+) and without (RT^-) the BioScript reverse transcriptase enzyme, to enable substitution of gene expression data caused by amplification of gDNA. Briefly, total RNA was diluted to a concentration of 125ng/µL in 8µL of DEPC-treated water (1µg) and combined with 10mM deoxynucleotide triphosphates (DNTP) mix (Bioline #BIO-39053) and 40µM Random Hexamers (Bioline #BIO38028) in RNase/DNase free PCR strip tubes. The samples were incubated at 70°C for 5 minutes using a DNA Engine Tetrad PCR cycler (MJ Research, Massachusetts, USA) and chilled for at least 1 minute on ice. 4µL of RT-Buffer, 1µL of RiboSafe RNase Inhibitor (Bioline #BIO65027), 1µL of BioScript Reverse Transcriptase (200u/µL) and 4µL of DEPC-treated water was then added to each reaction in a master-mix and tubes centrifuged to collect the contents at the bottom of the tubes. Samples were then incubated at 25°C for 10 minutes, 42°C for 30 minutes and then the reaction was terminated at 85°C for 5 minutes. Following incubation, reactions were cooled on ice, immediately diluted 1:15 with DEPC treated water and stored at -20°C until required.

2.18.3. TAQMAN RT-PCR

TaqMan RT-PCR was performed in 384 well plates using the QuantStudio 6 Flex Real-Time PCR System (Applied Biosystems, Life Technologies, Paisley, UK). Briefly, 9 µL of 1:15 diluted cDNA was loaded into each well of a 384 well plate (n=3 biological replicates with two technical replicates per sample) and the plate centrifuged at 300g for 2 minutes to collect the cDNA at the bottom of each well. 10µL of TaqMan Universal MasterMix II With UNG (Applied Biosystems, Life Technologies #4440045) and 1µL the PCR primers/probes for individual genes (table 2.7) were added to each well ensuring that both the 2X MasterMix II and the 20X primers/probes were both at 1X final concentrations in the well (TaqMan Universal MasterMix and the PCR primers/probes were combined and added to each well in one step to reduce variability due to pipetting error). One gene per plate was analysed (16 genes) with all samples included on each plate. Non-template controls (NTC's) were included (~ 6 wells per gene) where DEPC-treated water replaced the cDNA template.

Plates were sealed with MicroAmp optical adhesive film covers (Applied Biosystems, Life Technologies #4311971) and the contents mixed thoroughly be inverting 3-4 times. Plates were centrifuged at 300g for

4 minutes to collect the reaction products at the bottom of each well. Plates were then placed into the QuantStudio 6 Flex instrument and run at default running conditions, for 40 cycles, with detection set at FAM-NFQ for the detection of amplification fluorescence.

2.18.4. RT-PCR STATISTICAL ANALYSIS

Cycle threshold (Ct) values were exported from the QuantStudio software as tab-delimited text files and data were transferred to Microsoft Excel for downstream analysis. Ct values were converted to copy numbers of each gene and the RT^- value was substituted from the RT^+ value to correct for amplification of gDNA. Averages of duplicate (technical replicate) wells were calculated and sample copy numbers were then normalised by division against the housekeeper gene, glyceraldehyde-3-phosphate dehydrogenase (Gapdh*)*. Statistical significance was derived using analysis of variance (ANOVA) (n=3) with post-hoc Dunnett's test in TaqMan toolkit (Microsoft Excel plug-in).

2.19. Global Metabolomics Profiling

Liver and plasma samples were sent to Metabolon (Metablon Inc, Durham, NC, USA) on dry ice for global metabolomics analysis. In brief, samples underwent a methanol extraction to remove the protein fraction prior to being placed under a Zymark TurboVap (Biotage AB, Sweden) under nitrogen to remove the organic solvent. Samples were then split into equal parts for analysis on the GC/MS, LC/MS/MS, and polar LC platforms. For liquid chromatography (LC), the samples were stored under nitrogen overnight. For gas chromatography (GC), the samples were dried under vacuum overnight. Bioanalytical methods are briefly described below.

Please note: a pooled matrix sample, generated by taking a small volume of each experimental sample, was used as a technical replicate throughout the metabolomic analysis. This pooled sample was used to distinguish between biological and process derived variability and was randomly included amongst study samples.

Ultrahigh Performance Liquid Chromatography/Mass Spectroscopy (UPLC/MS/MS): The LC/MS portion of the platform was based on a Waters ACQUITY ultra-performance liquid chromatography (UPLC) and a Thermo Scientific Q-Exactive high resolution/accurate mass spectrometer interfaced with a heated electrospray ionisation (HESI-II) source and Orbitrap mass analyser operated at 35,000 mass

resolution. The sample extract was reconstituted in acidic or basic LC-compatible solvents, each of which contained 8 or more injection standards at fixed concentrations. One aliquot was analysed using acidic positive ion optimised conditions and the other using basic negative ion optimised conditions in two independent injections using separate dedicated columns (Waters UPLC BEH C18-2.1x100 mm, 1.7µm). Extracts reconstituted in acidic conditions were gradient eluted from a C18 column using water and methanol containing 0.1% formic acid. The basic extracts were similarly eluted from C18 using methanol and water, however with 6.5mM ammonium bicarbonate. The third aliquot was analysed via negative ionization following elution from a HILIC column (Waters UPLC BEH Amide 2.1x150 mm, 1.7 µm) using a gradient consisting of water and acetonitrile with 10mM ammonium formate. The MS analysis alternated between MS and data-dependent MS^2 scans using dynamic exclusion, and the scan range was from 80-1000 *m/z*.

Gas Chromatography-Mass Spectroscopy (GC-MS): The samples destined for analysis by GC-MS were dried under vacuum for a minimum of 18 h prior to being derivatised under dried nitrogen using bistrimethyl-silyltrifluoroacetamide. Derivatised samples were separated on a 5% diphenyl/95% dimethyl polysiloxane fused silica column (20 m x 0.18 mm ID; 0.18µm film thickness) with helium as carrier gas and a temperature ramp from 60° to 340°C in a 17.5 min period. Samples were analysed on a Thermo-Finnigan Trace DSQ fast-scanning single-quadrupole mass spectrometer using electron impact ionization (EI) and operated at unit mass resolving power.

Metabolon proprietary software was used to match ions to an in-house library of standards for metabolite identification and for metabolite quantitation by peak area integration. Metabolon maintains a library based on authenticated standards that contains the retention time/index (RI), mass to charge ratio (*m/z)*, and chromatographic data (including MS/MS spectral data) on all molecules present in the library. Biochemical identifications are based on three criteria: retention index within a narrow RI window of the proposed identification, accurate mass match to the library ± 0.005 amu, and the MS/MS forward and reverse scores between the experimental data and authentic standards. The MS/MS scores are based on a comparison of the ions present in the experimental spectrum to the ions present in the library spectrum. Peaks were quantified using area-under-the-curve. For studies spanning multiple days, a data normalisation step was performed to correct variation resulting from instrument inter-day tuning differences (pooled plasma). Essentially, each compound was corrected in run-day blocks by registering the medians to equal one (1.00) and normalising each data point proportionately. As such all data presented herein is expressed as scaled intensity of a median equal to 1.00.

3.0. MECHANISMS OF DIMT – GSK932121A INDUCED COMPLEX III INHIBITION

3.1. Introduction

As outlined in section 1.9.1, GSK932121A was developed as a 4(1H)-pyridone antimalarial drug and is a potent, reversible inhibitor of the mitochondrial respiratory chain complex III in *Plasmodium falciparum* (cytochrome bc1 IC_{50} = 0.007μM). The molecule inhibits the same target in mammalian species but with lower potency (two orders of magnitude less potent on the isolated protein target from rats and three orders of magnitude less potent in intact rodent cells). Despite this difference in potency, GSK932121A was withdrawn from development following FTIH trials, due to unexpected toxicology findings in rats, when dosed via the intraperitoneal (IP) route or orally as a pro-drug to increase exposure. Cross-over inhibition of mammalian complex III activity by GSK932121A was considered to be a possibility [127].

A package of investigative work was initiated to follow up on the toxicological findings and the possible role of ETC inhibition. The work presented here describes initial aspects of this investigative program whereby the conditions known to cause the acute toxicity were recreated in order to study the nature of the toxic response.

The analyses presented here provide additional weight of evidence that the main mechanism of toxicity with GSK932121A was mitochondrial complex inhibition and provide significant detail regarding the profile of downstream effects of such inhibition, including molecular adaptive changes. This comprehensive comparison of multiple endpoints also allows for better informed selection of endpoints for future mechanistic investigative studies where mitochondrial toxicity or therapeutic mitochondrial modulation is suspected and highlights the need to consider both *in vitro* and *in vivo* data together when interpreting mitochondrial effects. Finally, the data presented is of significant value in developing an AOP for mitochondrial ETC inhibition, and a follow-up study with earlier time points and a lower dose is presented in chapter 4, to add further detail in this regard.

3.1.1. CHAPTER AIMS

The present chapter describes the first phase of an investigative program which was initiated to explore the acute toxicity caused by GSK932121A, when dosed via the IP route of administration. In order to investigate the adverse effects caused by GSK932121A the conditions which caused the aforementioned acute toxicity were recreated. As such, the present chapter aimed to,

1. Analyse the effects of GSK932121A *in vitro* by treatment of isolated mitochondria from control animals to provide mechanistic detail and to allow comparison with the *in vivo* data.

2. Profile the acute effects of GSK932121A *in vivo*, based on the likelihood that the observed clinical signs in rat were due to complex III inhibition, via measurement of mitochondrial function, liver glutathione levels, hepatic microscopy, blood gasses and lactate/pyruvate ratio alongside gene expression profiling.

3.2. Results

3.2.1. Confirmation of Respiratory Chain Inhibition

The inhibitory effect of GSK932121A on the mammalian respiratory chain was assessed *in vitro* using a complex III activity assay (as described in section 2.8.6). GSK932121A was tested using 9 concentrations spanning the range 0.01nM to 100μM, to ensure accurate determination of an IC_{50}. GSK932121A caused a concentration-dependent reduction in complex III activity with an IC_{50} of 0.63μM (Fig.3.1). Data shown correspond to mean ± SD of measurements obtained with bovine heart mitochondria minus the rates obtained without mitochondria (negative control). The potency of GSK932121A on bovine heart mitochondria complex III was approximately 4.6x less than that of the gold standard complex III inhibitor antimycin A (IC_{50}=136nm as indicated by Cayman Chemicals, data not shown). Furthermore, potency was comparable to that obtained by Bueno *et al* (2012) for cytochrome bc1 inhibition in mammalian species (IC_{50} = 0.4μM with isolated target from HEK293 cells and 0.6μM with the isolated target from H9C2 cells) [127]. Further work is required to compare the effect of GSK932121A on mitochondrial complex III activity to other classical complex III inhibitors, in order to accurately assess potency. Furthermore, the selectivity of GSK932121A for the cytochrome bc1 complex should be assessed by measuring its effect on the other respiratory chain complexes in isolation.

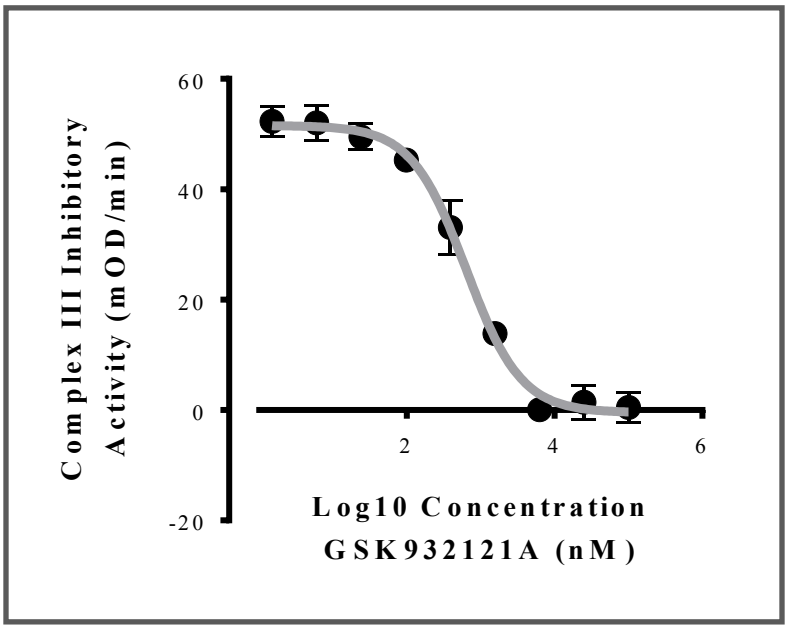


FIGURE 3.1: Complex III activity assay with GSK932121A. A concentration-dependent reduction in bovine heart mitochondrial complex III activity was observed following GSK932121A exposure (IC_{50}: 0.63µM). Data shown in mean ± SD of change in OD rate (per minute) representing conversion of cytochrome c from its oxidised to its reduced form (n=5).

Following confirmation of GSK932121A's complex III inhibitory activity, the effect of GSK932121A on other mitochondrial processes was assessed *in vitro*. Mitochondria were isolated from the liver of 3 control female Crl:CD (SD) rats and exposed to GSK932121A separately *in vitro.* Female rats were chosen for comparability with the sex and species used in the corresponding *in vivo* study (outlined in section 3.2.2 below) and as female rats have been shown to be more sensitive to GSK932121A toxicity than males in previous tolerability studies. Following treatment, OCR and CRC were assessed in order to better understand the direct effect of GSK932121A on mitochondria.

Exposure of isolated liver mitochondria from untreated rats to GSK932121A resulted in concentration-dependent decreases in basal respiration (IC_{50}: 9.5µM) and state 3 respiration (IC_{50}: 5.8µM), characteristic of a mid-respiratory chain inhibitor (Fig.3.2) Maximal respiratory rate and RCR were markedly reduced at 100µM and 10µM, with only minor effects on respiratory chain function observed at lower concentrations. It is however important to ackonowledge that maximal respiration is still stimulated by FCCP with the 10µM concentration of GSK932121A. This data suggests partial inhibition of the respiratory chain which is in contrast to the high level of potency observed in Fig.3.1. (IC_{50} : 0.63µM). Further work is required to better understand the effect of GSK932121A on oxygen consumption *ex vivo.*

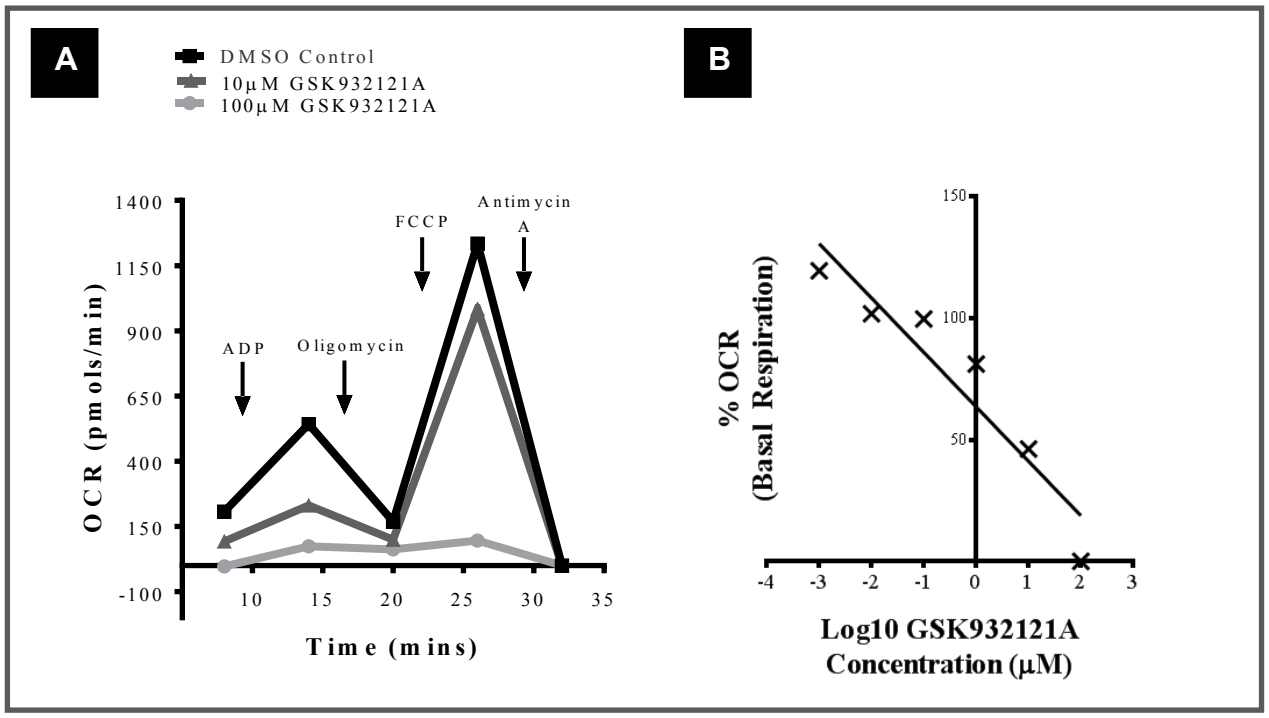


FIGURE 3.2: Analysis of liver mitochondrial OCR following in vitro treatment of control liver mitochondria with GSK932121A (measured using Seahorse XF24 analyser). (A) Exposure to 100µM GSK932121A (light grey) caused a significant reduction in OCR at all respiratory states ($p<0.001$) and a reduction in basal, state 3 and state 3u respiration at 10µM (dark grey) was noted. No other concentration (data not shown) significantly affected mitochondrial respiration compared to that with the 0.5% DMSO control (black). (B) GSK932121A reduced basal OCR in a concentration-dependent manner [IC_{50} = 9.5µM], correlation, R^2: 0.8937 (data is mean only, n=3).

CRC was calculated as the difference in OD between the point at which mitochondria are energised and begin to take up a given bolus of calcium to the point of undergoing MPT. GSK932121A (100µM-1µM) *in vitro* reduced the CRC in liver mitochondria from untreated animals in a concentration-dependent manner with an IC_{50} of 1.36µM (Fig.3.3).

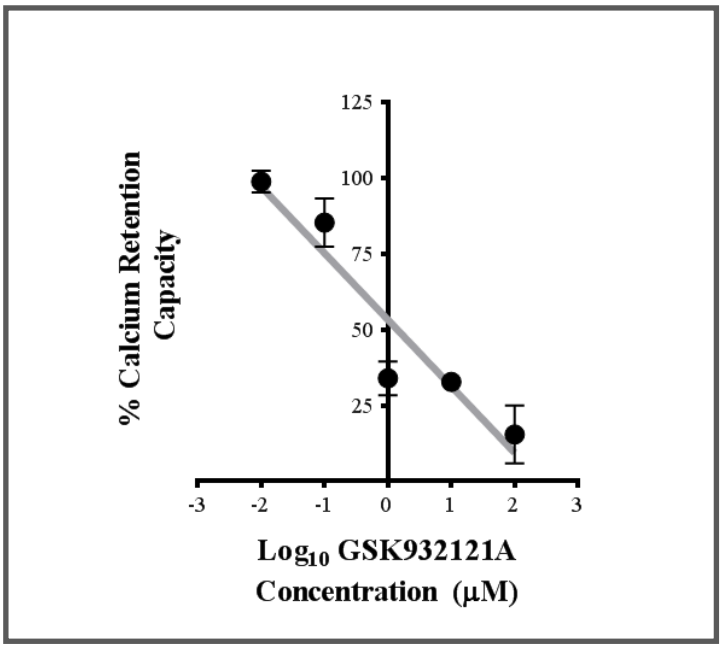


FIGURE 3.3: Assessment of the mitochondrial CRC. Freshly isolated liver mitochondria from female control Crl:CD(SD) rats were treated *in vitro* with GSK932121A. A concentration-dependent reduction in CRC was observed at 1μM, 10μM and 100μM of GSK932121A [IC_{50} = 1.36μM], correlation, R^2=0.9031. Data shown is mean ± SD (n=3).

3.2.2. ACUTE DOSE IN VIVO STUDY (NON MITOCHONDRIAL ENDPOINTS)

Female Crl:CD (SD) rats were dosed (via the IP route) with either 50mg/kg GSK932121A (n=12) or vehicle alone (n=12) and observed for a period of five hours (as described in section 2.1.1 and 2.3.1). Female rats were used because previous tolerability studies using GSK932121A showed slightly more marked in-life effects in female rats than in males. A dose of 50mg/kg was selected based on data generated in previous GSK932121A single-dose tolerability studies where dose-limiting clinical signs were noted in a proportion of the animals at approximately 5.5 hours post-dose. The aim of the investigation was to follow-up on the toxicological issue which led to GSK932121A's termination from development and therefore the 50mg/kg dose (which replicated the dose known to cause acute toxicity) was selected and a time-point of 5 hours was chosen (i.e. to induce mitochondrial derived toxicity whilst minimising in-life effects).

Clinical Signs.

Significant inter-animal variability was noted in terms of both the severity and speed of onset of clinical signs. Moderate clinical signs were observed approximately 3-5 hours post dose and included slight to moderate piloerection, hunched posture, slightly irregular or deep abdominal breathing and mildly

subdued behaviour. Reduction in body temperature was noted in some animals approximately 1.5h post dose, with body temperature continuing to fall by an average of 3.4°C by 5 hours post dose. The reduction in body temperature over the course of the study was highly variable but was closely associated with the plasma concentration of GSK932121A (R^2 0.9063) (Fig. 3.4).

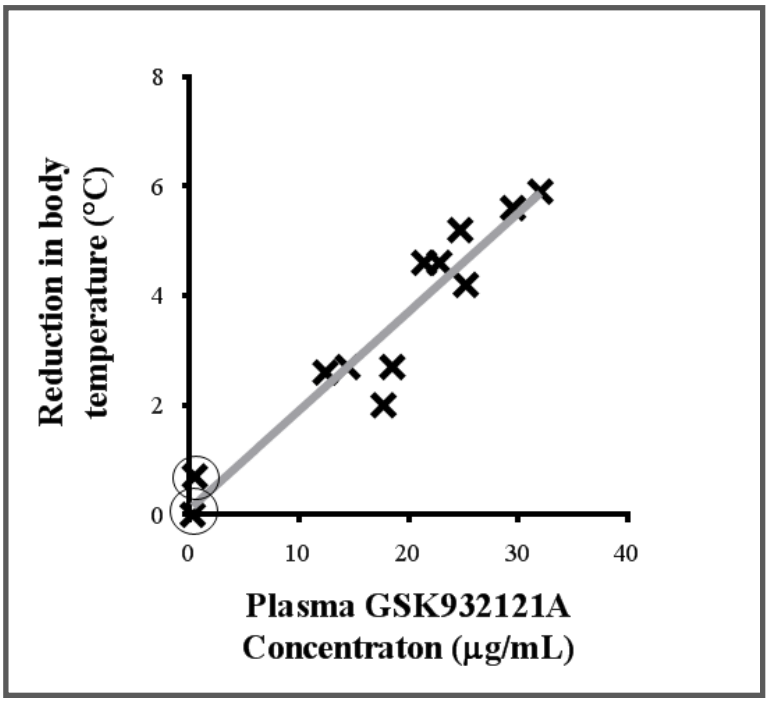


FIGURE 3.4: Relationship between core body temperature and plasma GSK932121A concentration. The correlation is shown between reduction in core body temperature observed at 3.5-5 hours (dependent on observed clinical signs) post treatment with GSK932121A (50 mg/kg) and plasma drug concentration (R^2=0.9063, $p<0.0001$). Two animals (circled) showed little reduction in body temperature but also had a very low systemic exposure (284-485ng/mL) to GSK932121A. These animals were excluded from all further analyses.

No body temperature reduction was observed in two females throughout the course of the treatment period but in these animals the terminal plasma concentrations of GSK932121A were very low (284ng/mL and 485ng/mL, respectively, with all other animals having exposures of ~10-35µg/mL). These animals were therefore excluded from all further analyses. Reduction in body temperature also correlated with adverse clinical signs, those animals with the greatest fall in body temperature showing the most severe clinical effects.

Arterial Blood Gas (pO2 and pCO2) and Bicarbonate (HCO3)

GSK932121A at a dose of 50 mg/kg produced a significant increase in pO_2 and a significant decrease in pCO_2 in arterial whole blood at approximately 5-6 hours post-dose (depending on observed clinical signs)(Fig.3.5). These findings are suggestive of impaired mitochondrial respiration in GSK932121A treated animals consistent with the mechanism of action (ETC inhibition). Bicarbonate (HCO_3) was also reduced in GSK932121A treated rats compared to VC (Fig.3.5) which suggests that metabolic acidosis is occurring following respiratory chain inhibition *in vivo*. This may be as a result of increased lactate production following a metabolic switch to glycolysis which will be presented in the next section.

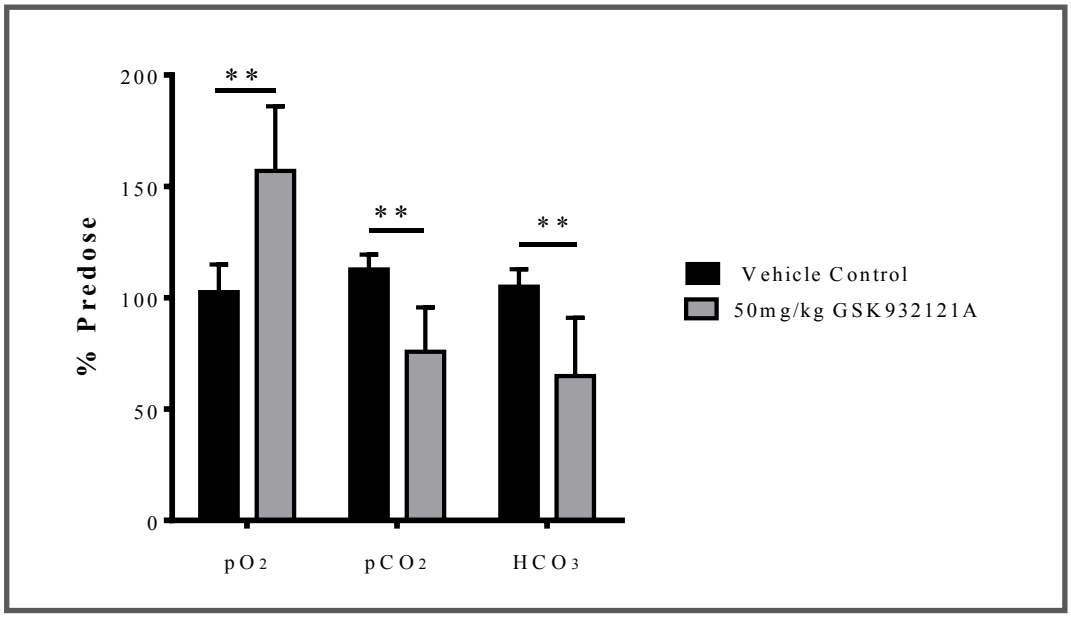


FIGURE 3.5: Analysis of arterial blood gasses ($p0_2$ and $pC0_2$) and bicarbonate (HCO_3) in whole blood of animals treated with GSK932121A (50mg/kg). GSK932121A (50mg/kg – grey bars) caused a significant reduction in arterial pCO_2 and $HC0_3$ at 5 hours post-dose compared with VC (black bars). A significant increase in arterial pO_2 was also observed in GSK932121A treated animals. Results are mean ± SD (n=6) **p<0.01.

The Metabolic Shift: Light and Electron Microscopy

Key histological alterations in the liver following exposure to GSK932121A *in vivo* were identified by light microscopy (Fig.3.6 A and B). Hepatocellular changes included an increase in periportal lipid (microvesicular steatosis) highlighted by prominent osmium tetroxide staining in the livers of the treated group. This is suggestive of a shift in metabolism within the liver towards glycolysis and/or a reduced level of mitochondrial β-oxidation.

Electron microscopy was utilised in order to assess the effect of GSK932121A treatment on mitochondrial ultrastructure. Mitochondria appeared swollen with a pale matrix with moderate to severe

disorganisation of the cristae. Mitochondrial diameter increased from approximately 0.45µm to 0.55µm on average and an increase in the number of condensed degenerating mitochondria was observed with mitochondria often observed within phagosomes (Fig 3.6 C and D). Further to the increase in lipid observed in LM analyses, a reduction in glycogen stores was evident in GSK932121A treated hepatocytes (peri-portal region). This supports LM observations of changes suggestive of increased glycolytic activity.

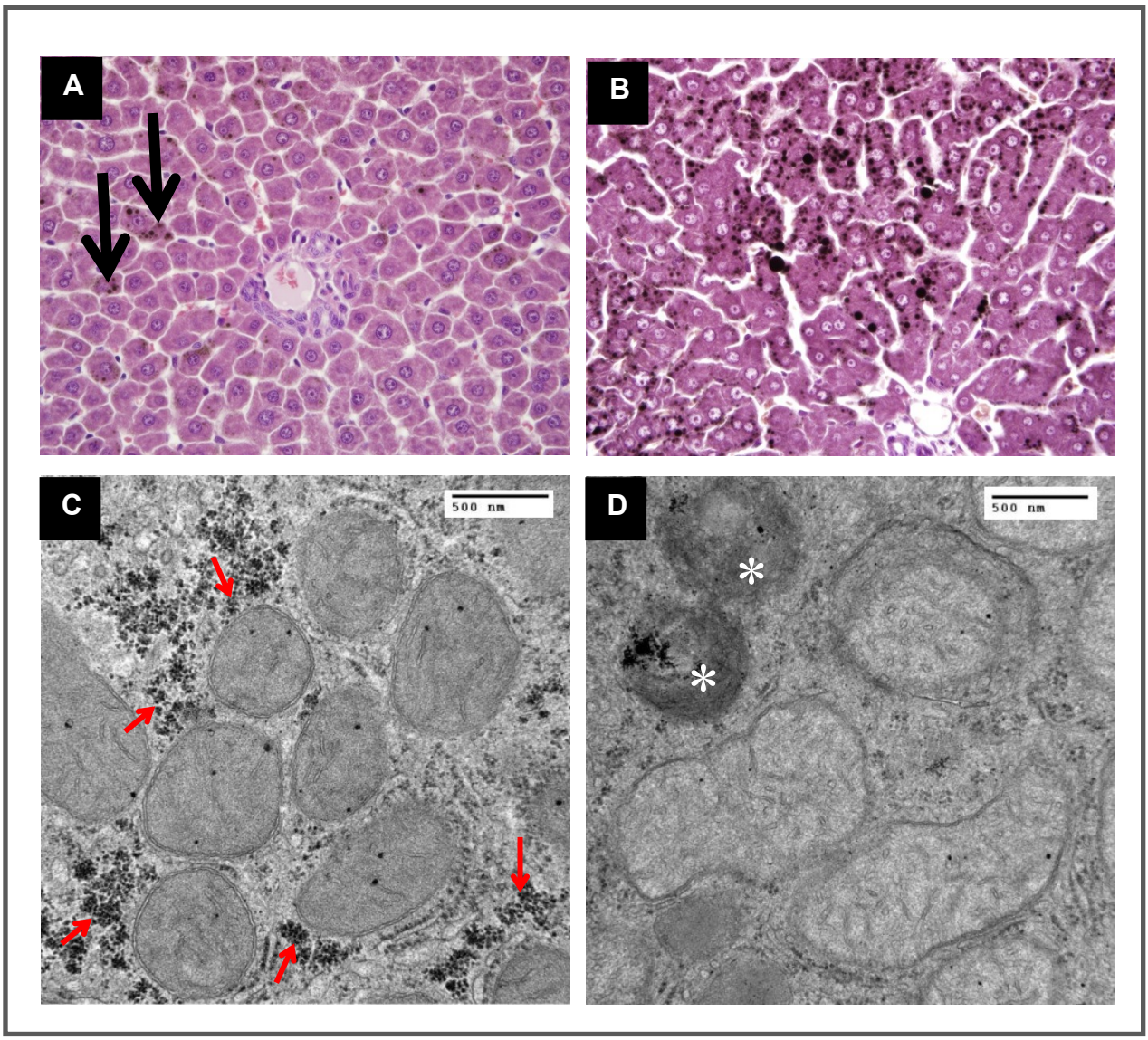


FIGURE 3.6: Effect of 50mg/kg GSK932121A on liver LM and TEM compared to VC. Panels A + B (200x magnification) show H&E stained liver sections post-fixed in osmium tetroxide. (A) VC rat, note the rare hepatocytes that contain a small number of osmium tetroxide-stained lipid droplets (black arrow depicted). (B) Rat treated with 50 mg/kg GSK932121A; note that the cytoplasmic droplets within hepatocytes are extensively and darkly stained with osmium tetroxide which confirms the accumulation of neutral lipid. Panels C+D show electron micrographs of rat hepatocytes from the right lateral lobe focussed on the mitochondria at 50,000X magnification (Images shown are taken from peri-portal regions of the liver). (C) Mitochondria from VC animal, with intact membrane structure and normal histology. Stores of glycogen are depicted by red arrows (D) Mitochondria from GSK932121A treated animal which appear swollen with pale matrices and a significant increase in the number of condensed degenerative mitochondria were observed (white stars). Glycogen stores (highlighted by red arrows in C) were reduced in animals treated with GSK932121A.

To confirm this metabolic shift (reported to be characteristic of mitochondrial dysfunction *in vivo)* circulating lactate and pyruvate were measured in whole blood. Animals given 50mg/kg GSK932121A

had higher blood lactate concentrations than controls (3.53-fold, $p<0.001$) and the lactate:pyruvate ratio was also increased by 1.66-fold ($p<0.01$) (Fig. 3.7). Elevated lactate/pyruvate ratios are indicative of deficiencies of the respiratory chain, tricarboxylic cycle or pyruvate metabolism. Change in lactate:pyruvate ratio correlated with plasma exposure of GSK932121A as shown in Fig.3.7B (R^2: 0.4689, $p<0.05$).

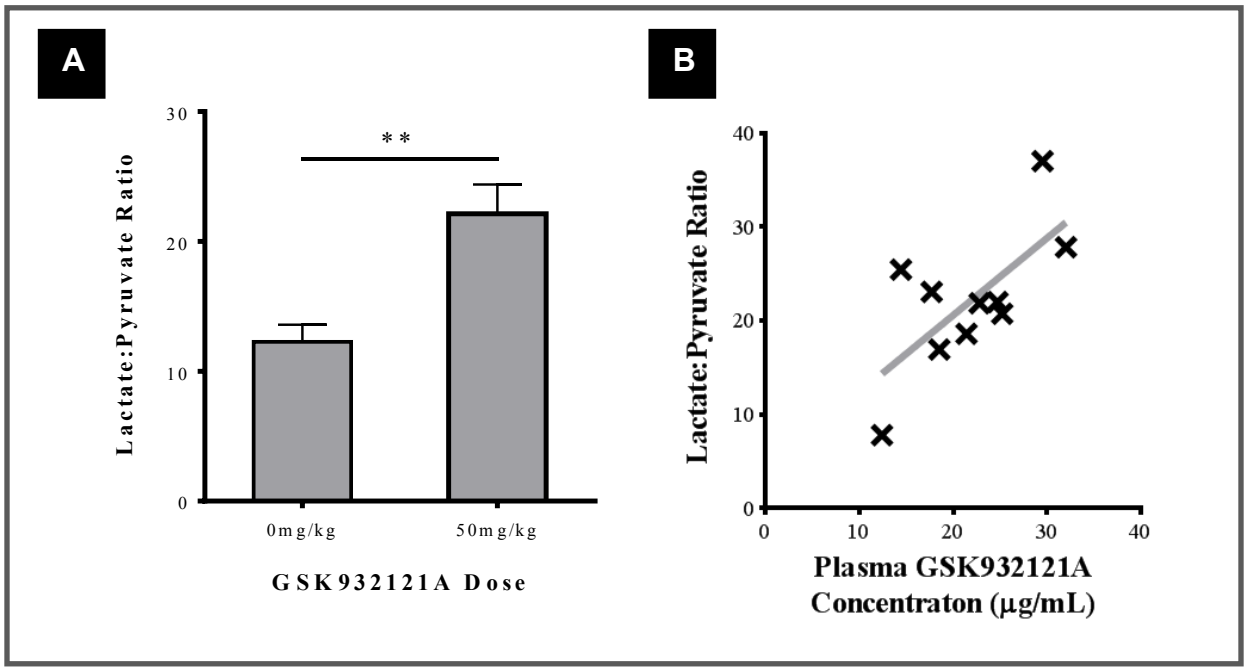


FIGURE 3.7: Effect of 50mg/kg GSK932121A on whole blood lactate:pyruvate ratio compared with blood taken from VC animals. (A) GSK932121A (50mg/kg, n=10) treatment caused a statistically significant increase in blood lactate:pyruvate ratio compared to blood taken from VC animals (n=12). ** $p<0.01$. (B) The correlation is shown between plasma GSK932121A concentration and blood lactate:pyruvate ratio (R^2: 0.4689, $p<0.05$)

Ratio of Reduced Glutathione (GSH) to Oxidised Glutathione (GSSG)

GSK932121A, at a dose of 50mg/kg caused a statistically significant (54.6%) reduction in the GSH:GSSG ratio in liver tissue at a terminal 5 hour time-point compared to VC animals ($p<0.001$) (Fig.3.8C). The reduced GSH:GSSG ratio manifests due to a significant reduction in reduced GSH compared to VC animals ($p<0.05$) and a significant increase in oxidised GSSG in the liver of treated animals compared to VC ($p<0.01$) (Fig.3.8 A and B). This data suggests that treatment of rats with 50mg/kg GSK932121A for 5 hours causes increased levels of oxidative stress and a resulting reduction in the glutathione antioxidant system, in the liver compared with time matched VC animals.

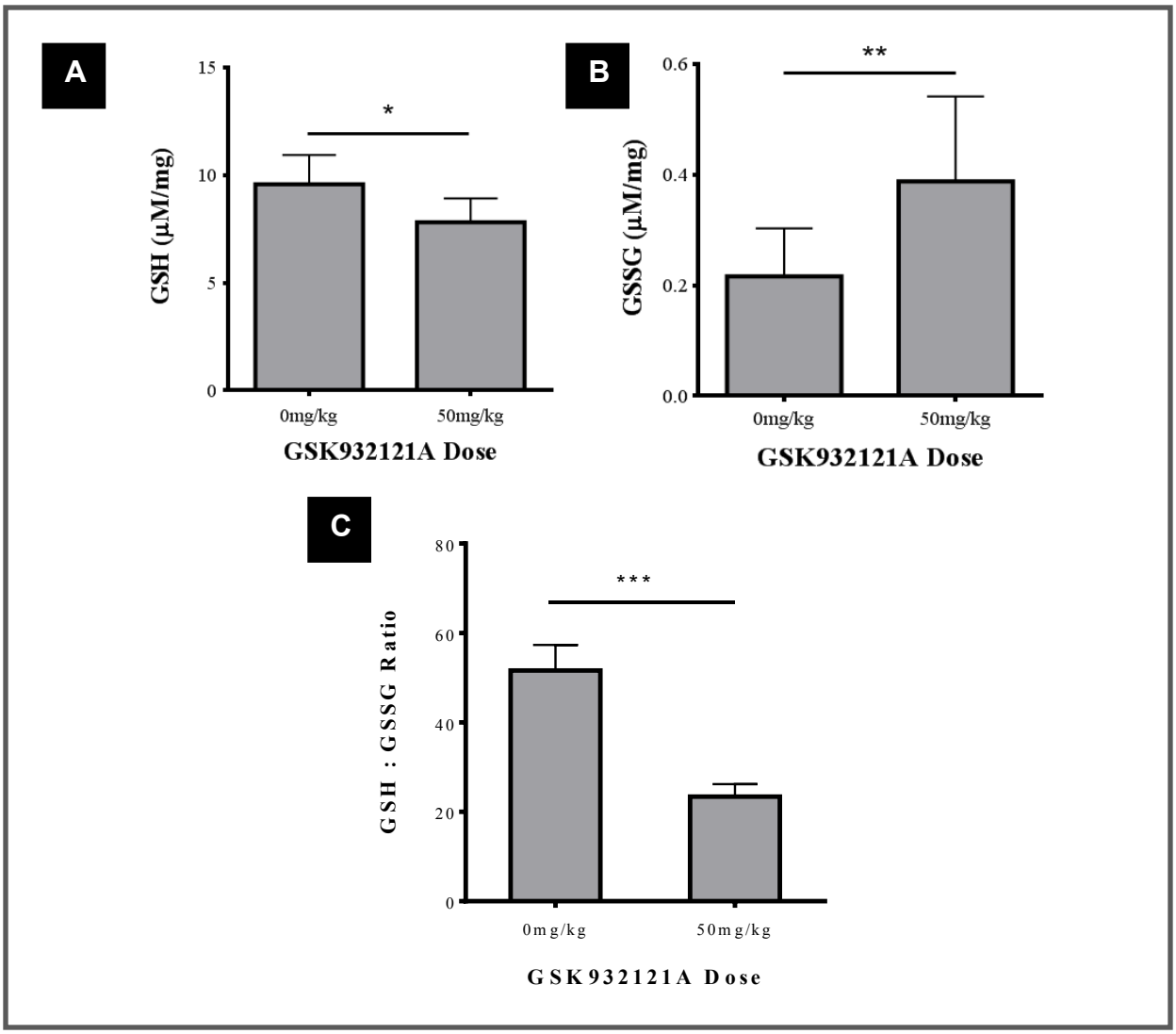


FIGURE 3.8: Analysis of liver GSH, GSSG and ratio of GSH:GSSG following treatment of rats with 50mg/kg GSK932121A compared to vehicle control. GSK932121A (50mg/kg – open bars, n=10) caused a significant reduction in GSH (panel A), a significant increase in GSSG (panel B) and a significant reduction in GSH:GSSG ratio (panel C) in the liver, compared with vehicle controls (0mg/kg - solid bars, n=12). Results are mean ± sd. *p<0.05, **p<0.01, ***p<0.001.

3.2.3. ACUTE DOSE IN VIVO STUDY (MITOCHONDRIAL ENDPOINTS)

Calcium Retention Capacity

In direct contrast to the effects of GSK932121A *in vitro* (Fig.3.3), the CRC of liver mitochondria isolated from rats treated *in vivo* with 50mg/kg GSK932121A was increased, (Fig.3.9A, for clarity only means for the kinetic data are shown). When calculated as delta-OD, the increase in liver mitochondria CRC

following GSK932121A treatment (n=10) was 79% ($p<0.01$) compared with mitochondria from control animals (n=12), (Fig. 3.9B). These data demonstrate a desensitisation to calcium-induced mPTP opening following *in vivo* treatment with GSK932121A. Increase in liver mitochondria CRC showed a mild degree of correlation to the plasma concentration of GSK932121A (R^2: 0.4939, $p<0.05$).

No effect was observed on CRC in mitochondria isolated from the heart or skeletal muscle of GSK932121A treated animals in comparison with VC ($p>0.05$, data not shown). There was also no correlation to plasma exposure levels of GSK932121A in these tissues. It is currently unknown whether this was a result of lower plasma exposure levels in these organs and follow-up pharmacokinetic analyses in multiple tissues are required.

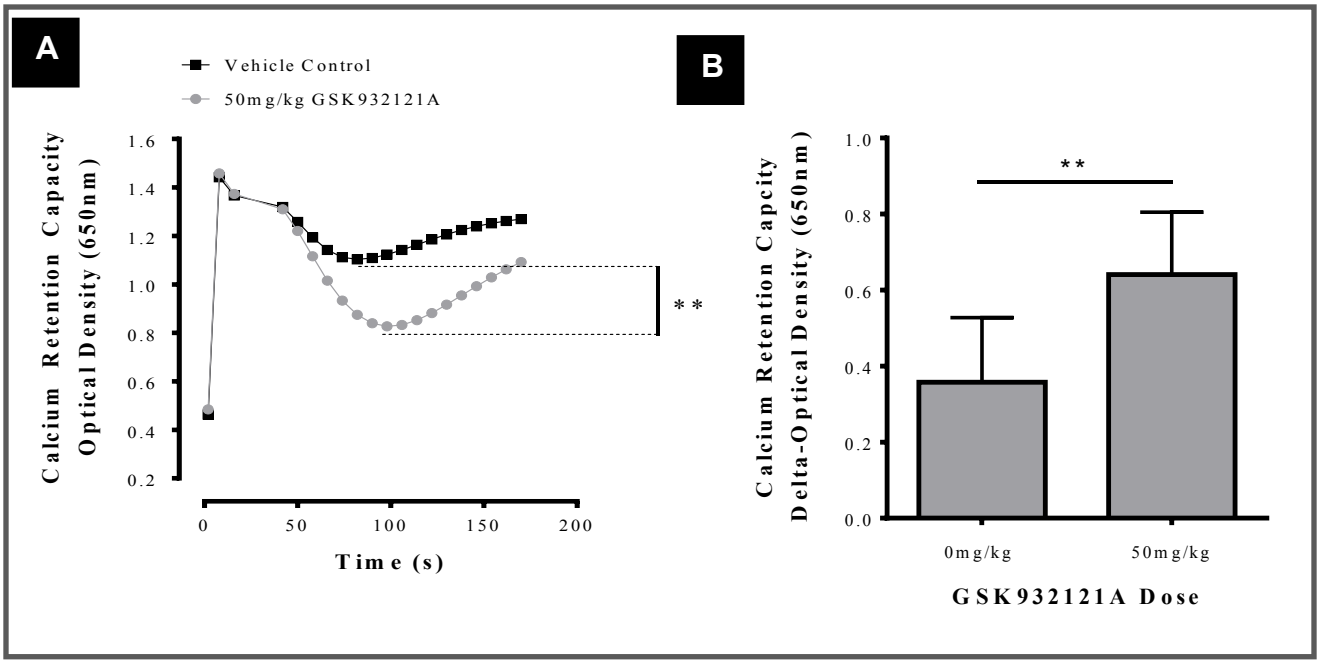


FIGURE 3.9: Analysis of liver mitochondrial CRC following treatment of rats with GSK932121A *in vivo*. (A) Mitochondria isolated from rats treated with 50 mg/kg GSK932121A (n=10, grey circles) displayed an increased CRC compared to control animals (n=12, black squares) treated with vehicle alone. Data shown in this kinetic trace are mean only (B) The increase in GSK932121A-induced CRC is displayed as increase in ΔOD (difference in OD between point of succinate substrate addition and mitochondria undergoing permeability transition, i.e. lowest OD value before calcium release). Data shown is mean ± SD. ** $p<0.01$.

Mitochondrial Bioenergetics

In contrast to the effects seen *in vitro*, mitochondria isolated from the livers of rats treated *in vivo* with GSK932121A, showed an increase in basal respiration of 30.3% compared to VC ($p<0.001$) (Fig. 3.10 A

and B). A similar degree of increased respiratory demand is maintained throughout state 3 (27.5%, $p<0.01$) and state 4 (28.4%, $p<0.001$), demonstrating increased background levels of oxygen consumption linked to ATP production (Fig. 3.10 A and B). This increase in OCR further coincides with an 11.9% ($p<0.001$) increase in proton leak across the inner mitochondrial membrane. Whilst increased proton leak is suggestive of a decline in efficiency of the OXPHOS machinery, the percentage of total OCR linked to ATP synthesis was the same in mitochondria from control and treated after normalisation to basal respiration (Fig. 3.10 C). Furthermore the RCR (state 3/state 4 ratio), often used as a gold-standard measure of general mitochondrial health, was not significantly altered between mitochondria isolated from control (4.25) and GSK932121A treated (4.20) rats ($p>0.05$ – data not shown). FCCP was used to uncouple mitochondria and determine the maximum respiration rate (often termed the maximal uncoupled or state 3u respiration). This was reduced by 24.7% in mitochondria isolated from GSK932121A treated rats ($p<0.001$) indicating a diminished maximal capacity for the ETC in the uncoupled state. This is particularly visible in Fig.3.10C where normalisation of data to basal respiration highlights the maximal OCR deficit following FCCP-induced uncoupling. Correlation analysis between the various respiratory states and the plasma concentration of GSK932121A revealed only marginal correlation to plasma exposure levels as shown in the R^2 values in Fig 3.10B.

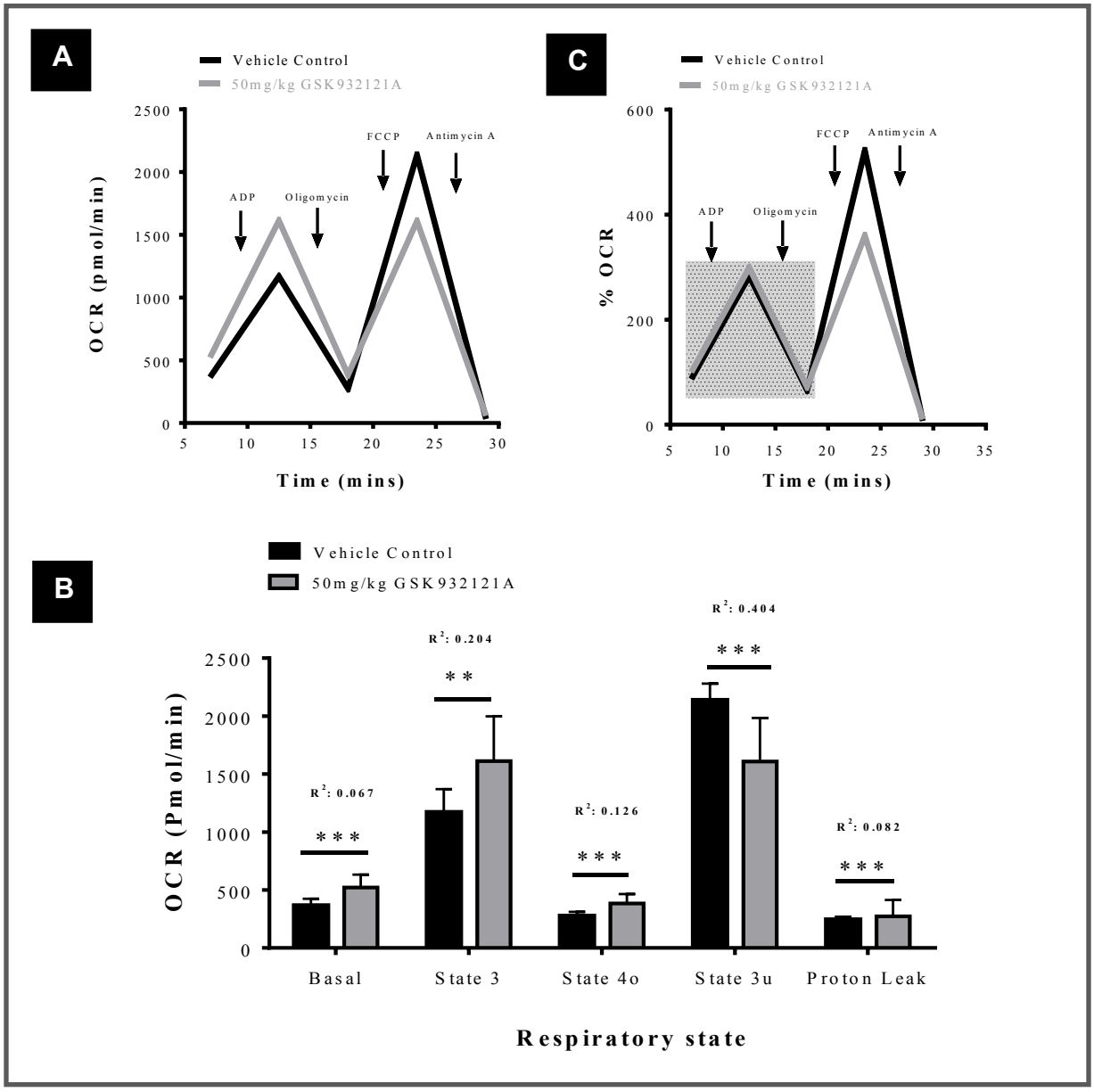


FIGURE 3.10: Analysis of liver mitochondrial bioenergetics using the Seahorse XF24 analyser following treatment of rats with GSK932121A *in vivo* (A) Representative OCR data for liver mitochondria isolated from animals treated with GSK932121A (grey line) or VC (black line). (B) Effect of GSK932121A treatment (grey bars) on basal, state 3, state 4o, state 3u respiration and on proton leak, compared with VC (black bars). R^2 values correspond to the correlation between OCR and the plasma concentration of GSK932121A (C) Normalisation of OCR data to basal respiration, demonstrating the lack of significant change in total ATP linked OCR (shaded box) between mitochondria isolated from control (black line) and treated (grey line) animals and the reduction in maximal uncoupled respiration. Data shown is mean ± SD (n=12 VC, n=10 GSK932121A treated). Each biological replicate is the mean of 5 technical replicate wells / XF24 plate ** $p<0.01$, *** $p<0.001$

Overall mitochondria from rats treated *in vivo* with GSK932121A showed a loss of mitochondrial reserve capacity ($p<0.001$, 74.47% reduction) calculated as the difference between state 3 and state 3u OCR

highlighting the potential for bioenergetic insufficiency should the cells require ATP levels beyond that which can be manufactured at a basal level.

No significant effect on OCR was observed in mitochondria isolated from the skeletal muscle or heart of GSK932121A treated animals compared to VC ($p>0.05$, data not shown). Isolated mitochondrial data presented in section 3.2.3 therefore suggests that the liver might be a key target organ in response to GSK932121A toxicity and no effects of GSK932121A was observed in skeletal muscle or heart mitochondria (in terms of mitochondrial function). The suggestion that the liver is a key target organ will be further explored in chapter 4.

3.2.4. TRANSCRIPTOMICS

Transcriptomic analysis was performed on liver samples from control and GSK932121A treated rats. The entire raw gene-data (discussed herein) has been deposited in NCBI's Gene Expression Omnibus (GEO) and are accessible through GEO Series accession number GSE65374 (http://www.ncbi.nlm.nih.gov/geo/query/acc.cgi?acc=GSE65374). Affymetrix data was normalised using the robust multichip average (RMA) method [145] and differentially expressed genes were defined as those with greater than 1.5 fold change in expression, at $p<0.05$. These genes were examined using a principal component analysis (PCA) and interestingly separation of data-points for treated animals from those for VC, correlated well with plasma drug concentration, as shown in Fig.3.11 below.

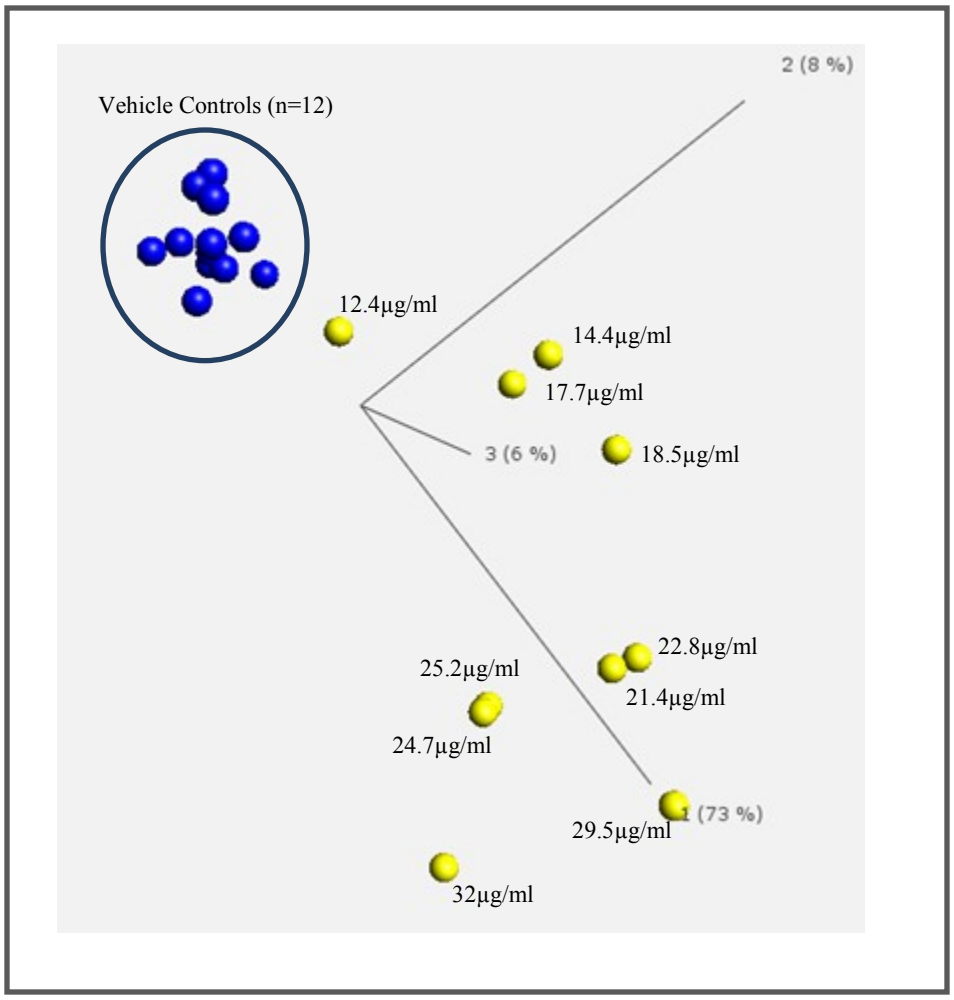


FIGURE 3.11: PCA of Affymetrix transcriptomics data (from liver of GSK932121A and VC animals) highlighting relationship between degree of experimental data separation and plasma drug concentration. PCA analysis showing the breadth of data separation between VC (blue circles) and GSK932121A treatment (yellow circles). Separation of data points in the PCA analysis appeared to correlate with plasma drug exposure levels (expressed in µg/ml).

Following PCA analysis, these genes were subjected to IPA analysis (Ingenuity Systems, Redwood City, CA). This analysis identified perturbation of pathways associated with the cellular response to glycogen depletion, with glucocorticoid receptor signalling the most significantly up-regulated. Other pathways identified were immunological (IL10, IL6 and Acute Phase response signalling) and activation of retinoic acid receptor responsive genes (data not shown). The ratio of genes involved in each identified pathway was low (less than 10%), for example for the glucocorticoid receptor signalling pathway 24/299 genes were altered (8.02%). Consideration of these data alongside the observed increase in blood lactate and observed depletion of cellular glycogen (TEM micrographs) did however prompt further analysis of genes

involved in the cellular response to glycogen depletion. Peroxisome proliferator-activated receptor gamma coactivator 1-alpha (Ppargc1a) was upregulated 8.2-fold ($p<0.001$) and Forkhead box protein O1 (Foxo1) expression increased 1.6-fold. Ppargc1a and Foxo1 interact to coordinate the expression of genes involved in gluconeogenesis, such as Pck1/PEPCK (1.9-fold; $p<0.001$) and Glucose-6-Phosphatase (G6pd). Ppargc1a and Foxo1 expression levels both correlated well with GSK932121A plasma concentrations (R^2: 0.6587 and 0.7493 respectively) (Fig. 3.12). Insulin Receptor Substrate 2 (Irs2) and Pyruvate Dehydrogenase Kinase 4 (Pdk4) expression levels, which were upregulated 4.8 and 2.2-fold respectively, also correlated well with GSK932121A plasma levels (Fig.3.12).

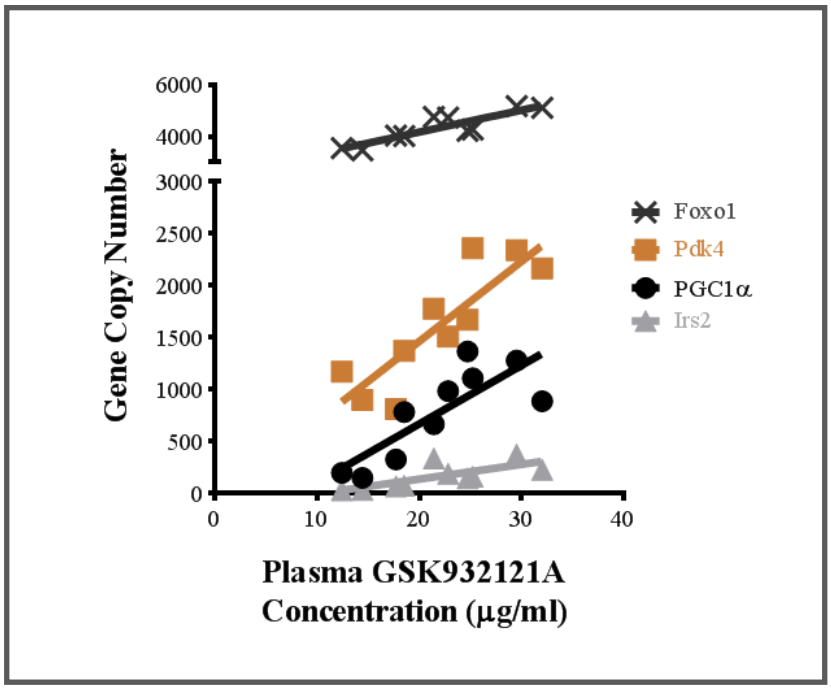


FIGURE 3.12: Correlative analysis of gene copy number for 4 significantly altered genes and GSK932121A plasma concentration. Correlation between terminal plasma GSK932121A concentration in treated rats and the copy number of 4 hepatic gluconeogenic response genes, Foxo1 (dark grey crosses) (R^2:0.7943), Pdk4 (orange squares) (R^2:0.7389), Ppargc1a (black circles) (R^2:0.6587) and Irs2 (light grey triangles) (R^2:0.5457). The expression of all four genes was significantly increased compared to VC ($p<0.001$).

3.3. Discussion

It is important for successful drug development that we improve our understanding of how mitochondrial toxicity is manifested in our preclinical test species. To this end, and as part of a mechanistic toxicology investigation, the present study profiled the acute toxicity caused by a candidate molecule

(GSK932121A), suspected of causing acute toxicity by complex III inhibition *in vivo*. The work highlighted the utility of a multi-system approach for detecting mitochondrial dysfunction *in vivo*, and should aid other investigators in designing studies and selecting endpoints for future studies with potentially mitochondrially active molecules. GSK932121A is a potent inhibitor of the mitochondrial respiratory chain complex III in the target species, *P. falciparum*. It is two orders of magnitude less potent on the isolated target from rats, and three orders of magnitude less potent in intact rodent cells [127]. At the dose of GSK932121A used in the present study, the plasma concentrations achieved were 2-6 times above the IC_{50} in rodent cells and, consistent with this, it was acutely toxic. Blood gas analysis in the present study confirmed inhibition of respiratory function highlighted by an increase in the levels of arterial O_2 and a reduction in arterial CO_2. It remains likely that the animals are in a state of "cytotoxic hypoxia", characterised by effective oxygen deprivation (i.e. inability of cells to utilise oxygen as opposed to impaired oxygen availability). This has been highlighted as a central cause of toxicity relating to other respiratory chain inhibitors such as cyanide [148].

Body temperature changes have been reported with a range of mitochondrial toxins acting by different mechanisms, for example, 2,4-DNP (mitochondrial uncoupling) causes hyperthermia [149] and 3-nitroproprionic acid (complex II inhibition) causes hypothermia [150]. In the present study, hypothermia was an early consequence of treatment of rats with GSK932121A, the magnitude of the response correlating well with plasma levels of the drug, suggesting that respiratory chain inhibition was the primary cause of the reduced thermal energy generation. Of the gross in-life measures, body temperature appeared to be the most sensitive marker of mitochondrial impairment, at least when monitored internally (core temperature) and measured regularly (15 minute intervals) via the implanted chips used in this study. The liver is a major thermoregulatory organ in the rat [151] and therefore the reduction in body temperature may be directly associated with disruption of mitochondrial function and morphology changes noted in this organ. The value of monitoring body temperature demonstrated here, combined with the ease of data collection when using implantable chips (which are primarily used for animal identification), means that this endpoint would be suitable for consideration in all *in vivo* studies with compounds suspected of having mitochondrial activity.

Lactic acidosis and an increase in hepatic lipid (steatosis) are common outcomes of mitochondrial dysfunction [152], as observed with the early nucleoside reverse transcriptase inhibitors [153]. Both of these outcomes were observed in this study. The increase in lactate/pyruvate ratio suggests an increase in glycolytic metabolism and this is supported by the TEM evidence of glycogen depletion in the liver of treated rats. Furthermore, the blood gas data was also suggestive of metabolic acidosis, with a reduction

in bicarbonate noted. Combined with body temperature, lactate levels are a potentially useful marker of DIMT [143] and it has been suggested that a rise in blood lactate concentrations alongside a reduction in core body temperature may be indicative of a generalised adverse event [154]. Further studies with GSK932121A at sub-toxic doses are on-going and it will be interesting to see if lactate:pyruvate ratio can be utilised as a marker of more mild underlying mitochondrial perturbation.

The switch in metabolism towards glycolysis, indicated by ultrastructural changes and blood lactate levels, was also reflected in the gene expression findings. Foxo1 was up-regulated following GSK932121A treatment and this gene has been shown to play a central role in the response to glycogen depletion via activation of gluconeogenesis [155]. Foxo1 interacts with PGC1α to regulate the expression of gluconeogenic genes by binding and activating promoter regions, for example, the PGC1α-dependent transcription of Pepck [156]. Pepck catalyses the first committed step in gluconeogenesis via conversion of oxaloacetate to phosphoenolpyruvate [157]. Foxo1 is also essential to the up-regulation of Pdk4 and Irs2 in response to glycogen depletion and fasting and these were up-regulated in the present study [155]. This fasted/starvation-like transcriptional response has previously been associated with respiratory chain deficiency and mitochondrial myopathy [158]. These gene findings demonstrate a potentially adaptive response to reduced liver glycogen by activation of gluconeogenesis via Foxo1 mediated transcription.

With regard to the functional mitochondrial endpoints, specifically OCR and CRC in this study, GSK932121A had effects both *in vivo* and *in vitro,* however the direction of change was not consistent. It is unlikely that this difference is due to a metabolite of GSK932121A since it is known that there is limited metabolism of the compound within the timescale applicable here. *In vitro*, GSK932121A reduced basal mitochondrial OCR in HepG2 cells, entirely consistent with its proposed complex III inhibitory activity and effects of other known respiratory chain inhibitors (shown in chapter 7) [6, 132]. The same effect was observed when isolated liver mitochondria from naïve control rats were directly exposed to GSK932121A. In contrast, the opposite was true with liver mitochondria isolated from rats treated with GSK932121A *in vivo*, where basal OCR was seen to be increased. In the same vein, the CRC of isolated liver mitochondria from naive control rats was reduced following direct exposure to GSK932121A, again consistent with the effects of other known respiratory chain inhibitor compounds, but opposite to the effect observed in mitochondria isolated from the livers of rats treated with GSK932121A *in vivo*.

It is clear then that the *in vitro* functional data are consistent with GSK932121A's proposed complex III inhibitory mechanism and published data regarding other tool ETC inhibitors. Likewise the body temperature findings, LM/TEM, gene expression, blood lactate and gas analyses findings also point

convincingly to GSK932121A blocking mitochondrial complex activity as expected. So why are the functional measures (OCR and CRC) obtained with the mitochondria isolated from animals treated with GSK932121A *in vivo* seemingly at odds with the overall picture?

In terms of the OCR data, it may be that GSK932121A washes out during isolation of the liver mitochondria from treated rats. However, here samples of isolated mitochondria from the *in vivo* experiment were analysed for GSK932121A and appreciable levels were detected (appendix 3). The was also a reduction in the maximal OCR following FCCP treatment and a clear effect in the CRC assay (discussed below) in the mitochondria isolated from treated animals, arguing against a complete washout of compound and reversal of effects during the isolation procedure. An alternate possibility is that the increase in OCR reflects a compensatory increase in the overall ETC activity within the isolated mitochondrial population as a result of increased proton leak due to ROS-induced mitochondrial damage. Consistent with other respiratory chain inhibitors (i.e. antimycin a [159]), there was evidence for an increase in oxidative stress in the livers of GSK932121A treated animals (significantly reduced GSH: GSSG ratio), but for ROS-induced damage to be a causative factor in the observed OCR increase, this would again rely on the de-inhibition of the ETC. A third possibility may be linked to stabilisation of the mitochondria and this is discussed below.

Mitochondria play a key role in regulating intracellular calcium concentrations during both normal and pathological states [134]. However, excess calcium is able to trigger the mPTP, characterised by a non-selective increase in the permeability of the inner mitochondrial membrane [135, 136]. mPTP activity is affected by compounds that interfere with mitochondrial function and this can be monitored by measurement of CRC in mitochondrial isolates. Exposure *in vitro* to respiratory chain inhibitors typically reduces the CRC of isolated mitochondria [160] and this is exactly what was observed with GSK932121A (IC_{50} of 1.36µM, well below the plasma concentrations of GSK932121A achieved in the *in vivo* study, ~30-75µM). In contrast liver mitochondria isolated from GSK932121A treated rats showed a significant and unexpected increase in CRC. It has been reported that the mPTP can be desensitised to calcium-induced opening during times of myocardial infarction due to a reduction in pH [161]. It is possible that the lactic-acidosis induced pH reduction, observed in rats treated with GSK932121A, may cause an effect on the mPTP *in vivo* that persists and is maintained throughout the isolation procedure and CRC assay, i.e. despite the mitochondria being prepared and the CRC assay being performed in neutral pH buffers. Furthermore, the observed desensitisation of mPTP triggering could act to stabilise the mitochondria during the stressful isolation process, resulting in a higher proportion of intact (non-permeabilised)

mitochondria per mg of measured protein; potentially explaining the increase in basal OCR level observed with mitochondria from the treated animals.

Mitochondria are capable of responding to increased energy demand or stress by utilising their spare respiratory reserve (i.e. the difference between basal respiration and maximal possible respiration rates) [39]. Significant depletion of this reserve capacity has been noted in response to increased ROS, aging, following drug exposure [162] and importantly, has been demonstrated to precede cell death [37]. One consistent functional effect observed both *in vitro* and *in vivo* in this study was an apparent reduction in the maximal respiration rate following GSK932121A exposure (i.e. uncoupled OCR following FCCP injection). This raises the question of whether monitoring erosion of maximal respiratory capacity, in the absence of overt clinical signs, could be a way to overcome a key limitation of current preclinical safety testing with respect to detecting mitochondrial toxicity; namely the use of healthy young animals with inherently high reserve capacity. This current pre-clinical model is at odds with the low underlying metabolic reserves of many key patient groups who are often elderly, on co-medications, have co-morbidities etc. A more detailed analysis of metabolic reserve capacity using doses of GSK932121A below that which cause overt clinical signs would help to test this possibility and this is on-going.

3.3.1. SUMMARY

The conclusions that can be drawn from this initial study with GSK932121A are as follows…

1. The *in vitro* and *in vivo* data presented here support the proposition that GSK932121A administered at 50mg/kg via the IP route causes acute toxicity in rats due to perturbation of mitochondrial function, most likely via inhibition of the ETC.

2. Building understanding around the progression of toxicity from complex III inhibition to adverse *in vivo* outcomes (clinical signs) required consideration of both the *in vitro* and *in vivo* data; neither on its own would have been sufficient. The *in vitro* data informed on the likely molecular initiating event and initial (non-confounded) respiratory response, whist the *in vivo* data provided a view of the integrated state of the mitochondria in response to the initial insult plus the compensatory adaptations made by the tissue and organism. The *in vivo* experiment also informed on the final adverse outcomes and provided a platform to investigate specific molecular and morphologic changes in a key tissue, for example, highlighting the role of the metabolic switch

gene Foxo1 and the downstream effectors PGC1α, Pepck, Pdk4 and Irs2 in the cellular response to glycogen depletion in the liver.

The data presented here provides the ground work for developing AOPs around ETC inhibition and also provides a platform for evaluating new methods for monitoring underlying mitochondrial perturbation. Further work based on a systems approach is required in order to further understand the downstream mechanisms and pathways [163], of which the metabolomics based follow-up investigation presented in chapter 4 overleaf is part.

4.0. A METABOLOMICS APPROACH TO UNDERSTANDING MECHANISMS OF DRUG-INUDCED RESPIRATORY CHAIN INHIBITION

4.1. Introduction

GSK932121A was a late stage drug, destined for the market as a novel 4(1H)-pyridone anti-malarial medicine with huge therapeutic potential, (i.e. due to the prevalence of malaria in the developing world). GSK932121A acts via inhibition of mitochondrial electron transport at complex III. The molecule was however withdrawn from development following observations of acute toxicity in rats at high plasma exposure levels following administration either via the oral route as a pro-drug or via the IP route as the parent compound alone.

Work outlined in chapter 3, described stage one of an investigative package which aimed to evaluate the acute toxicity caused by compounds, including GSK932121A, with potent respiratory chain inhibitory properties. The study revealed that, (in conjunction with the adverse in-life effects), respiratory chain inhibition caused a switch in metabolism to glycolysis (leading to metabolic acidosis, hepatic steatosis and liver glycogen depletion), rapid onset hypothermia and effects on mitochondrial ultra-structure and function (although the direction of change in two commonly used mitochondrial assays was opposite to that observed *in vitro)*. Transcriptomics analysis also identified gene changes indicative of a fasted-like state.

Although the initial study (described in chapter 3) was necessary to characterise the acute toxicity profile of GSK932121A *in vivo* at a dose associated with the adverse outcome, the high dose single time point experimental design made it a challenge to determine the events preceding overt clinical signs i.e. difficult to assess primary from adaptive toxicity. It was therefore important to follow up these findings with GSK932121A using a sub-toxic dose and earlier time points. Metabolomics was used to seek both early and progressive biochemical markers of respiratory chain inhibition.

In order to correlate the early biochemical effects to a functional and well characterised effect, the study parameters outlined in chapter 3 were repeated (i.e. an acute IP dose of 50mg/kg GSK9232121A over a 4 hour time point) with timed bleeds used for metabolite analyses in order to identify early biochemical changes. A lower dose group of 12.5mg/kg GSK932121A (a dose which was previously reported to be well tolerated) was included in order to identify markers of respiratory-chain inhibition which occur at sub-toxic doses of GSK932121A and to facilitate the determination of pathways involved in underlying mitochondrial adaptation and perturbation. Timed bleeds were taken as early as 30 minutes post dose in attempts to identify the earliest possible markers of dysfunction.

Biochemical metabolites are sensitive indicators of homeostatic changes (whether induced by genetics, the environment, drug treatment etc.). This makes them excellent candidates for biomarkers as they can be easily measured and, if present in blood, are accessible and translatable to the clinical situation. In addition, metabolites play a crucial role in the signalling and regulation of genes and proteins thus making them an ideal complement to other 'omics' assessments. Finally, because metabolic pathways are generally well understood and highly translatable across species, metabolomics data is often highly actionable in terms of assessing potential safely liability using a top-down systems biological approach [164]. Metabolites were mapped to their biochemical pathways and those that exhibited statistically significant, time/dose-dependent; compound-related changes in comparison to the time-matched control groups are herein discussed.

4.1.1. CHAPTER AIMS

The purpose of this study was to…

1. Confirm mitochondrial functional changes observed with GSK932121A in chapter 3 (with a 50mg/kg dose) and assess the effect of a well tolerated 12.5mg/kg dose on underlying mitochondrial function and clinical measures.

2. Evaluate potential plasma and liver biomarkers of mitochondrial toxicity (specifically mid-respiratory chain inhibition) using a global metabolomics approach and assess the pathways implicated in the toxicological response to complex III inhibition via analysis of plasma metabolites at progressive time points and liver metabolites at the terminal time point.

4.1.2. STUDY DESIGN

Crl:CD(SD) rats were exposed to GSK932121A essentially as described for chapter 3. Six or seven rats per group were sampled for plasma prior to compound treatment (pre-dose) and then exposed to either 12.5mg/kg GSK932121A (n=7), 50mg/kg GSK932121A (n=7) or vehicle alone (n=6). The number of animals for each group was based on the known potential for low systemic exposure levels using the IP route of administration for this compound and to provide sufficient statistical power for metabolomics assessment. Plasma samples were then taken at 0.5, 1, 2 and 4h with time-matched VC samples taken in

parallel. Terminal liver samples were also harvested at the end of each study for a total of 100 plasma samples and 20 liver samples for analysis.

Plasma and liver samples were stored at -80°C and sent to Metabolon on dry ice for analysis (as described in section 2.19). Liver tissue was also used to isolate fresh mitochondria in order to both confirm mitochondrial function changes highlighted in chapter 3 (increase in basal OCR and increase in CRC) and investigate whether these changes occur at a sub-toxic dose of GSK932121A. Blood toxicokinetics and lactate/pyruvate analysis were also performed.

4.1.3. METABOLOMICS DATA VISUALISATION

Metabolomics data presented throughout section 4.2 below can be interpreted based on the schematic shown in Fig.4.1 below. Plasma metabolite data is depicted using line charts to demonstrate the change in scaled ion levels throughout the 4 hour time period (mean ± standard error). Liver metabolite data is presented in the same y-axis scale although using a box and whisker plot to show the key statistical parameters. All data is presented as a scaled intensity of the total ion counts for each metabolite whereby the median ion level for each metabolite is equal to 1.00. Total ion counts were used as opposed to absolute quantification to ensure that the relative quantitation of each biochemical is consistently made on the parent ion for a specific platform (e.g. LC/neg, LC/pos, etc) and as it is the degree of change that determines the outcome, not the absolute level. This method ensures the quantitation of each biochemical is made consistently.

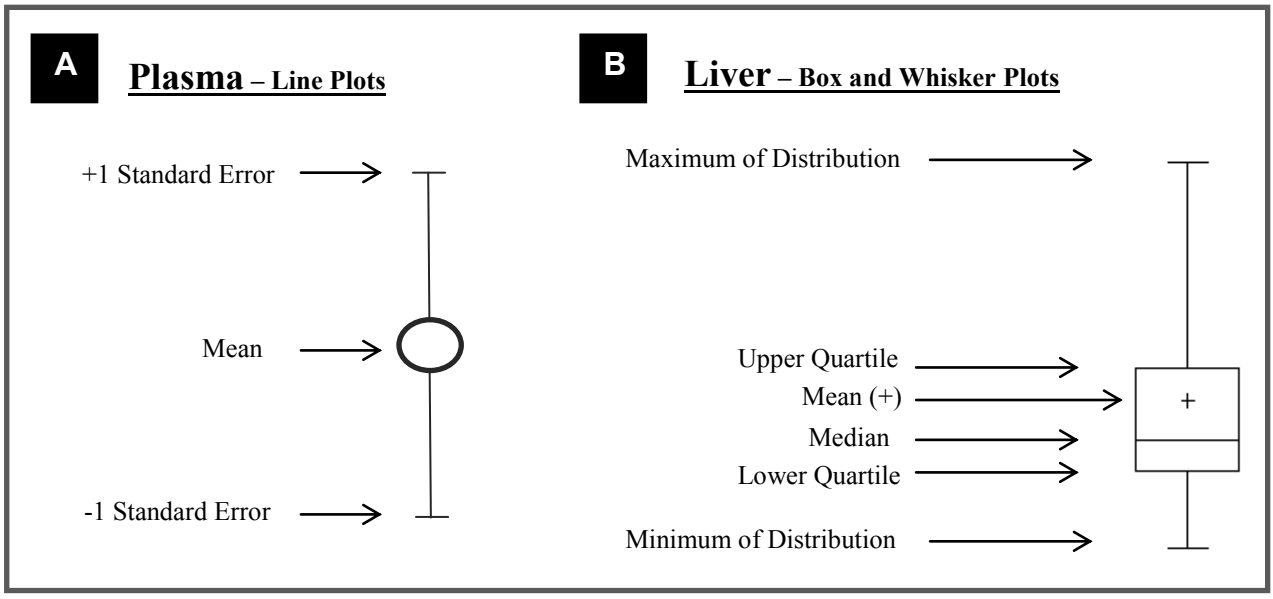


FIGURE 4.1: Metabolomics data visualisation. Visualisation of the study data in line or box plot format (A) Plasma data is represented by line plots with mean ± standard error plotted. (B) Box plots are used to convey the spread of the data with the middle 50% of the data represented by the boxes and the whiskers reporting the range of the data. The solid line across the box represents the median value of the data while the + is the mean. All metabolomics data are scaled such that the median value measured across all samples was set to 1.0.

4.2. Results and Discussion

In chapter 3 a single acutely toxic dose of GSK932121A was used in order to relate the observed in-life effects to functional effects. Whilst informative, this study design and dose were not designed to distinguish primary events from secondary consequences (rather just to characterise the acute toxicity). The first task of this follow-up study was to determine whether the key observations which occurred with a 50mg/kg (toxic) dose occurred with a 12.5mg/kg (well tolerated) dose to determine more subtle low dose effects of complex III inhibition *in vivo*.

4.2.1. In Life Effects and Comparison of Endpoints to Chapter 3 Study

The key observations made in chapter 3 with regard to the effect of GSK932121A *in vivo* were hypothermia, increase in both basal respiration and CRC compared to VC animals and an increased blood lactate:pyruvate ratio. The same endpoints were assessed in the present study.

Using the 12.5mg/kg dose led to an expected lower plasma drug concentration than in the 50mg/kg study outlined in chapter 3. The average plasma drug concentration was 4.45µg/mL (12.5mg/kg) compared with 18.3µg/mL at 50mg/kg in chapter 3. However here, the plasma concentration with the 50mg/kg dose was markedly different to that in the previous study, with a plasma concentration of only 5.40µg/mL being achieved in this follow up investigation. This data is striking as it shows that at 50mg/kg the animals had 3.4 times less exposure in the present study compared to the study described in chapter 3 (reason behind this discrepancy remains unknown). Furthermore the plasma concentration of GSK932121A at 4-hours post treatment with 50mg/kg was just 21% greater than that achieved with the 12.5mg/kg dose. The difference in the toxicokinetics between the 12.5mg/kg and 50mg/kg group is however greater in liver tissue where an average concentration of 3.38µg/mg was observed with 12.5mg/kg GSK932121A compared to 7.67µg/mg with 50mg/kg GSK932121A (2.7x difference). Together these data highlights that GSK932121A is rapidly deposited in the liver following IP dosing and suggests that animals in the present study were exposed to less drug than in the initial study. Despite this lower internal exposure at the 50mg/kg dose compared to the previous study described in chapter 3, the remainder of the results presented in this chapter are from the new 50mg/kg study and its paired 12.5mg/kg dose.

Consistent with the significant reduction in plasma exposure levels (compared to that described in chapter 3), no adverse clinical signs were observed at either 12.5mg/kg or 50mg/kg GSK932121A. Despite this, a significant reduction in body temperature was still observed in 50mg/kg animals compared to VC, with an average temperature reduction of 2.8°C observed ($p<0.01$) (Fig.4.2A). No effect on body temperature was observed at 12.5mg/kg ($p>0.05$, n=7). On this occasion reduction in body temperature showed no correlation with GSK932121A plasma concentration (R^2:0.3227, $p>0.05$) or liver concentration (R^2:0.5833, $p>0.05$). In contrast to results in chapter 3, no significant effect of GSK932121A treatment was observed on whole blood lactate:pyruvate ratio with either 12.5mg/kg or 50mg/kg groups (Fig.4.2B), compared to VC ($p>0.05$).

A statistically significant increase in liver mitochondria basal OCR was seen in mitochondria isolated from both 12.5mg/kg GSK932121A (n=7, $p<0.05$) and 50mg/kg GSK932121A (n=7, $p<0.01$) groups compared to VC (n=6) (Fig.4.2C). These data supports observations made in previous chapters and further confirms the opposite effect of GSK932121A in mitochondria isolated from GSK932121A-treated animals compared to *in vitro* treatment of control (not previously exposed) mitochondria. Similarly, GSK932121A caused a statistically significant and dose dependent increase in CRC in mitochondria isolated from the livers of both 12.5mg/kg ($p<0.05$, n=7) and 50mg/kg ($p<0.01$, n=7) animals compared to VC (n=6) (Fig.4.2D). Again this supports previous observations in terms of the direction of change

observed between mitochondria isolated from animals treated with GSK932121A in comparison to *in vitro* treatment of control mitochondria. These data support effects of GSK932121A on mitochondrial function at doses which are well tolerated which lends credence to the hypothesis that altered mitochondrial function is central to downstream toxicities as opposed to being a consequential effect.

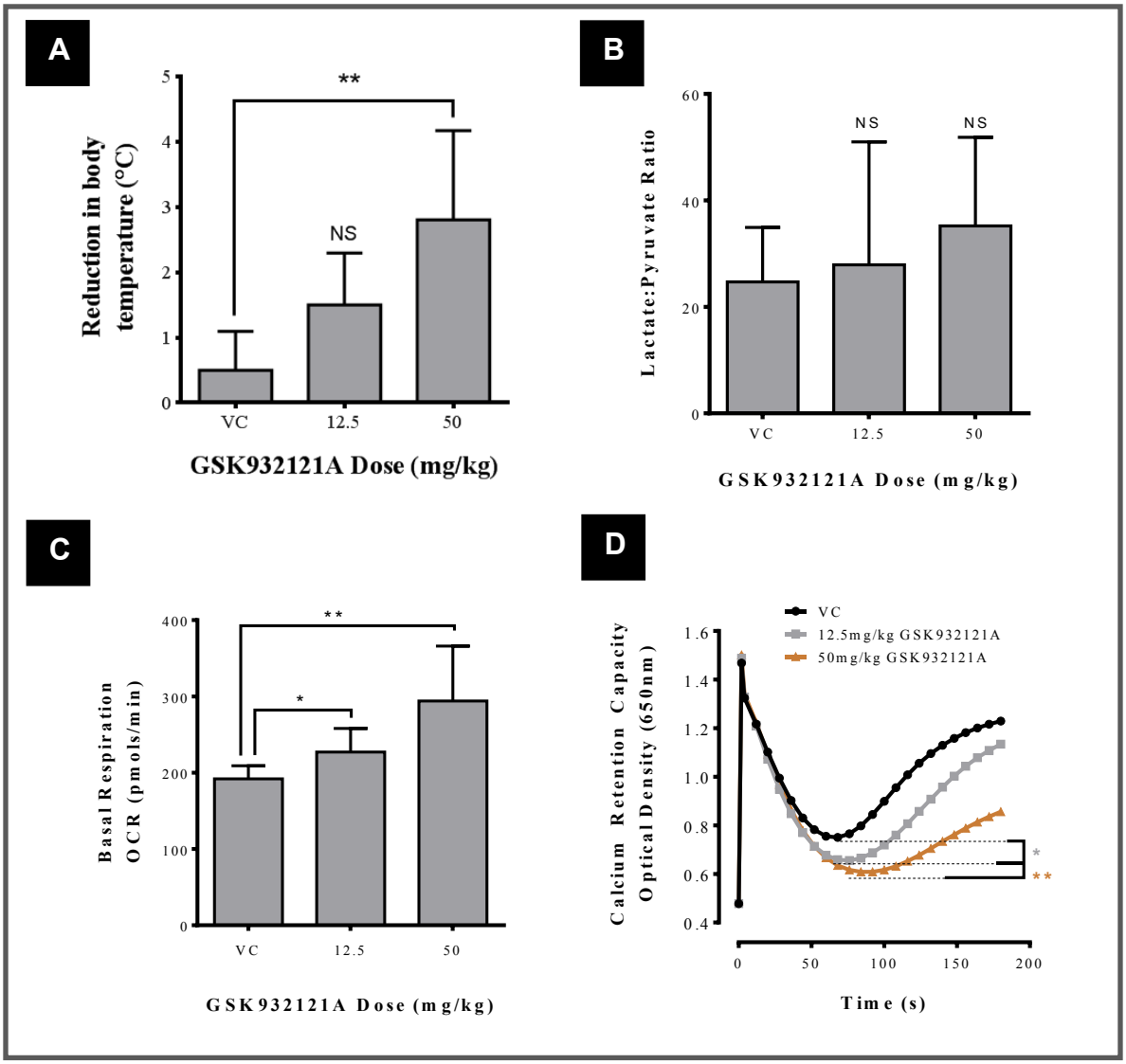


FIGURE 4.2: Effect of 12.5mg/kg and 50mg/kg GSK932121A on body temperature, blood lactate:pyruvate ratio and isolated liver mitochondria CRC and OCR. The data above shows the effect of 12.5mg/kg and 50mg/kg GSK932121A on the endpoints deemed pertinent from chapter 3. These were re-tested in the present study to assess the effect of a well tolerated 12.5mg/kg dose and to analyse the reproducibility of a 50mg/kg dose on body temperature (A), blood lactate:pyruvate ratio (B) and isolated liver mitochondria OCR (C) and CRC (D). All data shown is mean ± SD (VC, n=6, 12.5/50mg/kg, n=7). $p<0.05$*, $p<0.01$**

It is important to acknowledge that lactate/pyruvate data generated using clinical chemistry methods outlined in section 2.13 (and shown in Fig.4.2B) bared high degrees of similarity to the plasma lactate and pyruvate measures made by Metabolon (see Appendix 5). Metabolomic data described below (and shown in Appendix 5) showed a spike in plasma lactate both at 0.5 hours and 4 hours post-dose. The 50mg/kg dose of GSK932121A showed a significant elevation in lactate at 4 hours with the Metabolon dataset however, whereas the data shown in Fig.4.2B shows that the increase was merely trending.

4.2.2. Effect of GSK932121A on Total Metabolites in the Liver and Plasma

A high-level statistical summary of the data obtained from the metabolomics analyses is shown in table 4.1 below. A total of 609 and 658 identifiable/named metabolites were detected in the plasma and liver respectively. Metabolomics raw data (for the metabolites described in this chapter), can be found in Appendix 4. Within the plasma, there was a dose dependent effect of compound treatment on the metabolomic profiles observed in this study when compared to time-matched controls. The low dose of GSK932121A (12.5mg/kg) elicited changes beginning at ~2 hours post treatment whilst the high dose of GSK932121A (50mg/kg) had clear effects beginning at 1h post-treatment with some indication of significantly altered metabolites as early as 0.5h (though the number of changes was limited at this time point).

Similar to the plasma, the end of study liver samples also showed a more notable metabolomic impact with high dose, at which there was a 294% increase in significantly altered metabolites compared to low dose. The number of metabolite changes in the liver at 4 hours post-dose with both low dose and high dose of GSK932121A was much lower than the number of significant alterations observed in the plasma at the same time point. It is therefore possible that additional, non-hepatic effects of GSK932121A contribute to the plasma metabolomic shift that was observed herein. This lack of corroboration between the plasma and liver metabolome is evident elsewhere in the metabolomics data and therefore assessment of other tissues such as muscle, lung, heart and kidney may be warranted.

A	-12.5mg/kg	Significant Effect of 12/5mg/kg GSK932121A on Plasma Metabolites Compared to Time Matched VC				
		Pre Dose	**0.5 hours**	**1 hour**	**2 hours**	**4 hours**
Significant **up** | **down**		**51** | **8**	**30** | **17**	**4** | **34**	**55** | **30**	**54** | **55**
Percentage change in significant metabolites from pre dose (up or down)		-	-20%	-36%	+44%	+85%
Percentage of total detected metabolites changing (up or down)		9.9%	7.7%	6.2%	14%	17.9%

B	-50mg/kg	Significant Effect of 50mg/kg GSK932121A on Plasma Metabolites Compared to Time Matched VC				
		Pre Dose	**0.5 hours**	**1 hour**	**2 hours**	**4 hours**
Significant **up** | **down**		**47** | **3**	**41** | **19**	**37** | **50**	**81** | **104**	**128** | **71**
Percentage change in significant metabolites from pre dose (up or down)		-	+20%	+74%	+270%	+298%
Percentage of total detected metabolites changing (up or down)		8.2%	9.9%	14.3%	30.4%	32.7%

C	Effect of GSK932121A on Liver metabolites compared to VC	
GSK932121A Dose	**12.5mg/kg**	**50mg/kg**
Significant **up** | **down**	**26** | **8**	**70** | **64**
Percentage of total detected metabolites changing (up or down)	5.2%	20.4%

TABLE 4.1: Statistical summary of a plasma and liver metabolite changes. Data shown represents change in statistically significant metabolites in plasma following treatment with 12.5mg/kg GSK932121A (A) and 50mg/kg GSK932121A (B) compared to time-matched VC samples. Effect of both 12.5mg/kg and 50mg/kg doses on liver metabolites compared to VC is shown in table C. (**green = significant reduction in expression**, **red = significant increase in expression**).

4.2.3. METABOLOMICS: COMPLEX III INHIBITION HAS A PROMINENT IMPACT ON PLASMA TCA CYCLE INTERMEDIATES

Mitochondrial ETC function and TCA cycle energetics are intimately linked. Data shown below (Table 4.2) illustrate the impact that altering mitochondrial function at the level of complex III has on TCA

intermediates (TCAi) in the plasma. Acute treatment with 50mg/kg GSK932121A revealed a significant increase in all plasma TCAi at 4 hours post dose with the exception of succinate (trending increase but $p>0.05$) compared to VC. No effect on plasma TCAi was observed at 12.5mg/kg (data not shown). The absolute levels of these TCAi in the plasma with a 50mg/kg dose were however relatively low, with substantial effects noted only at 4 hours (and in conjunction with severe hypothermia). This is suggestive that alterations in plasma TCAi may only occur at a late stage in the AOP following GSK932121A administration or are secondary adaptive changes. This data suggests a delay in organ specific alterations in TCA cycle energetics which requires time to significantly impact the circulating plasma TCAi.

Metabolite	Pre Dose	0.5 Hours	1 Hour	2 Hours	4 Hours
Citrate	1.14	0.94	1.08	**1.17**	**1.39**
α-ketoglutarate	1.34	**0.62**	1.25	1.07	**2.47**
Succinate	1.77	1.18	0.69	**0.71**	2.74
Fumarate	1.51	1.22	1.02	1.07	**4.35**
Malate	1.57	1.22	1.07	1.09	**5.06**

TABLE 4.2: Impact of GSK932121A (50mg/kg) on plasma TCAi. Data shown represents fold change in TCAi compared to time matched VC samples. Statistical significance is represented by colour (**red = statistically significant increase**, **green = statistically significant reduction**).

Evaluation of terminal 4 hour liver TCAi did not reveal any major impact of compound on mitochondrial TCA cycle function in the liver (data not shown), in contrast to observations in the plasma. These data indicate that only higher dose/later stage mitochondrial dysfunction causes any change in TCA cycle energetics highlighted by plasma biomarkers. Additionally, the general lack of TCAi change within the liver suggested that the 4h plasma change may have originated in a non-hepatic target organ(s). Although increases in released TCAi have been previously demonstrated in response to complex III inhibition induced by antimycin A [165], the present data reveals this is not an early event and may either be a secondary consequence of other tissues or a downstream event in the AOP.

With respect to the overt increase in plasma TCAi, multiple carbon energy sources would be expected to become impacted by a loss of TCA cycle efficiency, glycogen metabolism including FA oxidation and amino acid catabolism. The next three sections will evaluate the impact of GSK932121A on these energy sources, both systemically (plasma) and in the liver.

4.2.4. METABOLOMICS: COMPLEX III INHIBITION CAUSES AN INCREASE IN GLYCOGENOLYSIS AND GLYCOLYSIS

Consistent with observations made in chapter 3, metabolomics analysis revealed a prominent metabolic switch in energy production, away from mitochondrial OXPHOS and towards glycogenolysis, glycolysis and substrate level phosphorylation. When mitochondrial function was altered by GSK932121A, a rapidly available alternative energy source would be from glycogen mobilisation and flow into glycolytic metabolism at the level of glucose-6-phosphate as shown in Fig.4.3 below.

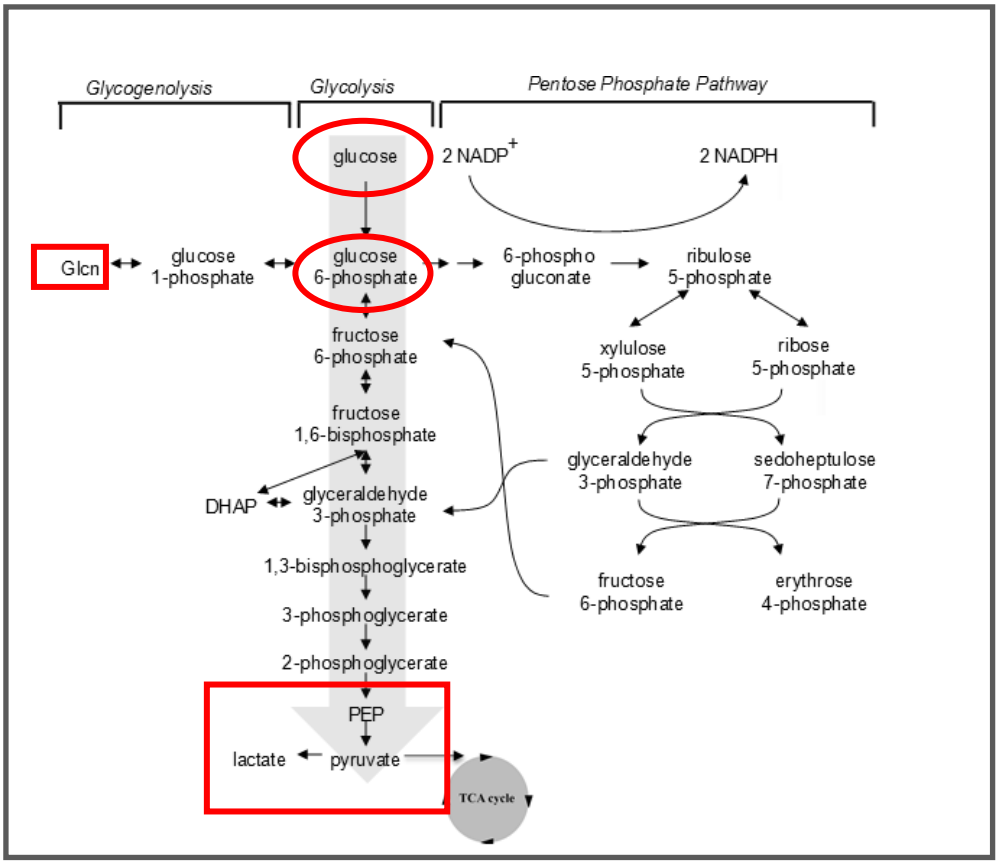


FIGURE 4.3: Schematic representation of the glycogenolysis, glycolysis and PPP. Biochemicals which showed significant changes on treatment with GSK932121A in the present study are presented in red boxes.

A major biochemical outcome of GSK932121A treatment shown in chapter 3 was the significant reduction in hepatocellular glycogen. Consistent with this observation a decrease in all liver starch/glycogen intermediates was observed in GSK932121A treated animals in the present study. This concentration dependent decrease in all liver glycogen was trending a decrease at the 12.5mg/kg dose and

reached statistical significance at 50mg/kg (Fig.4.4). Glycogen itself was however unchanged in the liver of 12.5mg/kg GSK932121A treated animals. Reduction in glycogen levels therefore manifest only at higher doses due to increased reliance on hepatic glycolysis (i.e. Reduction in glycogen is not a critical event following GSK932121A treatment *in vivo*).

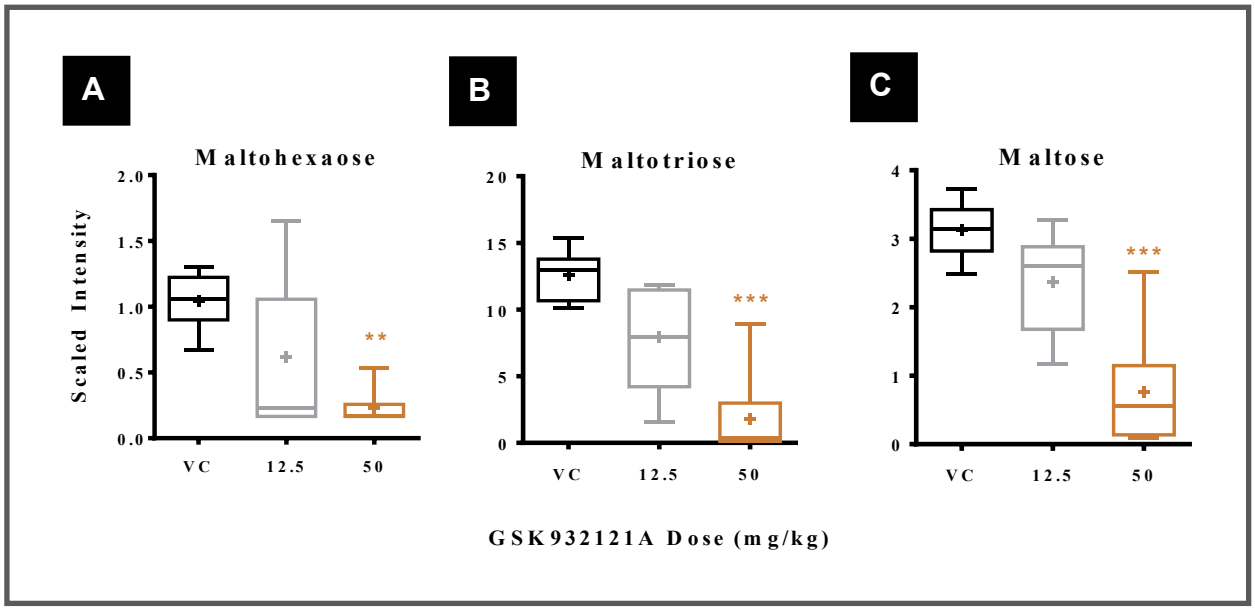


FIGURE 4.4: GSK932121A causes a dose dependent reduction in liver starch/glycogen intermediates at a 4 hour time point. Data shown represents scaled intensity of the total ion counts for each metabolite whereby the median ion is equal to 1. A significant reduction in maltohexaose (A), maltotriose (B) and maltose (C) was observed in the liver of animals treated with 50mg/kg GSK932121A (n=7, orange) compared to VC (n=6, black). All glycogen intermediates were trending a reduction at 12.5mg/kg (n=7). **p<0.01, ***p<0.001.

In line with the hypothesis of compensatory energy sourcing, the dramatic depletion of liver glycogen intermediates correlated with a progressive increase in liver glucose-6-phosphate, the input level at which increased glycogenolysis would be expected to impact glycolytic metabolism (Fig.4.5A). Additional support for increased glycolytic compensation was given by a statistically significant decrease in liver glucose levels, an elevation in the glycolysis intermediates 2-phosphoglycerate and phosphoenolpyruvate (PEP) and a significant decrease in both pyruvate and lactate with high dose acute exposure (Fig4.5 D and E). Importantly, while elevated glycolytic metabolism might be expected to result in elevated lactate levels within the liver, it is known that the liver is able to utilise lactate as a non-carbohydrate fuel source in order to generate glucose (gluconeogenesis) via the Cori cycle. This theory is supported by gene expression changes presented in chapter 3 which highlight up-regulation of genes involved in gluconeogenesis, i.e. Pck1, Foxo1 and PGC1α. The significant increase in lactate observed in the blood at late time points in chapter 3 (despite trending increase this was not evident in the present study, likely due

to lower drug exposure levels) is likely originating from the skeletal muscle although further work is required to better understand its origins. Furthermore, the observation that GSK932121A caused a significant increase in liver phosphoenolpyruvate (PEP) and a significant reduction in liver pyruvate/ lactate (with the 50mg/kg dose) is suggestive that the activity of pyruvate dehydrogenase kinase may be inhibited. This would support observations made in chapter 3 which showed an increased level of Pdk4 gene transcription in liver tissue of rats treated with 50mg/kg GSK932121A compared to VC. Further work is required to understand the effect of DIMT on both the activity and expression of the pyruvate kinase family of enzymes and the associated upstream substrates.

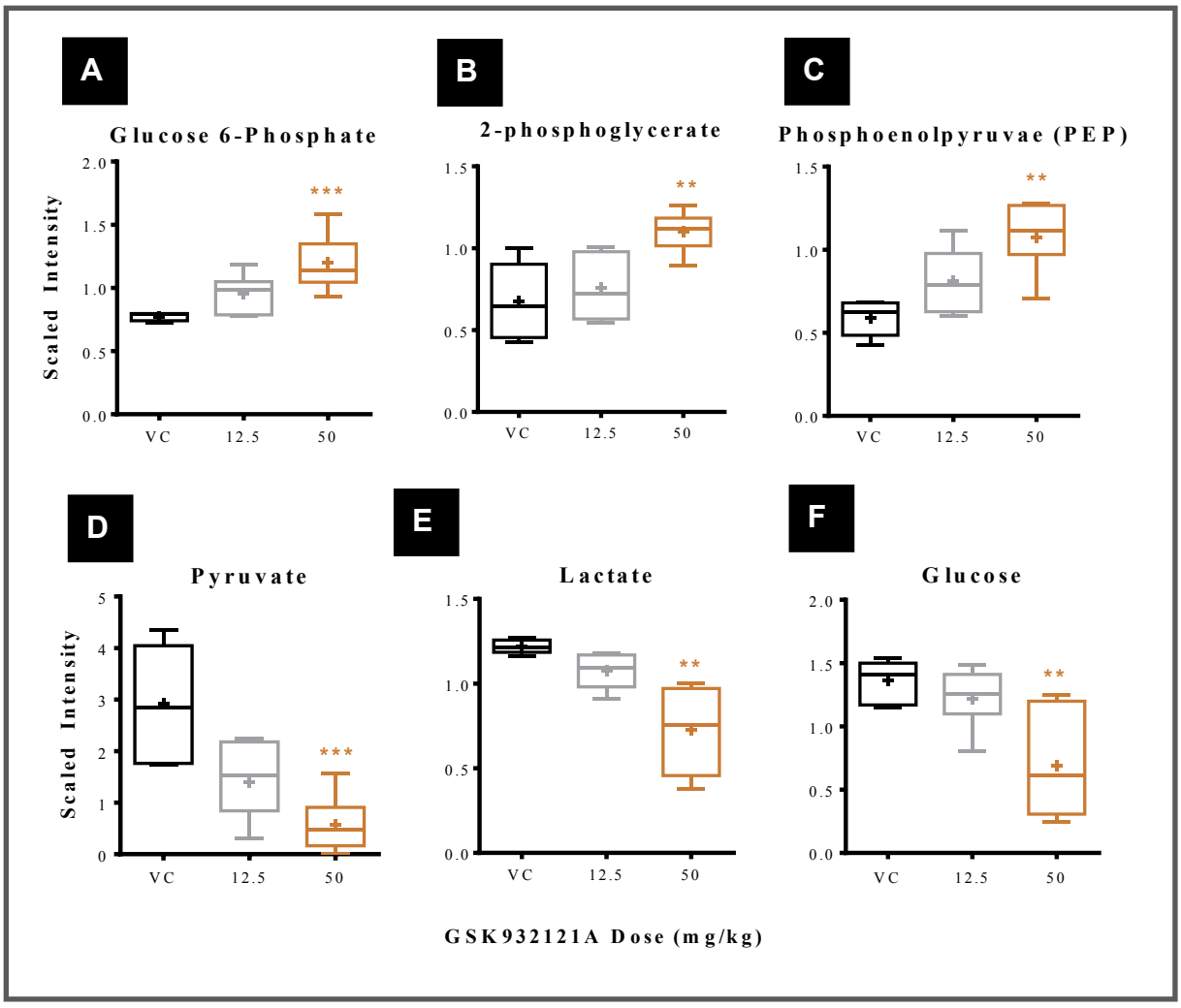


FIGURE 4.5: Effect of GSK932121A treatment on key glycolysis metabolites in the liver of GSK932121A and VC treated animals. Data shown represents scaled intensity of the total ion counts for each metabolite whereby the median ion is equal to 1. Data represents the differential effect of a 12.5mg/kg (n=7, grey) or 50mg/kg (n=7, orange) dose of GSK932121A on glucose-6-phosphate (A), 2-phosphoglycerate (B), phosphoenolpyruvate (C), pyruvate (D), lactate (E) and glucose (F) compared to VC livers (n=6, black). $p<0.01$**, $p<0.001$***

It is important to highlight that no biochemical involved in glycogenolysis or the glycolysis pathway was affected at the well-tolerated 12.5mg/kg dose. Lactate has long been regarded as a useful biomarker of mitochondrial dysfunction however the evidence obtained would suggest that the effect of complex III inhibition on circulating lactate is only apparent at high doses and in conjunction with severe clinical toxicity. It is currently unknown what level of mitochondrial dysfunction *in vivo* is required to provoke significant effects on circulating lactate. Despite this, the current data improves understanding of the effect of drug-induced respiratory chain inhibition on metabolic pathways in the liver. Further work exploring glycogen depletion and lactate generation at sub-toxic doses will be presented in chapter 7.

4.2.5. METABOLOMICS: COMPLEX III INHIBITION HAS AN EFFECT ON MITOCHONDRIAL FA OXIDATION

Elevation of plasma TCAi following high dose compound exposure indicated some level of altered energy metabolism, and presuming liver is a major target of compound toxicity, one would anticipate that altered hepatic FA β-oxidation may be the primary impact in the acute exposure situation. It is important to acknowledge that the general pathology relating to the effect of GSK932121A on cellular lipid relates to an increase in hepatocellular lipid and as such the metabolomic footprint downstream of GSK932121A may be likened to that described in studies following high fat diet feeding, observation of hepatic steatosis or insulin resistance (type II diabetes mellitus) [166].

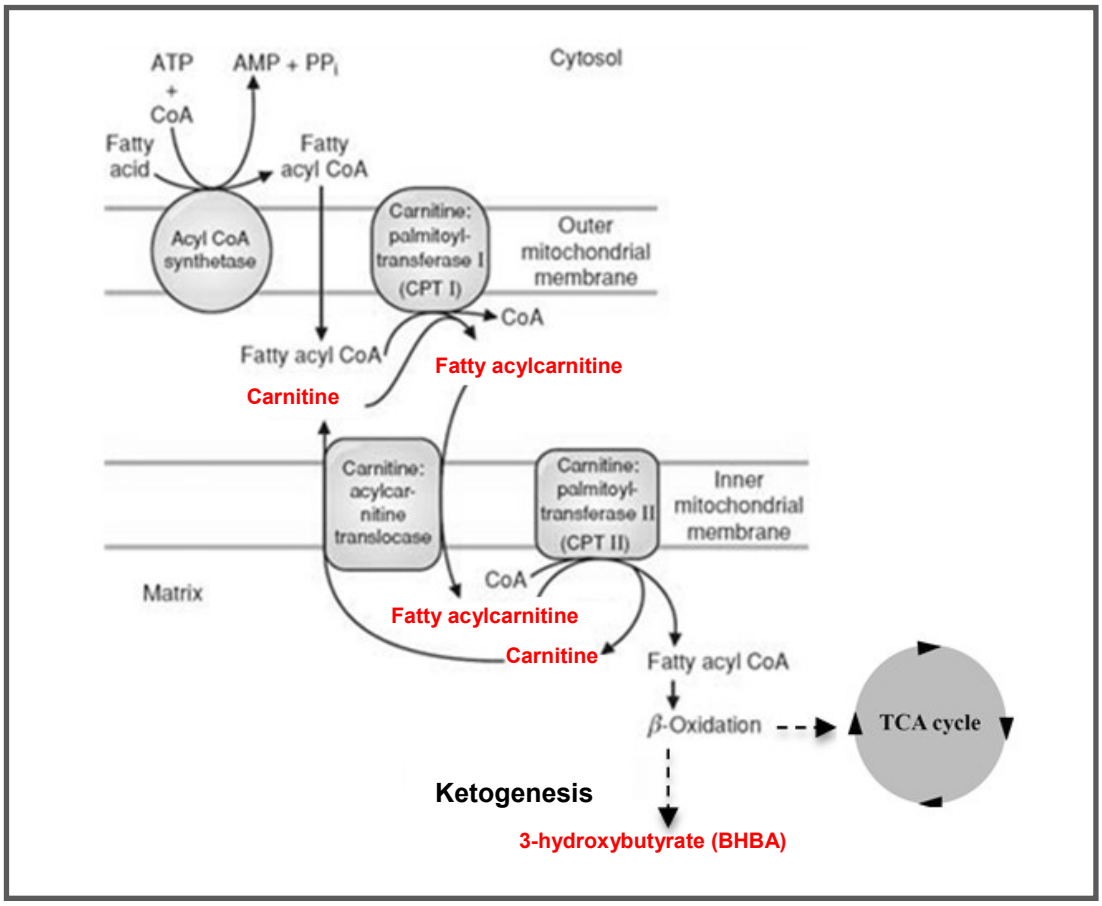


FIGURE 4.6: Schemiatic representation of the carnitine shuttle and ketogenesis. Biochemicals depicted in red were differentially affected due to GSK932121A's impact on FA β-oxdation.

Mitochondrial FA oxidation requires FA-conjugation with carnitine in order to facilitate transport across the IMM for FA β-oxidation to proceed (Fig.4.6 above). Consistent with increased FA conjugation (i.e. attempts to increase mitochondrial substrate for β-oxidation) a significant reduction in plasma carnitine (significant at 2h and 4h with low and high doses of GSK932121A) was observed compared to VC (Fig.4.7). End of study liver carnitine was not significantly altered compared to control.

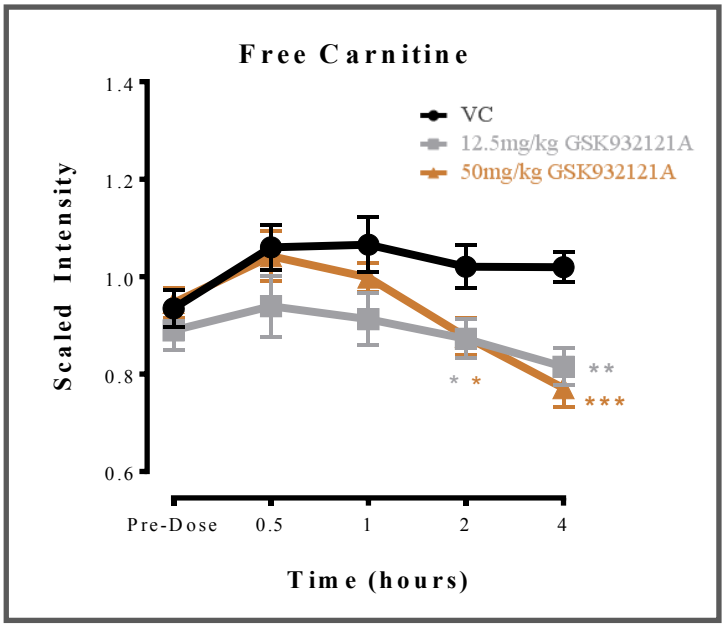


FIGURE 4.7: Effect of GSK932121A on plasma free carnitine. A significant reduction in free carnitine was observed in the plasma of 12.5mg/kg (grey line, n=7) and 50mg/kg (orange line, n=7) treated animals at 2 and 4 hours compared to VC animals (black line, n=6). Data shown represents scaled intensity of the total ion counts for each metabolite whereby the median ion is equal to 1 with mean ± SE shown. *p<0.05, **p<0.01, ***p<0.001.

Consistent with the metabolic attempts to increase β-oxidation shown by significant reduction in free-carnitine with escalating time and dose, an increase in a number of ketone bodies was observed. Efficient FA β-oxidation leads to the formation of acetyl-CoA, which is incorporated into the TCA cycle [167]. If this process is perturbed, efficient FA oxidation is diverted into ketogenic FA metabolism, resulting in the accumulation of ketone bodies (such as 3-hydroxybutyrate, BHBA) and the accumulation of upstream FA-acylcarnitines [168-170]. In the current study, a significant increase in both plasma and liver BHBA was observed compared to time matched VC animals (Fig.4.8 A and B). Increased levels of plasma BHBA have been previously observed in individuals with diabetes-related fatty liver [171]. This occurred alongside a significant increase in plasma long-chain acylcarnitines which lends further credence to the hypothesis that mitochondrial FA β-oxidation is altered with acute exposure (Fig.4.8 C, D and E). It is however important to acknowledge a trending yet appreciable increase in the three fatty acylcarnitines shown in Fig.4.8 at the pre-dose stage. Recent research has shown that elevations in the plasma concentrations of FA-acylcarnitines reflect mitochondrial dysfunction associated with metabolic disease states [168, 169, 172-175]. Furthermore, increased levels of circulating acylcarnitines have also been investigated as biomarkers, specifically of mitochondrial dysfunction following drug induced liver injury using acetaminophen [123]. Furthermore increased levels of circulating palmitoylcarnitine,

stearoylcarnitine and oleylcarnitine were observed in mice with increased levels of hepatic lipid after being fed a high fat diet [176].

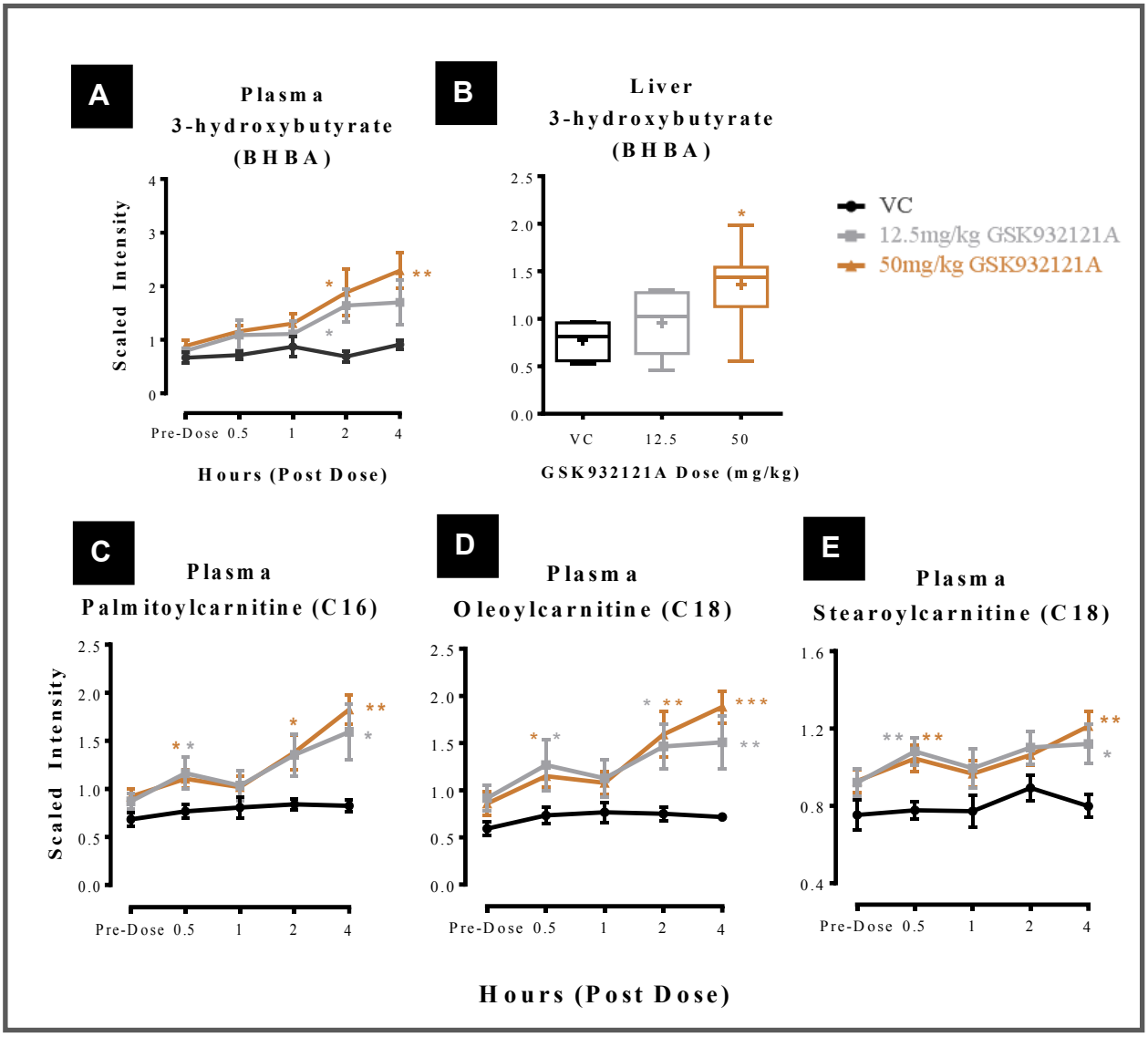


FIGURE 4.8: Effect of GSK932121A on plasma and liver BHBA and plasma FA-acylcarnitine levels. A significant increase in plasma (A) and liver (B) BHBA was observed in 12.5mg/kg (n=7) and 50mg/kg (n=7) GSK932121A treated animals compared to VC animals (n=6). Increases in the FA-acylcarnitines palmitoylcarnitine (C), oleoylcarnitine (D) and stearoylcarnitine (E) was observed as early as 0.5 hours post dose with both 12.5mg/kg (grey, n=7) and 50mg/kg (orange, n=7) line compared to VC animals (black, n=6). Data shown is mean ± SE. $p<0.05$*, $p<0.01$**, $p<0.001$***

Acylcarnitines are derivatives of long chain FA's which are essential for the transport of FA into the mitochondria [177]. Liver FA-acylcarnitines were not significantly affected by compound under any treatment condition (data not shown). This apparent lack of change could reflect a more substantial

baseline concentration of FA-acylcarnitines in the liver (as the major lipid metabolising organ) when compared to plasma baseline levels. Alternatively, this may reflect a shift from complete FA oxidation with TCA cycle incorporation towards increased ketogenesis which would fit with the increase in both plasma and liver BHBA. Similar to the discord between plasma and liver TCAi, the general lack of consistency between plasma and liver FA-acylcarnitine levels suggests that other, non-hepatic effects of the compound may contribute to plasma acylcarnitine accumulation. In any case, circulating acylcarnitines may have potential as a biomarker of drug induced respiratory chain dysfunction with increased expression levels observed at sub-toxic doses *in vivo* (12.5mg/kg) and as early as 0.5 hours post dose. Overall, these data indicate a significant impact of acute compound exposure on mitochondrial FA oxidation efficiency leading to increased ketogenesis.

4.2.6. METABOLOMICS: COMPLEX III INHIBITION HAS AN EFFECT ON AMINO ACID CATABOLISM

There are multiple upstream carbon energy sources that may be altered with a significant perturbation in mitochondrial TCA cycle efficiency. In addition to the predominant lipid source used by the liver, amino acid catabolism might also be anticipated to show changes with decreased mitochondrial function (Fig.4.9).

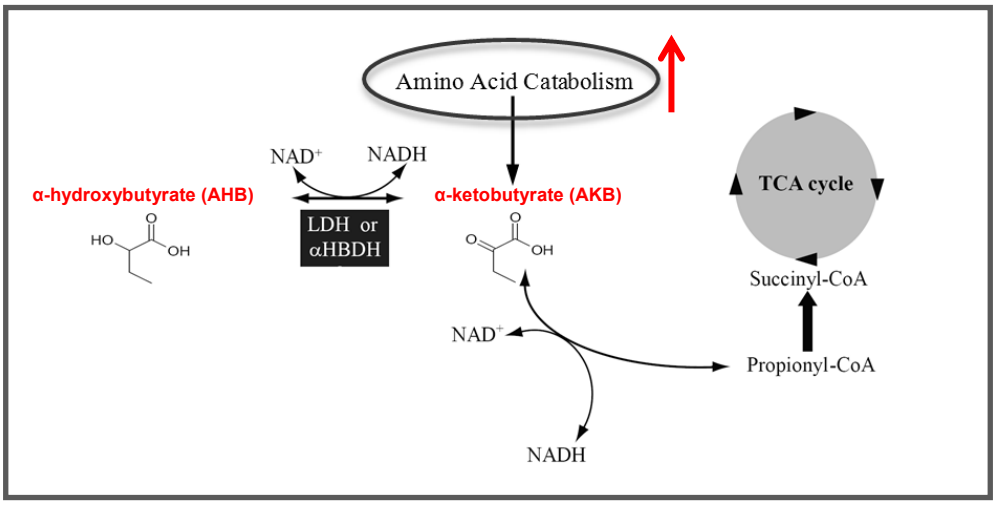


FIGURE 4.9: Schematic representation of α-ketobutyrate and α-hydroxybutyrate involvement in the supply of carbon sources to the TCA cycle.

A significant increase in the levels of several plasma and liver amino acids corroborated the hypothesis that mitochondrial amino acid catabolism was impacted by GSK932121A. Of particular interest was the notable increase in plasma branched chain amino acids (BCAA), 4 hours post-treatment with 50mg/kg GSK932121A (Fig.4.10 A-C). No significant difference in plasma BCAA's were observed following low dose administration of GSK932121A compared to VC. Increases in a number of BCAA were also observed in the liver at both 12.5mg/kg and 50mg/kg GSK932121A compared to VC (Fig.4.10D). These data suggest that hepatic amino acid catabolism is affected despite absence of clinical signs and these increases are only observed in the plasma at higher doses. Perturbations in BCAA metabolism have been shown to correlate with metabolic disease and the underlying mitochondrial dysfunction that is manifest in such disease states [170, 178-180]. Furthermore, increased levels of glycogenic and ketogenic amino acids (valine and leucine respectively) have been observed in states of hepatic insulin resistance due to fatty liver which is consistent with the pathological steatosis observed following GSK932121A treatment [181]. Similarly to this observation, the exact three amino acids which were increased in the plasma in this study (valine, leucine and isoleucine) were also significantly elevated in the plasma of human diabetes-induced fatty liver patients suggesting impaired short term metabolic control [171] although the exact mechanism for these elevations remains unknown.

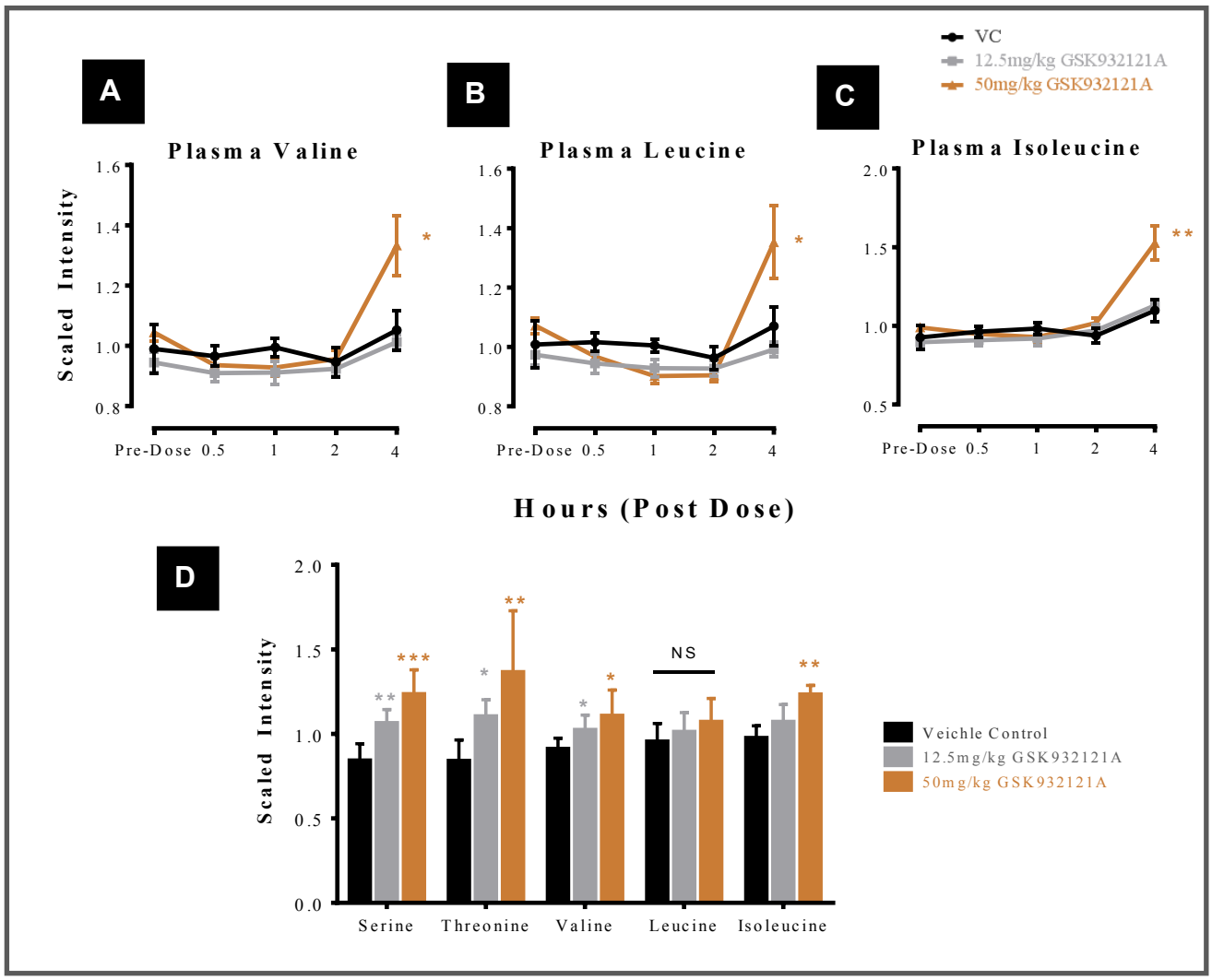


FIGURE 4.10: Effect of GSK932121A on plasma and liver BCAA's. To demonstrate the effect of GSK932121A on amino acid catabolism the effect of compound treatment on the BCAA's is displayed. A significant increase in plasma valine (A), leucine (B) and isoleucine (C) was observed at 4 hours post dose with 50mg/kg GSK932121A (orange line, n=7) compared to VC animals (black line, n=6). (D) A significant increase in liver BCAA's was also observed at both 12.5mg/kg (grey bars, n=7) and 50mg/kg (orange bars, n=7) compared to VC (black bars, n=6) 4-hours post dose with GSK932121A. All data displayed is mean ± SE. $p<0.05$*, $p<0.01$**, $p<0.001$***

Plasma concentrations of α-ketobutyrate (AKB) and its alternative metabolite, α-hydroxybutyrate (AHB) showed time and concentration dependent increases with acute exposure to GSK932121A (Fig.4.11). Recent publications have shown that elevated AHB serves as a marker of insulin resistance, a condition known to involve mitochondrial dysfunction [182-184] and provides one of the most notable markers of increased amino acid catabolism in the current model system. Accumulation of AHB is postulated to

occur when levels of AKB exceed the rate of its catabolism to propionyl-CoA which appears to be the case in the present study.

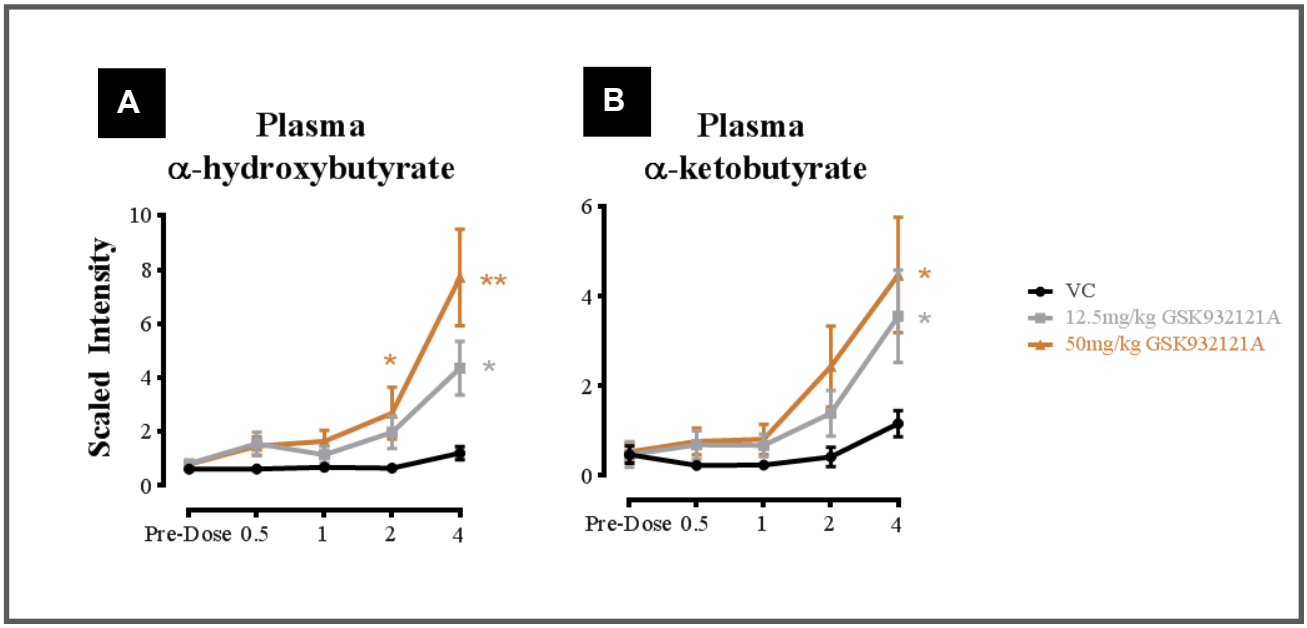


FIGURE 4.11: Effect of GSK932121A on plasma AKB and its downstream metabolite AHB over a 4 hour time course. GSK932121A causes a significant dose and time dependent increase in AHB (A) and AKB (B) with both 12.5mg/kg (grey line, n=7) and 50mg/kg (orange line, n=7) compared to VC animals (black line, n=6). Data shown is mean ± SE of scaled intensity (median = 1) of total metabolite counts. $p<0.05$*, $p<0.01$**

Whilst the metabolomics data point towards an insulin-resistance / metabolic syndrome-like phenotype it is important to acknowledge that, to date, no reports have appeared in the literature that an increase in circulating or hepatic BCAA or in circulating levels of AHB/AKB are markers of DIMT.

4.2.7. METABOLOMICS: INHIBITION OF COMPLEX III CAUSES INCREASED LEVELS OF HEPATIC OXIDATIVE STRESS

In addition to alterations in glycolytic metabolism shown in section 4.2.4, there was a notable shift in hepatic intermediates of pentose phosphate pathway (PPP) metabolism that suggest, at least in part, elevated glucose-6-phosphate was also being tapped as a source feeding PPP metabolism. PPP metabolism is commonly increased to serve two major purposes: 1) increase nucleotide biosynthesis in the context of elevated proliferation, or 2) increase the reducing NADPH equivalents necessary to reduce oxidised glutathione (GSSG) to the major tissue antioxidant GSH [167, 185]. Sedoheptulose-7-phosphate

was significantly elevated in the liver of animals with both low and high dose compound in the acute setting (Fig.4.12A), consistent with an increase in PPP metabolism. In the current model of acute compound-induced toxicity, this profile likely reflects an increased need to maintain antioxidant GSH levels in the liver (versus increased nucleotide biosynthesis).

Cysteine-glutathione disulphide is a reported marker of oxidative stress [186]. Increased liver cysteine-glutathione disulphide levels observed at both doses of the drug in the present study indicate elevated hepatic oxidative stress with GSK932121A exposure (Fig.4.12B). Importantly, liver GSH levels were not significantly diminished with low dose compound exposure, but were significantly decreased with acute high dose compound treatment (Fig.4.12D). These data indicate a compound related increase in oxidative stress with both low and high dose treatment, but an inability to maintain antioxidant GSH levels in the acute high dose setting vs. low dose treatment. In line with this observation was a significant increase in liver ophthalmate levels with low dose GSK932121A and a trending decrease in liver ophthalmate levels with high dose exposure (Fig.4.12C). Ophthalmate is co-ordinately synthesised alongside glutathione through the promiscuity of GSH biosynthetic enzymes [167, 185], but is typically a more stable marker of GSH biosynthesis than GSH itself (particularly within a changing redox environment). Altered ophthalmate levels suggested that GSH biosynthesis was appropriately up-regulated with low dose exposure, but appeared compromised at 50mg/kg. This data is consistent with a two-hit paradigm in the latter scenario, where altered energy metabolism could be coupled with significant impairment of a crucial redox response in the liver of animals treated with high dose GSK932121A, thus contributing to the observed toxicity.

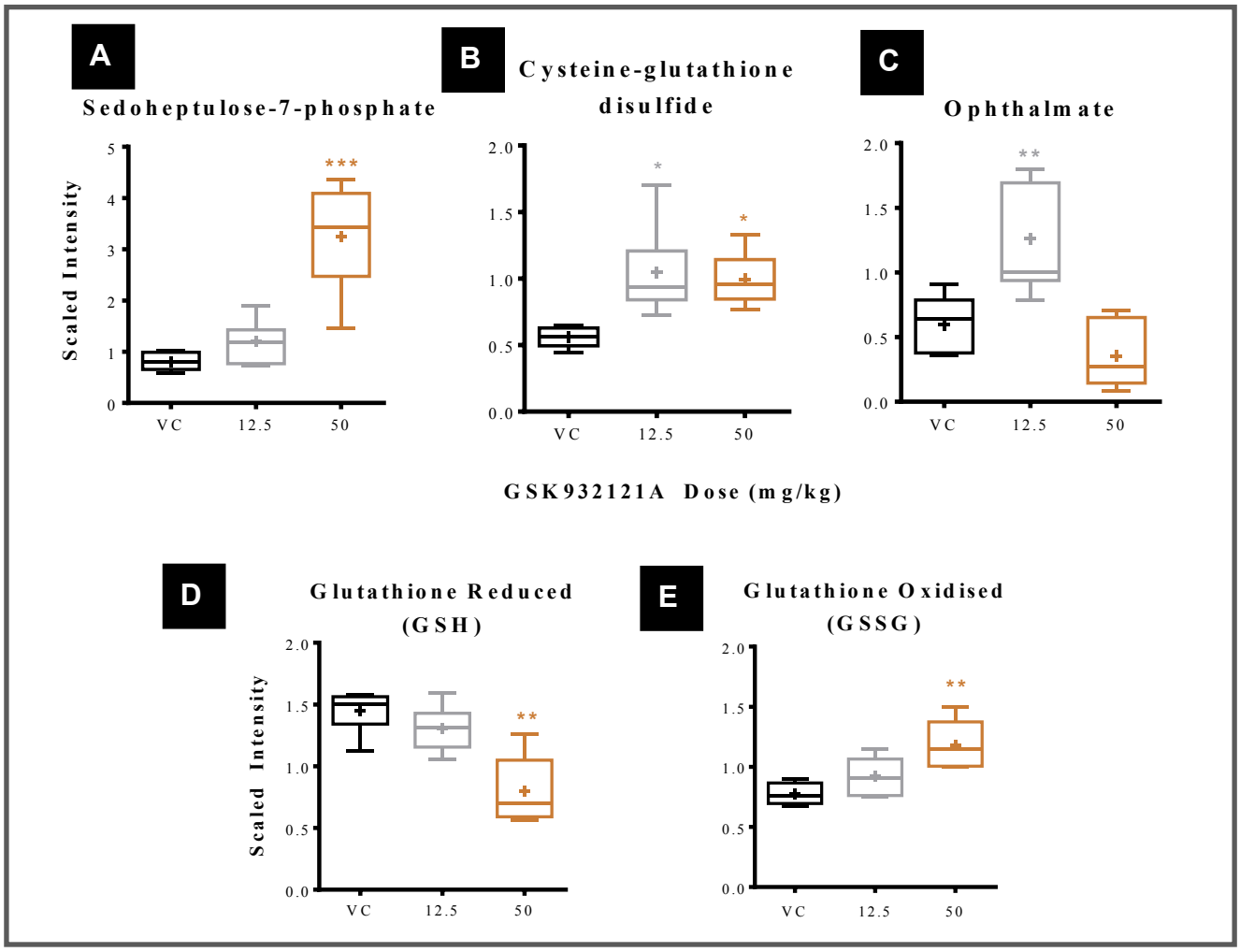


FIGURE 4.12: Effect of GSK932121A on oxidative stress and anti-oxidant stress response in the liver. GSK932121A had a significant effect on the liver oxidative stress markers cysteine glutathione disulphide (A) and sedoheptulose-7-phosphate (B). (C) A transient increase in opthalmate was observed with 12.5mg/kg GSK932121A (grey, n=7) which was significantly reduced at 50mg/kg (orange, n=7). Furthermore, 50mg/kg GSK932121A caused a significant reduction in reduced GSH (D) and a significant increase in oxidised GSSG (E) compared to VC (black, n=6). Data represented as scaled intensity whereby the median value is equal to 1.$p<0.05$*, $p<0.01$**, $p<0.001$***.

4.3. Further Discussion

4.3.1. METABOLOMICS

Metabolomics analysis identified biochemical changes occurring as a result of respiratory chain inhibition at both early time-points and at a sub-toxic dose of GSK932121A. The analysis demonstrated an increase in plasma TCA cycle intermediates, increased levels of hepatic oxidative stress, impaired mitochondrial β-oxidation / amino acid catabolism and an increased level of glycogenolysis. This metabolomic profile is similar to that observed in metabolic syndrome, fasting, fatty liver and insulin resistance. Furthermore the data outlined in this chapter correlates closely with clinical observations in patients with mitochondrial diseases caused by mutation to mtDNA [187]. Many of these disorders manifest in respiratory chain deficiencies and as such validate the translatability of the present work to patients with impaired bioenergetic capacity and mitochondrial myopathies. Particularly acute are increases in acylcarnitines, BCAA's and ketone bodies and future work will no doubt explore the effect of DIMT on these parameters further (i.e. during longer term dosing regimens).

The similarity of the metabolomics signatures in the present study to observations made in other studies of mitochondrial dysfunctions opens the possibility of a mechanism-independent metabolite footprint from generalized mitochondrial perturbation. This is supported by the authors of a recent review into the metabolic and biochemical effects of mitochondrial dysfunction *in vivo* [188].

Furthermore, it is important to acknowledge the current study showed a delayed and diminished toxic response to GSK932121A when compared to previous studies (outlined in chapter 3), i.e. 50mg/kg dose showed no adverse clinical signs and significantly lower plasma exposure levels. This would suggest that the response profiles may manifest earlier in a more typical scenario – thus providing the potential for markers at 0.5h with acute high dose. Drug-induced observations in the present study are therefore particularly sensitive in detecting underlying mitochondrial dysfunction as clinical signs were absent up to the 4 hour time-point.

4.4. Summary

In this chapter I have detailed the effect of GSK932121A (complex III inhibition) on early biochemical changes in plasma and liver. The following conclusions can be drawn for the experimental evidence in this chapter…

- With the exception of plasma lactate:pyruvate and clinical signs (no effect likely due to lower plasma exposure levels of GSK932121A), the key observations made in chapter 3 were reproducible with a 50mg/kg dose in the present study. Furthermore it has been confirmed that increases in basal OCR and increases in CRC occur 4-5 hours following administration with a well tolerated 12.5mg/kg dose confirming they are primary effects of drug-induced respiratory chain perturbation and not secondary events. This is especially apparent as no significant effect on body temperature was observed with a 12.5mg/kg dose.
- Analysis of plasma metabolites at progressive time points and liver metabolites at the terminal time point helped to identify key biochemical changes occurring as a result of GSK932121A treatment. Most notable was the increase in liver glycogenolysis, FA import and oxidative stress alongside impairment of amino acid catabolism and FA β-oxidation. These data suggest altered cell metabolism of all available substrates with continued metabolic efforts to feed carbon sources into the TCA cycle for generation of reducing equivalents, alongside substantial hepatic ROS production. Globally the metabolomics data shows a degree of similarity to the metabolomics signature of metabolic syndrome / hepatic insulin resistance and of human-clinical mitochondrial diseases. This opens up the possibility of a generalised metabolomic footprint of mitochondrial dysfunction although this requires further investigation.

In future studies it remains important to take tissue samples at early time points in order to identify any early biochemical / mitochondrial functional changes occurring at the tissue level. Validation work is also required to assess the utility of measuring metabolomic markers (e.g. acylcarnitines or ketone bodies) as biomarkers of mitochondrial dysfunction *in vivo*.

5.0. INTEGRATION OF GSK932121A DATA INTO AN AOP/MOA

5.1. Introduction – AOP/MOA of GSK932121A Toxicity

The aim of this thesis was to use a systems approach to improve current understanding of the mechanisms of DIMT. In essence, I attempted to devise AOP's in order to detail the key events leading from the molecular initiation event (MIE) to clinical toxicity. In any complex biological system there is however more than one plausible pathway leading to an adverse outcome, which therefore complicates the task of distinguishing key events from casual associated occurrences. This is especially pertinent within an acutely stressed system where it is likely multiple biological mechanisms/pathways are involved, with many events consequential as opposed to primary/causative. It is this multi-mechanism and multi-system response which makes defining causation (according to Bradford Hill considerations) so difficult. For this reason a hybrid AOP/MOA approach was taken to detail the integrated learning's from chapters 3 and 4 with regard to the acute toxicity caused by respiratory chain inhibitors (using both data from the literature and data generated with GSK932121A in rats). Whilst small differences exist between an MOA and an AOP (i.e. an AOP goes out to the population level whereas an MOA does not) a hybrid AOP/MOA enables the description of both parameters.

When building a hybrid AOP/MOA it was important to distinguish between four categories of event (see below, not including the MIE and adverse outcome). This approach takes into account the uncertainties surrounding each stage of the toxicological response and enables the AOP/MOA to develop gradually, from known key events to events which are merely associated…

- **Key events** (including the molecular initiating event if known): There should be good evidence that these are causally related and necessary for the adverse outcome. A key event is an empirically observable step or marker which is a necessary element of the MOA and is critical to the outcome. Key events are measurable and reproducible.
- **Possible key events (PKE)**: Those events which are plausible but for which there is not yet clear evidence.
- **Modifying factors**: These can affect the progression or magnitude of a key event but are themselves not essential for the outcome to occur.
- **Associated events**: Processes occurring in parallel with the key events, but not involved in the outcome.

There is likely to be little utility in generating single-compound AOP's unless in-depth investigations are required on a single compounds mechanism of action (i.e. if there is a late stage drug development issue).

It is therefore important to ensure data generated with GSK932121A is incorporated into a generalised AOP for complex III inhibition taking into account data from the literature. Taking this into consideration, key events (detailed in section 5.2) and possible key events (detailed in section 5.3) contain occurrences which are not necessarily specific to GSK932121A but are characteristic of complex III inhibition in general. Associated events (detailed in section 5.4) will then incorporate additional observations made specifically with GSK932121A which require further analysis.

I will therefore start by identifying just the key events known to be causal in the toxicological response to complex III inhibition (see Fig.5.1. below). The AOP/MOA will then be assembled based on possible key events (PKE) and associated events with the uncertainties at each level discussed.

5.2. Key Events: Complex III Inhibition

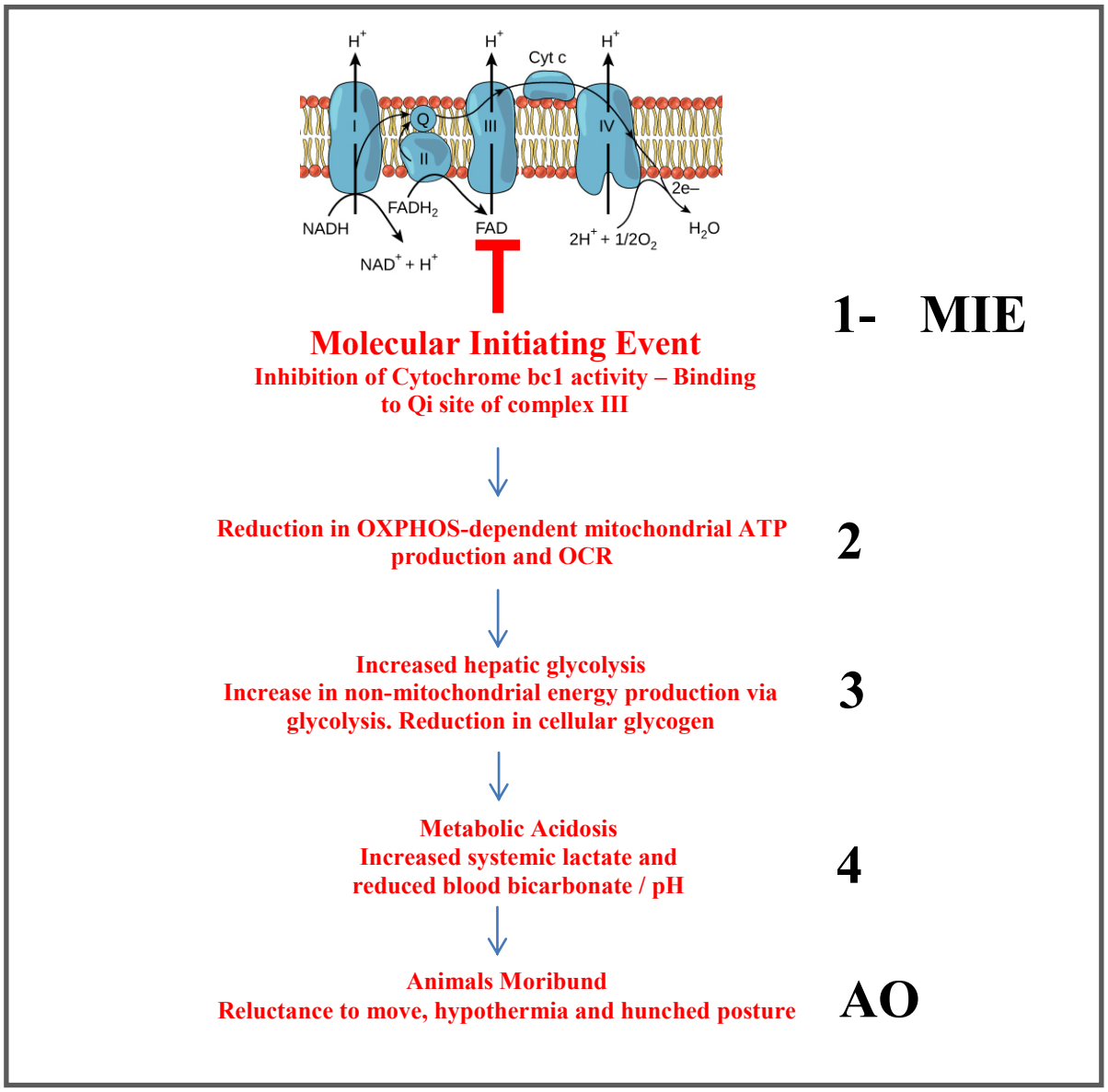


FIGURE 5.1.: Key events in the AOP/MOA for complex III inhibition. Detailed are the key events (labelled 1-4) which are observed downstream of the molecular initiating event (MIE) i.e. GSK932121A binding to the Qi site of cytochrome bc1 complex, to the adverse outcome (AO) in rats (moribund state/hypothermia).

The key events described in the above pathway clearly do not capture the complexity of the full response to respiratory chain inhibition *in vivo*. To be considered key events however, observations must be measurable, casually related (to each other and the outcome) and required for progression of the AOP. Table 5.1 below, details the experimental evidence or literature support which confirms the occurrence of

the key events (1-4, as labelled in Fig.5.1 above), and the plausibility for the relationship between the key events, including any remaining uncertainty.

KE	Experimental evidence	Literature support	Key event relationship plausibility and uncertainties
1 - MIE	Covalent binding of GSK932121A to the Qi binding site of the cytochrome Bc1 subunit.	Proven in X-ray crystallography study [189].	1-2+3: Literature and data suggests that inhibition of cytochrome bc1 activity causes ATP depletion and a metabolic switch to glycolysis due to inhibition of OXPHOS. 1-AO: Reduction in ETC activity provokes loss of temperature due to decreased metabolic rate. Uncertainty – It is uncertain whether GSK932121A causes reduction in mitochondrial oxygen consumption and ATP production. It is likely this energy deficit promotes the relationship to 2 and 4, rather than the MIE itself.
2	None	Primary event following respiratory chain perturbation is a reduction in mitochondrial oxygen consumption and a reduction in mitochondrial ATP synthesis following antimycin A and myxothiazol treatment [190]. This effect was also seen using rotenone and cyanide [191].	Difficulty in assessing and quantifying mitochondrial ATP *in vivo*. To date no evidence of ATP depletion observed however this may be as yields are supplemented by glycolytic substrate level phosphorylation. There is however strong evidence in the literature supporting its inclusion as a key event and reduction in OXPHOS activity (ATP and OCR output) is known to cause a switch in metabolism to glycolysis (key event 3).
3	Reduction in liver glycogen (TEM), metabolomics evidence of glycogenolysis, transcriptomic evidence of a liver fasted state.	Much evidence supporting switch in energy production [192]	3-4: Uncertainty – Lactate originating from other (non-hepatic) organs and tissues such as the skeletal muscle? Lactate likely being consumed by the liver for gluconeogenesis via the Cori cycle?
4	Increase in blood lactate	Clinical evidence of lactic acidosis from mitochondrial toxicants [193].	4-AO: Lactic acidosis widely acknowledged as a key event in the progression of a mitochondrially toxic event and a poor prognosis [194].
AO	Severe and rapid onset hypothermia observed *in vivo* alongside other clinical signs (e.g. hunched posture, reluctance to move etc).	Hypothermia noted downstream of other respiratory chain inhibitors such as 3-nitropropionic acid [150].	4-5: Hypothermia widely acknowledged as a key event in the progression of sepsis like toxicity [163, 195]. Reduced metabolic rate and temperature related effects on enzymatic function. Uncertainty - Is this of hepatic origin (liver is a key thermoregulatory organ in rat) and is this a local event in the short-term?

TABLE 5.1: Experimental and literature evidence of key events in the complex III AOP/MOA including the plausibility of the relationships between the key events and remaining uncertainties at each stage. Key events are labelled 1-4 (and AO) according to the numbering in Fig.5.1 above.

5.3. Possible Key Events: Complex III Inhibition

By adopting a hybrid "weight of evidence" based AOP/MOA approach it prevents the need to try and fit all endpoints into a single AOP. This is beneficial as some pathways may be occurring in parallel and are responsive as opposed to progressive (and as such do not fit the criteria as key events). These PKEs may be important in terms of detection for risk assessment purposes or for understanding the adaptation to mitochondrial perturbation but not enough evidence currently exists to definitively relate them to each other or the adverse outcome.

It is important to acknowledge that the below possible key events are supported by data in the literature using other tool complex III inhibitors (e.g. myxothiazol and antimycin A). This is especially important as within any given *in vivo* study it is not always possible to measure every step in the progression of a toxicological outcome. To date our knowledge is restricted to two studies and therefore gaps in our understanding remain. Furthermore, it was intended to generate a hybrid AOP/MOA for complex III inhibition and not GSK932121A toxicity which therefore requires additional data from other compounds with similar *in vitro* activities.

Detailed below, in the same AOP as the key events were portrayed, are the observations where experimental data or strong biological fundamentals suggest they are possibly important to the progression of the AOP but there is not yet sufficient evidence to classify them as key events (Fig.5.2).

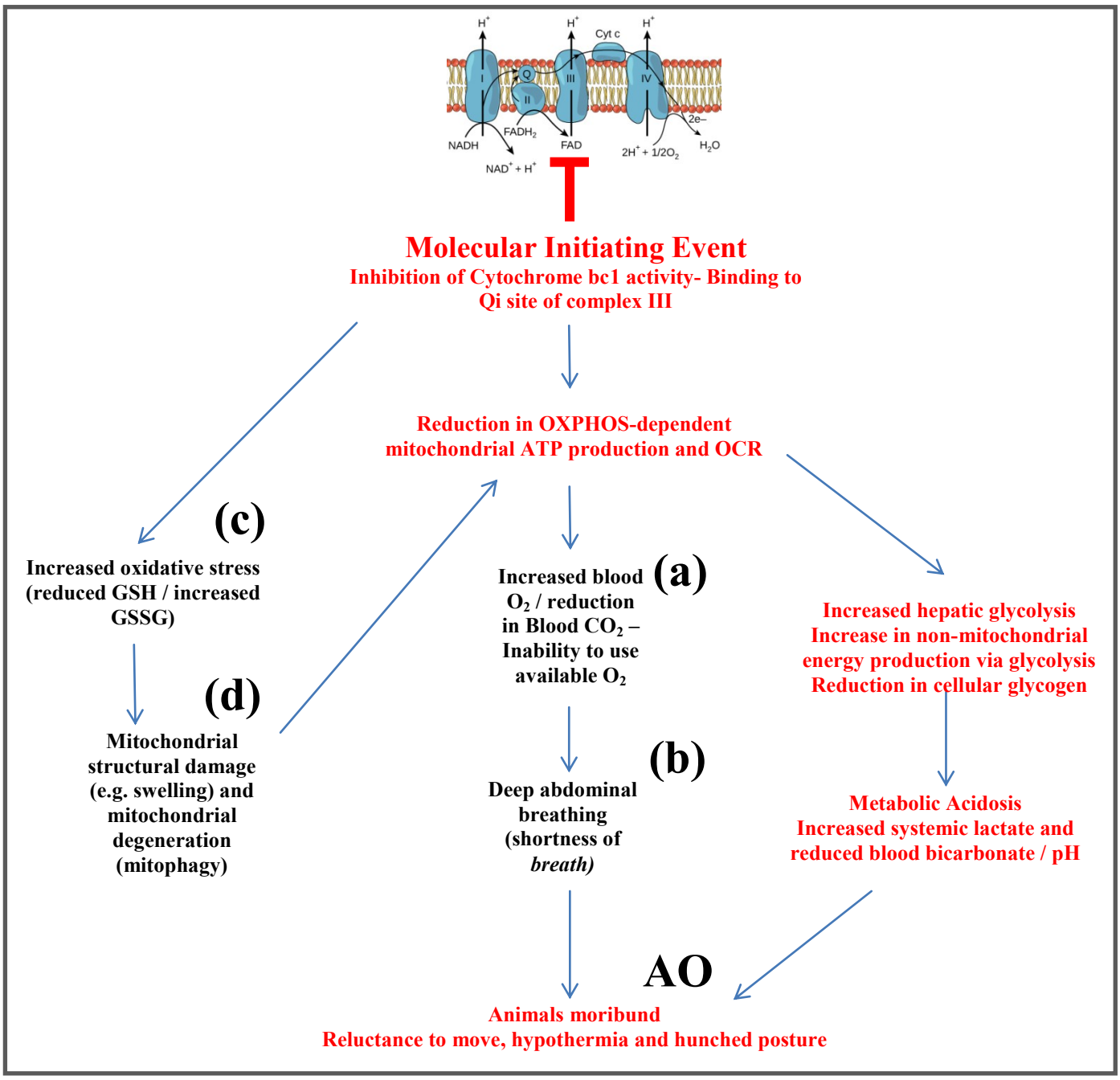


FIGURE 5.2: PKE's in the AOP for complex III inhibition. Insufficient evidence currently exists to definitively include the PKE's (black text and lettered a-d) as key events (red text).

The events shown in black in Fig.5.2 above are categorised as PKE's as not enough sufficient evidence currently exists to definitely conclude they are essential to the progression of the AOP/MOA (i.e. unclear whether they are casually related or whether they are a requirement in the progress of a toxicological response towards an adverse event). These events are however generally considered in the literature

and/or demonstrated downstream of GSK932121A to be potentially key to the AOP for complex III inhibition although further studies are required in order to generate a weight-of-evidence for re-categorisation as key events. Detailed in table 5.2 below, is both the evidence of their involvement in the AOP/MOA for drug-induced respiratory chain inhibition and the remaining uncertainties at each stage.

PKE	Evidence	Uncertainty
a	Blood gas data with 50mg/kg GSK932121A demonstrates an increase in plasma 0_2 and reduction in plasma CO_2 compared to VC.	High level of certainty that this observation is due to reduction in mitochondrial oxygen consumption. This observation is however under-reported in the literature and as such further work is required to assess whether this is common to other complex III inhibitors.
b	Experimental - Principle clinical observation with the 50mg/kg dose was deep abdominal breathing / respiratory depression at 4-5 hours post-treatment. Literature evidence of hypoventilation and respiratory depression *in vivo* with patients suffering cyanide poisoning (cyanide is an ETC inhibitor – complex iv) [196].	Patients with some degree of acidosis (key event 3) usually increase breathing rate, however this is a compensatory effect of increased blood CO_2 which is not observed in the present study. Breathing rate could be as a result of temperature effects as opposed to blood gas findings.
c	Increase in oxidative stress marker cysteine glutathione disulphide with low dose of GSK932121A. Over time oxidative stress overwhelms antioxidant response = Increase in GSSG and reduction in reduced GSH. Literature evidence of ROS generation following respiratory chain inhibition [197].	High level of certainty that ROS generation is primary to the MIE however uncertain what effect oxidative stress has in downstream events i.e. lipid oxidation and DNA damage?
d	Evidence of mitochondrial swelling and degeneration at 50mg/kg GSK932121A at a terminal time point. Mitochondria were often seen engulfed within phagosomes.	Likely to be due to a combination of factors (i.e. ATP depletion, drug binding) and not just caused by ROS. Unsure whether key to the adverse outcome or just an associated event?

TABLE 5.2: Evidence for, and remaining uncertainty surrounding, PKE's in the AOP/MOA of complex III inhibition. PKE's are labelled a-d according to the lettering shown in Fig.5.2 above.

5.4. Associated Events

Further to both the key events shown in Fig.5.1 and the PKE's shown in Fig.5.2 are a number of associated events which are likely occurring in parallel to the AOP, however are not likely essential to the progression toward the adverse effect. Please note that the associated events described below are more specific to the effects observed with GSK932121A and overlays the AOP/MOA developed in sections 5.2 and 5.3 above.

In the acute toxicological scenario the associated events are generally consequential adaptations, cellular responses to the key events or mitochondrial effects where uncertainty remains (i.e. with regard to the direction of change). These events may be extremely important in terms of chronic adaption to respiratory chain inhibition however are not key to the AOP in an acute scenario. Associated events which have been identified and their relationship to the key events and PKE's are shown in Fig.5.3 and are briefly described below.

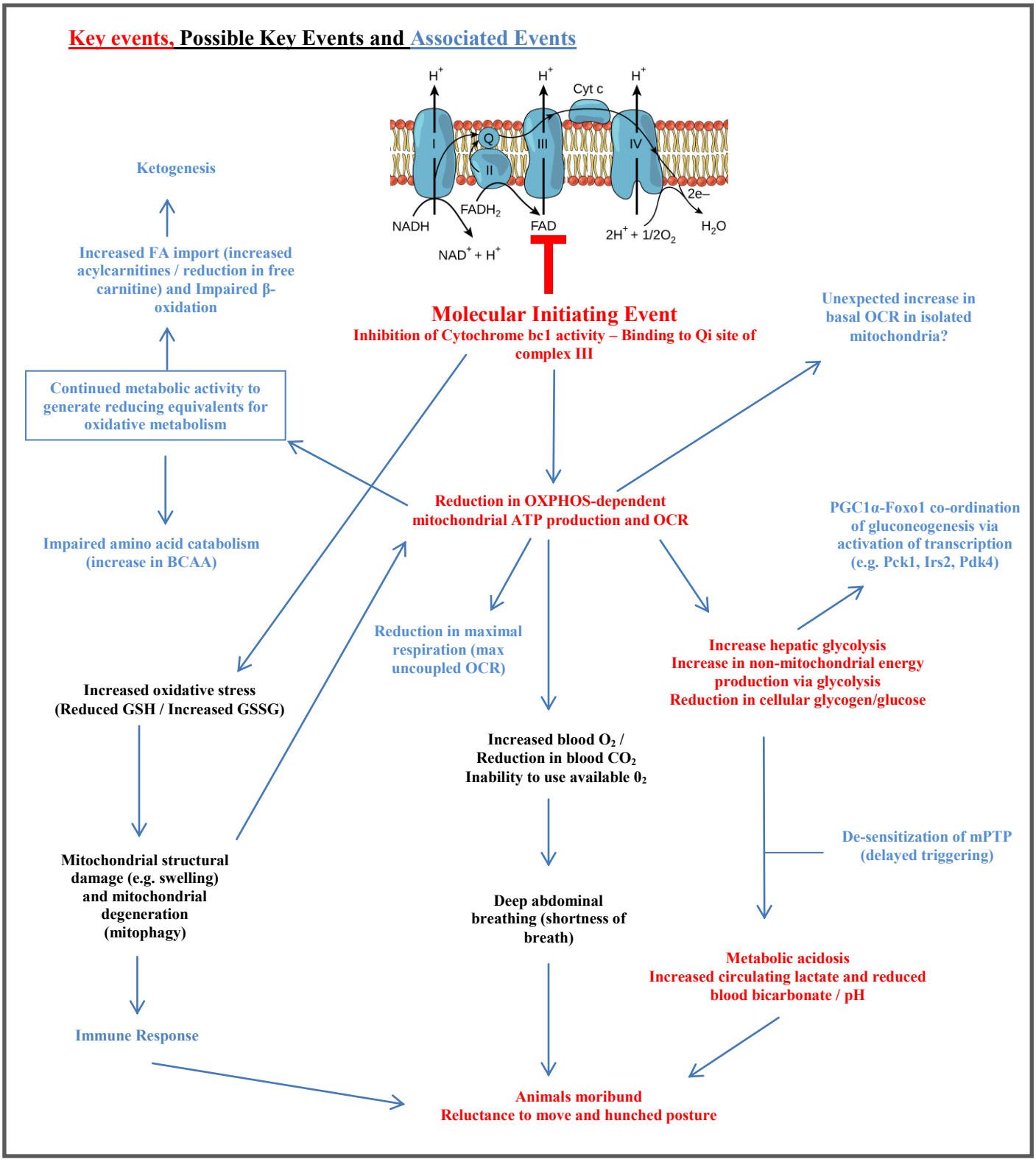


FIGURE 5.3: Hybrid AOP/MOA including key events, possible key events and associated events in the toxicological progression of complex III inhibition related toxicity. Key events (red), PKE's (black) and associated events (blue) are shown in order to detail the observable series of events leading from complex III inhibition to the adverse outcome (AO).

Unexpected increase in basal OCR in isolated mitochondria: An increase in basal OCR was observed in isolated mitochondria from GSK932121A treated rats. This is in contrast to data *in vitro* (both HepG2 cells and control isolated mitochondria treatment) and the cause remains unknown (hypotheses described in section 3.3). Whilst seemingly contradictory, these differences likely reflect an adapted state *in vivo* resulting from the initial insult in combination with compensatory changes made by the tissue to maintain energy production. Only the initial, unconfounded, response is observable *in vitro*. The increase was however shown at a 4 hour time point with both 12.5mg/kg and 50mg/kg GSK932121A and as such is a dose-dependent and sub-toxic marker of complex III inhibitory toxicity. All *in vivo* observations however suggest that GSK932121A does cause a reduction in mitochondrial OCR/ATP synthesis *in vivo* (i.e. blood gas findings, body temperature reduction etc). Increase in basal OCR in isolated mitochondria can therefore only be labelled an associated event as the mechanisms remain unclear and it likely does not represent what is occurring *in vivo*.

PGC1α-Foxo1 co-ordination of gluconeogenesis via activation of transcription (e.g. Pck1, Irs2, Pdk4): Increased levels of both PGC1α and Foxo1 alongside their downstream effectors Pck1, Irs2 and Pdk4 was observed in the liver of GSK932121A treated rats. These genes function to induce gluconeogenesis, the process of generating glucose from non-carbohydrate sources. This process is unlikely to be related to the adverse event as it is a consequence of drug-induced glycogenolysis and low liver glucose levels. Gluconeogenesis is likely activated to increase levels of substrate and therefore does not constitute a toxicologically progressive event.

Desensitisation / delayed triggering of mPTP: A dose dependent effect of GSK932121A was observed on the triggering of the mPTP in isolated mitochondria. This has been attributed to the acidification of the liver due to increased levels of glycolysis (a result of the metabolic switch to glycolysis). It has been widely documented that a pH below 7 can inhibit the action of the mPTP [161]. Inhibiting the mPTP is however generally a cyto-protective / anti-apoptotic effect and as such is likely a protective response and not key to the progression towards the adverse effect. Furthermore, and similarly to the increase in basal OCR described above, this observation was in contrast to *in vitro* observations and therefore enough uncertainty exists to classify this as an associated event.

Reduction in maximal respiration rate (maximal OCR): An effect seen with 50mg/kg GSK932121A was a reduction in the ability of the ETC to maximally increase activity (OCR) following dissipation of mitochondrial $\Delta\Psi$. This data suggests that mitochondria may be unable to increase the activity of the ETC should ATP be required beyond that which is produced at a basal level. This may be a key event in the

pathway towards the adverse outcome of GSK932121A-toxicity but to date it is unknown whether it is a requirement for the adverse event to take place and how reduced maximal respiration manifests. It also remains unclear how the reduction in maximal respiratory rate relates to overall ATP levels and whether this is observed *in vivo* (as opposed to just in isolated mitochondria from treated animals). Its lack of any downstream connection justifies its inclusion as an associated event as further data is required.

Continued metabolic activity to generate reducing equivalents for oxidative metabolism (increased FA import, impaired β-oxidation, Ketogenesis, impaired amino acid catabolism): Metabolomics data presented in chapter 4 has identified that cells and tissues (specifically hepatocytes) continue to drive cell metabolism relating to amino acid catabolism and FA oxidation in order to generate reducing equivalents for oxidative metabolism (despite acute respiratory failure). This is a cellular response to the reduction in mitochondrial ATP production and likely has little impact on the progression of the toxicological response towards the adverse outcome. Specific metabolites essential to these processes may however prove useful biomarkers of respiratory chain dysfunction (e.g. acylcarnitines, ketone bodies or α-hydroxybutyrate).

This exercise has highlighted that GSK932121A-related reduction in mitochondrial ATP synthesis and oxygen consumption is absolutely central to the AOP/MOA. However it remains only a PKE due to the present lack of experimental evidence. It is pivotal that future experiments focus on the effect of complex III inhibition on ATP levels *in vivo*. This is not a trivial measurement however and to date investigation into the effect of GSK932121A on high energy phosphate levels *in vivo* has been attempted using both magnetic resonance spectroscopy (MRS) and high-performance liquid chromatography (HLPC) with limited success. Furthermore, it is important that measurements are specific to mitochondrial ATP as it is hypothesised that global high energy phosphates may be unaffected due to glycolytic compensation.

Immune response: Evidence for the activation of the immune system following GSK932121A treatment is substantiated by data in the literature which shows that the inflammatory response is involved in the toxic response to respiratory chain inhibitors in general. Experimentally, transcriptional up regulation of genes involved in the control of inflammation both pro- and anti-inflammatory (IL-10, IL-6, Acute Phase Protein Response) was observed in chapter 3. In addition, the literature reports a link between ROS generation and immune response [198] and between immunostimulation and onset of acute toxicity [199]. It is however currently unknown whether transcriptional activation of immune response genes is representative of increased protein levels (i.e. of cytokines, white blood cells, chemokine's etc).

5.5. Modifying Factors

It is important to also acknowledge the involvement of modifying factors in the AOP/MOA of GSK932121A toxicity. A modifying factor is an event which can affect the magnitude or progression of a key event but is not itself essential to the adverse outcome. In the acute scenario differentiating modifying factors from other events is extremely challenging as the rapid deterioration in health of the animals gives only a narrow window to identify which endpoints constitute key events, associated events, modifying factors etc. Furthermore modifying factors could easily be mistaken for key events as inherently, anything which affects the magnitude of toxicity is clearly extremely important in terms of a toxicological response. The real difficulty is determining whether they are essential to the outcome i.e. does the adverse outcome still occur in the absence of the modifying factor? Does the adverse outcome manifest earlier or with an increased level of severity when the modifying factor is present?

From close examination of the above AOP/MOA (Fig.5.1-5.3) it could be postulated that the immune response for example, may be considered a modifying factor. Despite clear evidence which suggests the involvement of immunostimulation in adverse clinical reactions, it is likely that impaired energy metabolism would provoke the adverse outcome in the absence of the immune response. Importantly for classification as a modifying factor, it is likely that the involvement of the immune response (i.e. pro-inflammatory response, cytokine storm etc.) may increase the magnitude of the adverse effect but is likely not a pre-requisite for the clinical manifestation of GSK932121A toxicity.

Further work clearly needs to focus on how events interact within the AOP to effect either progression or magnitude as clearly not enough evidence currently exists in order to unequivocally identify modifying factors in the AOP of GSK932121A toxicity.

5.6. AOP/MOA of Respiratory Chain Inhibitors

When attempting to assemble an AOP/MOA for a novel compound, an informative exercise is to assess the similarity of the observations made to other compounds with similar mechanistic activities. The difficulty in terms of GSK932121A is the paucity of data in the literature which describe the toxicological effects of other respiratory chain inhibitors, at the toxic level, in *vivo*. Despite being unspecific to the cytochrome bc1 complex the toxicological effect of compounds which inhibit the activity of other respiratory chain complexes are likely to be similar. It is for this reason that the key comparator discussed below is the complex IV inhibitor cyanide. The toxicity of the classical inhibitors used experimentally to

study the mitochondrial respiratory chain (i.e. antimycin A and rotenone) has yet to be fully examined *in vivo*. Having said this, numerous *in vitro* studies have suggested that treatment with antimycin A causes a collapse in ΔΨ, ATP depletion and increase ROS production [200]. One *in vivo* study which was specific for complex III was with myxothiazol, however at the exposures tested the drug was well tolerated in mice[201].

Like GSK932121A, the anti-androgen medication and inhibitor of mitochondrial complex I, nilutamide, caused an inhibition of FA oxidation, however this was observed in isolated hepatocytes. In the same study nilutamide also caused ATP depletion and early onset cytotoxicity which was not observed when treated alongside glucose. This data suggests that, like with GSK932121A, the action of glycolysis in maintaining ATP levels is a pivotal event downstream of treatment with nilutamide [202]. Furthermore, nilutamide toxicity has been attributed to an increase in mitochondrial superoxide production and oxidative stress [203].

Cyanide is an extremely toxic respiratory chain complex IV (cytochrome oxidase) inhibitor found in fire and cigarette smoke but has also been used as a suicide/terrorist agent due to its potency. Like GSK932121A, the mechanism of cyanide toxicity is based on chemical asphyxiation via effective oxygen deprivation (i.e. inability of cells to use oxygen) and loss of cellular ATP [148]. Manifestations of cyanide toxicity are similar to those of GSK932121A and include respiratory depression, increased blood oxygenation, lactic acidosis and metabolic acidosis characterized by a pH of <7 and a reduction in circulating bicarbonate levels [196]. Furthermore metabolomics studies identified an acute effect of cyanide on bile acid metabolism and as such, and considering the potent effect of GSK932121A on liver function, this should be explored in future studies with GSK932121A [204].

From undertaking this review it appears that the toxicological response to GSK932121A is comparable to that of other respiratory chain inhibitors (independent of the site of inhibition). Clearly further work is however required. Future experiments should aim to assess the toxicity of more respiratory chain inhibitors in order to both validate the AOP/MOA and increase the confidence surrounding the relationships between key events and the adverse outcome.

5.7. Summary

In this chapter I have attempted to create a hybrid AOP/MOA for complex III inhibition, which details the toxicological series of events occurring between the MIE (drug binding to the Qi site of the cytochrome

bc1 complex) and the adverse effect (animals moribund/hypothermia). Key events and PKE's detailed in section 5.2 and 5.3 respectively identified the main mechanism-dependent effects anchoring the MIE to the adverse outcome for complex III inhibition. The associated events in section 5.4 adds further mechanistic details regarding compensatory/adaptive effects of GSK932121A which requires further investigation (including analysis post-treatment with tool respiratory chain inhibitors) in order to understand how they fit within the complex III inhibition AOP. In essence, further work is required in order to validate the proposed AOP/MOA with other compounds which inhibit the mitochondrial respiratory chain. With regard to GSK932121A, it is important to take tissue samples at early time points in order to identify any early biochemical / mitochondrial functional changes occurring at the tissue level. Validation work is also required to assess the utility of measuring metabolomic markers (e.g. acylcarnitines or ketone bodies) as biomarkers of mitochondrial dysfunction *in vivo*.

Following on from this comprehensive "systems" based analysis of DIMT (related to respiratory chain inhibition) it was decided to perform similar systems-based analyses of the toxicological effects of a compound with OXPHOS uncoupling activity *in vitro* and *in vivo*. This analysis is detailed in chapter 6.

6.0. MECHANISM OF DIMT – GSK2617971A INDUCED UNCOUPLING OF OXPHOS

6.1. Introduction

Uncouplers of OXPHOS inhibit the coupling between the mitochondrial ETC and ATP synthesis, by dissipation of the proton gradient between the IMM and the matrix. Uncouplers (reviewed in section 1.5.1) cause protons to bypass the F_0F_1 subunit of ATP-synthase, causing the collapse of mitochondrial $\Delta\Psi$ and the production of heat [205, 206].

Generally, OXPHOS uncouplers collapse both the pH gradient and electrochemical potential across the IMM, thereby stimulating substrate oxidation and oxygen consumption [27]. Classically, uncouplers often represent weak, hydrophobic, organic acids [207]. Furthermore, NSAIDs often have this biochemical characteristic, with many NSAIDs (such as diflunisal, mefenamic acid and flufenamic acid), demonstrating uncoupling activity albeit it with low potency (i.e. doses which are unlikely to be clinically relevant) [208, 209].

The risks associated with compounds that uncouple mitochondria are significant. 2,4-DNP is a classic example. Used in the 1930's as a weight loss drug, numerous 2,4-DNP associated side effects were recognised and it was eventually withdrawn from the market [5]. Although not licensed as a drug, 2,4-DNP is still misused as a fat burning agent, and numerous fatalities are still attributed to dinitrophenol poisoning per year [66]. DNP's potent effects underscore the potential risks associated with mitochondrial uncoupling agents and emphasises the importance of understanding and assessing the risk of DIMT pre-clinically.

As described in section 1.9.2, GSK2617971A is a pyrazole compound which was designed as a selective androgen receptor modulator (SARM) for the treatment of cachexia (muscle wastage). GSK2617971A has shown potent uncoupling activity *in vitro* and is acutely toxic *in vivo* when dosed at 60mg/kg. GSK2617971A was terminated early in development following observations of adverse toxicity in pre-clinical studies. Since GSK2617971A's termination from development, it has been used as a tool molecule for the study of DIMT. As molecules with some degree of OXPHOS uncoupling activity are regularly observed during preclinical assessment of compounds for mitochondrial activity, it was considered valuable to gain further understanding of its mechanism of toxicity *in vivo,* in order to better inform discovery groups of the potential safety liability of this class of mitochondrial toxicant.

6.1.1. CHAPTER AIMS

The experimental aims of this chapter were…

1. To assess the toxicological profile of GSK2617971, in order to better understand the downstream toxicological consequences of OXPHOS uncoupling *in vivo* and build an AOP/MOA of OXPHOS uncoupling.

2. To further current understanding of how *in vivo* outcomes relate to data generated using *ex vivo / in vitro* methods with molecules which uncouple mitochondrial respiration.

3. To identify endpoints which most sensitively detect the effect of OXPHOS uncoupling agents for future studies involving compounds with this potential mechanism of action. It was especially hoped to identify markers of mitochondrial dysfunction at sub-toxic doses of GSK2617971A.

6.2. Results

6.2.1. CONFIRMATION OF THE UNCOUPLING ACTIVITY OF GSK2617971A

In order to assess the uncoupling activity of GSK2617971A, isolated liver mitochondria from control rats were directly exposed to increasing concentrations of the drug and basal OCR was assessed. The response was compared to that with 2,4-DNP (selected as the comparator due to its history of adverse clinical toxicity associated with OXPHOS uncoupling) in order to gauge the relative potency of GSK2617971A. Uncoupling of OXPHOS generally causes an increase in OCR as the activity of the ETC increases due to the drop in charge difference across the IMM, i.e. it attempts to compensate for the collapse in $\Delta\Psi$ caused by the uncoupler.

Isolated liver mitochondria from naïve male Crl:Wi (Han) rats (12-14 weeks of age) were separately exposed to increasing concentrations of both GSK2617971A and 2,4-DNP following which, OCR was measured using the Seahorse XF24 analyser (Fig.6.1A). The experiment was repeated on three occasions. GSK2617971A induced a biphasic and dose-dependent increase in OCR with the peak response occurring at 1μM that led to a 1000% increase in OCR compared to DMSO control (although the low dose of 0.01μM GSK2617971A also induced an average increase in OCR of over 150% compared to the DMSO control). The uncoupling effect of GSK2617971A on isolated liver mitochondria was insensitive to

oligomycin, indicating compound-induced dissipation of the proton gradient following ATP-synthase inhibition (Fig.6.1B). Uncoupling activity is often observed in a biphasic (bell shaped) dose response as at high doses uncoupling agents can become toxic to the respiratory chain and ETC activity becomes inhibited [210]. There is however contradictory reports in the literature as the inhibition of ETC activity at high doses of uncoupler could be due to "non-specific toxicity" caused by binding to the IMM thus inhibiting electron flow [295], or due to decreased substrate availability to drive respiration [296]. These hypotheses are however in the whole cell scenario and therefore further investigations are required to understand the kinetics of this dose-response relationship with uncoupling agents within isolated mitochondria.

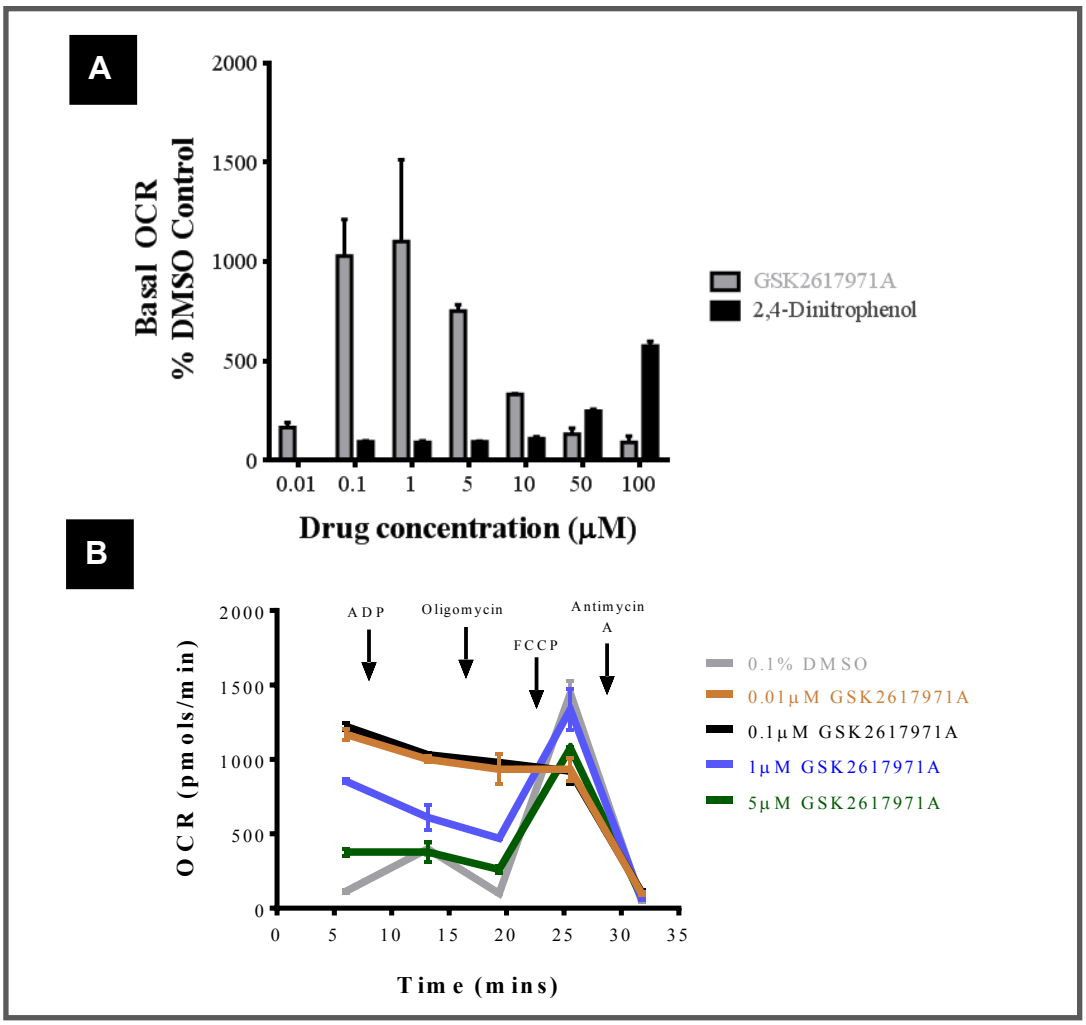


FIGURE 6.1: Comparison of the OXPHOS uncoupling activity of GSK2617971A to 2,4-DNP in control isolated liver mitochondria. (A) Freshly isolated liver mitochondria from naive Crl:Wi (Han) rats were exposed to increasing concentrations of GSK2617971A (0.001-100µM) or 2,4-DNP (0.1-100µM) and basal OCR was analysed. Data was compared to basal OCR readings from a 0.5% DMSO control and is expressed as a percentage of this control (mean ± SD, n=3). GSK2617971A (grey bars) induced a biphasic uncoupling of OXPHOS with peak uncoupling activity stimulated at 1µM. 2,4-DNP (black bars) caused a significant increase in OCR at 50-100µM (concentration of 0.01µM not tested). (B) Representative OCR trace showing the acute uncoupling effect of GSK2617971A following *ex vivo* treatment of control isolated liver mitochondria. GSK2617971A (doses up to 5µM shown for clarity) caused a dose dependent and biphasic uncoupling effect compared to a 0.1% DMSO control (grey line), mean ± SD data is shown (n=3).

Taking into account the concentrations tested, GSK2617971A induced maximal respiration with significantly higher potency than 2,4-DNP (over three orders of magnitude). Following these observations, GSK2617971A was profiled in the CRC assay to assess direct impact on mPTP function and calcium retention. The concentration range of GSK2617971A was modified based on the high potency observed in terms of OCR, and a six point dose response (0.02-2µM) was assessed.

Calcium Retention Capacity

GSK2617971A reduced the CRC in liver mitochondria from untreated animals in a concentration dependent manner with an IC_{50} of 0.16µM (Fig.6.2). The reduction in CRC observed was strongly dose-dependent in the concentration range assessed (R^2:0.9918). The classical uncoupler 2,4-DNP also reduced the CRC of control isolated liver mitochondria although only at doses above 10µM (IC_{50}=46.7µM). In terms of the dose required to inhibit CRC to 50% of that achieved by the 0.5% DMSO control, GSK2617971A was 292-fold more potent than 2,4-DNP.

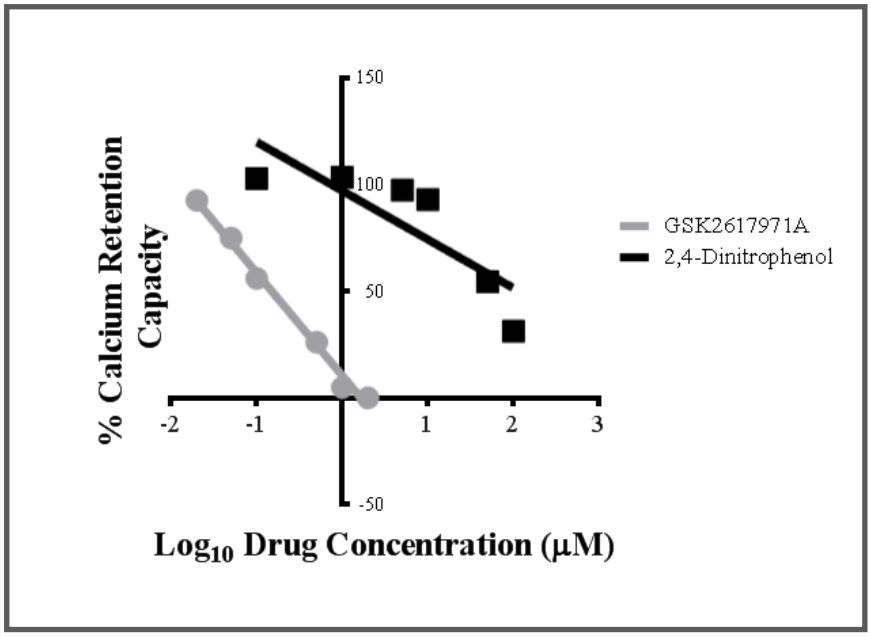


FIGURE 6.2: Assessment of the mitochondrial CRC following *in vitro* treatment of control liver mitochondria with GSK2617971A and 2,4-DNP. Freshly isolated liver mitochondria from male control Crl:Wi (Han) rats were treated *in vitro* with GSK2617971A (0.02-2µM) and 2,4-DNP (0.1-100µM) in order to assess the potency of the drugs on succinate-driven CRC (ΔOD upon addition of succinate and undergoing MPT expressed as percentage of DMSO control). [GSK2617971A IC_{50} =0.16µM, = R^2: 0.9918]. [2,4-DNP IC_{50}=46.7, correlation= R^2: 0.7012]. Data shown is mean only (n=3).

In summary, GSK2617971A is a potent uncoupler of OXPHOS. A concentration of 1µM causes the largest increase in OCR in control isolated liver mitochondria although substantial effects are noted down to 0.01µM. GSK2617971A reduces the CRC of control isolated liver mitochondria *in vitro* down to 0.05µM (IC_{50}: 0.16µM) in a strongly dose dependent manner. Both observations are evidence of the substantial uncoupling capacity of the molecule. The observed responses show that GSK2617971A is significantly more potent than the classical uncoupler, 2,4-DNP.

Following confirmation of GSK2617971A's uncoupling activity, GSK2617971A was administered to male Crl:Wi (Han) rats in order to assess the effect of OXPHOS uncoupling *in vivo*.

6.2.2. ACUTE DOSE *IN VIVO* STUDY WITH GSK2617971A – NON MITOCHONDRIAL ENDPOINTS

Male Crl:Wi (Han) rats were dosed (via the oral route) with either 30mg/kg GSK2617971A (n=2), 60mg/kg GSK2617971A (n=6) or vehicle alone (n=8) for a period of four hours (as described in section 2.1.2 and 2.3.2). Doses of 30mg/kg and 60mg/kg GSK2617971A were selected based on data generated in previous GSK2617971A single-dose tolerability studies where dose-limiting clinical signs were noted in a proportion of animals dosed with 60mg/kg GSK2617971A at approximately 5 hours post-dose and 30mg/kg appeared well tolerated. The aim of the investigation was to follow-up on the acute toxicity noted with the 60mg/kg dose and investigate any underlying functional effects in the well-tolerated 30mg/kg animals. Four hours was selected as the time point in order to induce the desired mitochondrial effects whilst minimising in-life effects.

Clinical Signs

All animals given 60mg/kg GSK2617971A showed clinical signs between 2-4 hours post dose which included slight to moderate piloerection, subdued behaviour, salivation and partially closed eyes. Although not quantifiable, there appeared to be a strong correlation between the severity of clinical observations at the time of necropsy, and the plasma concentration of GSK2617971A. Rapid increase in body temperature was noted in all animals treated with 60mg/kg approximately 1.5 hours post dose with body temperature continuing to rise by 2.68°C on average by 4 hours post dose. No increase in body temperature or clinical signs were observed in the two animals dosed with 30mg/kg GSK2617971A up to 4 hours. Similar to observations made in chapter 3 (relating to decline in body temperature following exposure to GSK932121A), the peak increase in body temperature following GSK2617971A administration was closely associated with the terminal plasma concentration of GSK2617971A (R^2 = 0.8198) (Fig.6.3) and the two animals at 30mg/kg that did not show an elevated body temperature had lower plasma concentrations of GSK2617971A.

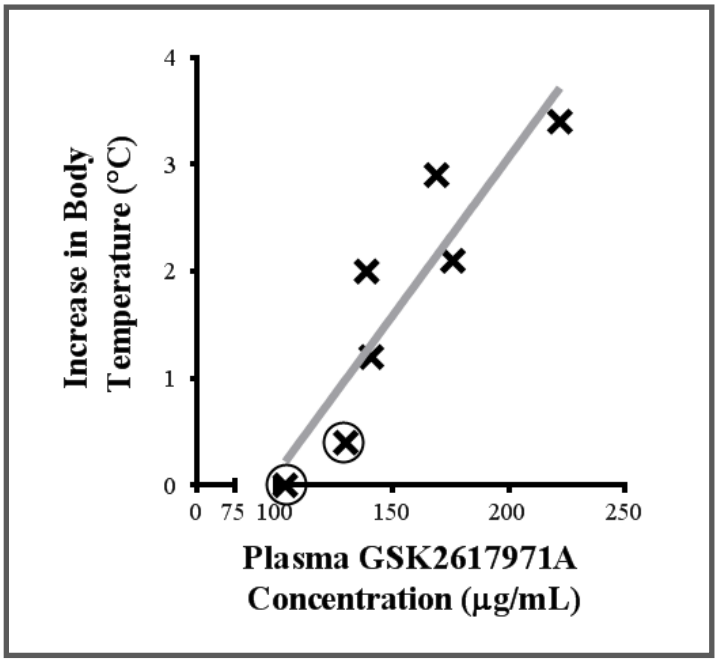


FIGURE 6.3: Relationship between core body temperature and plasma GSK2617971A concentration. The relationship is shown between increase in core body temperature (expressed as increase in body temperature compared to a pre-dose measurement) post treatment with GSK2617971A and plasma drug concentration. Two circled data-points correspond to animals treated with 30mg/kg dose (n=2) where no significant increase in body temperature was observed (<0.5°C increase). 60mg/kg (n=6) corresponds to un-circled data points (one animal not displayed due to being found moribund – no sample available for concentration analysis). (R^2=0.8198, $p<0.001$)

Lactate: Pyruvate

A significant increase in lactate:pyruvate ratio was observed in whole blood of animals given 60mg/kg GSK2617971A compared to blood from VC animals ($p<0.01$**) (Fig.6.4). GSK2617971A, dosed at 60mg/kg, caused a 135.3% increase in lactate:pyruvate ratio which is indicative of increased glycolytic metabolism. No effect on lactate or pyruvate was noted in animals dosed at 30mg/kg GSK2617971A which, when taken into consideration with the lack of clinical signs/body temperature change, indicate that 30mg/kg was a tolerated dose up to 4 hours in the present study.

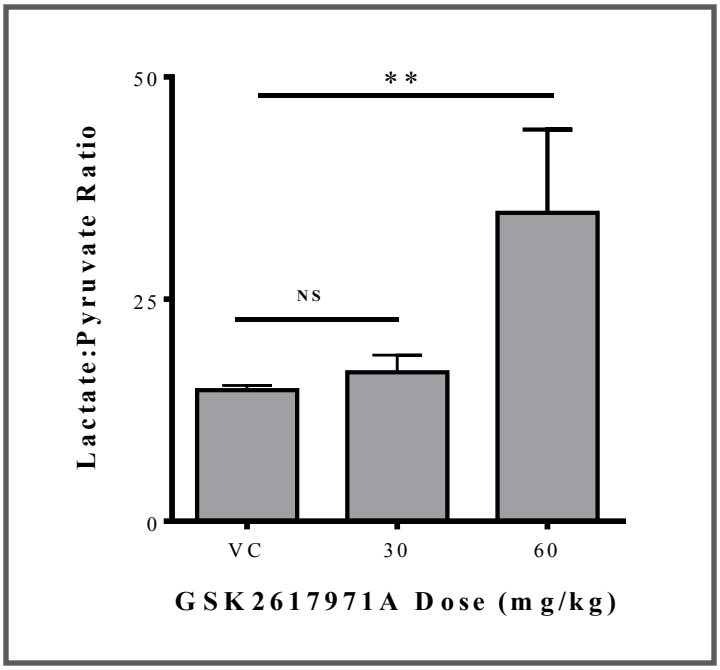


FIGURE 6.4: Effect of GSK2617971A treatment on blood lactate: pyruvate ratio compared to VC. Treatment of rats with 60mg/kg GSK2617971A causes an increase in lactate/pyruvate ratio (in whole blood) compared to VC blood samples ($p<0.01$**, n=6, mean ± sd). No effect on lactate: pyruvate ratio was observed in animals treated with 30mg/kg GSK2617971A (n=2, mean ± range) compared to VC ($p>0.05$).

Changes to Mitochondrial Ultra-structure in the Kidney (TEM Analysis)

TEM was employed to assess the effect of OXPHOS uncoupling on mitochondrial ultra-structure and general cell architecture. Small block sections of liver (median lobe) and kidney (cortex) tissue were fixed in 4% formaldehyde/1% glutaraldehyde, although adverse fixation artefacts prevented the reading of liver micrographs.

Treatment related effects were observed in kidney cortex tubular epithelial cells (Fig.6.5). Minimal to mild mitochondrial swelling and increased lysosomal activity/residual bodies, many of which contained mitochondrial-fragments (suggesting induction of mitophagy) were observed in 60mg/kg GSK2617971A treated animals in comparison to VC (arrowed). Furthermore, disorganisation of the congregated mitochondrial networks was noted and this is especially visible when comparing Fig.6.5B with Fig.6.5D. No ultra-structural effects were observed in animals treated with 30mg/kg GSK2617971A (images not shown).

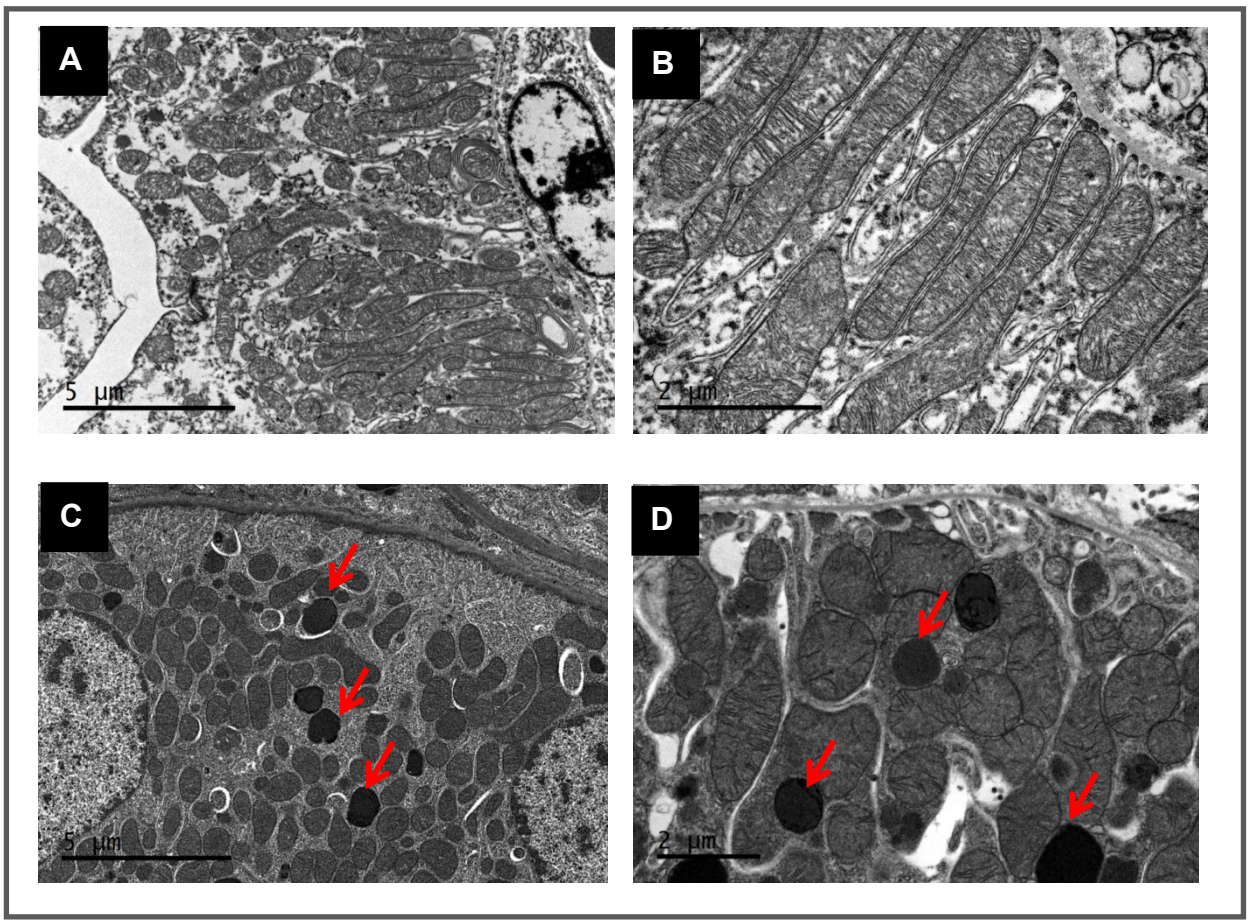


FIGURE 6.5: TEM analysis of kidney sections of rats treated with 60mg/kg GSK2617971A and VC. Panels A and B (10,000x & 25,000x magnification, respectively) show mitochondria from VC animal, with intact membrane structure and normal histology. Note the orderly arrangement of mitochondria within the tubular epithelium. Panels C and D (10,000x & 15,000x magnification, respectively) show mitochondria from GSK2617971A treated animals (60mg/kg) which appear mildly swollen. Increased lysosomal activity is also observed in these treated animals, highlighted by an increase in the number of residual bodies (depicted by red arrows). Disorganisation of mitochondrial networks / arrangement is also visible in treated sections.

6.2.3. ACUTE DOSE *IN VIVO* STUDY WITH GSK2617971A – MITOCHONDRIAL ENDPOINTS

Following administration of GSK2617971A (30mg/kg and 60mg/kg) or VC to Crl:Wi (Han) rats, mitochondrial fractions were isolated from the left lateral liver lobe and left kidney using methods described in section 2.8.1.

OCR Assessment (Seahorse Bioscience)

Mitochondria isolated from the liver and kidney of animals given 30mg/kg GSK2617971A showed no significant change in OCR compared to VC (data not shown).

In contrast to the increase in OCR observed following treatment of mitochondria isolated from a naive rat with GSK2617971A *in vitro* (Fig.6.1), mitochondria isolated from the kidney of rats treated *in vivo* with GSK2617971A showed a reduction in basal OCR by an average of 27.1% compared to VC (Fig.6.6 A and B). A significant reduction in OCR was further observed at state 3 (33.9% reduction), state 4 (25.8% reduction) and maximal (state 3u) respiration (38.7% reduction).

No significant effect on OCR was observed in mitochondria isolated from the liver of GSK2617971A (60mg/kg) treated rats compared to VC (Fig.6.6 C and D).

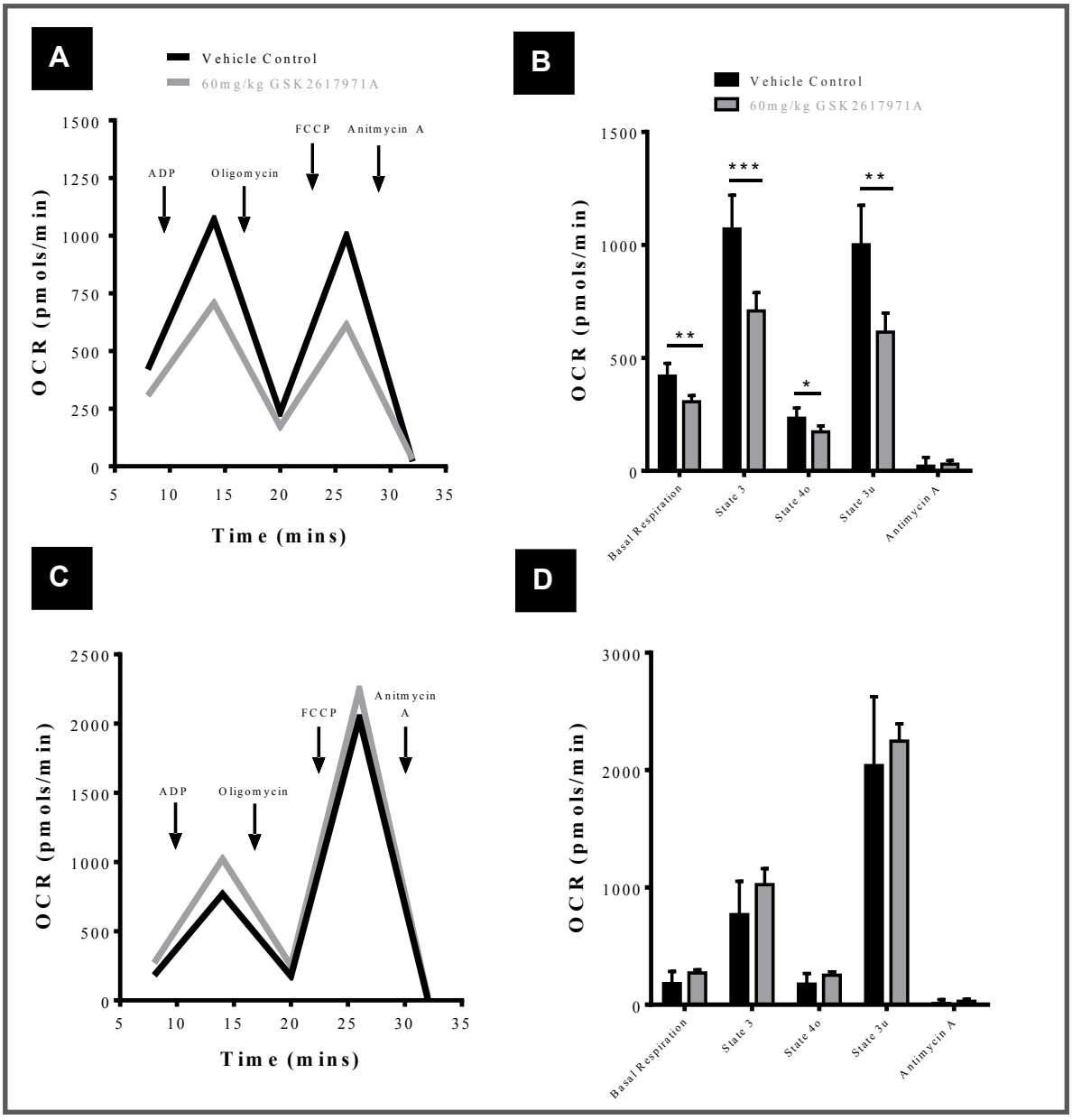


FIGURE 6.6: Analysis of kidney and liver mitochondrial bioenergetics using the Seahorse XF24 analyser following treatment of rats with GSK2617971A *in vivo*. (A) Representative OCR data for mitochondria isolated from the kidney of animals treated with GSK2617971A (grey line) or VC (black line). (B) GSK2617971A treatment (grey bars) caused a reduction in basal, state 3, state 4o and state 3u respiration in the kidney compared with VC (black bars). (C) Representative OCR data for mitochondria isolated from the liver of animals treated with GSK2617971A (grey line) or VC (black line). (D) GSK2617971A had no effect on OCR at any respiratory state in the liver compared to VC ($p>0.05$). Results shown are mean ± SD (GSK2617971A treated, n=6 and VC, n=8). *$p<0.05$, ** $p<0.01$, *** $p<0.001$.

The data shown in Fig.6.6 above was striking as mitochondrial uncouplers typically cause an increase in OCR when treated directly (*in vitro* and *ex vivo* treatment) whereas mitochondria isolated from

GSK2617971A (liver and kidney) showed either no response or a reduction in OCR. One potential hypothesis for this is that GSK2617971A may have been washed out of the mitochondrial preparations during the isolation procedure and therefore had limited effects in these isolates. For this to be the case however, we must assume that the effects of OXPHOS uncoupling on CRC and mitochondrial ΔΨ are more persistent and are irreversible (or only very slowly reversible) upon removal of the drug. Though further work is required, the data shown in Fig.6.7 confirms that the effect of GSK2617971A on OCR (using Seahorse Bioscience technology) *in vitro,* can be reversed upon removal of the drug (i.e. the drug and its effect can be "washed out").

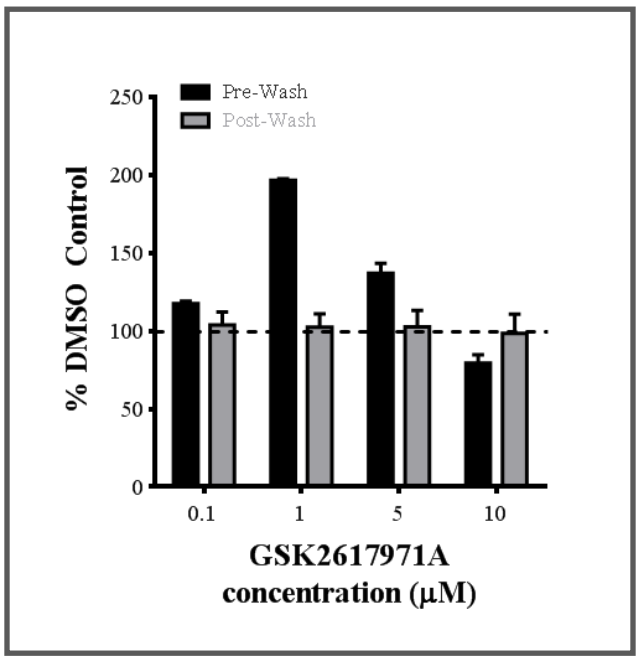


FIGURE 6.7: Reversibility of the uncoupling effect of GSK2617971A demonstrated *in vitro* in HepG2 cells. HepG2 cells were exposed to increasing doses of GSK2617971A (0.1-10μM) and a biphasic dose response was observed on basal OCR with a maximal respiratory rate noted at 1μM. Cells were then removed from the analyser, washed with PBS and the medium was replaced with Seahorse XF assay medium minus GSK2617971A. Removal of the compound reversed the uncoupling effect previously observed and no effect was observed in comparison with the 0.1% DMSO control. Data shown is mean ± SD (n=3).

Mitochondrial Membrane Potential

In order to further assess the effect of GSK2617971A on the ETC, mitochondrial ΔΨ was assessed using JC-1 dye. This dye concentrates and aggregates in the mitochondrial matrix. Any event that dissipates the ΔΨ (e.g. membrane damage or uncoupling) causes the dye to disperse out of the mitochondrial matrix and form green fluorescent monomers. This change in fluorescence can be detected in a multi-plate format fluorometrically.

A significant reduction in ΔΨ was observed in mitochondria isolated from the liver and kidney of animals treated with both 30mg/kg and 60mg/kg GSK2617971A compared to VC (Fig.6.8). At 60mg/kg (n=6, $p<0.001$) a 17.4% reduction in $\Delta\Psi$ was observed in liver mitochondria and a 15.5% reduction was observed in kidney mitochondria, meanwhile 30mg/kg (n=2) reduced ΔΨ *by* 30.7% ($p<0.01$) and 25.5% ($p<0.001$) respectively.

This effect was observed despite the absence of any increase in OCR being observed in the Seahorse BOFA assay in these two tissues (Fig.6.6). An increase in OCR would have been expected in any mitochondria with a loss of ΔΨ due to increased ETC activity to drive proton motive force. This suggests that the JC-1 mitochondrial ΔΨ assay is more sensitive in terms of detecting changes in ΔΨ caused by the MOA of an OXPHOS uncoupler, compared to the Seahorse Bioanalyser.

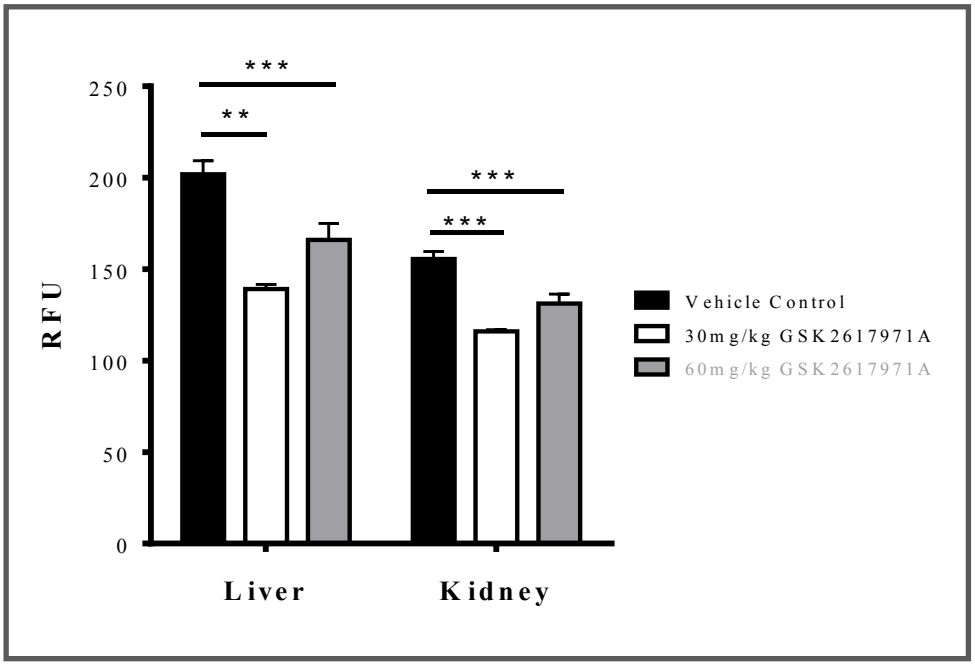


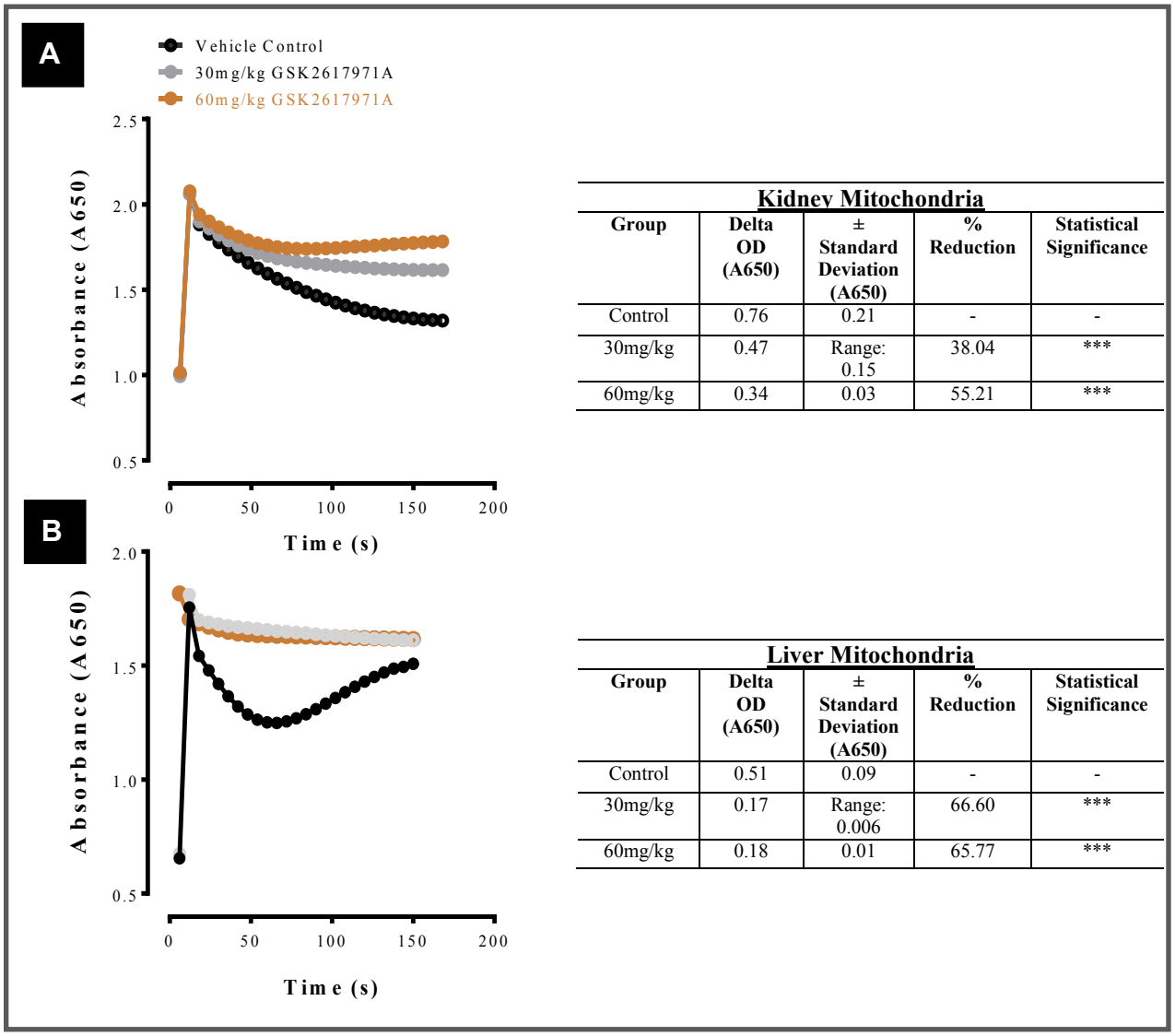
FIGURE 6.8: Analysis of mitochondrial ΔΨ (JC-1) in liver and kidney mitochondria from animals treated with GSK2617971A compared to VC. A significant reduction in mitochondrial ΔΨ was noted in mitochondria isolated from the liver and kidney of both 30mg/kg (n=2, mean ± range, clear bars) and 60mg/kg (n=6, mean ± SD, grey bars) GSK2617971A treated animals compared to VC (n=8, mean ± SD, black bars) is plotted. $p<0.01$ **, $p<0.001$ ***

Calcium Retention Capacity

Mitochondria isolated from the liver and kidney of GSK2617971A treated animals had a decreased level of CRC compared to VC (Fig.6.9). These data are consistent with findings generated *in vitro* which show that GSK2617971A directly reduced the CRC of naïve mitochondria from control animals (Fig.6.2).

Mitochondria isolated from the kidney of GSK2617971A treated animals showed a significant reduction in CRC compared to VC animals. This reduction occurs in a dose dependent manner with 30mg/kg provoking a 38% reduction ($p<0.001$***), whilst 60mg/kg reduced the CRC by 55.2% ($p<0.001$***) (Fig.6.9). The reduction in CRC in the kidney appears to be as a result of earlier potentiation of mPTP triggering following calcium pre-loading.

Similarly, mitochondria isolated from the liver of GSK2617971A treated animals (dosed at both 30mg/kg and 60mg/kg) also showed a reduced CRC compared to mitochondria isolated from VC animals, reducing the CRC by 66.6% and 65.8% respectively (Fig.6.9). The data shows a similar degree of inhibition in calcium uptake between 30mg/kg and 60mg/kg despite no evidence of body temperature increase, clinical signs, lactate generation or mitochondrial ultra-structure changes in animals given 30mg/kg GSK2617971A.



Kidney Mitochondria

Group	Delta OD (A650)	± Standard Deviation (A650)	% Reduction	Statistical Significance
Control	0.76	0.21	-	-
30mg/kg	0.47	Range: 0.15	38.04	***
60mg/kg	0.34	0.03	55.21	***

Liver Mitochondria

Group	Delta OD (A650)	± Standard Deviation (A650)	% Reduction	Statistical Significance
Control	0.51	0.09	-	-
30mg/kg	0.17	Range: 0.006	66.60	***
60mg/kg	0.18	0.01	65.77	***

FIGURE 6.9: Analysis of mitochondrial CRC in kidney and liver mitochondria isolated from GSK2617971A treated rats and VC. Mitochondria isolated from the kidney (A) and liver (B) of rats treated with 30mg/kg GSK2617971A (light grey, n=2) and 60mg/kg GSK2617971A (orange, n=6), showed a statistically significant reduction in average CRC (calculated as the ΔOD between the point of energising with succinate and mitochondria undergoing calcium induced permeability transition) compared to VC (black, n=6). Tables show average (±SD/Range) delta OD along with % reduction compared to VC. $p<0.001$***

6.2.4. IDENTIFYING MECHANISMS OF TOXICITY FOLLOWING OXPHOS UNCOUPLING *IN VIVO* USING TRANSCRIPTOMICS

Global transcriptomic assessment was performed in the liver of GSK2617971A treated animals. The liver was chosen for analysis due to the effects observed in this organ in terms of reduction in CRC and $\Delta\Psi$ and to allow comparative analysis to be undertaken between the gene expression signatures downstream of both OXPHOS uncoupling (GSK2617971A – present chapter) and complex III inhibition (GSK932121A- chapters 3-5). The aim of the transcriptomics was to identify downstream pathways or cellular functions which are differentially affected by drug-induced OXPHOS uncoupling, compared to VC and build these into an AOP. It was also hoped that early marker genes of OXPHOS uncoupling activity might be identified.

GSK2617671A dosed at 30mg/kg caused 1250 gene transcripts to be differentially expressed (1.5 fold ±, $p<0.05$) compared with VC of which 452 (36.16%) were protein coding. Despite the onset of severe toxicity occurring at a dose of 60mg/kg GSK2617971A, fewer genes were differentially altered compared to VC. 60mg/kg GSK2617971A caused the increase or decrease of 1019 gene transcripts (1.5 fold ±, $p<0.05$) with 271 of those transcripts (26.59%) mapped to protein coding genes. Table 6.1 below shows the direction of change in expression of protein coding genes across the study.

Direction of Change	30mg/kg GSK2617971A	60mg/kg GSK2617971A
Increased	169 (37.39%)	175 (64.58%)
Decreased	283 (62.61%)	96 (35.42%)

TABLE 6.1: Direction of change in protein coding gene expression in GSK2617971A treated rat livers.

PCA analysis of the data was performed using Qlucore Omics Explorer (OE) 3.0. 64-bit (Qlucore, Lund, Sweden). The entire raw data set (following normalisation by the RMA method) was incorporated into Qlucore OE and a PCA plot was generated (Fig.6.10A). This was based on data variance observed across the entire array and limited separation of the data was visible (i.e. the PCA was unable to identify principal components which suitably explain the variation of the raw data).

Qlucore OE facilitates the user to adapt the statistical parameters from a lenient to stringent statistical significance, and identify the genes that best separate the experimental variables Qlucore OE is therefore

a useful tool both to identify the key components within large gene expression data sets (i.e. the most significantly affected genes in terms of separating control vs treatment) and to visualise this effect within a dynamic-PCA plot in real time.

A multi-group statistical comparison was employed between both 30mg/kg and 60mg/kg groups versus the VC with the aim of separating GSK2617971A treatment (for both dose groups) in terms of the top 30-40 gene transcripts. The user is then able to view the corresponding effect on the PCA plot (Fig.6.10B). Using a variance level of 0.29, $p \leq 0.05$ and fold-change of 1.5x reduced the number of significant variables to 67 of which 32 were protein coding genes.

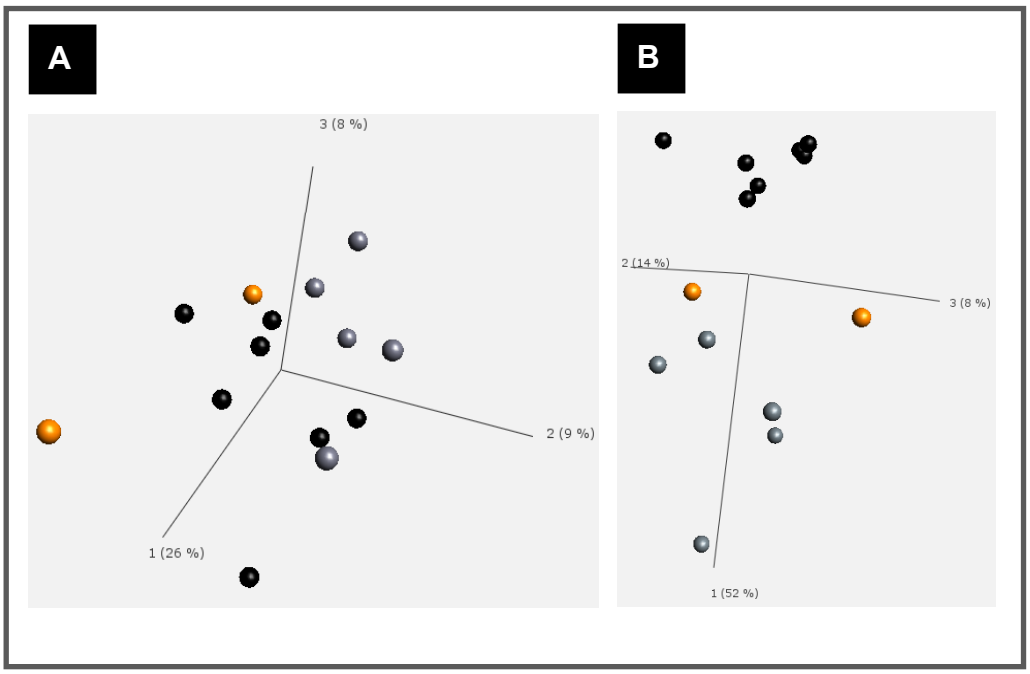


FIGURE 6.10: PCA analysis of global hepatic transcriptional data pre and post statistical refinement. (A) PCA analysis of the full raw data set which shows limited separation between VC (black circles), 30mg/kg GSK2617971A (orange circles) or 60mg/kg GSK2617971A (grey circles). (B) Qlucore OE permits the user to adjust the statistical stringency of the data-set. Upon refining the data (0.29 variance, $p<0.05$ and 1.5 fold change in expression), only the most statistically significant gene expression changes are included in the PCA analysis thus producing a more robust separation of control and treated data. Such analysis reduced the number of significantly affected variables to 67, of which 32 were protein coding transcript (used in subsequent pathway analysis).

The 32 most statistically important protein-coding genes identified to best separate GSK2617971A treatment from control (as determined by PCA analysis) were then selected for IPA analysis with the aim of identifying key biological themes characteristic of GSK2617971A toxicity (as pathway analysis is unbiased the theme analysis is not simply reflective of OXPHOS uncoupling). It was decided to input

only the top most statistically significant genes into pathway analysis as submission of all genes differentially expressed following GSK2617971A produced an unspecific pathway prediction (biased towards most studied transcriptional responses e.g. tumourgenesis and neurodegenerative disorders). The gene list was filtered by IPA based on known biological function and mapped into interaction networks which were ranked quantitatively. These networks indicate functional association between genes which were affected by GSK2617971A treatment and other known genes within a biological pathway (Table 6.2 below). This functional association is ranked by score with the top three biological functions associated with each gene network provided.

Network Rank	Genes in Network	Score	Focus Genes	Biological Function
1	ADRB, Alp,**ATF3**, Cyclin A, **CYP1A1**, ERK1/2, estrogen receptor, **G0S2**, **GADD45B**, GOT, **GOT1**, Hdac, **HSPB1**, **HSPH1**, **IGFBP1**, IgG, IL1, **IRS2**, **JUN**, KLF6 LDL, **LPIN1**, MAP2K1/2, MEF2, **mir-122**, **MT1E**, PDGF BB, PEPCK, **PPARGC1A**, RGS16, RNA polymerase II, **SIK1**, **SLC38A2**, thyroid hormone receptor, Tnf (family)	47	16	Cell Death and Survival, Lipid Metabolism, Molecular Transport
2	ACOT13, AIP, CCDC64B, **CHAC1**, CHP1, CMSS1, CTDNEP1, DAG1, ECI2, ETHE1, GCKR, Gstm3, HNF4A, MEF2BNB-MEF2B, **MID1**, **MID1IP1**, **MT1E**, MT1H, NDUFA1, NDUFB5, NDUFV1, NECAP1, NUF2, **P4HA1**, POR, **PPP1R3B**, PWP1, **RAB30**, **SDS**, SLC30A7, SRP19, TMC6, TRIP11, TRMT61B, UBC	15	8	Cell Death and Survival, Cellular Assembly and Organization, Cellular Compromise
3	ADRA2A, Akt, **BTG2**, CDKN2D, Cebpd, Cg, CYP17A1, ERK, FSH, GPC1, Histone h4, Igf, Insulin, Interferon alpha, Jnk, lipoxin A4, Mapk, **MT1E**, NFkB (complex), P38 MAPK, Pdgf (complex), **PDK4**, PI3K (complex), Pka,Pkc(s), PTP4A1, RGS16, **S1PR1**, SRC (family), TCR, **TNFAIP2**, tyrosine kinase, **USP18**, vitamin K1	15	6	Cell Morphology, Cellular Development, Molecular Transport

TABLE 6.2: IPA network analysis (biological theme analysis) of top 32 protein coding genes differentially altered in response to GSK2617971A (30 and 60mg/kg). Direction of change is indicated by colour (**Red= increased**, **Green = decreased**). Genes not coloured red or green have known (experimentally proven) interactions with other members of the network. Scores are calculated from p-values (-log10p) and equate to the likelihood of the focus genes (differentially changing in response to GSK2617971A treatment) being associated by chance. Biological function indicates the top three biological themes corresponding to each network.

The top ranked network (due to the high score value, i.e. low likelihood that focus genes changing in GSK2617971A treated livers are associated in the network due to chance) relates to cell death and survival, lipid metabolism and molecular transport cell functions. Biological functions which were

inferred with less confidence by second and third ranked networks also include cell death / survival, effect on cell morphology, cellular compromise and cellular development.

Changes in genes such as Atf3, Irs2, Lpin1 and PGC1α (incorporated in the top rank network) were also observed following GSK932121A treatment (shown in chapter 3) and this may be suggestive of mitochondrial-toxicity signature genes. This concept will be explored further in chapter 7.

The 32 most significant protein coding transcripts which were altered by GSK2617971A treatment were subjected to an IPA-Tox analysis (Table 6.3). This analysis compares the user's gene signatures with other sets of genes known to change when perturbed by particular compounds and go on to provoke downstream pathology. The IPA-Tox-analysis describes adaptive, defensive, or reparative responses to xenobiotic insult and was used to better understand the potential tox specific downstream pathways, as suggested by gene expression analyses. Table 6.3 below includes a column which, where applicable, links the toxicological pathways generated by IPA (and indicative of the gene signatures differentially altered) to relevant observable effects which occurred in the current study and are presented in the current chapter.

Ingenuity Tox Lists	-log (p-value)	Ratio	Focus genes	Observable link to current study?
Acute Renal Failure Panel (Rat)	5.23E00	6.45E-02	JUN, ATF3, IGFBP1, MT1E	Evidence of renal toxicity (CRC, OCR, TEM, $\Delta\Psi$)
Liver Necrosis/Cell Death	3.92E00	1.85E-02	JUN, GADD45B, IGFBP1, MT1E, PPARGC1A	Evidence of hepatic mitochondrial toxicity (CRC and $\Delta\Psi$)
Nongenotoxic Hepatocarcinogenicity Biomarker Panel	3.06E00	9.09E-02	BTG2, MT1E	No relevant measurement
Renal Proximal Tubule Toxicity Biomarker Panel (Rat)	2.91E00	7.41E-02	IGFBP1, HSPB1	Evidence of renal toxicity (CRC, OCR, TEM, $\Delta\Psi$)
Aryl Hydrocarbon Receptor Signalling	2.57E00	1.88E-02	CYP1A1, JUN, HSPB1	No relevant measurement
PXR/RXR Activation	2.31E00	2.99E-02	IGFBP1, PPARGC1A	No relevant measurement
Liver Proliferation	2.14E00	1.39E-02	JUN ,IGFBP1, MT1E	No pathology available
Increases Liver Steatosis	2.1E00	2.74E-02	LPIN1, PPARGC1A	No pathology available
p53 Signalling	2.01E00	2.02E-02	JUN, GADD45B	No relevant measurement
Hepatic Fibrosis	1.86E00	2.08E-02	mir-122, IGFBP1	No pathology available
Decreases Permeability Transition of Mitochondria and Mitochondrial Membrane	1.85E00	1.43E-01	BTG2	Decrease in CRC noted *in vitro* and *in vivo*
Mechanism of Gene Regulation by Peroxisome Proliferators via PPARα	1.85E00	2.11E-02	JUN, PPARGC1A	No relevant measurement
Genes Downregulated in Response to Chronic Renal Failure (Rat)	1.75E00	1E-01	CYP1A1	Evidence of renal toxicity (CRC, OCR, TEM, $\Delta\Psi$)
FA Metabolism	1.74E00	1.69E-02	CYP1A1, SDS	Increased levels of lactate (likely corresponding effect on lipid metabolism)
Decreases Respiration of Mitochondria	1.7E00	9.09E-02	MT1E	Decrease OCR in kidney mitochondria
Increases Renal Proliferation	1.66E00	1.56E-02	JUN, MT1E	No relevant measurement
Cytochrome P450 Panel - Substrate is a Xenobiotic (Human)	1.56E00	5E-02	CYP1A1	No relevant measurement
Increases Depolarization of Mitochondria and Mitochondrial Membrane	1.53E00	5.88E-02	BTG2	Evidence of depolarization in kidney and liver mitochondria (MMP)
Cardiac Hypertrophy	1.52E00	8.04E-03	JUN, ATF3, PPARGC1A	No pathology or other relative assessments available
Cardiac Fibrosis	5.43E-01	5.52E-03	ATF3	No pathology or other relative assessments available

TABLE 6.3: IPA-Tox analysis of top 32 protein coding genes differentially altered in response to GSK2617971A. Top 20 toxicity pathways or functions linked to the 32 gene signatures inputted following GSK2617971A treatment (30 & 60mg/kg). –log(p-value) shows significance that the focus gene is not simply included in the toxicity pathway by chance. The ratio refers to the ratio of focus genes compared to total number of genes in the toxicity pathway (IPA database). These ratios are low but this is largely due to the fact only 32 transcripts were submitted for analysis. Any toxicity pathways arising from IPA-Tox analysis which is supported by other observations in this chapter are shown in orange with supporting evidence described.

Of the top 20 pathways generated via IPA-Tox analysis (with the 32 protein coding genes most significantly altered by GSK2617971A treatment used as the comparator), 8 of the pathways could be supported by other experimental data presented in this chapter (40%). In these cases many of the pathways identified by this method were very specific to the experimental data generated (e.g. decreases in permeability transition of mitochondria and increased depolarisation of mitochondria). Caution must however be advised as many of these Tox-pathway predictions are based on alterations in just a single gene. Furthermore, this analysis is not suggesting that gene expression data in one tissue can predict a toxic effect in another, just that (as a resource for toxicologists) the IPA-Tox analysis can identify gene-signatures which are suggestive of certain toxic effects, independent of the tissue or organ. In the present studies these suggestions were deemed fairly predictive and were substantiated by functional endpoints. I believe further studies of this kind are required in order to better assess the true utility of the IPA package.

These data do however suggest that if the genes inputted for IPA analysis are first filtered to only the most significant (i.e. in terms of separating control versus treatment) then the output from pathway analysis appears to be more robust.

6.3. Discussion

Uncouplers of OXPHOS are a common class of mitochondrial toxicant seen in pre-clinical screening [211]. Despite this, few studies have been reported which detail the AOP arising from drug-induced OXPHOS uncoupling *in vivo*. Since they are a common class of mitochondrial toxicant, it is important to understand their toxicological effect *in vivo,* in order to better advise discovery groups of the potential risk involved with progressing such molecules and offer strategies to manage their development when required. This is especially important considering OXPHOS uncouplers are considered attractive therapeutic agents for the treatment of many disorders [212] including non-alcoholic fatty liver disease [213], type 2 diabetes [214], ischemia reperfusion injury [215] and acute neurological injury [216].

To provide a benchmark for the evaluation of *in vitro* assays of mitochondrial dysfunction, the present study investigated the MOA of the acute toxicity caused by an uncoupler of OXPHOS in rats. To facilitate the assembly of an AOP, a single administration (mid and high dose) study which was likely to cause an adverse outcome was performed in male Crl:Wi (Han) rats, and a systems approach was used to detect downstream consequences.

Uncouplers of OXPHOS have been shown to cause hyperthermia *in vivo*. An example of this is the hyperthermic response caused by 2,4-DNP which has been linked to fatal incidences in recent years following the use of DNP as a dieting aid [149, 217, 218]. Hyperthermia has also been reported *in vivo* following administration of other known uncouplers such as tolcapone [219]. This is not unexpected considering uncoupling of OXPHOS is the fundamental mechanism of non-shivering thermogenesis in brown adipose tissue [220]. Uncoupling proteins (UCP's), specifically UCP1 (or thermogenin), decrease the proton gradient generated by the ETC by increasing the permeability of the IMM to protons [221, 222]. In the present study, hyperthermia was an early consequence of treatment of rats with GSK2617971A, the magnitude of the response correlating well with plasma levels of the drug suggesting that drug-induced OXPHOS uncoupling is the primary cause of increased thermal energy generation. Interestingly however, no effect on body temperature was noted at 30mg/kg GSK2617971A, despite abnormalities in mitochondrial function noted at this dose. This observation is suggestive that OXPHOS related hyperthermia is downstream in the AOP from mitochondrial effects such as reduction in $\Delta\Psi$ and CRC. It is likely that compensatory mechanisms are able to maintain whole body temperature regulation following milder mitochondrial uncoupling and heat generation is confined to the tissue-level during the early stages.

As discussed, 30mg/kg GSK2617971A did not affect either body temperature or provoke adverse clinical signs up to four hours post dose but did cause a marked and statistically significant reduction in CRC and $\Delta\Psi$ in the liver and the kidney (also observed at 60mg/kg). Firstly, it is important to acknowledge that all observations with 30mg/kg require validation because of the low number of experimental repeats (due to study circumstances beyond control). Having said this, samples obtained for all endpoints at 60mg/kg were taken at a time-point where the animals showed clinical signs but those at 30mg/kg were obtained from animals which were to all appearances normal. This highlights that endpoints significantly altered with a 30mg/kg dose (i.e. CRC and $\Delta\Psi$) are representative of underlying sub-toxic DIMT and that endpoints significantly affected by the 60mg/kg dose group may be attenuated with the high level of toxicity. Furthermore, this surprising observation suggests that membrane depolarisation and impaired CRC does not necessarily cause an adverse clinical reaction and that these events most certainly occur at lower toxicity (dose) levels than the observed increases in body temperature and effects on mitochondrial ultra-structure.

Induction of MPT has been noted with other compounds with known uncoupling activity such as the selective serotonin reuptake inhibitor sertraline [223] and the tyrosine kinase inhibitor regorafenib [224], with both groups speculating that MPT induction was a key mechanism of hepatocyte injury. Further

work should explore whether reduction in CRC and $\Delta\Psi$ observed in mitochondria isolated from animals treated with 30mg/kg GSK2617971A is recoverable at later time points (i.e. due to turnover of the mitochondrial pool through dynamic processes such as mitophagy and biogenesis) or whether a dose of 30mg/kg provokes adverse toxicity following repeated administrations. The present study does however show a correlation between observations made *in vitro* and *in vivo* and demonstrates the potential utility of the CRC assay, both as a potential screening aid and as an early marker of mitochondrial uncoupling.
One difficulty in assessing uncoupling-induced effects on OCR is the bell-shaped nature of the dose response. A valid hypothesis for the limited effects observed in response to GSK2617971A treatment using the Seahorse Bioanalyser is that the concentration of the drug in the plasma was high (~270µM and ~540µM with 30mg/kg and 60mg/kg respectively) and this high concentration is likely to be represented in the tissues (drug tissue concentration data not available). The peak uncoupling response *in vitro* (in terms of OCR) was observed at just 1µM and concentrations above this were toxic to the respiratory chain.

Another feasible hypothesis is that GSK2617971A may have been washed out of the mitochondrial preparations during the isolation procedure and therefore has limited effects in these isolates. For this to be the case however, we must assume that the effects of OXPHOS uncoupling on CRC and mitochondrial $\Delta\Psi$ are more persistent and are irreversible (or only very slowly reversible) upon removal of the drug. Data presented in this chapter (Fig.6.7) does however show that the effect of GSK2617971A can be reversed upon removal of the drug; however this experiment was performed *in vitro* and further work is required. This analysis does however raise questions about the utility of assessing direct effects on mitochondrial function in *in vivo* studies by subcellular fractionation, although this "wash out" effect would not apply to all compounds and other endpoints (e.g. CRC) look to be persistent. This observation is however pertinent when considering it amongst other compromises already associated with isolating mitochondria (i.e. representative of *in vivo* scenario, structural damage etc). Novel methods, such as using primary cell isolates, and *in vivo* biomarkers, should continue to be evaluated as better ways of assessing the effects of mitochondrial toxicants *in vivo* are sought.

An increase in lactate:pyruvate ratio was observed at 4 hours post-dose with 60mg/kg GSK2617971A. Lactic acidosis has previously been noted following administration of uncouplers both *in vitro and vivo* [225, 226]. Lactate is known to be a biomarker of mitochondrial dysfunction *in vivo* as energy metabolism is switched to glycolysis in attempts to maintain ATP levels following perturbation of OXPHOS, to the detriment of increased levels of local lactate generation (also shown in chapters 3-5 following complex III ETC inhibition). Alongside increases in lactate:pyruvate ratio, mitochondrial ultra-

structural observations were also observed at 60mg/kg (although unfortunately data was not obtained in the liver). Ultra-structural observations noted in the present study were comparable to those induced *in vivo* by the classical mitochondrial uncoupler 2,4-DNP [227] and the mild uncoupler, indomethacin [228]. When noted in preclinical studies, these observations (mitochondrial swelling and disorganisation of mitochondrial networks) should in the future, alert drug safety scientists to the possibility that the compound may have functional effects on mitochondria and thus prompt further investigations.
As there was no effect observed on lactate:pyruvate ratio or mitochondrial ultrastructure at 30mg/kg, it appears these endpoints are only affected in conjunction with the adverse outcome and not at sub-toxic doses (this will be further explored in chapter 7). Importantly however, as functional changes (such as reduction in both $\Delta\Psi$ and CRC*)* were observed in mitochondria isolated from 30mg/kg GSK2617971A treated animals, we can say that increases in blood lactate and alterations in mitochondrial ultra-structure occur downstream in the AOP. This may suggest that the point at which lactate is raised in whole blood and/or when mitochondrial ultra-structure becomes affected, might be key pathological events underpinning the onset of adverse clinical signs following OXPHOS uncoupling.

Microarray analysis was used to identify downstream pathways or cellular functions which were differentially affected by GSK932121A treatment. Statistical parameters were adopted which helped to reduce the number of differentially expressed genes to the top 32 most significant for separating the experimental variables. These 32 genes were then subjected to both biological theme and IPA-Tox analysis. Biological theme analysis identified that a number of genes affected by GSK2617971A uncoupling belong to a network of transcripts involved in cell death and survival. Kuruvilla and colleagues in 2003, explored the molecular events downstream of OXPHOS uncoupling *in vitro* and they observed comparable transcriptional patterns with FCCP as observed here with GSK2617971A [229]. They suggest that an early consequence of uncoupling is DNA damage, characterised by changes in genes such as *Gadd153, Gadd45, p21/Waf1* and *Fas,* with consequences observed on cell cycle control and cell death at later time points. These data correspond to gene expression data / biological theme analysis in the present study which demonstrates transcriptional activation of genes such as *Gadd45b* and *Jun* alongside identification of gene networks involved in cell death (although no absolute measure of cell death was made). This observation opens up the possibility that the mechanisms underlying FCCP and GSK2617971A toxicity may be comparable. Meanwhile, IPA-Tox analysis identified specific toxicological events which correlated well to other functional data within the present study (e.g. membrane depolarisation and reduction in mitochondrial respiration). Importantly however the levels of confidence in these analyses are questionable when toxicological themes are generated based on alteration of single genes.

Overall, data presented in this chapter (alongside evidence reported in the literature with other tool mitochondrial uncouplers e.g. 2,4-DNP) enabled the assembly of a proposed AOP/MOA for OXPHOS uncoupling *in vivo* (Fig.6.11). Whilst some endpoints do not fully-fit the AOP/MOA framework outlined in chapter 5 (i.e. not measurable, causally related or too broad e.g. generalised mitochondrial insufficiency) this is a starting point for further refinement in more focussed future studies. This AOP can be referred to when molecules with uncoupling activity are identified *in vitro,* in order to aid selection of the most robust endpoints for *in vivo* assessment or to better understand the potential safety liabilities of this class of mitochondrial toxicant.

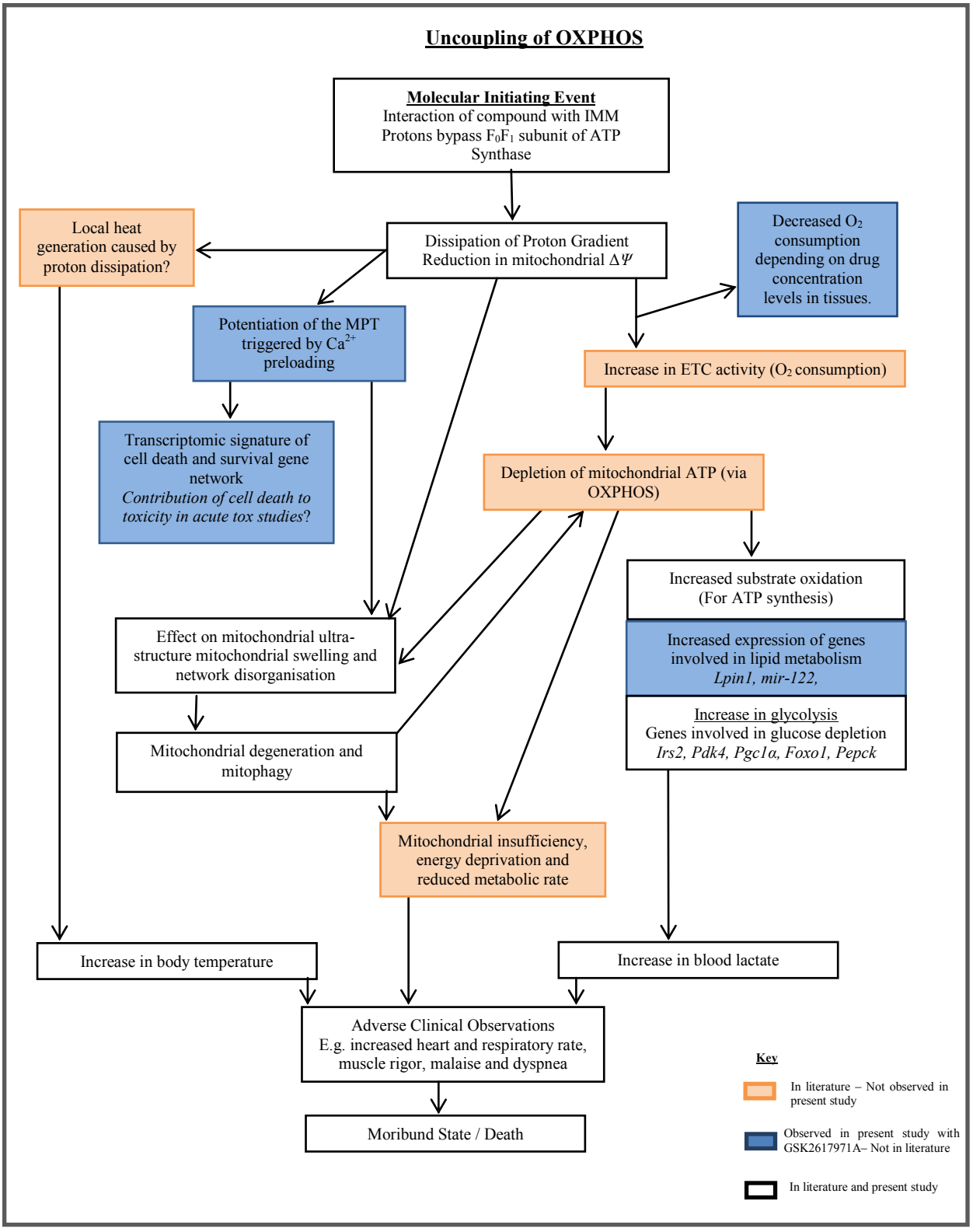


FIGURE 6.11: Proposed AOP/MOA for mitochondrial OXPHOS uncoupling *in vivo*. Events which are supported by experimental data presented in this chapter (for GSK2617971A) and which are generally not reported (or are under-reported) in the literature, are shown in **blue boxes.** Events which are reported widely in the literature for OXPHOS uncouplers but which were either not observed or measured in the present study are shown in **orange boxes**. Clear boxes show endpoints which are acknowledged in the literature and were observed in the present study. It is anticipated that various key events in the AOP have consequences on uncoupling-induced toxicity but in general it is considered that ATP depletion increased body temperature, increased substrate oxidation and lactic acidosis are the primary causative factors.

6.4. Summary

To summarise, GSK2617971A was toxic when dosed at 60mg/kg to rats, with hyperthermia and adverse clinical signs observed at 4 hours post-dose. A dose of 30mg/kg was well tolerated despite functional changes in mitochondria being observed (reduction in $\Delta\Psi$ and CRC*),* highlighting the utility of these endpoints as possible early markers of mitochondrial uncoupling at sub-toxic doses.

In general, data generated *in vivo* correlated well with that produced by *in vitro* investigations suggesting utility of these approaches for screening of uncoupling agents. The exception was the decrease in OCR observed in mitochondria isolated from the kidney of rats treated with 60mg/kg GSK2617971A *in vivo,* compared with the increase in OCR observed when control isolated mitochondria were treated directly with GSK2617971A *in vitro* (although potential reasons for this discrepancy have been highlighted). At higher doses, mitochondrial uncoupling caused ultra-structural changes to mitochondria in the kidney, although analyses in other tissues are required. In addition there was an increase in blood lactate, reflecting attempts to maintain ATP levels via glycolysis. It is likely that these effects, together with acute hyperthermia are the principal causes of the acute toxicity observed downstream of OXPHOS uncoupling *in vivo*.

Transcriptomics highlighted activation of gene-networks involved in cell death (although there was no confirmation that this was actually occurring) and lipid metabolism with IPA-Tox analysis proving a useful tool with regards to predicting toxicological outcomes (many of which were supported by data within the study) using a selection of the most statistically significant gene changes. The major limitation of IPA-Tox theme analysis was however, that conclusions were based around changes in just a small number of genes. This chapter highlights the critical importance of using a systems approach to understand and build AOP's with the use of both higher (toxic) and lower (not overtly toxic) doses to aid determination of upstream and downstream (primary/adaptive) effects.

The acute natures of the studies outlined in chapters 3-6 have however made identification of endpoints at sub-toxic doses challenging (i.e. measures of underlying un-attenuated DIMT). Chapter 7 below, explores potential underlying markers of DIMT both as biomarkers and to differentiate primary from adaptive toxicological events.

7.0. THE EFFECT OF SUB-CYTOTOXIC CONCENTRATIONS OF GSK932121A AND GSK2617971A IN VITRO AND COMPARISON WITH A BIOINFORMATICALLY SELECTED 'SIMILAR' CHEMICAL

7.1. Introduction

Systems toxicology investigations presented in chapters 3-6, have identified a range of endpoints which are differentially affected by DIMT, specifically following respiratory chain inhibition and OXPHOS uncoupling *in vivo* and a number of common observations were made. Most notable was a metabolic switch to glycolysis, elevation in plasma lactate concentration, ultra-structural effects on mitochondria, effects on mitochondrial function and similar patterns of hepatic gene expression including alterations to genes involved in cell metabolism and cell stress. Taken together, these changes reflect the metabolic adaptation in the liver to drug-induced compromise in ATP synthesis via the ETC / OXPHOS (be this via inhibition of the mitochondrial complexes or uncoupling). Even with the use of well-tolerated doses of both GSK932121A (12.5mg/kg used in chapter 4) and GSK2617971A (30mg/kg used in chapter 6), a gap in the investigations completed to date is the difficulty in distinguishing primary from secondary events in the resulting AOP's for both drugs. Furthermore, it remained to be determined whether the observed downstream effects (i.e. the metabolic switch) are specific cellular adaptations following mitochondrial perturbation or common stress responses.

To address these questions a study was designed *in vivo* whereby animals would be killed at progressive time points in order to analyse the effect of mitochondrial perturbation at the tissue level and thus potentially determine the sequential order in which the key changes take place. Due to time and practical constraints this wasn't possible. As an alternative, the progression of events was explored *in vitro* and importantly at concentrations of drug which were not grossly toxic to the cells. I was especially interested in exploring the narrow window whereby compound-induced alterations in respiratory function were observable, prior to the onset of gross cellular cytotoxicity. It was hoped this analysis would help to determine both the order in which these fundamental events occur and the utility of *in vitro* systems in terms of replicating the *in vivo* effects.

Furthermore, I wanted to better understand whether the transcriptional response to GSK932121A and GSK2617971A in the liver was similar to that of any other previously studied compound and whether any connected compound was a mitochondrial toxicant. It was hoped to identify other reference compounds to further study mitochondrial toxicity and determine whether the endpoints being studied are common to mitochondrial toxicants or whether they occur in response to compounds with different modes of action.

Importantly the cells used in this chapter were cultured in a media supplemented with galactose rather than glucose. Human liver hepatocellular carcinoma cells lines (HepG2) are heavily reliant upon

glycolysis for energy production which has been shown to desensitise them to drug-induced mitochondrial perturbation (a phenomenon reported in the literature as the Crabtree effect) [106]. This effect can be circumvented by conditioning the HepG2 cells in galactose rather than glucose media and thus increasing the cells reliance on OXPHOS for ATP-production. This occurs as oxidation of galactose to pyruvate yields no net ATP, which forces cells to oxidize pyruvate (via OXPHOS) to survive. This model has shown increased sensitivity for detecting drug-induced mitochondrial perturbation in the pre-clinical setting [230]. This approach does however have certain limitations such as the reduced growth rate and changes in the cellular and mitochondrial proteome.

7.1.1. EXPERIMENTAL AIMS

The experimental aims of the work outlined in this chapter were…

1. To identify the concentration range of GSK932121A and GSK2617971A where mitochondrial function was compromised in the absence of gross cellular cytotoxicity. Using this narrow concentration window would build confidence that any observed effect was due to the perturbation of mitochondrial function as opposed to being secondary adaptive consequences to cytotoxicity.

2. At the concentrations determined in (1), to assess the impact of DIMT on lactate generation, mitochondrial ultrastructure and on a TaqMan gene expression panel consisting of genes pertinent to the toxicological response of both compounds *in vivo*. Furthermore, to identify the order in which these effects occur to be able to determine causal from consequential effects and thus validate early molecular events reported in the proposed GSK932121A and GSK2617971A AOP/MOAs.

3. To perform connectivity mapping analysis on liver transcriptomics data from GSK932121A and GSK2617971A treated animals, and identify novel tool compounds which may mimic the biological action of both drugs based on the genes which are differentially altered. Any connected compounds would then be screened in the Seahorse analyser to assess any effect on mitochondrial function and using the aforementioned *in vitro* methods to explore mechanistic similarity to both GlaxoSmithKline compounds.

7.2. Results

7.2.1. Identifying Effectual Sub-Cytotoxic Concentrations

The mitochondrial effects of GSK932121A and GSK2617971A were assessed *in vitro*. Following which, any concentration of drug found to affect the mitochondrial (OCR) or glycolytic (ECAR) cellular metabolism of HepG2 cells was assessed using a measure of cell viability. The objective was to identify concentrations of both compounds which caused metabolic compromise but showed no signs of gross cellular cytotoxicity.

GSK932121A – Complex III Inhibition

Exposure of HepG2 cells to GSK932121A *in vitro* (n=3) resulted in decreases in key bioenergetic parameters, demonstrated using a mitochondrial stress test (Fig.7.1A). The response observed was typical of a mid-respiratory chain inhibitor, i.e. reducing the amount of molecular oxygen consumed at mitochondrial complex IV via inhibition of the ETC. Statistically significant and concentration-dependent reductions in basal respiration and ATP-synthase linked respiration (concentrations of 7.5µM and above) were observed alongside a reduction in maximal respiration (concentrations of 0.75µM and above) following GSK932121A treatment *in vitro* (Fig.7.1B). OCR parameters were calculated as described in ([231]-supplementary). Concentrations of GSK932121A were chosen to match plasma drug concentrations achieved *in vivo* (i.e. up to ~75µM). With statistically significant effects on respiratory chain function noted as low as 0.75µM GSK932121A in HepG2 cells, cytotoxicity was assessed at concentrations of 0.75µM and above.

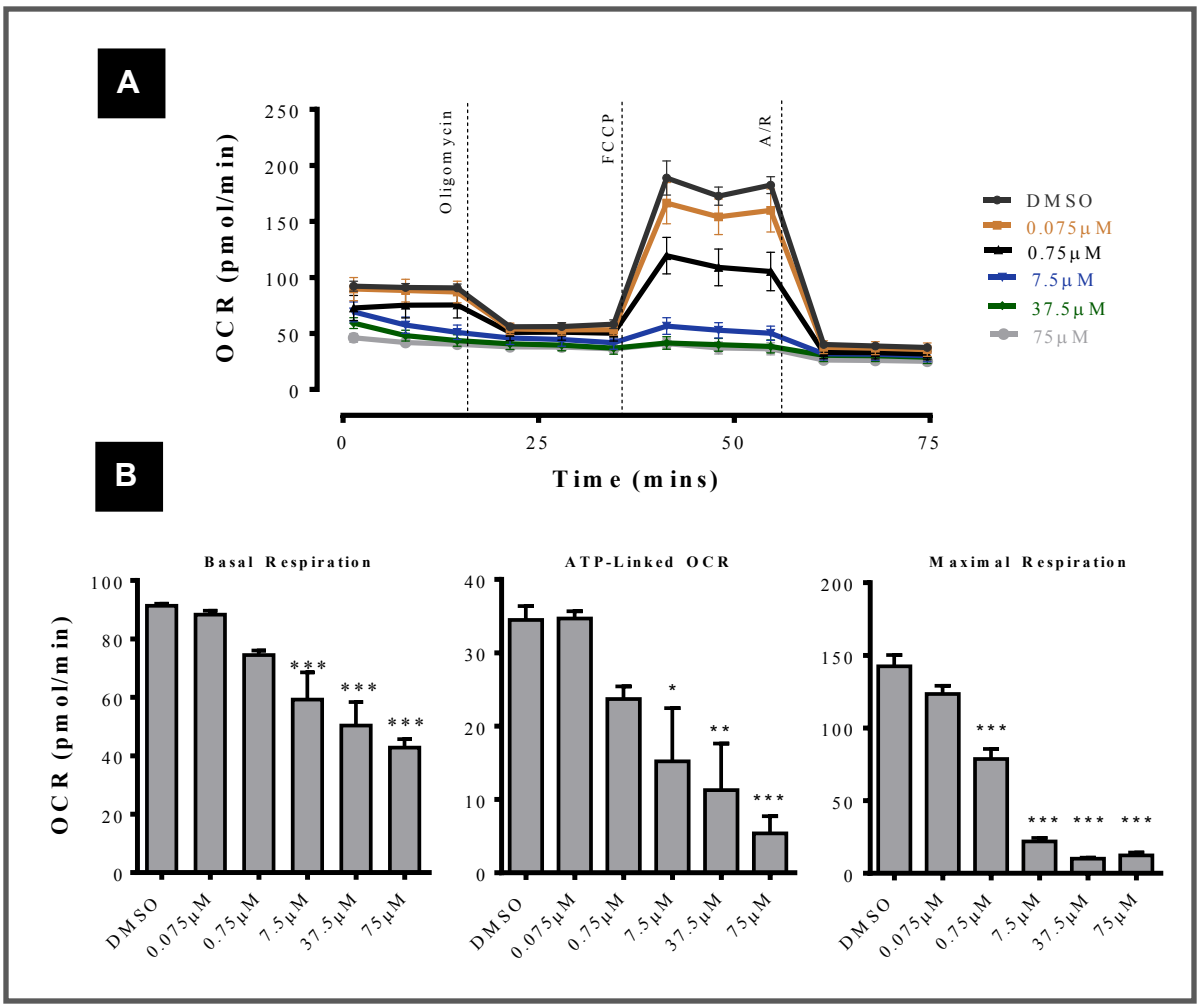


FIGURE 7.1: Analysis of HepG2 mitochondrial OCR following acute *in vitro* treatment with GSK932121A (measured using Seahorse XF$_e$96 analyser). HepG2 cells were treated *in vitro* with GSK932121A (0.075µM-75µM, 15 technical replicates per plate) and OCR was assessed. A mitochondrial stress test was then performed in order to assess the effect of GSK932121A on key bioenergetic parameters (n=3). (A) A representative graph of OCR outputs from the XF$_e$96 analyser of DMSO control (black line) and GSK932121A treated (various colours, 0.075µM-75µM) and the response to oligomycin, FCCP and Antimycin A /Rotenone (A/R). (B) Effect of GSK932121A on basal respiration, ATP-linked respiration and maximal respiration. OCR parameters were calculated as described in ([231]-supplementary). Data shown is mean ± SD (n=3), mid-point OCR. Significance stars depict reduction in OCR compared to DMSO control *p<0.05, **p<0.01, ***p<0.001.

Cytotoxicity was assessed using a LDH assay, at an 8 hour time point (Fig.7.2.). LDH leakage and light microscopy analyses (not shown) were used as the measures of cytotoxicity in the present study as many other cytotoxicity detection assays are in fact measures of mitochondrial activity (e.g.ATP assays, MTT Tetrazolium assay) and as such may over-predict cytotoxicity to mitochondrial-acting compounds. This time point was selected as subsequent *in vitro* experiments (section 7.2.2-7.2.4 below) were performed up to a maximum of 8-hours post treatment (as I wanted to assess effects due to mitochondrial perturbation

using an acute experimental design as all aforementioned *in vivo* studies involved short periods of exposure).

LDH was measured in spent media following an 8 hour treatment with GSK932121A or 0.1% DMSO control. 1% (v/v) Triton-X-100 detergent (in cell culture media) was used as a positive control (as described by [232]) and data were expressed as a percentage of leaked LDH compared to total LDH (calculated from a lysed cell sample prepared used 200µL Cell Lytic per well (Sigma Aldrich, #C2978). Significant effect on cell viability was observed at concentrations of 25µM, 50µM and 75µM GSK932121A compared to a 0.1% DMSO control ($p<0.001$, n=3). No effect on LDH leakage was observed at 0.75µM, 5µM or 10µM GSK932121A compared to the DMSO control ($p>0.05$).

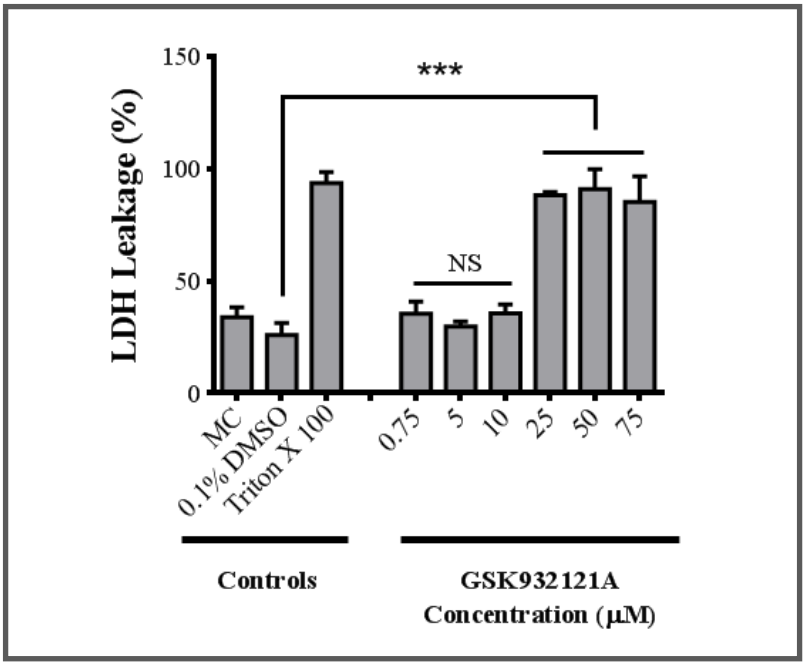


FIGURE 7.2: The effect of GSK932121A on HepG2 cytotoxicity using an LDH leak/lyse assay. The cytotoxicity of GSK932121A (at an 8 hour time point) was assessed *in vitro* in HepG2 cells by measurement of LDH leakage. Triton-X-100 was used as a positive control and the effect on media alone (MC) was also measured. Data is expressed as a percentage of LDH leaked compared to total LDH in the cells (i.e. lysed sample analysed following Cell Lytic treatment). Data is expressed as mean ± sd. ***$p<0.001$.

Concentrations of GSK932121A selected for further analysis therefore were 1µM, 5µM and 10µM. These were the concentrations which were defined by experiment to be sub-cytotoxic up to an 8 hour time point whilst causing a significant acute effect on respiratory chain function.

GSK2617971A – OXPHOS Uncoupling

The effect of GSK2617971A on HepG2 cell metabolic function was assessed using the Xf_e96 analyser (Fig.7.3 below). A significant increase in glycolytic metabolism (represented by increase in ECAR with statistical significance depicted using # in Fig.7.3. below) was observed at doses of 0.1µM ($p<0.05$), 1µM ($p<0.001$), 5µM ($p<0.001$) and 10µM ($p<0.01$) of GSK2617971A compared to a 0.1% DMSO control, with a peak response observed at 5µM. The peak concentration in terms of effect on OCR was at 1µM with an 80.2% increase in OCR observed compared to the DMSO control. A significant reduction in OCR was observed following treatment with 50µM as GSK2617971A becomes toxic to the respiratory chain at high concentrations (typical of a mitochondrial uncoupler and as shown in Fig.5.1 following *ex vivo* treatment with GSK2617971A of control isolated liver mitochondria). As all concentrations tested had a significant effect on metabolic function, all were analysed in the LDH leak/lyse assay to assess where the onset of cytotoxicity occurs.

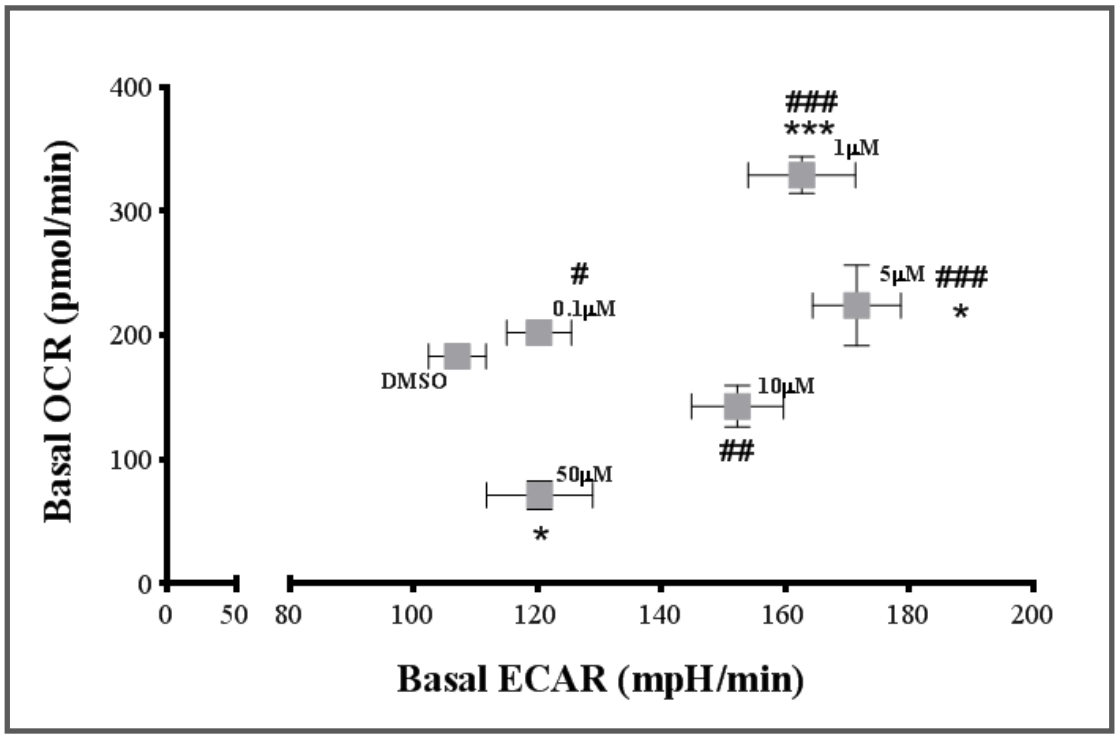


FIGURE 7.3: Effect of GSK2617971A (OXPHOS uncoupling) on HepG2 cell metabolism (OCR and ECAR). The effect of increasing concentrations of GSK2617971A (0.1µM-50µM, + 0.1% DMSO control) on both OCR (y-axis) and ECAR (x-axis) is shown. Statistical significance is highlighted using stars (*) for OCR and hash tags (#) for ECAR. A bell shaped dose response was observed with both OCR and ECAR following GSK2617971A treatment. Peak response in terms of ETC function (OCR) was observed at 1µM ($p<0.001$, n=3) and the peak response relating to glycolytic activity (ECAR) was observed at 5µM GSK2617971A ($p<0.001$), compared to DMSO control. */# $p<0.05$, **/## $p<0.01$, ***/### $p<0.001$.

Following an 8 hour exposure to either GSK2617971A (0.1µM-50µM), 0.1% DMSO control, media alone (MC) or a 1% Triton-X-100 positive control, spent media was analysed for LDH leakage. A significant increase in leaked LDH (indicating compound related cytotoxicity) was observed at 10µM ($p<0.05$) and 50µM ($p<0.001$) GSK2617971A compared to DMSO alone (Fig.7.4). Despite no evidence of LDH leakage with 5µM GSK2617971A, light microscopy evaluation identified a minor degree of vacuolation in the HepG2 cell appearance which was absent at lower doses and in the DMSO control (not shown). Taking this observation into consideration it was decided that 5µM would not be used in subsequent investigations due to minor observations which could be considered adverse effects. Instead doses of 0.1µM, 1µM and 2.5µM were selected for further analysis.

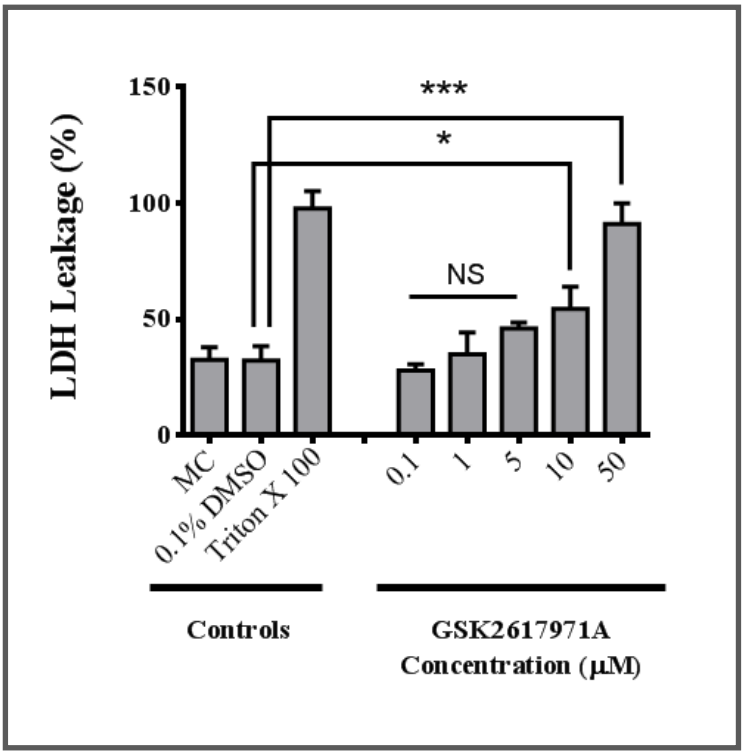


FIGURE 7.4: Effect of GSK2617971A on HepG2 cell cytotoxicity using an LDH leak/lyse assay. The cytotoxicity of GSK2617971A (at an 8 hour time point) was assessed *in vitro* in HepG2 cells by measurement of LDH leakage. Triton-X-100 was used as a positive control and the effect on media alone (MC) was also measured. Data is expressed as a percentage of LDH leaked compared to total LDH in the cells (i.e. lysed sample analysed following Cell Lytic treatment). Data is expressed as mean ± SD (n=3), $p<0.05$*, $p<0.001$***

Having identified effective sub-cytotoxic concentrations of GSK932121A and GSK2617971A, these concentrations were then tested in HepG2 cells for up to 8 hours to assess the effect on lactate generation, mitochondrial/cellular morphology and gene expression.

7.2.2. IN VITRO LACTATE GENERATION

An increased level of blood lactate was observed in rats following treatment with both GSK932121A and GSK2617971A *in vivo*. Mechanistically, mitochondrial perturbation causes an increase in lactate as cells switch metabolism away from impaired mitochondrial OXPHOS and towards cytoplasmic glycolysis. Glycolysis offers cells an opportunity to produce cellular ATP, independent of mitochondrial ETC function via substrate level phosphorylation however the process is far less efficient and lactate generation is a consequence of this response.

Preliminary Experiment: Prior to exploring the effect of both tool compounds on lactate generation *in vitro,* it was important to perform a preliminary experiment to determine the optimum media glucose concentration to ensure the cells had sufficient glycolytic substrate to optimise subsequent lactate generation. As proof of concept, compounds which are known to increase lactate *in vitro* due to mitochondrial inhibition were used. Oligomycin (2μg/mL) and antimycin A (1μM) were chosen with concentrations based on evidence in the literature showing these concentrations induced the desired lactate response [233].

In galactose-conditioned cell maintenance media alone, both oligomycin and antimycin A induced a statistically significant increase in supernatant lactate at both 1 hour and 4 hours post treatment (highlighted by # in Fig.7.5 below). However, the relative increase in lactate was significantly greater when treatment was made alongside addition of increasing concentrations of glucose (2.5mM, 5.5mM and 11mM). The increase in lactate generation following oligomycin/antimycin A treatment in glucose supplemented cells was significantly higher than the relative response in galactose alone at 1 hour with 11mM glucose (Fig.7.5A) and significantly higher than galactose alone with 2.5mM, 5.5mM and 11mM glucose at 4 hours (Fig.7.5B). These data suggest that supplementing the media with glucose significantly improves the lactate response to mitochondrial perturbation and this effect is enhanced both with time and glucose concentration.

In order to ensure that the lactate generated was as a result of the exogenous glucose which was provided (i.e. lactate produced *de novo* by the action of glycolysis) 2-deoxyglucose (2-DG), a potent glycolytic inhibitor, was used. 2-DG is a competitive inhibitor of hexokinase and as such completely inhibits the production of glucose-6-phosphate from glucose. In the present study, 50mM 2-DG (with the same increasing concentrations of glucose) inhibited the lactate production which was observed following oligomycin and antimycin A treatment with glucose supplementation (minus 2-DG). This data confirms

that the lactate produced following treatment with both mitochondrial toxicants is directly linked to the levels of glucose supplemented to the cell maintenance media. As 2-DG blocks glycolysis at the level of hexokinase (i.e. glucose conversion to glucose-6-phospate) it has no effect on galactose uptake into glycolysis, as galactose enters the glycolysis pathway directly at glucose-6-phosphate (via glucose-1-phosphate).

The effect of glucose treatment alone on lactate generation in galactose treated cells was also examined with no significant increase observed (data not shown).

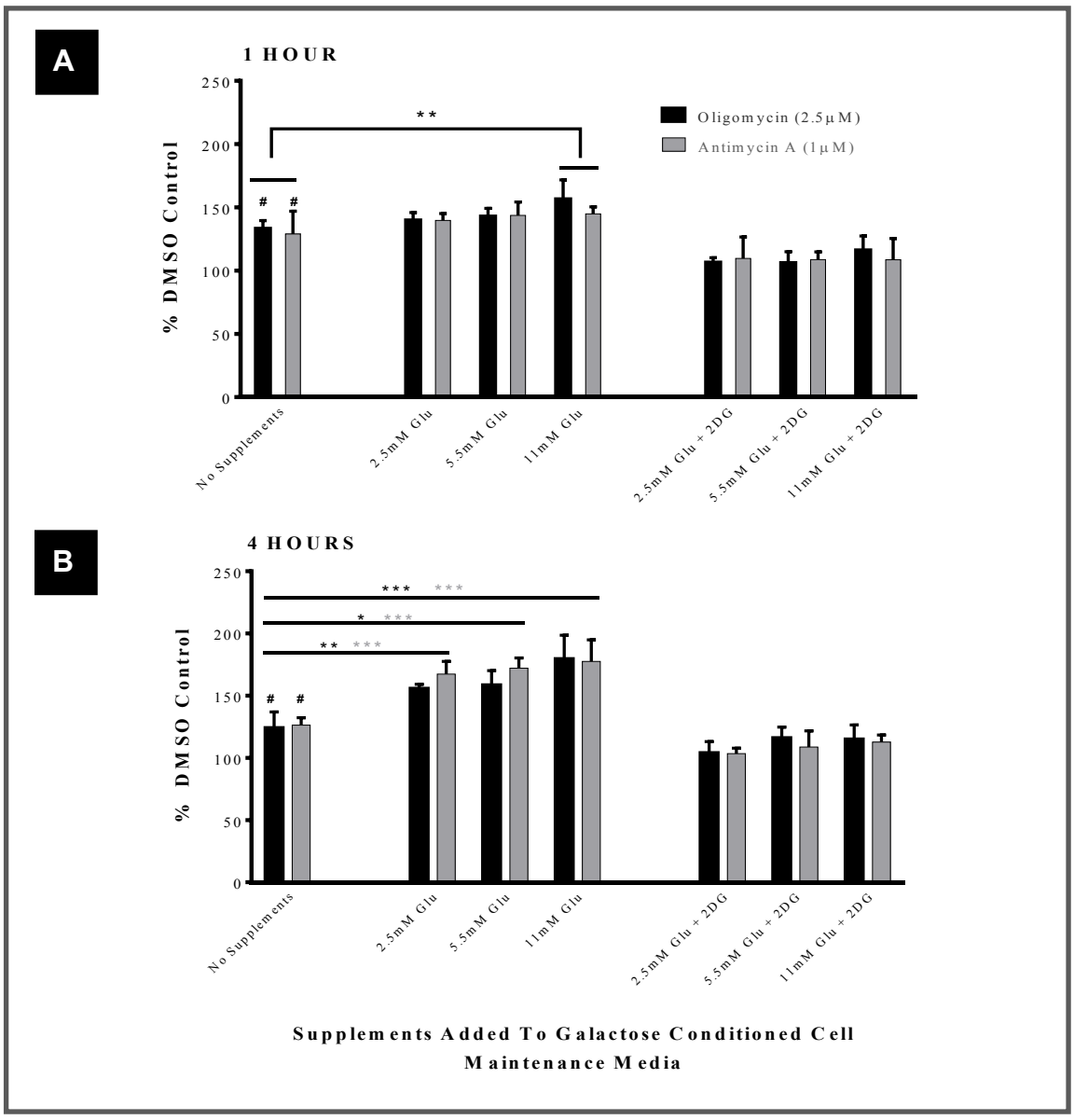


FIGURE 7.5: Effect of glucose concentration on the generation of lactate in HepG2 cell supernatant following treatment with Oligomycin and Antimycin A. HepG2 cells were incubated for 1 hour (A) and 4 hours (B) with either oligomycin (2.5µM) or Antimycin A (1µM) in galactose conditioned media provoking a statistically significant increase in lactate (marked with an # and labelled as no supplements). Relative increase in lactate was however significantly increased with both compounds whereupon oligomycin and antimycin A were treated alongside increasing doses of glucose (in galactose conditioned media). 2-DG (50mM) inhibited antimycin A / oligomycin induced lactate generation. Data is expressed as a percentage of the response elicited to a 0.1% DMSO control. Data shown is mean ± sd (n=3), $p<0.05$*, $p<0.01$**, $p<0.001$***

Following analysis of the effect of glucose concentration on oligomycin and antimycin A induced lactate generation, it was decided that 11mM of glucose would be supplemented to the cell maintenance media upon treatment with both GSK932121A and GSK2617971A to ensure an optimal window for observing treatment related effects on lactate generation. It was hoped that the addition of glucose, only at the time

of compound-treatment, would provide the substrate required to facilitate metabolic switching (to a detectable level using the methods available) but not negate the effects of culturing in galactose. Further experimentation is however required to assess how long it takes for media supplementation (i.e. glucose addition) to have a significant effect on underlying metabolic activities.

Assessment of lactate generation following treatment of HepG2 cells with sub-cytotoxic concentrations of GSK932121A and GSK2617971A: The aim of the experiment was to analyse the acute effect of GSK932121A/GSK2617971A on lactate generation (including speed of onset), both *in vitro* and at sub-toxic concentrations. As such three concentrations of both GSK932121A (1, 5 and 10μM) and GSK2617971A (0.1, 1 and 2.5μM) were tested over an 8 hour acute time-course. Supernatant samples were taken at 1 hour, 2 hours, 4 hours and 8 hours post-treatment for analysis of lactate (as described in section 2.14). Data shown is represented as a percentage of a 0.1% DMSO control (n=3).

A significant increase in lactate was observed at 4 hours post-treatment with 5μM (146.2% ±14.3, $p<0.05$) and 10μM (170.6% ± 13.1, $p<0.01$) GSK932121A and at 8 hours post-treatment with 10μM (147.8% ± 18.5, $p<0.05$) GSK932121A alone, compared to time matched DMSO controls (Fig.7.6A). No effect was observed with either dose at 1 hour or 2 hours post-treatment. No effect on lactate was observed at 1μM GSK932121A at any time point ($p>0.05$).

Only a minor effect on lactate production was observed following uncoupling of OXPHOS with GSK2617971A *in vitro* (Fig.7.6B). A significant increase in lactate was only observed at 2.5μM GSK2617971A at the 8-hour time point (138.3% ± 5.7, $p<0.05$, n=3) compared to a time matched 0.1% DMSO control. No effect was seen at lower concentrations or earlier time points.

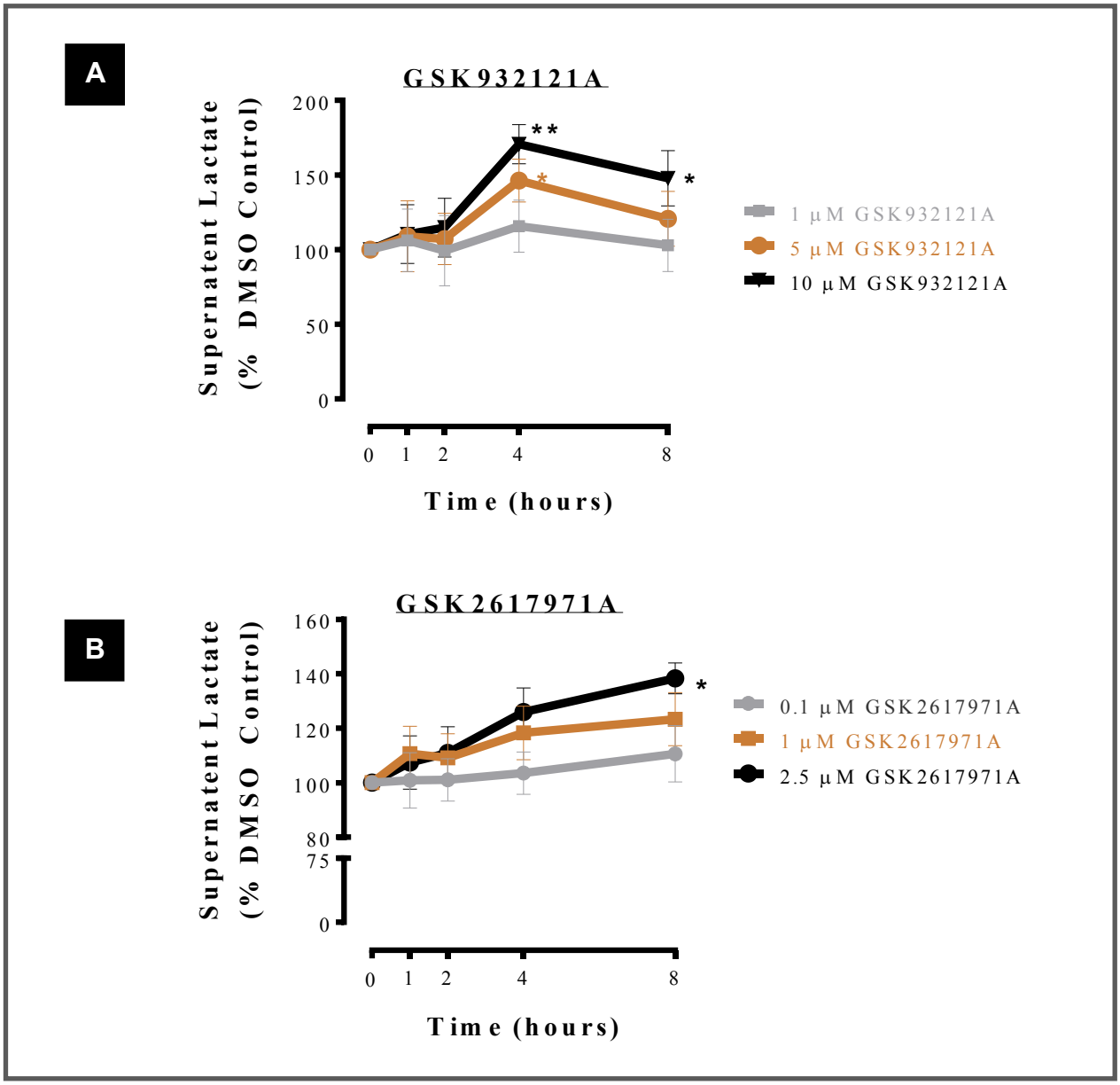


FIGURE 7.6: Effect of sub-cytotoxic concentrations of GSK932121A and GSK2617971A on HepG2 cell lactate generation up to 8 hours. (A) Effect of GSK932121A (1µM, 5µM and 10µM) and (B) GSK2617971A (0.1µM, 1µM and 2.5µM) on lactate concentration in HepG2 cell media up to 8 hours post treatment. All data is expressed as a percentage of time matched DMSO control lactate concentration and plotted as mean ± SD (n=3). $p<0.05$*, $p<0.01$**

These data show that lactate is increased in HepG2 cells at concentrations of both GSK932121A and GSK2617971A which are not grossly cytotoxic to the cells, at 4-8 hours post-treatment. To further investigate the early biochemical effects of complex III inhibition and OXPHOS uncoupling *in vitro* and using well tolerated concentrations, gene expression profiling was used. A gene panel was assembled

based on data obtained *in vivo* with both compounds. As the main metabolic event observed in the proposed AOP of both compounds was the switch towards glycolysis, the genes selected primarily involved cellular glycolytic function alongside genes involved in lipid metabolism, gluconeogenesis and cell stress responses.

7.2.3. RT-PCR – METABOLIC SWITCH GENE PANEL

The aim of this work was to identify early gene expression changes occurring as a result of subtle complex III inhibition and OXPHOS uncoupling *in vitro* (i.e. at sub-cytotoxic concentrations). The same experimental conditions, as described above for the lactate assay, were repeated to enable comparisons to be drawn between gene expression alterations and onset of lactate stimulation. Identification of genes responding early following exposure to these compounds may provide the opportunity to, a) better understand the early mechanisms of toxicity following the molecular initiating event for both drugs, and b), identify any potential "marker genes" which could be measured in future studies to assess potential underlying changes in mitochondrial function.

As described above, a gene panel was assembled based on *in vivo* microarray data with both compounds in rat liver. The gene panel was selected in a supervised manner, which enabled selection of genes pertinent to the mechanisms under investigation. This was deemed preferable to selecting genes based on statistical significance (i.e. an unsupervised approach) as this method does not account for the known fundamental mechanisms. Table 7.1 below describes the genes selected for analysis in this experiment.

Gene symbol	Gene name	Fold change and stat sig following complex III inhibition (50mg/kg) (GSK932121A)	Fold change and stat sig following OXPHOS uncoupling 30mg/kg and 60mg/kg (GSK2617971A)	Headline summary of biochemical function	Reason for inclusion in gene-panel
NR4a1	Nuclear receptor subfamily 4, group a, member 1	**5.42x*** **	**1.27x** **1.76x***	Ligand-independent transcription factors which function as immediate or early response genes. Key transcriptional regulators of hepatic glucose and lipid homeostasis. Key review can be found in [234].	Upregulated with both compounds *in vivo* and heavily linked to cell metabolism in the liver.
NR4a2	Nuclear receptor subfamily 4, group a, member 2	**2.69x** **	**1.25x** **2.00x** **		
NR4a3	Nuclear receptor subfamily 4, group a, member 3	**5.22x*** **	**1.24x** **2.26x***		
Ppargc1a (PGC1α)	Peroxisome proliferator-activated receptor gamma, coactivator 1 alpha	**8.18x*** **	**1.05x** **3.76x*** **	Transcriptional co-activator and central co-ordinator of gluconeogenesis and mitochondrial biogenesis in the liver [235, 236].	Upregulated with both compounds *in vivo* and heavily linked to cell metabolism in the liver.
Foxo1	Forkhead box 01	**1.56x***	**1.59x*** **2.08x***	Forkhead transcription factor. Plays pivotal role in glucose metabolism and the action of insulin on glucogenic processes [237].	Upregulated with both compounds *in vivo* and heavily linked to cell metabolism in the liver.
Pck1	Phosphoenolpyruvate carboxykinase 1	**1.94x** **	**1.22x** **1.48x***	Rate limiting step in gluconeogenesis – Converts oxaloacetate to phosphoenolpyruvate (substrate for gluconeogenesis) [157].	Upregulated with both compounds *in vivo* – Linked to gluconeogenesis
G6pd	Glucose-6-phosphate dehydrogenase	**-1.05x**	**-1.38x** **-1.28x**	Catalyses reaction between glucose (in the form of G6p) and 6-phosphogluconolactone in the PPP.	No change observed *in vivo* but key gene involved in glycolysis/PPP
Irs2	Insulin receptor substrate 2	**4.78x*** **	**1.41x** **3.37x*** **	Irs2 is phosphorylated by the Insulin receptor during signal transduction and plays subsequent role in glucose metabolism in the liver [238].	Upregulated with both compounds *in vivo* and heavily linked to cell metabolism in the liver.
Pdk4	Pyruvate dehydrogenase kinase isozyme 4	**2.22x** **	**1.17x** **3.76x** **	Inhibits pyruvate dehydrogenase complex by phosphorylation which prevents pyruvate conversion to acetyl-coA. Pyruvate instead converted to oxaloacetate for gluconeogenesis. [239]	Upregulated with both compounds *in vivo* and heavily linked to cell metabolism in the liver.

Hmox1	Heme oxygenase 1	**2.22x****	**-1.04x** **3.06x*****	An essential enzyme in heme catabolism, cleaves heme to form biliverdin, which is subsequently converted to bilirubin by biliverdin reductase, and carbon monoxide. Involved in cytoprotection to hepatocyte injury *in vivo* [240].	Upregulated with both compounds *in vivo* and heavily linked to the response to physiological stress.
Lpin1	Lipin 1	**4.65x*****	**1.15x** **3.30x****	Controls the metabolism of FAs at different levels. Phosphatidate phosphatase enzyme which catalyses the conversion of phosphatidic acid to diacylglycerol during triglyceride biosynthesis. Acts as a nuclear transcriptional coactivator for PGC1α /Ppar-α to modulate lipid metabolism gene expression [241].	Upregulated with both compounds *in vivo* and heavily linked to liver cell metabolism.
Ppar-α	Peroxisome proliferator-activated receptor alpha	**1.01**	**1.27x** **1.88x****	Among other functions, Ppar-α plays a role in regulating lipid metabolism via Lpin1 and PGC1α during periods of fasting or increased FA supply [242].	Upregulated following GSK2617971A treatment *in vivo* and heavily involved in the Lpin1/PGC1α control of lipid metabolism.
Chac1	Chac, Cation Transport Regulator Homolog 1	**12.72x*****	**-1.08x** **1.62x***	Pro-apoptotic component of the unfolded protein response pathway by mediating the pro-apoptotic effects of the ATF4-ATF3-DDIT3/CHOP cascade	Upregulated with both compounds *in vivo* and linked to cell stress response.
Atf3	Activating transcription factor 3	**8.73x*****	**1.28x** **5.36x*****	Transcriptional repressor and induced by many stress signals. Plays a role in downstream signalling of the unfolded protein response pathway and in control of gluconeogenic Pck1 expression in the liver [243] Also involved in EIF2 kinase stress pathway following amino acid starvation [244].	Upregulated with both compounds *in vivo* and linked to cell stress responses.

TABLE 7.1: Genes selected for use in TaqMan gene-panel. The table describes the genes which were incorporated into a custom TaqMan gene-panel aimed at identifying early gene expression signatures downstream of mitochondrial perturbation *in vitro*. Genes were selected based on observations *in vivo* and the effect of both GSK932121A and GSK2617971A on the induction of all genes is indicated (fold change, and statistical significance, $p<0.05$*, $p<0.01$**, $p<0.001$***). The proposed mechanism of action for each gene is provided alongside the main justification for use in this gene panel.

The focus of the gene panel was largely on the metabolic adaptation which occurred downstream of mitochondrial perturbation induced by both molecules, however a small number of genes involved in cell-stress responses (i.e. Chac1 and Atf3) were also included. This experiment was performed alongside the lactate investigation described above. As such, GSK932121A, GSK2617971A and a 0.1% DMSO control were introduced to a confluent monolayer of HepG2 cells in cell maintenance media supplemented with 11mM glucose. After 1 hour, 2 hours, 4 hours and 8 hours, the cell media was removed and cells were lysed with RNA Lysis Buffer (Promega SV RNA Isolation Kit). Triplicate wells were pooled and the experiment was repeated on three separate occasions (n=3). Data was represented in a heat map format with statistically significant alterations in gene expression following GSK932121A (Fig.7.7) and GSK2617971A (Fig.7.8) treatment compared to the 0.1% DMSO control shown.

GSK932121A (Complex III Inhibition) – Gene Panel Data (Fig.7.7)

The NR4A Gene Family: GSK932121A (complex III inhibition) caused a significant induction of the nuclear receptor 4-alpha genes Nr4a1 and Nr4a3 over the time course with Nr4a1 upregulated with all concentrations at 4 hours and with 5μM and 10μM at 8 hours ($p<0.01$). Nr4a3 was significantly elevated at 2 hours with 5μM GSK932121A (1.7x, $p<0.01$) and then with 5μM and 10μM at 4 hours (1.58x and 2.12x respectively) and finally with all concentrations at 8 hours post treatment ($p<0.001$). These data indicate that effect of GSK932121A on induction of the NR4a genes has a trend towards being more time-dependent than dose dependent. Despite efficient target amplification, no effect on Nr4a2 compared to the 0.1% DMSO control was observed throughout the study.

PGC1α/Foxo1 Gene Expression: GSK932121A induced a consistent increase in gene expression of PGC1α and Foxo1 which are known as metabolic switch/master regulator genes. The increase in expression of both genes was highly significant at 1 hour post treatment with all concentrations, compared to the DMSO control ($p<0.01$). An increase in PGC1α expression (with all concentrations of GSK932121A) was then observed throughout the time course with the exception of with 0.1μM GSK932121A at a 4 hour time point (trending increase but $p>0.05$). At later time points (4 hour and 8 hour), Foxo1 expression was only increased with the higher doses of 5μM and 10μM GSK932121A however data for both genes suggests they play a key role in the control of cell metabolism following complex III inhibition *in vitro*.

PGC1α-Foxo1 Effectors: As anticipated, the downstream effector genes of PGC1α and Foxo1 were generally induced later in the time course than Foxo1 and PGC1α. However, a significant induction of Pck1 (involved in the rate limiting step of gluconeogenesis) was observed at all concentrations at 1 hour

post treatment compared to the DMSO control. Pdk4 was also increased at 1 hour with 5μM GSK932121A however a significant reduction in expression was observed with 10μM GSK932121A, which makes interpretation of data with Pdk4 challenging at early time points. G6pd was increased at 1μM ($p<0.01$) and 10μM ($p<0.05$) although data with this gene appeared highly variable. Only minor effects on the downstream effector genes were observed at 2 hours post-treatment with the exception of Pck1 which remained significantly elevated with all concentrations compared to the DMSO control. At 4 hours post-treatment a significant increase in the expression of Irs2 was observed with all concentrations and with high fold-changes (2.1x with 5μM and 6.6x with 10μM GSK932121A). The activation of Irs2 was however temporary as no effect was noted at 8 hours. GSK932121A caused only minor effects on Pdk4 and Hmox1 expression at 4 hours, with a slight reduction in the expression of both genes. At 8 hours post-treatment a significant increase in the expression of Hmox1 and G6pd was observed at all concentrations suggesting that induction of these genes occurred later or downstream to the observed increase in Foxo1, PGC1α and Pck1 expression.

Lpin1-Ppar-α and the stress response genes Atf3 and Chac1: Induction of Lpin1 (involved in activating FAO) was observed at 4 hours post treatment with both 5μM and 10μM GSK932121A (1.64x and 2.98x respectively). This increase preceded a respective increase in both Lpin1 and Ppar-α at 8 hours post-treatment with all concentrations of GSK932121A compared to DMSO control. This suggests that transcriptional activation of Lpin1/Ppar-α mediated FAO was delayed and was a later consequence of the action of GSK932121A although Lpin1 expression preceded that of Ppar-α. Similarly, a significant reduction in the expression of two genes involved in the cell stress/unfolded protein response (Chac1 and Atf3) was observed at 1 hour and 2 hour post-treatment with GSK932121A. Increases in the expression of both genes appeared however to be time dependent with all concentrations of GSK932121A inducing a significant increase in the expression of both genes by 8 hours.

These data show that treatment with well tolerated concentrations of GSK932121A caused an early increase in the regulator genes PGC1α, Foxo1 and Pck1. Transcriptional effects on other genes appear to be time dependent rather than dose dependent and include induction of Nr4a1/3, Gdpd, Hmox1, Lpin1, Ppar-α, Chac1 and Atf3.

GSK932121A (Complex III Inhibition) – Gene Panel Data

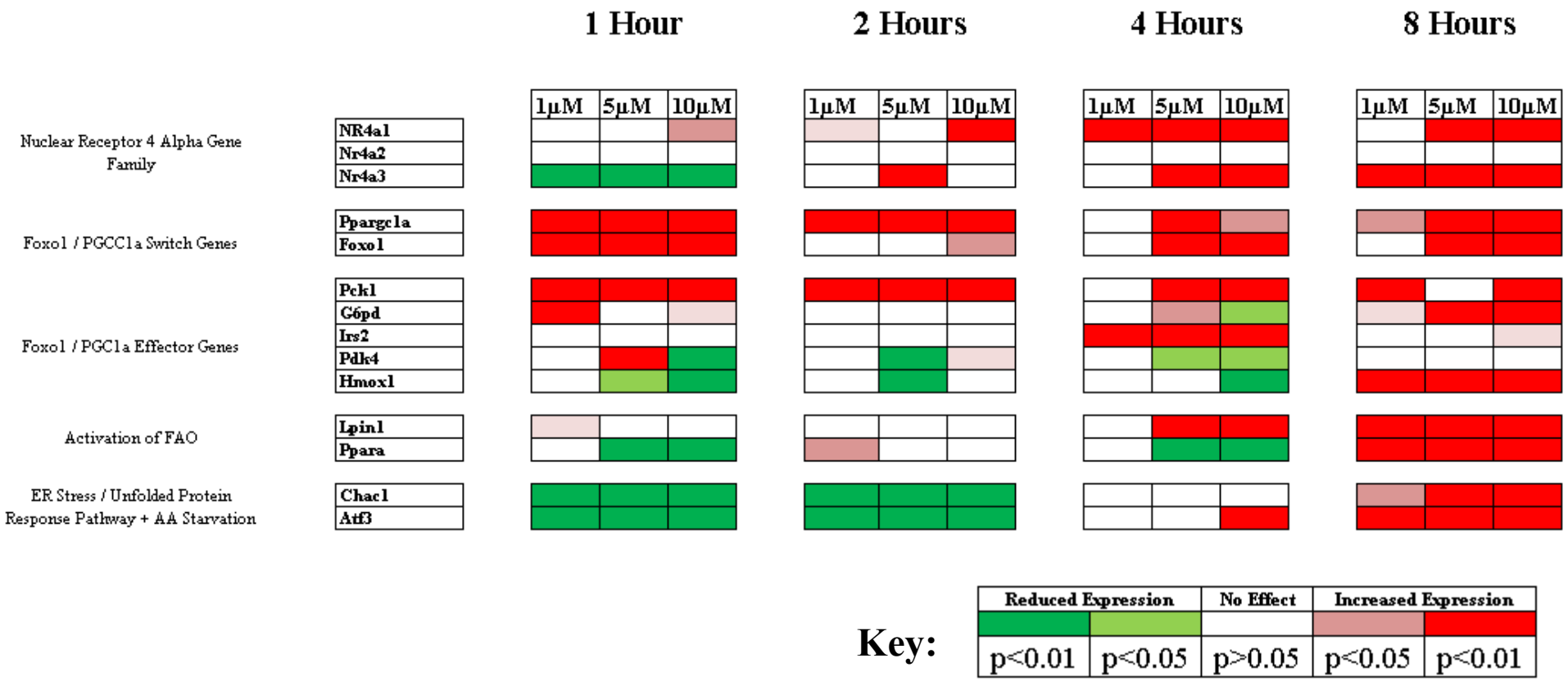


FIGURE 7.7: Heat map showing the effect in HepG2 cells of GSK932121A on a selection of pertinent genes involved in the response to DIMT. Data shown represents a heat map of statistically significant changes in the expression of a number of genes following GSK932121A treatment *in vitro*. Experiments were repeated on three occasions (n=3) and fold change (and statistical significance) was calculated against a 0.1% DMSO control. Any changes in gene expression where $p<0.05$ are shown (in either direction).

GSK2617971A (OXPHOS Uncoupling) – Gene Panel Data (Fig.7.8)

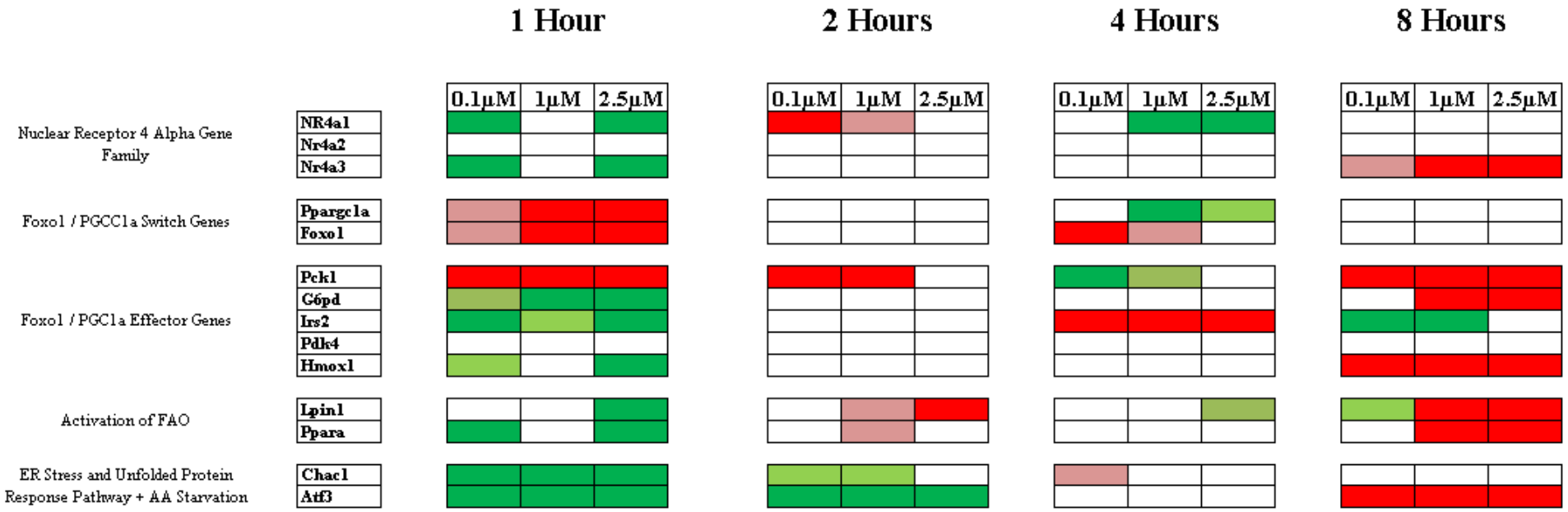
Like observations made with GSK932121A, the OXOHOS uncoupling agent GSK2617971A caused a time dependent increase in the expression of most genes over the time course studied. At 1 hour post treatment 9 of the 14 genes on the panel had lower levels of expression than the corresponding 0.1% DMSO control. Most notably, there was a significant reduction in both of the stress response genes, Chac1 and Atf3, with all concentrations of GSK2617971A. Furthermore, a reduction in the expression of Nr4a1/3 at 0.1μM and 2.5μM GSK2617971A was observed alongside reductions in Irs2, Hmox1, G6pd, Lpin1 and Ppar-α, especially with the 2.5μM concentration. However, as observed with GSK932121A, the expression of regulator genes PGC1α and Foxo1, alongside Pck1 (gene encoding the rate limiting enzyme involved in gluconeogenesis) was increased with all concentrations.

At 2 hours post treatment with GSK2617971A, (with the exception of Pck1 which remained transcriptionally up-regulated) all downstream effector genes of the action of PGC1α / Foxo1 (Hmox1, Pdk4, Irs2, G6pd) were unchanged compared to control. Likewise the expression of Chac1 and Atf3 remained reduced compared to the DMSO control. A significant increase in expression was however observed with Lpin1 at 1μM ($p<0.01$, 1.2x) and 2.5μM ($p<0.01$, 1.7x) and these data suggest early transcriptional activation of FAO genes. At 2 hours a significant increase in the expression of Nr4a1 at 0.1μM and 1μM was observed although no effect was seen with 2.5μM.

The transcriptional response to GSK2617971A remained fairly subtle at the 4 hour time point with many genes involved in the cell stress response, activation of FAO and glycolytic / gluconeogenic processes not significantly changed compared to DMSO control. However, when compared to data at 1 and 2 hours where many of these genes had significantly reduced expression levels compared to control, it may be inferred that the expression of these genes was in fact gradually increasing. Like observations noted with GSK932121A, the expression of Irs2 was maximally induced at 4 hours with fold changes of 5.1, 7.6 and 13.5 observed with 0.1μM, 1μM and 2.5μM respectively ($p<0.001$). Despite an increase in the expression of Foxo1 persisting with 0.1μM and 1μM GSK2617971A, a reduction in the expression of PGC1α was observed with 1μM and 2.5μM GSK2617971A and it was apparent that the transcriptional activity of these regulator genes was starting to decline.

At 8 hours post-treatment with GSK2617971A (the only time-point in which an increase in lactate was observed), a statistically significant induction of Atf3, Lpin1, Ppar-α, Hmox, G6pd, Pck1 and Nr4a3 was observed with either all GSK2617971A concentrations or with 1μM and 2.5μM. This data represents a more similar pattern of gene expression to observations made *in vivo*. At 8 hours post treatment the expression of both PGC1α and Foxo1 was not significantly altered compared to control highlighting a reduction in the expression of these co-ordinators of the metabolic response. No effect on Pdk4 was observed throughout the study at any time points or with any concentration of compound.

GSK2617971A (OXPHOS uncoupling) – Gene Panel Data



Key:

Reduced Expression		No Effect	Increased Expression	
p<0.01	p<0.05	p>0.05	p<0.05	p<0.01

FIGURE 7.8: Heat map showing the effect in HepG2 cells of GSK2617971A on a selection of pertinent genes involved in the response to DIMT. Data shown represents a heat map of statistically significant changes in the expression of a number of genes following GSK2617971A treatment *in vitro*. Experiments were repeated on three occasions (n=3) and fold change (and statistical significance) was calculated against a 0.1% DMSO control. Any changes in gene expression where $p<0.05$ are shown (in either direction).

The following conclusions can be drawn from the gene expression data with both compounds…

- PGC1α, Foxo1 and Pck1 were the earliest response genes studied in this experiment and were induced at 1 hour post-treatment with both GSK932121A and GSK2617971A. In response to complex III inhibition these genes remain constitutively active over the 8 hour time course whereas following OXPHOS uncoupling expression of these genes gradually declines.
- In general the expression of the majority of genes is more time-dependent than dose dependent. This is highlighted by the down-regulation in many genes in the panel at early time points and increases in expression at late time points. This is especially pertinent with regards to the effect of both compounds on Chac1 and Atf3, the FAO induction genes, Lpin1 and Ppar-α, as well as Hmox1 and G6pd.
- The transcriptional activity of Irs2 appears to be transient with a significant elevation of expression observed at 4 hours post-treatment with both compounds and little effects observed at other time points.
- The nuclear receptor 4-alpha genes, Nr4a1 and Nr4a3, appear to play a role in downstream adaptation to DIMT, also in a time dependent manner (up to 8 hours) although no effect was observed with Nr4a2 throughout the experiment.

7.2.4. IN VITRO ELECTRON MICROSCOPY

Another key observation noted *in vivo* with both compounds was the effect of DIMT on mitochondrial ultrastructure (both GSK932121A and GSK2617971A) and on the levels of cellular glycogen / free lipid in hepatocytes (GSK932121A alone). TEM investigations to date have however only been performed at late time points and largely in conjunction with severe clinical toxicity. The present work sought to investigate the effects of low concentrations of both GSK932121A (complex III inhibition) and GSK2617971A (OXPHOS uncoupler) on HepG2 cell ultra-structure with a particular emphasis being placed on mitochondrial structure and cellular glycogen / lipid levels.

An important consideration of this experiment was however that TEM analysis is costly and low throughput. Concentrations and time-points selected for analysis were therefore based on effects seen on lactate generation and gene expression (sections 7.2.2 and 7.2.3 above) and as such were concentrations where effect on HepG2 cell structure was most likely to be observed. Taking this into account, the effect

of GSK932121A on HepG2 cell ultrastructure was assessed at 4 hours and 8 hours post-treatment with 5µM and 10µM concentrations. TEM analysis was performed on GSK2617971A treated cells only at 8 hours and with 1µM and 2.5µM concentrations. Following compound treatment (and at the defined time point), cells were prepared for TEM analysis as described in section 2.10.2. HepG2 cells were assessed for mitochondrial morphological abnormalities compared to a time-matched 0.1% DMSO control. Glycogen and lipid content was assessed (per 100 cells) by counting those containing glycogen clusters and those which contained more than 1 lipid droplet. Data is shown below in Table 7.2.

A

Compound and Concentration	Time Point (Hours post dose)	% of Cells with Glycogen clusters	% of Cells with Lipid droplets
DMSO Control (0.1%)	**4**	**26**	**16**
GSK932121A (5µM)	4	9	21
GSK932121A (10µM)	4	10	9

B

Compound and Concentration	Time Point (Hours post dose)	% of Cells with Glycogen clusters	% of Cells with Lipid droplets
DMSO Control (0.1%)	**8**	**21**	**19**
GSK932121A (5µM)	8	25	20
GSK932121A (10µM)	8	12	14
GSK2617971A (1 µM)	8	12	13
GSK2617971A (2.5 µM)	8	22	12

TABLE 7.2: Effect of GSK932121A and GSK2617971A on the intracellular levels of HepG2 cell glycogen and lipid. (A) The percentage of cells (per 100 cells counted) containing glycogen clusters and >1 lipid droplet was assessed following a 4 hour treatment with 5µM or 10µM GSK932121A. (B) The same assessment was made at 8 hours post treatment with GSK932121A (at the same concentrations as in A) and with 1µM or 2.5µM GSK2617971A.

Whilst providing an interesting insight the lack of experimental repeats makes drawing experimentally and statistically significant conclusions from the TEM data a challenge. The data shown in Table 7.2 should therefore be viewed as preliminary. At 4 hours post treatment, a reduction in the percentage of cells containing glycogen clusters was observed following treatment with 5µM and 10µM GSK932121A. Inconsistent with *in* vivo observations however was the reduction in cells containing lipid droplets with 10µM GSK932121A. At 8 hours post-treatment with GSK932121A, reductions in glycogen levels were again observed with 10µM GSK932121A. As cultured cells are more reliant on glucose for cell metabolism (as opposed to fatty acid), perhaps this explains the lack of lipid accumulation.

A reduction in glycogen stores was also observed with 1µM GSK2617971A at 8 hours although this was a concentration which showed no effect on lactate generation *in vitro* and under the same experimental

conditions and no effect was observed with 2.5μM. A moderate reduction in lipid levels was observed with GSK2617971A at both 1μM and 2.5μM however it is presently unknown whether this is a significant observation (although it would fit with the hypothesis of increased substrate utilization following OXPHOS uncoupling).

Mitochondrial Morphology

In the same survey sections, the effect of both GSK932121A and GSK2617971A on mitochondrial morphology was assessed. Analysis of TEM micrographs (data not shown) supports observations made *in vivo* which suggest that mitochondrial structural changes occur only at higher exposure levels and at concentrations which provoke adverse effects. To confirm this (and to validate that mitochondrial ultra-structural effects can be detected with these compounds *in vitro*), mitochondrial morphology would need to be assessed following *in vitro* treatment with higher concentrations of both drugs, which are grossly cytotoxic, however time, budget and experimental throughput constraints prevented such analysis in the present study.

7.2.5. COMPOUND CONNECTIVITY MAPPING

Compound connectivity mapping was performed using SScMap (statistically significant connections' map) program as described in [146, 147]. It was hoped to identify other molecules with similar downstream transcriptomic profiles to those of GSK932121A and GSK2617971A, which therefore, may also modulate mitochondrial function. These could then be used as tools in order to validate observations made to test if changes are mechanism specific rather than compound-dependent. The 34 most statistically significant, differentially regulated protein coding genes following GSK932121A treatment and the 32 most significant genes for GSK2617971A were input into SScMap. These genes were the most contributory to the separation of experimental variables via principal component analysis (i.e. effect of drug treatment on gene expression in rat livers). The most significant genes were determined using Qlucore OE (as described in section 6.2.4). Only the most statistically significant gene alterations were selected for comparison to avoid connection with other compounds based on marginally changed genes. Table 7.3 below shows the genes which were submitted to compound connectivity mapping categorised into their reported cellular function. Common genes which were altered as a result of administration of both compounds are highlighted in red.

Genes Submitted for Connectivity Mapping		
Cellular Function	**Gene Symbols**	
	GSK932121A	**GSK2617971A**
Cell metabolism	**Sds**, **Ppargc1a, Irs2, Sik1, Lpin1**, Nr4a1, Nr4a3, Coq10b	**Sds**, **Ppargc1a, Irs2, Sik1, Lpin1,** Got1, Ppp1r3b, Mir-122, Pdk4
Cell signalling / signal transduction	**Jun**, Gem, Trib1	**Jun**, Rab30, Rgs16
Cell cycle control / apoptosis	**Mir-505**, Insc, Zfp354a, Gdf15, Rhob, **Btg2**	**Mir-505, Btg2,** G0s2, Klf6
Cell stress response	**Atf3, Chac1**, Gadd45b, Sult2a1, Sult2a2, Gadd45g, Il1rn, Alp1, Gstm3	**Atf3, Chac1,** Hsph1, Hspb1, Upp2, Tnfaip2, Gadd45b, Cyp1a1 (xenobiotic metabolism)
Transporters	Slc16a6 (lactate/ pyruvate, amino acids, ketones) **Slc38a2** (amino acid transporter), Atp1b1 (Na+ / K+), Slc1a4 (amino acid transporter)	**Slc38a2** (amino acid transporter)
Other cell processes	Doc2a (calcium sensing), Egr1 (mitogenesis and differentiation), Mt2a (binds heavy metals), Ccrn4l (circadian rhythm)	Igfbp1 (cell growth), Eif4ebp3 (protein translation), Mt1a (binds heavy metals), S1pr1 (cell migration), Usp18 (protein deubiquination), P4ha1 (collagen synthesis), Midlip1 (unknown)

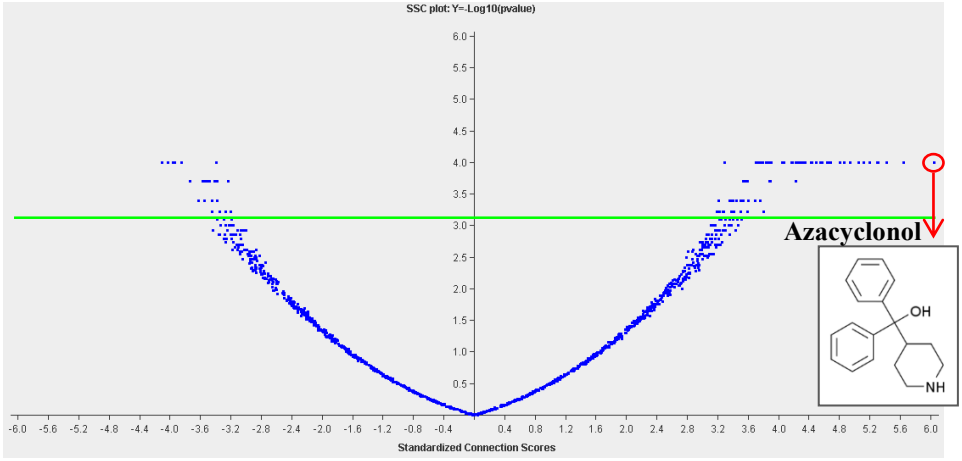
TABLE 7.3: Genes submitted for connectivity mapping analysis. The most statistically significant genes in terms of separating VC gene expression from GSK932121A (34 genes) and GSK2617971A (32 genes) treatment are shown. Genes have been separated according to biological function (according to the NCBI, Entrez database – accessed April 2015). Genes shown in **red** are commonly altered genes with both GSK932121A and GSK2617971A.

Despite the fact that GSK932121A (ETC inhibitor) and GSK2617971A (uncoupler) perturb mitochondrial function with differing mechanisms, they share 11 transcripts within their respective top significant gene lists. This opens up the possibility that, independent of mechanism, a common transcriptional response may exist following treatment with mitochondrially toxic agents. Connectivity mapping analysis was performed as described in section 2.17.6.

The expression signatures for both compounds were analysed separately with connection scores and p-values plotted as volcano diagrams (as shown in Fig.7.9). The connection score is calculated from comparison of query gene signatures with the reference database and therefore any closely related compounds appear on the far right of the x-axis. Statistically significant data points are located above a threshold (highlighted by the green line in Fig.7.9A) and therefore closely connected compounds which have a statistically significant comparison index are located as far right and as high as possible (the top 10

connected compounds for both GSK932121A and GSK2617971A are shown in Fig.7.9B). Analysis of volcano plots for both GSK932121A and GSK2617971A identified a single "top-hit" molecule (azacyclonol) which was highly significant for both drugs in terms of similarity of gene expression signatures.

A



B

GSK932121A Connected Compounds	Connection Score
Azacyclonol	7.35
Disulfiram	6.73
Mometasone	6.50
Ciclopirox	6.47
Mefloquine	6.38
Perphenazine	6.35
Astemizole	6.10
Maprotiline	6.04
Tribenoside	6.03
Iocetamic acid	6.02

GSK2617971A Connected Compounds	Connection Score
Azacyclonol	6.04
Ikarugamycin	5.64
Helveticoside	5.42
Lanatoside C	5.31
Strophanthidin	5.29
Haloperidol	5.20
Clozapine	5.12
Econazole	5.06
Dosulepin	5.06
Disulfiram	4.94

FIGURE 7.9: Exemplar volcano plot for GSK2617971A / GSK932121A connectivity map and top ten connected compounds: (A) The sscMap volcano plot generated during comparison of the most statistically significant genes altered following GSK932121A/GSK2617971A treatment to a reference data set. The x-axis shows connection score while the y-axis relates to –log10 p-value. The green horizontal line represents a pre-set threshold of p-value with any data points above the line considered significant. Circled is the most significant and highly connected compound, Azacylonol (inset).(B) Tables showing top ten connected compounds for both GSK932121A and GSK2617971A. Connection scores are calculated from comparison of query gene signatures with the reference database (higher the connection score the more significant the transcriptional similarity). Azacylondol was the top-hit connection for both GSK932121A and GSK2617971A.

Following identification of azacyclonol as the most significantly connected compound for both GSK932121A and GSK2617971A, I wanted to explore whether this connection was due to effects on

mitochondrial function or whether it was due to induction of similar genes via a different mechanism. In order to assess whether azacyclonol provokes a high degree of similarity in gene expression to GSK932121A and GSK2617971A due to mitochondrial toxicity, I analysed the acute effect of azacyclonol (purchased from Selleck Chemicals, #S3196) on ETC function and OXPHOS efficiency using the Seahorse Bioanalyser. The analysis was performed *in vitro* (in HepG2 liver cells) and *ex vivo* (isolated liver mitochondria from a control rat). Data is shown in Fig.7.10 below. Further work is required to assess whether other significantly connected compounds (listed in Fig.7.9B), cause adverse effects on mitochondrial function.

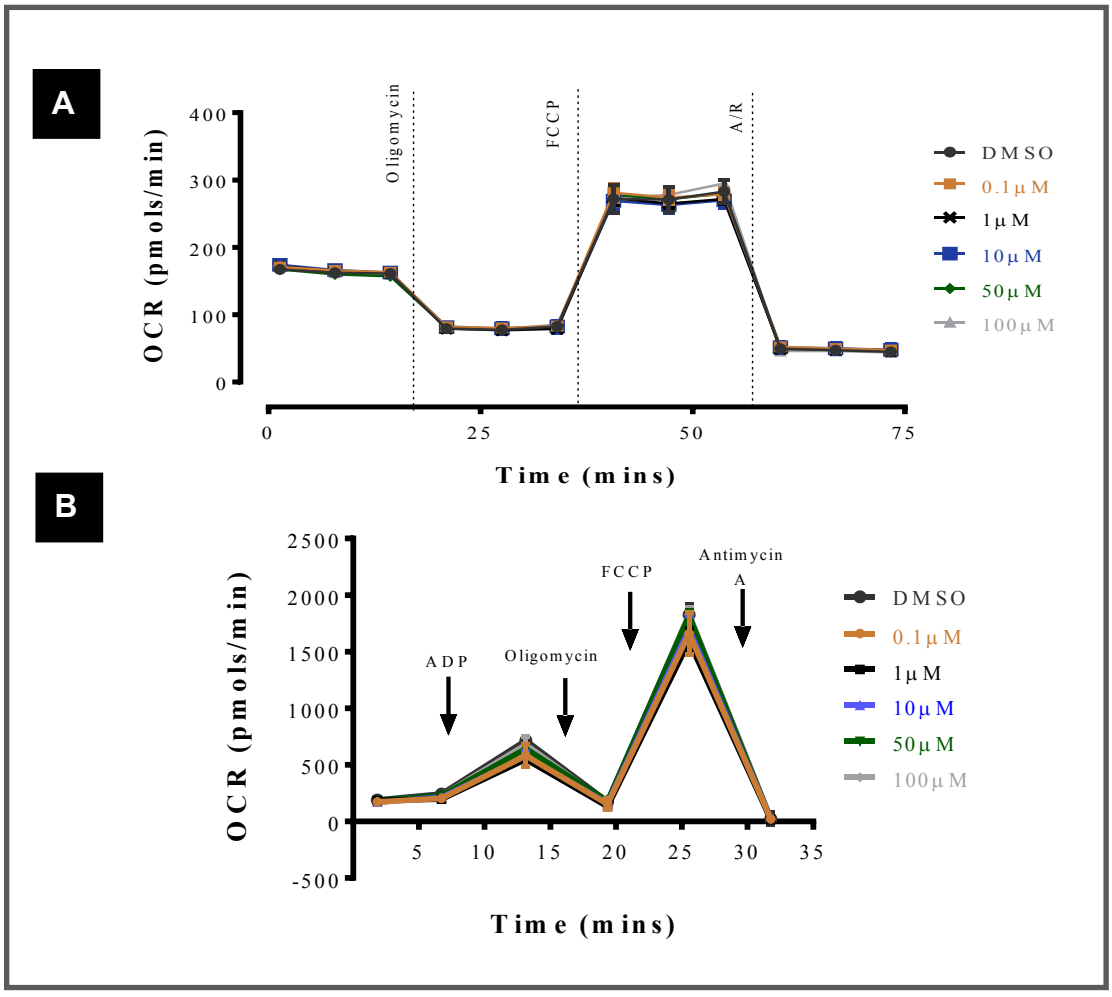
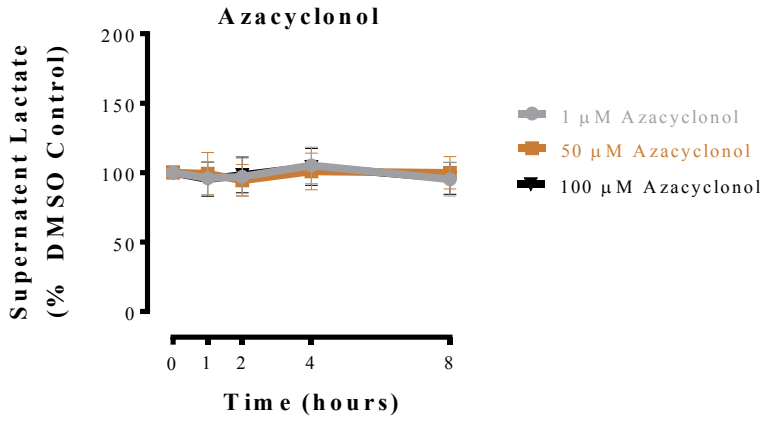


FIGURE 7.10: Effect of azacyclonol on mitochondrial OCR in both HepG2 cells and isolated control liver mitochondria. At the concentrations tested (0.1µM-100µM, n=3) azacyclonol had no significant effect on OCR in either HepG2 cells (A) or isolated liver mitochondria (B), $p>0.05$ (mean ± SD).

No difference was observed in OCR following treatment with azacyclonol (0.1µM-100µM, n=3) compared to the DMSO control in either HepG2 cell cultures (Fig.7.10A) or in naive isolated liver mitochondria (Fig.7.10B). This data suggests that the similarity in transcriptional response between azacyclonol and both GSK tool mitochondrial toxicants was not due to any effect on the respiratory chain (either acceleration or inhibition).

To further investigate any mechanistic similarity between azacyclonol and GSK932121A/GSK2617971A the effect of the compound on both lactate and on intracellular glycogen / lipid stored was investigated (essentially as described in section 7.2.2 and 7.2.4. above). As shown in Fig.7.11 below no significant effect on HepG2 cell media lactate concentration was observed following treatment with azacyclonol (1µM, 50µM and 100µM) compared to a 0.1% DMSO control (n=3, $p>0.05$). Furthermore, no effect on the percentage of cells containing intracellular glycogen stores was observed following TEM analysis of azacyclonol (at 50µM and 100µM only) treated cells at 8 hours. A moderate reduction in the percentage of cells containing >1 lipid droplet was observed in a dose dependent manner, however further work and experimental repeats are required to assess whether this change is statistically significant. In addition, TEM micrographs of HepG2 cells treated with azacyclonol were assessed for the effect of compound treatment on mitochondrial morphology, however, no effect was observed compared to the DMSO control (data not shown).

A



B

Compound and Concentration	Time Point (Hours)	% of Cells with Glycogen clusters	% of Cells with Lipid droplets
DMSO Control (0.1%)	8	21	19
Azacyclonol (50µM)	8	25	11
Azacyclonol (100µM)	8	18	5

FIGURE 7.11: Effect of azacyclonol on both HepG2 cell lactate generation and on the intracellular level of glycogen clusters and lipid droplets. (A) Effect of azacyclonol (1µM-100µM) on HepG2 cell media lactate concentration compared to a 0.1% DMSO control ($p>0.05$, n=3). Data shown is mean ± SD and expressed as a percentage of DMSO control. (B) The table shows the percentage of cells (per 100 cells counted) containing glycogen clusters and greater than 1 lipid droplet following an 8 hour treatment with 50µM + 100µM azacyclonol.

These data indicate that azacyclonol (up to a high concentration of 100µM) has no observable effect on mitochondrial function and extremely limited effects on cellular metabolism (potential reduction in intracellular lipid stores). It was therefore decided to perform gene expression analysis, using the same gene panel as described in section 7.2.3, on cells following treatment with 1, 10 and 100µM azacyclonol (Fig.7.12). It was hoped this experiment would, (a) help to confirm the connection between azacyclonol and the two tool GlaxoSmithKline mitochondrial toxic compounds and, (b) help to understand whether changes in genes on the panel are evoked specifically by mitochondrial toxicants or whether mitochondrially-inactive compounds (i.e. azacyclonol) induce these genes in the present model.

Azacyclonol – Gene Panel Data

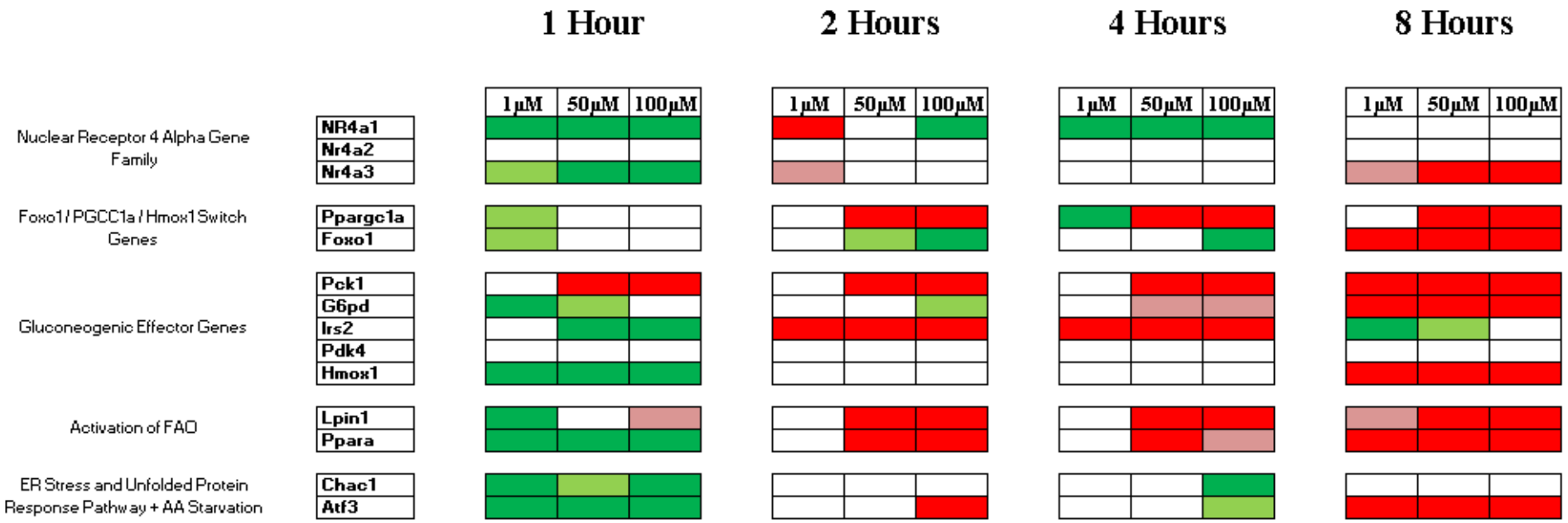


FIGURE 7.12: Heat map showing the effect in HepG2 cells of azacyclonol on a selection of pertinent genes involved in the response to DIMT. Data shown represents a heat map of statistically significant changes in the expression of a number of genes following azacyclonol treatment *in vitro*. Experiments were repeated on 3 occasions (n=3) and fold change (and statistical significance) was calculated against a 0.1% DMSO control. Any changes in gene expression where $p<0.05$ are shown (in either direction).

The gene expression data presented in Fig.7.12 lends further credence to the significant connection (identified using connectivity mapping analysis) between azacyclonol and GSK932121A/GSK2617971A in terms of the transcriptional response to drug exposure. As observed with both GlaxoSmithKline compounds, gene expression following azacyclonol treatment appears time dependent rather than dose dependent with 11 of the 14 genes down-regulated at 1 hour post-treatment compared to a 0.1% DMSO control and 9 of 14 up regulated by 8 hours post-treatment. In contrast to observations with GSK932121A and GSK2617971A, azacyclonol treatment does not cause an early (~1-2 hour) induction of the regulator genes Foxo1 and PGC1α, rather, these genes are induced over time in a similar manner to that of their downstream effectors. Pck1 is however constitutively up-regulated over the duration of the experimental time course and this is similar to the response shown with both GSK932121A and GSK2617971A. Unlike both GSK932121A and GSK2617971A, Nr4a1 and Chac1 do not appear to be effected by azacyclonol treatment *in vitro*.

Despite the similarity in transcriptional responses, I have demonstrated that, unlike both GlaxoSmithKline tool mito-toxicants, azacyclonol has no effect on the mitochondrial ETC or OXPHOS or on lactate generation *in vitro*. There was also no change in the levels of glycogen stores in HepG2 cells although a slight reduction in lipid stores was noted following TEM analysis. This highlights that induction of genes included in the present gene-panel can be stimulated by compounds with no effect on mitochondrial function and therefore lacks specificity.

7.3. Discussion

7.3.1. Mitochondrial Toxicity, Cytotoxicity and Lactate Generation

A key gap of the *in vivo* studies performed to date is the ability to differentiate primary from adaptive changes due to the use of high doses and/or late time points. Essential for the detailed characterisation of a toxicological event these experimental studies are not designed to determine the toxicological sequence of events. The ideal scenario would be to perform an *in vivo* study with multiple time points after dosing of the animals in order to analyse the order in which the key changes take place. However, due to time and practical constraints this was not possible. As an alternative, the progression of events was explored *in vitro* and importantly at concentrations of drug which were not notably toxic. Studying endpoints which had proven sensitive *in vivo* (i.e. lactate, electron microscopy and gene expression analysis) it was

possible to identify essential changes which, a) are primary to the mechanism of action for the drugs and may be key to the downstream events within the AOP and b) could be measured in future studies to assess potential underlying damage to mitochondria.

The effect of both GSK932121A (ETC inhibitor) and GSK2617971A (uncoupler) on both cell metabolism and cytotoxicity was assessed in HepG2 cells. For both drugs a concentration range was determined whereby drug-induced effects were observed on cell metabolism but at an exposure level where no obvious signs of cytotoxicity was evident. It was hypothesised that this would be a narrow concentration range due to the classical steep dose-response often exhibited by mitochondrial toxicants [245]. This hypothesis proved relatively valid in relation to GSK932121A and GSK2617971A with a concentration range of 1μM-10μM and 0.1μM-2.5μM selected for analysis respectively. LDH leakage and light microscopy analyses (not shown) were used as the measure of cytotoxicity in the present study as many other cytotoxicity detection assays are in fact measures of mitochondrial activity (e.g. ATP assays, MTT tetrazolium assay) and as such may over-predict cytotoxicity to our mitochondrial acting compounds [246]. Disadvantages of the LDH leak/lyse assay however includes the lack of sensitivity to mild cytotoxic insult and the limited half-life of LDH in culture medium. Following identification of the optimal concentration window for studying more subtle underlying mitochondrial effects, the consequence of both GSK932121A and GSK2617971A treatment on a selection of pertinent endpoints relating to the effects observed *in vivo* was assessed.

Increases in blood lactate were observed *in vivo* following treatment with both GSK932121A and GSk2617971A although generally at high exposure levels. The present work sought to understand whether sub-toxic concentrations of mitochondrial toxicants provoke an increase in lactate at the cellular level. These data show that both compounds do cause an increase in media lactate although the effect was only observed at 4 and 8 hours with ETC inhibition and 8 hours only following uncoupling. This is in contrast to immediate increases in ECAR observed following OXPHOS uncoupling *in vitro* however, as described by Dranka and colleagues it is important to acknowledge that ECAR measurement is based on pH alteration and is therefore not a direct measure of glycolysis [247]. Lactate has been suggested as a potential biomarker of mitochondrial perturbation and this may be justified based on its continued presence downstream of mitochondrial toxicity [230]. Whilst a useful mechanistic indicator, the data presented here suggests that increases in lactate in systemic circulation or in cell media is not an early consequence of mitochondrial dysfunction, but rather its generation is a delayed consequence of the

metabolic disruption and a significant switch to glycolysis. This is supported by Limonciel *et al* [143] who propose that lactate is a more promising biomarker of cell stress in long term repeat dose *in vitro* toxicology testing with many of the compounds used to validate their findings modulators of mitochondrial function.

7.3.2. GENE PANEL DISCUSSION

A gene panel was assembled based on key genes affected by both GlaxoSmithKline tool compounds *in vivo*. Striking similarity was observed in the transcriptomic signatures in rats following treatment with both compounds opening up the possibility of creating a gene panel for the detection of mechanism-independent/generalised DIMT. The main issues relating to gene panels are however that gene expression does not necessitate protein translation and inferring biological function from changes in gene expression remains extremely challenging. This is especially pertinent in the present study as the gene panel was comprised largely of stress-response genes and as such the induction of many genes on the panel have previously been reported following a diverse array of signals and for a wide range of cellular functions. For example the expression of PGC1α has been attributed to the control of cell metabolism [248], mitochondrial biogenesis [249], the anti-oxidant system [250], the determination of muscle fibre type [251] amongst others, and this leaves the precise nature of its induction unknown. Furthermore, the expression of many of the genes on this panel have been described following administration of various xenobiotics with very differing MOA's suggesting they are unsuitable as specific biomarkers of mitochondrial dysfunction. Despite this, it is important to acknowledge that no inferences have to date been made between any genes involved in the panel and DIMT. As such they all constitute novel mitochondrial-toxicity signature genes.

GSK932121A and GSK2617971A induced the expression of PGC1α and Foxo1 *in vivo* and *in vitro*. As well as its role in inducing mitochondrial biogenesis, PGC1α is induced under numerous stress conditions such as fasting (i.e. periods of low glucose) or energy deprivation. PGC1α in turn coordinates the activity of several transcription factors on the promoters of genes involved in the control of cell metabolism (β-oxidation, ketogenesis and heme-biosynthesis) within or external to the mitochondrion [252]. Additionally PGC1α co-activates the transcription factor, Foxo1, which in turn coordinates the expression of genes involved in insulin-regulated gluconeogenesis [155, 253]. In the present study both PGC1α and Foxo1 were the earliest genes to be differentially up-regulated following treatment with GSK932121A

and GSK2617971A (by 1 hour post-treatment). Induction is therefore likely a primary response but inferring the biological function of their up regulation is a challenge. However, taking into account the increase in expression is observed prior to induction of numerous PGC1α-Foxo1 downstream effector genes (i.e. Pck1, Irs2, Pdk4, Lpin1, Hmox1 and G6pd) it can be speculated its induction is related to control of energy metabolism and specifically induction of gluconeogenesis. There is however a distinct paucity of data in the literature which describes the effect of various drug-toxicities on the PGC1α -Foxo1 axis and therefore, further work is required to understand their role within a toxicological response pathway.

In the present experiment the induction of the majority of PGC1α -Foxo1-dependent effector genes occur at later time points following PGC1α -Foxo1 co-activation. The exception is however the Pck1 gene which encodes the phosphoenolpyruvate carboxykinase 1 enzyme, responsible for the first committed step in gluconeogenesis [254]. This gene is induced following activation of the Pck1 promoter by the PGC1α -Foxo1 complex however, in the present study, its expression appears to be increased alongside both PGC1α and Foxo1 at the 1 hour time point. Induction of Pck1 may therefore be an early biochemical adaptation of impaired mitochondrial function with this conclusion suggestive that cells can sense the requirement to generate glucose from non-carbohydrate sources very early in the AOP following mitochondrial perturbation.

Another key effect noted *in vivo* was the effect of both compounds on the NR4a gene family and in the present study both mitochondrial toxicants induced expression of Nr4a1 and Nr4a3 in a time dependent manner up to 8 hours. The early-response Nr4a genes are induced by various extracellular signals and stressors (e.g. glucose, growth factors, inflammation and apoptotic signals) and with this diversity of pathways regulating Nr4a expression it is likely that the biological function of these receptors is cell-type specific [255]. In the liver however there is strong evidence linking NR4a expression with cellular regulation of hepatic glucose metabolism with activation caused by reduced glucose levels [255]. This data is the first known link between NR4a induction and DIMT with induction likely due to increased levels of glycogenolysis. Drug induced agonists which promote expression of the NR4a gene family have been described (e.g. 6-mercaptopurine [256] and both the benzimidazole [257]/isoxazolopyridinone [258] chemical classes) but without direct association to perturbation of mitochondrial function.

Metabolomics data in chapter 4 identified continued efforts to drive FA β-oxidation despite respiratory chain compromise. This adaptation was generally under-represented in terms of the transcriptomic analysis with a significant increase in Lpin1 being the only sign of transcriptional regulation of FAO. In relation to OXPHOS uncoupling it is widely acknowledged that FA substrate utilization is a key feature of the resulting AOP and again Lpin1 was significantly up-regulated. Lpin1 is also activated by PGC1α and together they selectively activate a subset of PGC1α target pathways including FAO. Lpin1 is known to induce activation of Ppar-α and this was observed in the present study whereby generally Lpin1 activation appears earlier than Ppar-α induction. Importantly Lpin1 also has a role in the cytosol as a Mg^{2+}-dependent phosphatidate phosphatase type-1 (PAP1) involved in the synthesis of glycerolipids. Despite its up-regulation alongside PGC1α and Ppar-α (suggesting its role is related to its function as a transcriptional co-activator in the nucleus), its expression for the purposes of its cytosolic enzymatic function cannot be ruled out. Either way, Lpin1 upregulation was observed with both compounds *in vitro* and *in vivo* and as such the data suggests it plays a central role in the progression of mitochondrial toxicity by promoting FAO.

Large increases in both Atf3 and Chac1 were noted in the liver *in vivo* following DIMT with both mitochondrial toxicants (especially GSK932121A). Chac1 specifically, is heavily implicated in the ER stress pathway and is pro-apoptotic with glutathione degrading activity (GSH reduction being a key event in the progression of GSK932121A toxicity) [259]. Meanwhile, Atf3 is a well-known stress response gene which is induced to a wide range of stress signals including drug toxicity [260]. Atf3 is able to both repress and activate gene expression and is reportedly involved in the inflammatory response [261], the regulation of ER stress mediated pathways, eukaryotic initiation factor kinase 2 stress response, amino acid starvation [244], mediation of glucose homeostasis [262, 263], tumorigenesis [264] and cell death [265]. Like many other genes induced in this study, the wide range of cell processes reportedly associated with Atf3 makes building mechanistic assessments challenging. Further data is required to better understand the exact role of both Chac1 and Atf3 in the cell stress response following mitochondrial perturbation.

7.3.3. THE LINK BETWEEN AZACYCLONOL AND GSK932121A AND GSK2617971A

The striking similarity in the transcriptional response to both GSK932121A and GSK2617971A was highlighted upon performing connectivity mapping analysis. Despite their very different MOA's the

transcriptional response they elicit was significantly connected with one other compound within a database of over 1000 small molecules. The connection between the transcriptomic profile following azacyclonol treatment and exposure to both GSK932121A and GSK2617971A was highly statistically significant and opened up the possibility that azacyclonol may be toxic to mitochondria. Azacyclonol could rationally then be used to validate mechanistic observations with both GlaxoSmithKline compounds and as a new tool compound of DIMT. It is important to acknowledge however that despite the differing mechanisms of action of GSK932121A and GSK2617971A (i.e. complex III inhibition versus OXPHOS uncoupling), the resulting hepatocellular transcriptional similarity may be due to shared key events in the resulting AOP/MOA's (most notably perhaps being a decline in ATP and increased glycolytic function).

Mechanistic investigations suggest that, unlike GSK932121A or GSK2617971A azacyclonol (up to 100μM), does not adversely affect mitochondrial function nor provoke an increase in supernatant lactate levels. Furthermore azacyclonol has no effect on mitochondrial morphology or on the levels of intracellular glycogen clusters although a moderate reduction in the levels of lipid was observed. This data suggests very little similarity in the biochemical response following azacyclonol treatment compared to both GlaxoSmithKline compounds despite a similar transcriptional response being first suggested (by connectivity mapping) and then confirmed (gene-panel data in the present study).

Azacylonol is best known as the N-dealkylation product of terfendaine metabolism [266]. Terfenadine was withdrawn from development due to reports of QT-interval prolongation and cardiac arrhythmias and although rapidly metabolized in the liver, azacyclonol was never attributed to the terfenadine toxicity [267]. In fact, azacyclonol was briefly investigated as an anti-psychotic agent in schizophrenic individuals and although not being sufficiently efficacious, it was well tolerated in humans which, unlike both GlaxoSmithKline mitochondrial toxicants, sums up its minimal safety profile [268, 269]. It remains unknown why it induces a similar gene expression signature to two potent mitochondrial toxins.

Computational analyses were performed to assess whether transcriptional similarity was caused by any chemical/structural similarity between azacyclonol and either/both of GSK932121A/GSK2617971A. Using Tanimoto coefficient, essentially as described in [270], low comparative similarity scores of 0.16 and 0.13 were achieved in terms of comparing azacyclonol to GSK932121A and GSK2617971A respectively (with a score of 1 indicating high structural similarity). In addition, a ligand based target

prediction was performed in ChEMBL, to assess any overlap between azacyclonol and either/both of GSK932121A/GSK2617971A from a target-based perspective. Taking into account the top ten target predictions for all three compounds, no overlap was observed. These analyses (raw data not shown) suggests no theoretical association between azacyclonol and either GlaxoSmithKline tool compound based on structural similarity or target prediction.

This association does however provide some important learnings for the future. Whilst the present work has highlighted the involvement of genes such as PGC1α, Foxo1, Irs2, Pdk4, Pck1, Lpin1, Nr4a1 and Atf3 in the response to mitochondrial perturbation, similar responses are observable following treatment with mitochondrially-inactive compounds (i.e. azacyclonol). This therefore suggests that these genes are unsuitable as specific biomarkers of mitochondrial toxicity. Furthermore, the present work emphasises that transcriptional similarity does not always correspond to mechanistic-likeness and as such, the process of searching for and validating highly specific single-gene or gene-panel biomarkers always requires additional context and validation. The implication is also that, whilst the lack of a gene change likely rules out involvement, existence of such a change on its own does not confirm involvement in an effect. Furthermore, gene changes cannot be used as strong-supporting evidence in the construction of an AOP/MOA.

7.3.4. SUMMARY

In summary the following conclusions can be drawn from this study.

- Concentrations of 0.75µM-10µM GSK932121A (complex III inhibition) and 0.1µM-2.5µM GSK2617971A (OXHOS uncoupling) cause significant perturbation to mitochondrial function but are sub-cytotoxic in HepG2 cells at a gross cell level.
- Sub-toxic concentrations of both GSK932121A and GSK2617971A only effect HepG2 cell lactate generation at 4-8 hours post-treatment and as such this may be a delayed adaptive response to perturbation of energy production rather than an early mechanistic event.
- PGC1α, Foxo1 and Pck1 are early response genes following GSK932121A/GSK2617971A treatment which is followed by time-dependent up-regulation in the NR4a genes (NR4a1/3), the PGC1α -Foxo1 effector genes (Hmox1, G6pd and Irs2), the FAO activation gene (Lpin1) and the stress response genes (Atf3 and Chac1).

- Minimal effects on mitochondrial or cellular morphology were observed up to 8 hours post treatment with GSK932121A and GSK2617971A suggesting structural changes occur at later stages and at higher (potentially toxic) concentrations.
- Compound connectivity mapping analysis identified azacyclonol as the most statistically significant similar compound compared with both GSK932121A and GSK2617971A in terms of the respective transcriptional response to drug treatment. This striking observation highlights the similarity in transcriptional response following complex III inhibition and OXPHOS uncoupling *in vivo*. Despite transcriptional similarity, azacyclonol did not mimic the biological action of either compound as no effect on mitochondrial function, lactate generation or glycogen stores was observed *in vitro*. Gene expression analysis confirmed transcriptional similarity to both GlaxoSmithKline compounds suggesting that the gene panel used in this study is not specific to DIMT.
- This study supports the use of a systems approach as a combination of endpoints, in a multivariate model (e.g. genes and metabolites/ functional changes etc.), may be required for good early predictions.

Further work should involve a timed-kill study in rats, in order to assess the effect of compound treatment at the tissue-level, at both early and progressive time points *in vivo*. Further work should also involve the effect of GSK932121A and GSK2617971A on PGC1α, Foxo1 and Pck1 protein concentration (i.e. using Western blot) as these genes constitute the earliest transcriptional markers induced following treatment with tolerated concentrations of mitochondrial toxicants studied to date. Further work may also focus on whether any of the top 10 similar compounds for both GSK932121A and GSK2617971A effect mitochondrial function as only azacyclonol was explored in the present work.

8.0. THESIS DISCUSSION

Drug induced mitochondrial dysfunction is associated with some severe clinical toxicities resulting in adverse human suffering. Despite the progress made, defining mechanisms of DIMT even in the common pre-clinical test species (e.g. rat and mouse) remains difficult and the challenge is even greater when extrapolating to humans. The overall aim of this thesis was to use a systems approach (i.e. the use of a wide range of endpoints which are multi-faceted in scope) to improve current understanding of the mechanism and consequences of DIMT *in vivo* and relate these findings to *in vitro* observations using tool compounds.

On personal reflection and by the very nature of the project, this was an ambitious challenge. In hindsight, I would have focussed more on a particular area in the field (i.e. mechanisms of DIMT specifically in liver injury or with a particular sub-set of mitochondrial toxicants) as this added level of focus may have aided more tailored investigations and as such, further progress. Despite this, the challenge provided the opportunity for substantial scientific advancement and project diversity.

The overall aim of the thesis was broken down into a series of sub-objectives which are discussed below.

8.1. Manifestation of Mitochondrial Toxicity *in vitro* versus *in vivo*

The first sub-objective was to test the hypothesis that *in vitro* assessment of mitochondrial function (i.e. *in vitro* cell lines or *in vitro* testing of drugs on naïve isolated mitochondria) adequately reflects what occurs *in vivo* and is therefore a useful means of assessing the potential for mitochondrial toxicity in preclinical hazard identification. *In vitro* analysis of DIMT is used in the pharmaceutical industry both for screening activities and for making mechanistic assessments. The effect of two tool compounds, GSK932121A (complex III ETC inhibitor) and GSK2617971A (OXPHOS uncoupler) was assessed, to identify how mitochondrial toxicity manifested both *in vitro* and *in vivo*.

In vitro, both GSK932121A and GSK2617971A acted as expected and in line with other respiratory chain inhibitors and OXPHOS uncouplers respectively. With regards to the effect of both compounds on OCR *in vitro*, the direction of change observed was as anticipated i.e. GSK932121A caused a reduction in OCR and GSK2617971A caused a biphasic increase in OCR. As expected, both compounds decreased the CRC of freshly isolated control liver mitochondria *in vitro* due to impairment of the mitochondrial $\Delta\Psi$. This suggests that *in vitro* studies have utility in assessing mechanisms of DIMT (i.e. by comparing the

response to classical tool-molecules with similar mechanisms) though on a number of occasions, the direction of change observed *in vitro* was seen to be opposite to that observed *in vivo*.

Mitochondria isolated from the kidney of rats treated *in vivo* with GSK2617971A showed an unexpected decrease in all OCR parameters This is likely due to high levels of exposure in the kidney since the drug is predominantly cleared via the renal route, coupled with the fact that OXPHOS uncouplers generally exhibit a bell-shaped response curve (i.e. reducing OCR at high concentrations). This is a key learning with regard to selecting the most sensitive endpoints to detect drug-induced OXPHOS uncoupling following *in vivo* treatment in future studies. Assays of CRC and $\Delta\Psi$ in mitochondria isolated from treated animals provided a more sensitive indication of OXPHOS related toxicity in the present studies than OCR, with findings more consistent with the OXPHOS mechanism of action (i.e. dissipation of the $\Delta\Psi$ and reduction in CRC). It is therefore advisable to use these assays, in preference to the OCR assay, when analysing the effect of OXPHOS uncouplers *in vivo*.

Mitochondria isolated from rats treated *in vivo* with GSK932121A demonstrated unexpected yet clear differences with data obtained *in vitro*, namely an increase in basal OCR and CRC in mitochondria from treated animals compared to control. Whilst seemingly contradictory these observations likely represent an adapted state *in vivo* resulting from the initial insult in combination with the compensatory response of the animal/tissue to energy deprivation. Only the initial, unconfounded response is observable *in vitro*. Whilst acidosis and the resulting densitisation of the mPTP to calcium-induced pore triggering is proposed to be the cause of the increase in CRC in mitochondria from GSK932121A treated rats, the exact reason for the increase in OCR remains unknown. Hypotheses include washout of GSK932121A during the isolation procedure, increased levels of ROS-induced proton leak and stabilisation of a mitochondrial subpopulation in GSK932121A treated animals due to reduced mPTP triggering.

Whatever the mechanisms involved, it is now evident that consideration of both the *in vitro* and *in vivo* data is essential; neither on its own would have been sufficient. The *in vitro* data informs on the likely molecular initiating event and initial (non-confounded) respiratory response, whist the *in vivo* data provides a view of the integrated state of the mitochondria in response to the initial insult plus the compensatory adaptations occurring in the tissues and organism.

8.2. The Use of a Systems Approach to Generate AOP's

The second sub-objective was to assess the utility of using a systems approach in order to highlight the underlying mechanisms downstream of mitochondrial perturbation *in vivo*. Systems toxicology encompasses the integration of classical toxicology (e.g. pathology, clinical chemistry) with, a) novel methods of evaluation, in this case functional mitochondrial changes and b) with the quantitative analysis of large networks of molecular changes occurring across multiple layers of biological organisation, in this case transcriptomic and metabolomics assessments. A systems approach is particularly useful when the mechanisms are either completely unknown or where only little understanding exists. To build upon already existing knowledge of an adverse drug reaction, targeted evaluations may be more useful. Given the complexity of the downstream mechanisms of DIMT relating to respiratory chain inhibition (chapters 3-5) or OXPHOS uncoupling (chapter 6) *in vivo,* a systems approach seemed the most suitable.

For GSK932121A, evaluations included classical toxicology (serum biochemistry and histopathology), novel methods of evaluating mitochondrial function, glutathione profiling, TEM, body temperature etc; along with the use of global "omics" approaches (transcriptomics and metabolomics). Whilst this provided a truly system-level view from which to build an AOP for complex III inhibition (described in chapter 5) determining the key events between the primary molecular initiation event (compound binding to the Qi site of cytochrome bc1 and inhibiting ETC) and the adverse outcome was very challenging. This was made harder in this case here because the progression of toxicity was so rapid (within 5 hours), making identification of the order of events difficult. For this reason, the study design is of paramount importance and generation of AOP/MOA's should be augmented by existing literature data with other compounds with similar mechanistic activities.

Effects of both time and dose should be investigated. The complex nature of toxicological adaptation makes identifying primary consequences from adaptive secondary events a major challenge. For example, despite extensive investigations throughout this thesis looking into lactate generation, it still remains unknown whether this is a primary event following DIMT or whether this occurs downstream of prolonged perturbation in energy production. This example highlights a key learning. Regardless of the number of endpoints selected for analysis, the study design is fundamentally crucial to be able to generate AOP's. Time and dose responses are required in order to make informed judgements of the key events in an AOP and answer difficult questions such as; in the absence of any single key event does the adverse

outcome manifest? Are there any modifying factors, which when present, effect the progression or severity of the adverse outcome?

For both GSK932121A and GSK2617971A further work is required in order to investigate lower doses and earlier time points, using data presented in this thesis as a starting point to help design the studies and select endpoints that will provide the best possible opportunity to clarify uncertainties remaining in both AOP's. An example of such a study would be to investigate the effect of a 14-day repeat dose exposure to the well-tolerated 12.5mg/kg dose of GSK932121A to identify effects on liver histopathology, mitochondrial function and body temperature. This would bring insight from the present work into the repeat-dose scenario and therefore be more representative of the study designs used commonly in drug development with small molecules.

In addition, it is important to acknowledge that observations made post-treatment with both GSK932121A and GSK2617971A cannot purely be attributed to their toxicological effects. For example, observations made following administration of GSK2617971A *in vivo* may be caused by the drugs action as a selective androgen receptor modulator as oppose to simply its effects on mitochondrial uncoupling. A way of delineating "on target" therapeutic effects (i.e. effects as a SARM) from "off-target" effects (i.e. effects as an uncoupler) would be to have included a positive control non-SARM OXPHOS uncoupler (e.g. 2,4-DNP) in all studies, alongside GSK2617971A and compared the differential responses (e.g. transcriptomic signatures) to both molecules. Although this was not feasible due to time constraints this work is necessary to validate the AOP/MOAs.

The definitive list of AOP's which are validated to-date are on the AOP-Wiki web-page [https://aopkb.org/aopwiki/index.php/Main_Page] along with guidance documentation, written by the Organisation for Economic Co-operation and Development (OECD), on developing and assessing AOP's [271]. This was based around advancement (but importantly not replacement) of the existing, mode of action (MOA) approach which involved the description of a biologically plausible sequence of key events and processes. This document proposes a weight-of evidence based approach with a tailored set of Bradford Hill considerations whereby the level of confidence of all endpoints is scrutinised for biological plausibility, reproducibility, relationships between key events and apical endpoint, assay reliability and key event essentiality [272]. Table 8.1 below represents the differences between toxicity pathways, MOA's, AOP's and source to outcome pathways.

<table>
<tr><td>Environmental Containment</td><td>Exposure</td><td>MIE</td><td>Organelle and Molecular Effects</td><td>Cellular Effects</td><td>Tissue Effects</td><td>Organ Effects</td><td>Organ Systems Effects</td><td>Individual Effects</td><td>Population Effects</td><td>Community Effects</td></tr>
<tr><td></td><td></td><td colspan="3">Toxicity Pathways</td><td></td><td></td><td></td><td></td><td></td><td></td></tr>
<tr><td></td><td></td><td colspan="6">Mode of Acton</td><td></td><td></td><td></td></tr>
<tr><td></td><td></td><td colspan="7">Adverse Outcome Pathway</td><td></td><td></td></tr>
<tr><td colspan="11">Source to Outcome Pathway</td></tr>
</table>

TABLE 8.1: Representation of the relationships between Toxicity Pathways, Mode of Action Pathways, Adverse Outcome Pathways, and Source to Outcome Pathways. Orange bars represent the breadth of reach common to these concepts. The grey boxes represent the theoretical extent of the concepts. Adapted from [271].

The weight-of evidence based approach described in the OECD white-paper is similar in many regards to the AOP/MOA hybrid approach taken in chapter 5 to detail the observed acute toxicity with GSK932121A (complex III inhibition). The approach was not taken with GSK2617971A (chapter 6) due to having less data available in order to distinguish key events from PKE's and associated events.

Consideration of alternative explanations for the key AOP observations is imperative as there is often more than one plausible pathway and as a result, the hybrid AOP/MOA framework is a useful progressive step in the development of a fully validated AOP. For any investigation which aims to identify a mechanism of toxicity, the intelligent use of a systems approach is helpful and in some cases crucial. Following initial identification of fundamental key events and the preparation of a draft AOP/MOA hybrid (such as that displayed in chapter 5), studies should then be designed for more targeted evaluations, with refined doses and time-points to clarify uncertainties in the AOP/MOA and progress towards a full AOP. The AOP-Wiki provides a validation-procedure which provides the opportunity for other users to comment and edit AOP proposals prior to formal review by both the OECD and Extended Advisory Group on Molecular Screening and Toxicogenomics (EAGMST). This level of peer-review is critical for the generation of reliable and informative AOP's which have utility in future drug/chemical risk-assessment.

8.3. Markers of DIMT in the Absence of Overt Toxicity

The third sub-objective of the thesis was to set the groundwork for identifying markers of DIMT that change prior to the onset of overt toxicity. Importantly, this effect can be assessed either at low (sub-toxic) doses or at earlier time-points with a higher (toxic) dose.

In the past, drugs have been withdrawn from the market due to toxicity which was subsequently identified to be associated with mitochondrial dysfunction that was not overtly evident throughout pre-clinical and clinical trials (troglitazone being a key example). This may be due to the fact that damage to mitochondria was not detected in preclinical trials since mitochondrial functional changes have historically not been assessed or because the underlying effects are asymptomatic (e.g. erosion of reserve capacity). Mitochondria are able to respond to a certain level of direct or indirect stress by utilisation of an innate reserve capacity and this mitochondrial-resilience prevents the immediate onset of toxicity early in drug development. *In vivo* markers of mitochondrial damage which change prior to the onset of overt toxicity would be of immense value in monitoring the potential safety of molecules with some degree of mitochondrial activity but which are generally well tolerated in animals.

The most striking sub-toxic marker of underlying mitochondrial changes *in vivo* (identified in the present work) was measurement of CRC; for example administration of GSK2617971A to rats at a dose which caused no adverse clinical effects or body temperature alterations (30mg/kg) caused a significant depletion of CRC in isolated liver and kidney mitochondria. Mitochondrial functional measures, particularly CRC, may therefore be an informative marker of potential underlying DIMT in preclinical studies and this potential is now being investigated further in follow up studies within GlaxoSmithKline. Although extremely valuable in pre-clinical evaluations, CRC analysis in isolated mitochondrial fractions is not easily translatable to human trials due to the need for tissue. It is for this reason that more accessible markers of DIMT; for example, in bio-fluids or biopsy samples are being sought. Hence the plasma metabolite findings, described in chapter 4, are of particular value.

Metabolomics analyses identified a number of potential markers of DIMT prior to the onset of clinical signs following GSK932121A treatment. These included changes in the fatty acyl carnitines palmitoylcarnitine, oleylcarnitine and stearoylcarnitine, the ketone body BHBA and amino acid catabolism marker AHB. Importantly, whilst these metabolomic changes can inform about the metabolic

adaptation due to perturbed energy generation the fact is they closely resemble other conditions such as metabolic syndrome and insulin resistance. Consequently any markers derived from this work need to be applied with this in mind until further validation work is performed. For example, they may be best used in scenarios where mitochondrial activity is known or suspected with a candidate molecule and used for monitoring purposes rather than as routine biomarkers run on every *in vivo* study, such as standard clinical pathology makers. It is however my opinion that further work is warranted due to the potential translatability of these measurements to humans. Without taking these findings forward and generating further data with other mitochondrial toxicants it is impossible to determine the potential utility of these endpoints in terms of DIMT.

Chapter 7 focussed on identifying markers of DIMT *in vitro* at sub-cytotoxic concentrations of both GSK932121A and GSK2617971A using endpoints shown to be sensitive *in vivo*. Genes involved in the induction of gluconeogenesis, specifically the switch genes PGC1α and Foxo1 and the gene encoding the rate-limiting step in gluconeogenesis (Pck1) were induced early following treatment of HepG2 cells with sub-cytotoxic concentrations of both drugs. Like the mitochondrial functional endpoints described above, measurement of these genes may prove valuable in future pre-clinical assessments although, connectivity mapping analysis raised questions about their specificity as markers of DIMT, as the expression of many changed in response to a molecule with no obvious effect on mitochondrial function (azacyclonol).

In addition to the potential identification of biomarkers, the work presented here has provided invaluable mechanistic insight. Sub-toxic markers help identify primary toxicity from adaptive cell events in the development of an AOP/MOA (as described above). For example, studies presented here have revealed that potentiation of calcium-induced mPTP does not necessarily provoke a clinical outcome and is therefore an early event in the AOP. Additionally it has been noted that, induction of genes involved in the gluconeogenic response is an early consequence and biomarker of dysfunctional mitochondrial ETC/OXPHOS systems.

The withdrawal of a number of drugs due to toxicity which was later discovered to involve perturbation of mitochondrial function highlights a gap in current drug development methodologies, namely the apparent insensitivity of the commonly used animal models to mitochondrial perturbation. This may reflect the metabolic state of the animals currently used in pre-clinical studies that are generally young, healthy and possess a large reserve capacity allowing them to readily adapt to stress. This is at odds with

many patient groups whose metabolic capacities are eroded by co-morbidities, co-medication, age, genetics, lifestyle etc. This apparent lack of concordance between the current pre-clinical animal model and the patient population is illustrated by Fig.8.1 below.

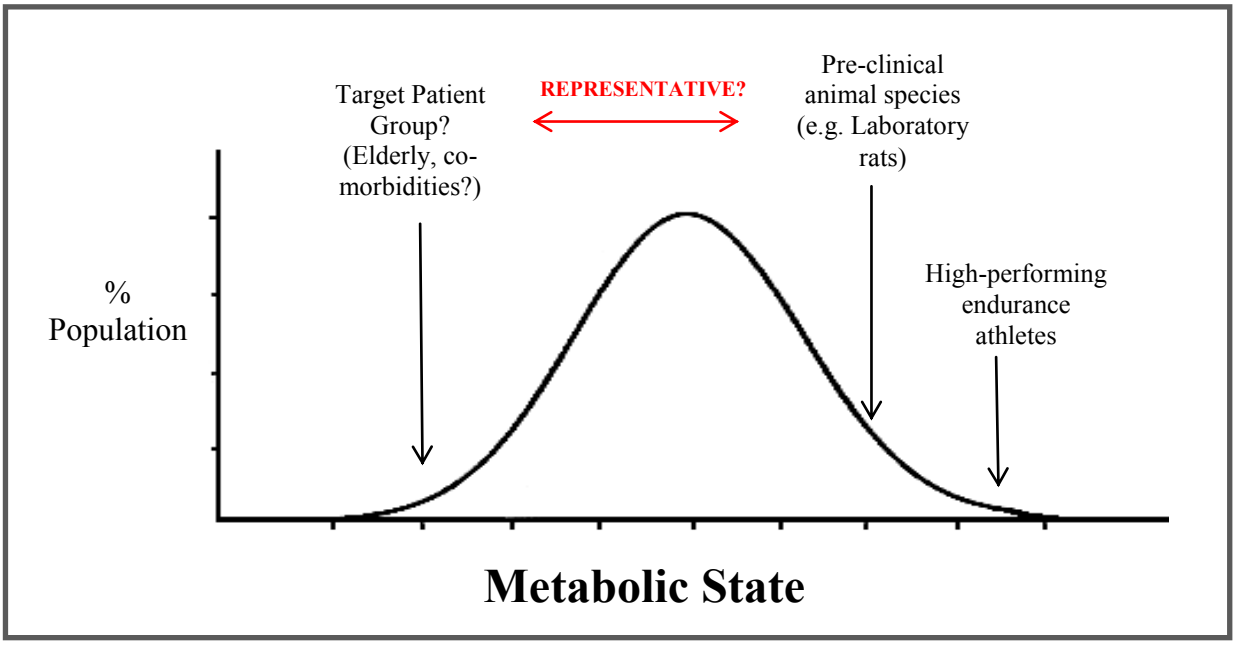


FIGURE 8.1.: Graphical representation of the relative metabolic states of potential target patient populations and the commonly used preclinical animal species.

A potential option to address this issue is to increase the metabolic burden on the animals alongside drug treatment, for example increasing the exercise demand, co-administering with other molecules which alter metabolic demand/function or using older animals. For example, in a recent GlaxoSmithKline study (data not shown) a candidate drug which had been well-tolerated in 14 day oral toxicity studies (despite histopathological changes in cardiac tissue) was co-administered with dobutamine (a cardiac β_1 receptor agonist used to stimulate heart contraction). This uncovered physiological changes in cardiovascular function which were absent in either drug alone or dobutamine alone controls. Other options are to explore the use of transgenic animal models in which metabolic capacity is affected, which may be more representative of patients in terms of underlying mitochondrial function. An example would be $Sod2^{+/-}$ mice which have been shown to be more sensitive to troglitazone-induced liver injury highlighting the increased sensitivity of this mouse model to DIMT [273].

What remains clear is that markers which can inform on mitochondrial perturbation prior to the onset of overt toxicity or the use of animals models that are more representative of patients with regard to metabolic status would be of immense value. This would enable improved monitoring of molecules with some degree of mitochondrial activity *in vitro* and ultimately improve drug safety for patients.

8.4. Future Work

Validation work with additional tool compounds is required to confirm that the observations made with GSK932121A and GSK2617971A are mechanism related and not specific to the individual compounds (i.e. many of the effects observed following administration of GSK2617971A for example may be due to its activity as a SARM as opposed to just its uncoupling effects). Compounds such as antimycin A, and 2,4-DNP or other terminated GlaxoSmithKline molecules with the right properties, could be considered. Future studies should include tissue-collection at early time-points to determine exactly when mitochondrial functional changes occur and to provide a time course for more in depth transcriptomic work.

Critically, the potential markers highlighted by the *in vivo* studies presented (ranging from body temperature, through biochemical analyses to mitochondrial functional endpoints) should be tested in chronic repeat-dose studies with mitochondrially-active compounds, at tolerated doses, to see if low level chronic reductions in mitochondrial function can be detected in the absence of overt toxicity. These studies should accurately represent the study designs used for standard regulatory toxicology work to test the utility of these markers in a standard study setting. Potential biomarkers of DIMT in plasma (i.e. acylcarnitines, BHBA and AHB) should also be tested to see if they are robust and reproducible and as such, potentially translatable to the clinic.

As described in section 8.3 above, the animal models currently used in drug safety assessment appear relatively insensitive to DIMT. This represents a significant gap that might be improved by the use of more sensitive animal models (although there is a dynamic move to reduce reliance on animal models in R&D and replace them with non-animal approaches where possible). Early investigations should follow up on existing work using the $Sod2^{+/-}$ mouse model (increased levels of oxidative stress) or with co-administration study designs. Ethically it will be important not to place the animals under unnecessary

stress. Any observed exacerbation of toxicity with known mito-toxicants compared to the effects observed in controls may indicate a more suitable model for the detection of underlying, asymptomatic DIMT.

The corresponding protein levels of the key genes identified following DIMT (e.g. PGC1α, Foxo1 and Pck1) should also be explored downstream of DIMT both *in vitro* and *in vivo,* via Western blot, as gene expression changes are not always representative of protein translation/expression. It would also be interesting to modulate the expression of these genes via RNA interference (RNAi) *in vitro,* and analyse the effect of this knockdown following treatment with mitochondrial toxicants, specifically whether gene knockdown confers resistance or exacerbates the effect of DIMT.

Further work should also focus on the intelligent mining of existing data relating to mitochondrial function in the pharmaceutical industry. The creation of computational tools to visualise, analyse and identify compounds and structures with varying degrees of mitochondrial activity (not just necessarily toxicity) would be invaluable both in selection of tool molecules, re-positioning of assets between discovery programmes (i.e. a compound which inhibits the mPTP, and thus delays cell death, may not be beneficial to oncology programmes but may be extremely beneficial to stress and repair groups), and to build structure activity relationship (SAR) paradigms.

8.5. Summary

This thesis has focused on using a systems approach to understand mechanisms of drug induced mitochondrial toxicity *in vitro* and *in vivo,* specifically using compounds which inhibit the mitochondrial ETC complex III (GSK932121A, chapters 3-5) or uncouple OXPHOS (GSK2617971A, chapter 6). This type of evaluation is rarely seen in the literature, particularly with novel pharmaceutical candidates (albeit terminated ones) and as such will be of particular interest to those who are faced with designing safety studies for mitochondrially active drugs and potential mito-toxicants. *In vitro* investigations were performed to assess the effect of sub-toxic concentrations of the two tool compounds on endpoints which had been identified as informative from *in vivo* studies (i.e. TEM, gene expression and lactate – chapter 7).

This project has answered some of the questions posed and in doing so has contributed to our general knowledge of the mechanisms of DIMT and the downstream biological consequences. It is clear that the

use of a systems approach can be of significant value when defining an initial mechanistic overview and therefore as a starting point for developing a AOP/MOA for a particular toxicity. Systems-based evaluations lay the groundwork for more tailored and detailed follow-up studies aimed at clarifying the key events to result in a final AOP (a robust resource for use in the risk assessment of other compounds with similar mechanistic activity). This in turn will help reduce costly compound attrition, reduce the time to get new drugs to market and ultimately improve the safety profile of medicines for patients by preventing future cases of DIMT in humans.

REFERENCES

1. Nadanaciva, S. and Y. Will, *Investigating mitochondrial dysfunction to increase drug safety in the pharmaceutical industry.* Curr Drug Targets, 2011. **12**(6): p. 774-82.
2. Nadanaciva, S. and Y. Will, *Current concepts in drug-induced mitochondrial toxicity.* Curr Protoc Toxicol, 2009. **Chapter 2**: p. Unit 2 15.
3. Saha, S., et al., *Investigation of the role of the thiazolidinedione ring of troglitazone in inducing hepatotoxicity.* Toxicol Lett, 2010. **192**(2): p. 141-9.
4. Dykens, J.A., L.D. Marroquin, and Y. Will, *Strategies to reduce late-stage drug attrition due to mitochondrial toxicity.* Expert Rev Mol Diagn, 2007. **7**(2): p. 161-75.
5. Hamilton, B.F., et al., *In vivo assessment of mitochondrial toxicity.* Drug Discov Today, 2008. **13**(17-18): p. 785-90.
6. Scatena, R., et al., *The role of mitochondria in pharmacotoxicology: a reevaluation of an old, newly emerging topic.* Am J Physiol Cell Physiol, 2007. **293**(1): p. C12-21.
7. Pereira, C.V., et al., *Investigating drug-induced mitochondrial toxicity: a biosensor to increase drug safety?* Curr Drug Saf, 2009. **4**(1): p. 34-54.
8. Ernster, L. and G. Schatz, *Mitochondria: a historical review.* J Cell Biol, 1981. **91**(3 Pt 2): p. 227s-255s.
9. Palade, G.E., *The fine structure of mitochondria.* Anat Rec, 1952. **114**(3): p. 427-51.
10. Benard, G. and R. Rossignol, *Ultrastructure of the mitochondrion and its bearing on function and bioenergetics.* Antioxid Redox Signal, 2008. **10**(8): p. 1313-42.
11. Lazarow, A. and S.J. Cooperstein, *Studies on the enzymatic basis for the Janus green B staining reaction.* J Histochem Cytochem, 1953. **1**(4): p. 234-41.
12. Siekevitz, P. and M.L. Watson, *Cytochemical studies of mitochondria. II. Enzymes associated with a mitochondrial membrane fraction.* J Biophys Biochem Cytol, 1956. **2**(6): p. 653-69.
13. Azzone, G.F. and L. Ernster, *Respiratory control and compartmentation of substrate level phosphorylation in liver mitochondria.* J Biol Chem, 1961. **236**: p. 1501-9.
14. Kagawa, Y., *[Reconstitution of oxidative phosphorylation system].* Tanpakushitsu Kakusan Koso, 1971. **16**(9): p. 775-86.

15. Berman, S.B., F.J. Pineda, and J.M. Hardwick, *Mitochondrial fission and fusion dynamics: the long and short of it.* Cell Death Differ, 2008. **15**(7): p. 1147-52.
16. Detmer, S.A. and D.C. Chan, *Functions and dysfunctions of mitochondrial dynamics.* Nat Rev Mol Cell Biol, 2007. **8**(11): p. 870-9.
17. Su, B., et al., *Abnormal mitochondrial dynamics--a novel therapeutic target for Alzheimer's disease?* Mol Neurobiol, 2010. **41**(2-3): p. 87-96.
18. Collins, T.J. and M.D. Bootman, *Mitochondria are morphologically heterogeneous within cells.* J Exp Biol, 2003. **206**(Pt 12): p. 1993-2000.
19. Yi, M., D. Weaver, and G. Hajnoczky, *Control of mitochondrial motility and distribution by the calcium signal: a homeostatic circuit.* J Cell Biol, 2004. **167**(4): p. 661-72.
20. Wallace, K.B. and A.A. Starkov, *Mitochondrial targets of drug toxicity.* Annu Rev Pharmacol Toxicol, 2000. **40**: p. 353-88.
21. Picard, M., et al., *Mitochondria: isolation, structure and function.* J Physiol, 2011. **589**(Pt 18): p. 4413-21.
22. Mitchell, P., *Coupling of phosphorylation to electron and hydrogen transfer by a chemi-osmotic type of mechanism.* Nature, 1961. **191**: p. 144-8.
23. Poyton, R.O. and J.E. McEwen, *Crosstalk between nuclear and mitochondrial genomes.* Annu Rev Biochem, 1996. **65**: p. 563-607.
24. Gray, M.W., G. Burger, and B.F. Lang, *The origin and early evolution of mitochondria.* Genome Biol, 2001. **2**(6): p. REVIEWS1018.
25. O'Brien, T.W., *Properties of human mitochondrial ribosomes.* IUBMB Life, 2003. **55**(9): p. 505-13.
26. Van Houten, B., V. Woshner, and J.H. Santos, *Role of mitochondrial DNA in toxic responses to oxidative stress.* DNA Repair (Amst), 2006. **5**(2): p. 145-52.
27. Wallace, K.B., *Mitochondrial off targets of drug therapy.* Trends Pharmacol Sci, 2008. **29**(7): p. 361-6.
28. Taylor, R.W. and D.M. Turnbull, *Mitochondrial DNA mutations in human disease.* Nat Rev Genet, 2005. **6**(5): p. 389-402.
29. Sondheimer, N., et al., *Neutral mitochondrial heteroplasmy and the influence of aging.* Hum Mol Genet, 2011. **20**(8): p. 1653-9.
30. Brandon, M., P. Baldi, and D.C. Wallace, *Mitochondrial mutations in cancer.* Oncogene, 2006. **25**(34): p. 4647-62.
31. Rich, P.R., *The molecular machinery of Keilin's respiratory chain.* Biochem Soc Trans, 2003. **31**(Pt 6): p. 1095-105.
32. Mogilevskaya, E., O. Demin, and I. Goryanin, *Kinetic model of mitochondrial Krebs cycle: unraveling the mechanism of salicylate hepatotoxic effects.* J Biol Phys, 2006. **32**(3-4): p. 245-71.

33. Papa, S., et al., *The oxidative phosphorylation system in mammalian mitochondria.* Adv Exp Med Biol, 2012. **942**: p. 3-37.

34. Saada, A., *The use of individual patient's fibroblasts in the search for personalized treatment of nuclear encoded OXPHOS diseases.* Mol Genet Metab, 2011. **104**(1-2): p. 39-47.

35. Maslov, L.N., et al., *[Uncoupling proteins and their role in the regulation of brain and heart tolerance to impact of ischemia and reperfusion].* Ross Fiziol Zh Im I M Sechenova, 2011. **97**(8): p. 761-80.

36. Velours, J., et al., *Mitochondrial F1F0-ATP synthase and organellar internal architecture.* Int J Biochem Cell Biol, 2009. **41**(10): p. 1783-9.

37. Perron, N.R., C. Beeson, and B. Rohrer, *Early alterations in mitochondrial reserve capacity; a means to predict subsequent photoreceptor cell death.* J Bioenerg Biomembr, 2013. **45**(1-2): p. 101-9.

38. Desler, C., et al., *Is There a Link between Mitochondrial Reserve Respiratory Capacity and Aging?* J Aging Res, 2012. **2012**: p. 192503.

39. Hill, B.G., et al., *Importance of the bioenergetic reserve capacity in response to cardiomyocyte stress induced by 4-hydroxynonenal.* Biochem J, 2009. **424**(1): p. 99-107.

40. Maaswinkel-Mooij, P.D., et al., *Depletion of mitochondrial DNA in the liver of a patient with lactic acidemia and hypoketotic hypoglycemia.* J Pediatr, 1996. **128**(5 Pt 1): p. 679-83.

41. Thomas, C., et al., *Hydroxyl radical is produced via the Fenton reaction in submitochondrial particles under oxidative stress: implications for diseases associated with iron accumulation.* Redox Rep, 2009. **14**(3): p. 102-8.

42. Ott, M., et al., *Mitochondria, oxidative stress and cell death.* Apoptosis, 2007. **12**(5): p. 913-22.

43. Han, D., E. Williams, and E. Cadenas, *Mitochondrial respiratory chain-dependent generation of superoxide anion and its release into the intermembrane space.* Biochem J, 2001. **353**(Pt 2): p. 411-6.

44. Adam-Vizi, V. and C. Chinopoulos, *Bioenergetics and the formation of mitochondrial reactive oxygen species.* Trends Pharmacol Sci, 2006. **27**(12): p. 639-45.

45. Soubannier, V. and H.M. McBride, *Positioning mitochondrial plasticity within cellular signaling cascades.* Biochim Biophys Acta, 2009. **1793**(1): p. 154-70.

46. Grivennikova, V.G. and A.D. Vinogradov, *Generation of superoxide by the mitochondrial Complex I.* Biochim Biophys Acta, 2006. **1757**(5-6): p. 553-61.

47. Grijalba, M.T., A.E. Vercesi, and S. Schreier, *Ca2+-induced increased lipid packing and domain formation in submitochondrial particles. A possible early step in the mechanism of Ca2+-stimulated generation of reactive oxygen species by the respiratory chain.* Biochemistry, 1999. **38**(40): p. 13279-87.

48. Armstrong, J.S., *The role of the mitochondrial permeability transition in cell death.* Mitochondrion, 2006. **6**(5): p. 225-34.

49. McConkey, D.J., *Biochemical determinants of apoptosis and necrosis.* Toxicol Lett, 1998. **99**(3): p. 157-68.

50. Ow, Y.P., et al., *Cytochrome c: functions beyond respiration.* Nat Rev Mol Cell Biol, 2008. **9**(7): p. 532-42.

51. McIlwain, D.R., T. Berger, and T.W. Mak, *Caspase functions in cell death and disease.* Cold Spring Harb Perspect Biol, 2015. **7**(4).

52. Tait, S.W. and D.R. Green, *Caspase-independent cell death: leaving the set without the final cut.* Oncogene, 2008. **27**(50): p. 6452-61.

53. Zamzami, N., et al., *Inhibitors of permeability transition interfere with the disruption of the mitochondrial transmembrane potential during apoptosis.* FEBS Lett, 1996. **384**(1): p. 53-7.

54. Miyoshi, H., *Structure-activity relationships of some complex I inhibitors.* Biochim Biophys Acta, 1998. **1364**(2): p. 236-44.

55. Degli Esposti, M., *Inhibitors of NADH-ubiquinone reductase: an overview.* Biochim Biophys Acta, 1998. **1364**(2): p. 222-35.

56. Wojtovich, A.P., et al., *Physiological consequences of complex II inhibition for aging, disease, and the mKATP channel.* Biochim Biophys Acta, 2013. **1827**(5): p. 598-611.

57. Lemarie, A., et al., *Specific disintegration of complex II succinate:ubiquinone oxidoreductase links pH changes to oxidative stress for apoptosis induction.* Cell Death Differ, 2011. **18**(2): p. 338-49.

58. Linnett, P.E. and R.B. Beechey, *Inhibitors of the ATP synthethase system.* Methods Enzymol, 1979. **55**: p. 472-518.

59. Ueno, Y., *The toxicology of mycotoxins.* Crit Rev Toxicol, 1985. **14**(2): p. 99-132.

60. Dabbeni-Sala, F., G. Schiavo, and P. Palatini, *Mechanism of local anesthetic effect on mitochondrial ATP synthase as deduced from photolabelling and inhibition studies with phenothiazine derivatives.* Biochim Biophys Acta, 1990. **1026**(1): p. 117-25.

61. Palmeira, C.M., A.J. Moreno, and V.M. Madeira, *Mitochondrial bioenergetics is affected by the herbicide paraquat.* Biochim Biophys Acta, 1995. **1229**(2): p. 187-92.

62. Wei, Y.H., et al., *Inhibition of the mitochondrial Mg2+-ATPase by propranolol.* Biochem Pharmacol, 1985. **34**(7): p. 911-7.

63. Snoeij, N.J., A.H. Penninks, and W. Seinen, *Biological activity of organotin compounds--an overview.* Environ Res, 1987. **44**(2): p. 335-53.

64. Petrescu, I. and C. Tarba, *Uncoupling effects of diclofenac and aspirin in the perfused liver and isolated hepatic mitochondria of rat.* Biochim Biophys Acta, 1997. **1318**(3): p. 385-94.

65. Moreno-Sanchez, R., et al., *Inhibition and uncoupling of oxidative phosphorylation by nonsteroidal anti-inflammatory drugs: study in mitochondria, submitochondrial particles, cells, and whole heart.* Biochem Pharmacol, 1999. **57**(7): p. 743-52.

66. Miranda, E.J., et al., *Two deaths attributed to the use of 2,4-dinitrophenol.* J Anal Toxicol, 2006. **30**(3): p. 219-22.

67. Ilivicky, J. and J.E. Casida, *Uncoupling action of 2,4-dinitrophenols, 2-trifluoromethylbenzimidazoles and certain other pesticide chemicals upon mitochondria from different sources and its relation to toxicity.* Biochem Pharmacol, 1969. **18**(6): p. 1389-401.

68. Terada, H., *The interaction of highly active uncouplers with mitochondria.* Biochim Biophys Acta, 1981. **639**(3-4): p. 225-42.

69. Starkov, A.A., *"Mild" uncoupling of mitochondria.* Biosci Rep, 1997. **17**(3): p. 273-9.

70. Reed, P.W., *Ionophores.* Methods Enzymol, 1979. **55**: p. 435-54.

71. Terada, H., et al., *The cyanine dye triS-C4(5) as a cationic uncoupler of oxidative phosphorylation: interaction with mitochondria detected by derivative spectrophotometry.* Cell Struct Funct, 1983. **8**(2): p. 161-70.

72. Parry, J.D., et al., *Pivotal role for two electron reduction in 2,3-dimethoxy-1,4-naphthoquinone and 2-methyl-1,4-naphthoquinone metabolism and kinetics in vivo that prevents liver redox stress.* Chem Res Toxicol, 2009. **22**(4): p. 717-25.

73. Gant, T.W., et al., *Redox cycling and sulphydryl arylation; their relative importance in the mechanism of quinone cytotoxicity to isolated hepatocytes.* Chem Biol Interact, 1988. **65**(2): p. 157-73.

74. Walker, U.A. and E. Byrne, *The therapy of respiratory chain encephalomyopathy: a critical review of the past and current perspective.* Acta Neurol Scand, 1995. **92**(4): p. 273-80.

75. Brand, M.D. and D.G. Nicholls, *Assessing mitochondrial dysfunction in cells.* Biochem J, 2011. **435**(2): p. 297-312.

76. Liebecq, C. and R.A. Peters, *The toxicity of fluoroacetate and the tricarboxylic acid cycle. 1949.* Biochim Biophys Acta, 1989. **1000**: p. 254-69.

77. Goncharov, N.V., R.O. Jenkins, and A.S. Radilov, *Toxicology of fluoroacetate: a review, with possible directions for therapy research.* J Appl Toxicol, 2006. **26**(2): p. 148-61.

78. Kerner, J., et al., *Characterization of the malonyl-CoA-sensitive carnitine palmitoyltransferase (CPTo) of a rat heart mitochondrial particle. Evidence that the catalytic unit is CPTi.* J Biol Chem, 1994. **269**(11): p. 8209-19.

79. Stanley, W.C., G.D. Lopaschuk, and J.G. McCormack, *Regulation of energy substrate metabolism in the diabetic heart.* Cardiovasc Res, 1997. **34**(1): p. 25-33.

80. Wolf, H.P., *Possible new therapeutic approach in diabetes mellitus by inhibition of carnitine palmitoyltransferase 1 (CPT1).* Horm Metab Res Suppl, 1992. **26**: p. 62-7.
81. Ankarcrona, M., F. Mangialasche, and B. Winblad, *Rethinking Alzheimer's disease therapy: are mitochondria the key?* J Alzheimers Dis, 2010. **20 Suppl 2**: p. S579-90.
82. Nishimura, J., et al., *Possible involvement of oxidative stress in fenofibrate-induced hepatocarcinogenesis in rats.* Arch Toxicol, 2008. **82**(9): p. 641-54.
83. Camara, A.K., E.J. Lesnefsky, and D.F. Stowe, *Potential therapeutic benefits of strategies directed to mitochondria.* Antioxid Redox Signal, 2010. **13**(3): p. 279-347.
84. Juhaszova, M., et al., *The identity and regulation of the mitochondrial permeability transition pore: where the known meets the unknown.* Ann N Y Acad Sci, 2008. **1123**: p. 197-212.
85. Rao, V.K., E.A. Carlson, and S.S. Yan, *Mitochondrial permeability transition pore is a potential drug target for neurodegeneration.* Biochim Biophys Acta, 2014. **1842**(8): p. 1267-72.
86. Halestrap, A.P. and A.P. Richardson, *The mitochondrial permeability transition: a current perspective on its identity and role in ischaemia/reperfusion injury.* J Mol Cell Cardiol, 2015. **78**: p. 129-41.
87. Hausenloy, D.J., et al., *Inhibiting mitochondrial permeability transition pore opening: a new paradigm for myocardial preconditioning?* Cardiovasc Res, 2002. **55**(3): p. 534-43.
88. St John, J.C., et al., *Mitochondrial DNA transmission, replication and inheritance: a journey from the gamete through the embryo and into offspring and embryonic stem cells.* Hum Reprod Update, 2010. **16**(5): p. 488-509.
89. Lewis, W., B.J. Day, and W.C. Copeland, *Mitochondrial toxicity of NRTI antiviral drugs: an integrated cellular perspective.* Nat Rev Drug Discov, 2003. **2**(10): p. 812-22.
90. Kakuda, T.N., *Pharmacology of nucleoside and nucleotide reverse transcriptase inhibitor-induced mitochondrial toxicity.* Clin Ther, 2000. **22**(6): p. 685-708.
91. Walker, U.A., et al., *Depletion of mitochondrial DNA in liver under antiretroviral therapy with didanosine, stavudine, or zalcitabine.* Hepatology, 2004. **39**(2): p. 311-7.
92. Mazat, J.P., et al., *What do mitochondrial diseases teach us about normal mitochondrial functions...that we already knew: threshold expression of mitochondrial defects.* Biochim Biophys Acta, 2001. **1504**(1): p. 20-30.
93. FDA, *Guidance for industry: Antiviral product development - Conducting and submitting virology studies to the agency.* 2006.
94. Yakes, F.M. and B. Van Houten, *Mitochondrial DNA damage is more extensive and persists longer than nuclear DNA damage in human cells following oxidative stress.* Proc Natl Acad Sci U S A, 1997. **94**(2): p. 514-9.

95. Garrabou, G., et al., *Reversible inhibition of mitochondrial protein synthesis during linezolid-related hyperlactatemia.* Antimicrob Agents Chemother, 2007. **51**(3): p. 962-7.

96. Oerter, D., et al., *Effect of chloramphenicol and thiamphenicol on mitochondrial components and the possible relationship to drug toxicity.* Postgrad Med J, 1974. **50 Suppl 5**: p. 65-8.

97. McKee, E.E., et al., *Inhibition of mammalian mitochondrial protein synthesis by oxazolidinones.* Antimicrob Agents Chemother, 2006. **50**(6): p. 2042-9.

98. Jafarian, I., et al., *Toxicity of valproic acid in isolated rat liver mitochondria.* Toxicol Mech Methods, 2013. **23**(8): p. 617-23.

99. Silva, M.F., et al., *Valproic acid metabolism and its effects on mitochondrial fatty acid oxidation: a review.* J Inherit Metab Dis, 2008. **31**(2): p. 205-16.

100. Nadanaciva, S., et al., *Target identification of drug induced mitochondrial toxicity using immunocapture based OXPHOS activity assays.* Toxicol In Vitro, 2007. **21**(5): p. 902-11.

101. Labbe, G., D. Pessayre, and B. Fromenty, *Drug-induced liver injury through mitochondrial dysfunction: mechanisms and detection during preclinical safety studies.* Fundam Clin Pharmacol, 2008. **22**(4): p. 335-53.

102. Gross, V.S., et al., *Isolation of functional mitochondria from rat kidney and skeletal muscle without manual homogenization.* Anal Biochem, 2011. **418**(2): p. 213-23.

103. Zhao, X., et al., *Phosphoproteome analysis of functional mitochondria isolated from resting human muscle reveals extensive phosphorylation of inner membrane protein complexes and enzymes.* Mol Cell Proteomics, 2011. **10**(1): p. M110 000299.

104. Horton, A.A. and J.A. Spencer, *Decline in respiratory control ratio of rat liver mitochondria in old age.* Mech Ageing Dev, 1981. **17**(3): p. 253-9.

105. Robinson, B.H., et al., *Nonviability of cells with oxidative defects in galactose medium: a screening test for affected patient fibroblasts.* Biochem Med Metab Biol, 1992. **48**(2): p. 122-6.

106. Marroquin, L.D., et al., *Circumventing the Crabtree effect: replacing media glucose with galactose increases susceptibility of HepG2 cells to mitochondrial toxicants.* Toxicol Sci, 2007. **97**(2): p. 539-47.

107. Nadanaciva, S. and Y. Will, *New insights in drug-induced mitochondrial toxicity.* Curr Pharm Des, 2011. **17**(20): p. 2100-12.

108. Armstrong, J.S., *Mitochondrial medicine: pharmacological targeting of mitochondria in disease.* Br J Pharmacol, 2007. **151**(8): p. 1154-65.

109. Ash, A.S. and H.T. Toh, *Oxidative phosphorylation in heart mitochondria isolated from chlorpromazine-treated animals.* Br J Pharmacol, 1970. **38**(2): p. 436P-437P.

110. Leont'eva, I.V., et al., *[The use of positron emission tomography for noninvasive diagnosis of mitochondrial dysfunction and assessment of myocardial compensatory reserve in children with cardiomyopathies]*. Kardiologiia, 2002. **42**(1): p. 80-5.

111. Penn, A.M., et al., *Generalized mitochondrial dysfunction in Parkinson's disease detected by magnetic resonance spectroscopy of muscle.* Neurology, 1995. **45**(11): p. 2097-9.

112. Thyfault, J.P., et al., *Rats selectively bred for low aerobic capacity have reduced hepatic mitochondrial oxidative capacity and susceptibility to hepatic steatosis and injury.* J Physiol, 2009. **587**(Pt 8): p. 1805-16.

113. Ong, M.M., C. Latchoumycandane, and U.A. Boelsterli, *Troglitazone-induced hepatic necrosis in an animal model of silent genetic mitochondrial abnormalities.* Toxicol Sci, 2007. **97**(1): p. 205-13.

114. Kirby, K., et al., *RNA interference-mediated silencing of Sod2 in Drosophila leads to early adult-onset mortality and elevated endogenous oxidative stress.* Proc Natl Acad Sci U S A, 2002. **99**(25): p. 16162-7.

115. Shoubridge, E.A., *A debut for mito-mouse.* Nat Genet, 2000. **26**(2): p. 132-4.

116. Graham, B.H., et al., *A mouse model for mitochondrial myopathy and cardiomyopathy resulting from a deficiency in the heart/muscle isoform of the adenine nucleotide translocator.* Nat Genet, 1997. **16**(3): p. 226-34.

117. Trifunovic, A., et al., *Premature ageing in mice expressing defective mitochondrial DNA polymerase.* Nature, 2004. **429**(6990): p. 417-23.

118. Ahting, U., et al., *Neurological phenotype and reduced lifespan in heterozygous Tim23 knockout mice, the first mouse model of defective mitochondrial import.* Biochim Biophys Acta, 2009. **1787**(5): p. 371-6.

119. Horobin, R.W., S. Trapp, and V. Weissig, *Mitochondriotropics: a review of their mode of action, and their applications for drug and DNA delivery to mammalian mitochondria.* J Control Release, 2007. **121**(3): p. 125-36.

120. Zhang, H., et al., *In silico prediction of mitochondrial toxicity by using GA-CG-SVM approach.* Toxicol In Vitro, 2009. **23**(1): p. 134-40.

121. Shikuma, C.M., et al., *Mitochondrial oxidative phosphorylation protein levels in peripheral blood mononuclear cells correlate with levels in subcutaneous adipose tissue within samples differing by HIV and lipoatrophy status.* AIDS Res Hum Retroviruses, 2008. **24**(10): p. 1255-62.

122. Fannin, R.D., et al., *Acetaminophen dosing of humans results in blood transcriptome and metabolome changes consistent with impaired oxidative phosphorylation.* Hepatology, 2010. **51**(1): p. 227-36.

123. McGill, M.R., et al., *Circulating acylcarnitines as biomarkers of mitochondrial dysfunction after acetaminophen overdose in mice and humans.* Arch Toxicol, 2014. **88**(2): p. 391-401.

124. Waters, M., et al., *Systems toxicology and the Chemical Effects in Biological Systems (CEBS) knowledge base.* EHP Toxicogenomics, 2003. **111**(1T): p. 15-28.

125. Sturla, S.J., et al., *Systems toxicology: from basic research to risk assessment.* Chem Res Toxicol, 2014. **27**(3): p. 314-29.

126. Plant, N., *Can systems toxicology identify common biomarkers of non-genotoxic carcinogenesis?* Toxicology, 2008. **254**(3): p. 164-9.

127. Bueno, J.M., et al., *Exploration of 4(1H)-pyridones as a novel family of potent antimalarial inhibitors of the plasmodial cytochrome bc1.* Future Med Chem, 2012. **4**(18): p. 2311-23.

128. Lote, C., *Principles of Renal Physiology; 4th Edition.* Springer, 2000.

129. Frezza, C., S. Cipolat, and L. Scorrano, *Organelle isolation: functional mitochondria from mouse liver, muscle and cultured fibroblasts.* Nat Protoc, 2007. **2**(2): p. 287-95.

130. Kristian, T., et al., *Isolation of mitochondria with high respiratory control from primary cultures of neurons and astrocytes using nitrogen cavitation.* J Neurosci Methods, 2006. **152**(1-2): p. 136-43.

131. Gostimskaya, I. and A. Galkin, *Preparation of highly coupled rat heart mitochondria.* J Vis Exp, 2010(43).

132. Nadanaciva, S., et al., *Assessment of drug-induced mitochondrial dysfunction via altered cellular respiration and acidification measured in a 96-well platform.* J Bioenerg Biomembr, 2012. **44**(4): p. 421-37.

133. Rogers, G.W., et al., *High throughput microplate respiratory measurements using minimal quantities of isolated mitochondria.* PLoS One, 2011. **6**(7): p. e21746.

134. Bernardi, P. and V. Petronilli, *The permeability transition pore as a mitochondrial calcium release channel: a critical appraisal.* J Bioenerg Biomembr, 1996. **28**(2): p. 131-8.

135. Bernardi, P., *The permeability transition pore. Control points of a cyclosporin A-sensitive mitochondrial channel involved in cell death.* Biochim Biophys Acta, 1996. **1275**(1-2): p. 5-9.

136. Petronilli, V., et al., *Regulation of the permeability transition pore, a voltage-dependent mitochondrial channel inhibited by cyclosporin A.* Biochim Biophys Acta, 1994. **1187**(2): p. 255-9.

137. Oliveira, P.J., et al., *Inhibitory effect of carvedilol in the high-conductance state of the mitochondrial permeability transition pore.* Eur J Pharmacol, 2001. **412**(3): p. 231-7.

138. Billiard, J., et al., *Quinoline 3-sulfonamides inhibit lactate dehydrogenase A and reverse aerobic glycolysis in cancer cells.* Cancer Metab, 2013. **1**(1): p. 19.

139. Szanto, M., et al., *Poly(ADP-ribose) polymerase-2 depletion reduces doxorubicin-induced damage through SIRT1 induction.* Cardiovasc Res, 2011. **92**(3): p. 430-8.

140. Seligman, A.M., H.L. Wasserkrug, and J.S. Hanker, *A new staining method (OTO) for enhancing contrast of lipid--containing membranes and droplets in osmium tetroxide--fixed tissue with osmiophilic thiocarbohydrazide(TCH).* J Cell Biol, 1966. **30**(2): p. 424-32.

141. Marbach, E.P. and M.H. Weil, *Rapid enzymatic measurement of blood lactate and pyruvate. Use and significance of metaphosphoric acid as a common precipitant.* Clin Chem, 1967. **13**(4): p. 314-25.

142. Babson, A.L. and G.E. Phillips, *A rapid colorimetric assay for serum lactic dehydrogenase.* Clin Chim Acta, 1965. **12**(2): p. 210-5.

143. Limonciel, A., et al., *Lactate is an ideal non-invasive marker for evaluating temporal alterations in cell stress and toxicity in repeat dose testing regimes.* Toxicol In Vitro, 2011. **25**(8): p. 1855-62.

144. Van Gelder, R.N., et al., *Amplified RNA synthesized from limited quantities of heterogeneous cDNA.* Proc Natl Acad Sci U S A, 1990. **87**(5): p. 1663-7.

145. Irizarry, R.A., et al., *Exploration, normalization, and summaries of high density oligonucleotide array probe level data.* Biostatistics, 2003. **4**(2): p. 249-64.

146. Zhang, S.D. and T.W. Gant, *A simple and robust method for connecting small-molecule drugs using gene-expression signatures.* BMC Bioinformatics, 2008. **9**: p. 258.

147. Zhang, S.D. and T.W. Gant, *sscMap: an extensible Java application for connecting small-molecule drugs using gene-expression signatures.* BMC Bioinformatics, 2009. **10**: p. 236.

148. Nelson, L., *Acute cyanide toxicity: mechanisms and manifestations.* J Emerg Nurs, 2006. **32**(4 Suppl): p. S8-11.

149. Grundlingh, J., et al., *2,4-dinitrophenol (DNP): a weight loss agent with significant acute toxicity and risk of death.* J Med Toxicol, 2011. **7**(3): p. 205-12.

150. Nony, P.A., et al., *3-Nitropropionic acid (3-NPA) produces hypothermia and inhibits histochemical labeling of succinate dehydrogenase (SDH) in rat brain.* Metab Brain Dis, 1999. **14**(2): p. 83-94.

151. Stoner, H.B., *The role of the liver in non-shivering thermogenesis in the rat.* J Physiol, 1973. **232**(2): p. 285-96.

152. Rotig, A., et al., *Pearson's marrow-pancreas syndrome. A multisystem mitochondrial disorder in infancy.* J Clin Invest, 1990. **86**(5): p. 1601-8.

153. Claessens, Y.E., et al., *Bench-to-bedside review: severe lactic acidosis in HIV patients treated with nucleoside analogue reverse transcriptase inhibitors.* Crit Care, 2003. **7**(3): p. 226-32.

154. Murray, B.J., *Severe lactic acidosis and hypothermia.* West J Med, 1981. **134**(2): p. 162-6.

155. Gross, D.N., A.P. van den Heuvel, and M.J. Birnbaum, *The role of FoxO in the regulation of metabolism.* Oncogene, 2008. **27**(16): p. 2320-36.

156. Postic, C., R. Dentin, and J. Girard, *Role of the liver in the control of carbohydrate and lipid homeostasis.* Diabetes Metab, 2004. **30**(5): p. 398-408.

157. Quinn, P.G. and D. Yeagley, *Insulin regulation of PEPCK gene expression: a model for rapid and reversible modulation.* Curr Drug Targets Immune Endocr Metabol Disord, 2005. **5**(4): p. 423-37.

158. Tyynismaa, H., et al., *Mitochondrial myopathy induces a starvation-like response.* Hum Mol Genet, 2010. **19**(20): p. 3948-58.

159. Chen, Q., et al., *Production of reactive oxygen species by mitochondria: central role of complex III.* J Biol Chem, 2003. **278**(38): p. 36027-31.

160. Zoratti, M. and I. Szabo, *The mitochondrial permeability transition.* Biochim Biophys Acta, 1995. **1241**(2): p. 139-76.

161. Lemasters, J.J., et al., *The mitochondrial permeability transition in toxic, hypoxic and reperfusion injury.* Mol Cell Biochem, 1997. **174**(1-2): p. 159-65.

162. Dranka, B.P., B.G. Hill, and V.M. Darley-Usmar, *Mitochondrial reserve capacity in endothelial cells: The impact of nitric oxide and reactive oxygen species.* Free Radic Biol Med, 2010. **48**(7): p. 905-14.

163. Carre, J.E. and M. Singer, *Cellular energetic metabolism in sepsis: the need for a systems approach.* Biochim Biophys Acta, 2008. **1777**(7-8): p. 763-71.

164. Collino, S., F.P. Martin, and S. Rezzi, *Clinical metabolomics paves the way towards future healthcare strategies.* Br J Clin Pharmacol, 2013. **75**(3): p. 619-29.

165. Shaham, O., et al., *A plasma signature of human mitochondrial disease revealed through metabolic profiling of spent media from cultured muscle cells.* Proc Natl Acad Sci U S A, 2010. **107**(4): p. 1571-5.

166. Roberts, L.D., A. Koulman, and J.L. Griffin, *Towards metabolic biomarkers of insulin resistance and type 2 diabetes: progress from the metabolome.* Lancet Diabetes Endocrinol, 2014. **2**(1): p. 65-75.

167. Stryer, L., *Biochemistry*. Fourth Edition ed. 1995, New York, NY: W.H.Freeman and Co. 1064.

168. Bain, J.R., et al., *Metabolomics applied to diabetes research: moving from information to knowledge.* Diabetes, 2009. **58**(11): p. 2429-43.

169. Muoio, D.M. and C.B. Newgard, *Mechanisms of disease: molecular and metabolic mechanisms of insulin resistance and beta-cell failure in type 2 diabetes.* Nat Rev Mol Cell Biol, 2008. **9**(3): p. 193-205.

170. Newgard, C.B., *Interplay between lipids and branched-chain amino acids in development of insulin resistance.* Cell Metab, 2012. **15**(5): p. 606-14.

171. Suhre, K., et al., *Metabolic footprint of diabetes: a multiplatform metabolomics study in an epidemiological setting.* PLoS One, 2010. **5**(11): p. e13953.

172. Frye, R.E., S. Melnyk, and D.F. Macfabe, *Unique acyl-carnitine profiles are potential biomarkers for acquired mitochondrial disease in autism spectrum disorder.* Transl Psychiatry, 2013. **3**: p. e220.

173. Mihalik, S.J., et al., *Increased levels of plasma acylcarnitines in obesity and type 2 diabetes and identification of a marker of glucolipotoxicity.* Obesity (Silver Spring), 2010. **18**(9): p. 1695-700.

174. Mai, M., et al., *Serum levels of acylcarnitines are altered in prediabetic conditions.* PLoS One, 2013. **8**(12): p. e82459.

175. Sampey, B.P., et al., *Metabolomic profiling reveals mitochondrial-derived lipid biomarkers that drive obesity-associated inflammation.* PLoS One, 2012. **7**(6): p. e38812.

176. Gruber, L., et al., *High fat diet accelerates pathogenesis of murine Crohn's disease-like ileitis independently of obesity.* PLoS One, 2013. **8**(8): p. e71661.

177. Schooneman, M.G., et al., *Acylcarnitines: reflecting or inflicting insulin resistance?* Diabetes, 2013. **62**(1): p. 1-8.

178. Newgard, C.B., et al., *A branched-chain amino acid-related metabolic signature that differentiates obese and lean humans and contributes to insulin resistance.* Cell Metab, 2009. **9**(4): p. 311-26.

179. Shah, S.H., et al., *Branched-chain amino acid levels are associated with improvement in insulin resistance with weight loss.* Diabetologia, 2012. **55**(2): p. 321-30.

180. Shah, S.H., L.P. Svetkey, and C.B. Newgard, *Branching out for detection of type 2 diabetes.* Cell Metab, 2011. **13**(5): p. 491-2.

181. Jesús Zacarías Villarreal-Pérez, J.Z.V.-M., Fernando Javier Lavalle-González, María del Rosario Torres-Sepúlveda, Consuelo Ruiz-Herrera, Ricardo Martín Cerda-Flores, Erik Rubén Castillo-García, Irám Pablo Rodríguez-Sánchez and Laura Elia Martínez de Villarreal, *Plasma and urine metabolic profiles are reflective of altered beta-oxidation in non-diabetic obese subjects and patients with type 2 diabetes mellitus.* Diabetology & Metabolic Syndrome, 2014. **6**.

182. Gall, W.E., et al., *alpha-hydroxybutyrate is an early biomarker of insulin resistance and glucose intolerance in a nondiabetic population.* PLoS One, 2010. **5**(5): p. e10883.

183. Gall, W.E., et al. *Alpha-hydroxybutyrate reduces mitochondrial ATP synthesis in human muscle*. in *American Diatetic Association, 70th Session*. 2011. Orlando, FL.

184. Cobb, J., et al., *A novel fasting blood test for insulin resistance and prediabetes.* J Diabetes Sci Technol, 2013. **7**(1): p. 100-10.

185. Voet, D.V., J.G., and C.W. Pratt, *Fundamentals of Biochemistry*. 1999: John Wiley & Sons, Inc.

186. Berkeley, L.I., et al., *Hepatoprotection by L-cysteine-glutathione mixed disulfide, a sulfhydryl-modified prodrug of glutathione.* J Biochem Mol Toxicol, 2003. **17**(2): p. 95-7.

187. Parikh, S., et al., *Diagnosis and management of mitochondrial disease: a consensus statement from the Mitochondrial Medicine Society.* Genet Med, 2014.

188. Demine, S., et al., *Unraveling biochemical pathways affected by mitochondrial dysfunctions using metabolomic approaches.* Metabolites, 2014. **4**(3): p. 831-78.

189. Capper, M.J., et al., *Antimalarial 4(1H)-pyridones bind to the Qi site of cytochrome bc1.* Proc Natl Acad Sci U S A, 2015. **112**(3): p. 755-60.

190. Lyamzaev, K.G., et al., *Inhibition of mitochondrial bioenergetics: the effects on structure of mitochondria in the cell and on apoptosis.* Acta Biochim Pol, 2004. **51**(2): p. 553-62.

191. Watabe, M. and T. Nakaki, *ATP depletion does not account for apoptosis induced by inhibition of mitochondrial electron transport chain in human dopaminergic cells.* Neuropharmacology, 2007. **52**(2): p. 536-41.

192. Lee, S.J., et al., *Mitochondrial dysfunction induces formation of lipid droplets as a generalized response to stress.* Oxid Med Cell Longev, 2013. **2013**: p. 327167.

193. Pao, D., et al., *Hyperlactataemia and hepatic steatosis: mitochondrial toxicity of nucleoside reverse transcriptase inhibitors.* Sex Transm Infect, 2001. **77**(5): p. 381-4.

194. Timbrell, S., et al., *Lactic acidosis secondary to metformin overdose: a case report.* J Med Case Rep, 2012. **6**: p. 230.

195. Clemmer, T.P., et al., *Hypothermia in the sepsis syndrome and clinical outcome. The Methylprednisolone Severe Sepsis Study Group.* Crit Care Med, 1992. **20**(10): p. 1395-401.

196. Borron, S.W., *Recognition and treatment of acute cyanide poisoning.* J Emerg Nurs, 2006. **32**(4 Suppl): p. S12-8.

197. St-Pierre, J., et al., *Topology of superoxide production from different sites in the mitochondrial electron transport chain.* J Biol Chem, 2002. **277**(47): p. 44784-90.

198. Yang, Y., et al., *Reactive oxygen species in the immune system.* Int Rev Immunol, 2013. **32**(3): p. 249-70.

199. Gribble, E.J., et al., *Toxicity as a result of immunostimulation by biologics.* Expert Opin Drug Metab Toxicol, 2007. **3**(2): p. 209-34.

200. Ma, X., et al., *Mitochondrial electron transport chain complex III is required for antimycin A to inhibit autophagy.* Chem Biol, 2011. **18**(11): p. 1474-81.

201. Davoudi, M., et al., *A mouse model of mitochondrial complex III dysfunction induced by myxothiazol.* Biochem Biophys Res Commun, 2014. **446**(4): p. 1079-84.

202. Berson, A., et al., *Inhibition by nilutamide of the mitochondrial respiratory chain and ATP formation. Possible contribution to the adverse effects of this antiandrogen.* J Pharmacol Exp Ther, 1994. **270**(1): p. 167-76.

203. Fau, D., et al., *Mechanism for the hepatotoxicity of the antiandrogen, nilutamide. Evidence suggesting that redox cycling of this nitroaromatic drug leads to oxidative stress in isolated hepatocytes.* J Pharmacol Exp Ther, 1992. **263**(1): p. 69-77.

204. Nath, A.K., et al., *Chemical and metabolomic screens identify novel biomarkers and antidotes for cyanide exposure.* FASEB J, 2013. **27**(5): p. 1928-38.

205. Kadenbach, B., *Intrinsic and extrinsic uncoupling of oxidative phosphorylation.* Biochim Biophys Acta, 2003. **1604**(2): p. 77-94.

206. Kessler, R.J., et al., *Uncouplers and the molecular mechanism of uncoupling in mitochondria.* Proc Natl Acad Sci U S A, 1977. **74**(6): p. 2241-5.

207. Finkelstein, A., *Weak-acid uncouplers of oxidative phosphorylation. Mechanism of action on thin lipid membranes.* Biochim Biophys Acta, 1970. **205**(1): p. 1-6.

208. McDougall, P., et al., *The mechanism of inhibition of mitochondrial oxidative phosphorylation by the nonsteroidal anti-inflammatory agent diflunisal.* Biochem Pharmacol, 1983. **32**(17): p. 2595-8.

209. Mahmud, T., et al., *Nonsteroidal antiinflammatory drugs and uncoupling of mitochondrial oxidative phosphorylation.* Arthritis Rheum, 1996. **39**(12): p. 1998-2003.

210. Norman, C., et al., *Salicylic acid is an uncoupler and inhibitor of mitochondrial electron transport.* Plant Physiol, 2004. **134**(1): p. 492-501.

211. Porceddu, M., et al., *Prediction of Liver Injury Induced by Chemicals in Human with a Multiparametric Assay on Isolated Mouse Liver Mitochondria.* Toxicol Sci, 2012.

212. Cunha, F.M., et al., *Mild mitochondrial uncoupling as a therapeutic strategy.* Curr Drug Targets, 2011. **12**(6): p. 783-9.

213. Perry, R.J., et al., *Controlled-release mitochondrial protonophore reverses diabetes and steatohepatitis in rats.* Science, 2015. **347**(6227): p. 1253-6.

214. Tao, H., et al., *Niclosamide ethanolamine-induced mild mitochondrial uncoupling improves diabetic symptoms in mice.* Nat Med, 2014. **20**(11): p. 1263-9.

215. Silachev, D.N., et al., *Neuroprotective effect of glutamate-substituted analog of gramicidin A is mediated by the uncoupling of mitochondria.* Biochim Biophys Acta, 2014. **1840**(12): p. 3434-42.

216. Maragos, W.F., et al., *Pre- or post-treatment with the mitochondrial uncoupler 2,4-dinitrophenol attenuates striatal quinolinate lesions.* Brain Res, 2003. **966**(2): p. 312-6.

217. Kamour, A., et al., *Increasing frequency of severe clinical toxicity after use of 2,4-dinitrophenol in the UK: a report from the National Poisons Information Service.* Emerg Med J, 2014.

218. Wise, J., *Increase in reports of toxicity from fat burning supplement seen in UK.* BMJ, 2014. **348**: p. g4188.

219. Haasio, K., et al., *Effects of entacapone and tolcapone on mitochondrial membrane potential.* Eur J Pharmacol, 2002. **453**(1): p. 21-6.

220. van Marken Lichtenbelt, W., *Brown adipose tissue and the regulation of nonshivering thermogenesis.* Curr Opin Clin Nutr Metab Care, 2012. **15**(6): p. 547-52.

221. Samudio, I., M. Fiegl, and M. Andreeff, *Mitochondrial uncoupling and the Warburg effect: molecular basis for the reprogramming of cancer cell metabolism.* Cancer Res, 2009. **69**(6): p. 2163-6.

222. Matthias, A., et al., *Thermogenic responses in brown fat cells are fully UCP1-dependent. UCP2 or UCP3 do not substitute for UCP1 in adrenergically or fatty scid-induced thermogenesis.* J Biol Chem, 2000. **275**(33): p. 25073-81.

223. Li, Y., et al., *Mitochondrial dysfunction induced by sertraline, an antidepressant agent.* Toxicol Sci, 2012. **127**(2): p. 582-91.

224. Weng, Z., et al., *Regorafenib impairs mitochondrial functions, activates AMP-activated protein kinase, induces autophagy, and causes rat hepatocyte necrosis.* Toxicology, 2015. **327**: p. 10-21.

225. Melmed, C., G. Karpati, and S. Carpenter, *Experimental mitochondrial myopathy produced by in vivo uncoupling of oxidative phosphorylation.* J Neurol Sci, 1975. **26**(3): p. 305-18.

226. Felser, A., et al., *Hepatocellular toxicity of benzbromarone: effects on mitochondrial function and structure.* Toxicology, 2014. **324**: p. 136-46.

227. Haasio, K., K. Lounatmaa, and A. Sukura, *Entacapone does not induce conformational changes in liver mitochondria or skeletal muscle in vivo.* Exp Toxicol Pathol, 2002. **54**(1): p. 9-14.

228. Somasundaram, S., et al., *Mitochondrial damage: a possible mechanism of the "topical" phase of NSAID induced injury to the rat intestine.* Gut, 1997. **41**(3): p. 344-53.

229. Kuruvilla, S., et al., *Effects of minimally toxic levels of carbonyl cyanide P-(trifluoromethoxy) phenylhydrazone (FCCP), elucidated through differential gene expression with biochemical and morphological correlations.* Toxicol Sci, 2003. **73**(2): p. 348-61.

230. Dykens, J.A. and Y. Will, *Drug-induced mitochondrial dysfunction*. 1st ed. 2008: Wiley.

231. Wang, G., et al., *Modeling the mitochondrial cardiomyopathy of Barth syndrome with induced pluripotent stem cell and heart-on-chip technologies.* Nat Med, 2014. **20**(6): p. 616-23.

232. Murata, S., et al., *Antitumor effect of 1, 8-cineole against colon cancer.* Oncol Rep, 2013. **30**(6): p. 2647-52.

233. Garedew, A., S.O. Henderson, and S. Moncada, *Activated macrophages utilize glycolytic ATP to maintain mitochondrial membrane potential and prevent apoptotic cell death.* Cell Death Differ, 2012.

234. Zhao, Y. and D. Bruemmer, *NR4A orphan nuclear receptors: transcriptional regulators of gene expression in metabolism and vascular biology.* Arterioscler Thromb Vasc Biol, 2010. **30**(8): p. 1535-41.

235. Liu, C. and J.D. Lin, *PGC-1 coactivators in the control of energy metabolism.* Acta Biochim Biophys Sin (Shanghai), 2011. **43**(4): p. 248-57.

236. Handschin, C., *The biology of PGC-1alpha and its therapeutic potential.* Trends Pharmacol Sci, 2009. **30**(6): p. 322-9.

237. Kousteni, S., *FoxO1, the transcriptional chief of staff of energy metabolism.* Bone, 2012. **50**(2): p. 437-43.

238. Guo, S., *Insulin signaling, resistance, and the metabolic syndrome: insights from mouse models into disease mechanisms.* J Endocrinol, 2014. **220**(2): p. T1-T23.

239. Araki, M., Y. Nozaki, and K. Motojima, *[Transcriptional regulation of metabolic switching PDK4 gene under various physiological conditions]*. Yakugaku Zasshi, 2007. **127**(1): p. 153-62.

240. Sass, G., R. Barikbin, and G. Tiegs, *The multiple functions of heme oxygenase-1 in the liver.* Z Gastroenterol, 2012. **50**(1): p. 34-40.

241. Ishimoto, K., *[Lipin 1 in lipid metabolism]*. Yakugaku Zasshi, 2011. **131**(8): p. 1189-94.

242. Finck, B.N., et al., *Lipin 1 is an inducible amplifier of the hepatic PGC-1alpha/PPARalpha regulatory pathway.* Cell Metab, 2006. **4**(3): p. 199-210.

243. Allen-Jennings, A.E., et al., *The roles of ATF3 in liver dysfunction and the regulation of phosphoenolpyruvate carboxykinase gene expression.* J Biol Chem, 2002. **277**(22): p. 20020-5.

244. Jiang, H.Y., et al., *Activating transcription factor 3 is integral to the eukaryotic initiation factor 2 kinase stress response.* Mol Cell Biol, 2004. **24**(3): p. 1365-77.

245. Shoichet, B.K., *Interpreting steep dose-response curves in early inhibitor discovery.* J Med Chem, 2006. **49**(25): p. 7274-7.

246. Riss, T.L., et al., *Cell Viability Assays*, in *Assay Guidance Manual*, G.S. Sittampalam, et al., Editors. 2004: Bethesda (MD).

247. Dranka, B.P., et al., *Assessing bioenergetic function in response to oxidative stress by metabolic profiling.* Free Radic Biol Med, 2011. **51**(9): p. 1621-35.

248. Liang, H. and W.F. Ward, *PGC-1alpha: a key regulator of energy metabolism.* Adv Physiol Educ, 2006. **30**(4): p. 145-51.

249. Scarpulla, R.C., *Metabolic control of mitochondrial biogenesis through the PGC-1 family regulatory network.* Biochim Biophys Acta, 2011. **1813**(7): p. 1269-78.

250. Valle, I., et al., *PGC-1alpha regulates the mitochondrial antioxidant defense system in vascular endothelial cells.* Cardiovasc Res, 2005. **66**(3): p. 562-73.

251. Lin, J., et al., *Transcriptional co-activator PGC-1 alpha drives the formation of slow-twitch muscle fibres.* Nature, 2002. **418**(6899): p. 797-801.

252. Finck, B.N. and D.P. Kelly, *PGC-1 coactivators: inducible regulators of energy metabolism in health and disease.* J Clin Invest, 2006. **116**(3): p. 615-22.

253. Puigserver, P., et al., *Insulin-regulated hepatic gluconeogenesis through FOXO1-PGC-1alpha interaction.* Nature, 2003. **423**(6939): p. 550-5.

254. Stark, R., et al., *A role for mitochondrial phosphoenolpyruvate carboxykinase (PEPCK-M) in the regulation of hepatic gluconeogenesis.* J Biol Chem, 2014. **289**(11): p. 7257-63.

255. Pei, L., et al., *NR4A orphan nuclear receptors are transcriptional regulators of hepatic glucose metabolism.* Nat Med, 2006. **12**(9): p. 1048-55.

256. Wansa, K.D., et al., *The AF-1 domain of the orphan nuclear receptor NOR-1 mediates trans-activation, coactivator recruitment, and activation by the purine anti-metabolite 6-mercaptopurine.* J Biol Chem, 2003. **278**(27): p. 24776-90.

257. Dubois, C., B. Hengerer, and H. Mattes, *Identification of a potent agonist of the orphan nuclear receptor Nurr1.* ChemMedChem, 2006. **1**(9): p. 955-8.

258. Hintermann, S., et al., *Identification of a series of highly potent activators of the Nurr1 signaling pathway.* Bioorg Med Chem Lett, 2007. **17**(1): p. 193-6.

259. Crawford, R.R., et al., *Human CHAC1 Protein Degrades Glutathione and mRNA Induction is Regulated by the Transcription Factors ATF4 and ATF3 and a Bipartite ATF/CRE Element.* J Biol Chem, 2015.

260. Hai, T., et al., *ATF3 and stress responses.* Gene Expr, 1999. **7**(4-6): p. 321-35.

261. Gilchrist, M., et al., *Activating transcription factor 3 is a negative regulator of allergic pulmonary inflammation.* J Exp Med, 2008. **205**(10): p. 2349-57.

262. Kim, J.Y., et al., *Chronic ethanol consumption inhibits glucokinase transcriptional activity by Atf3 and triggers metabolic syndrome in vivo.* J Biol Chem, 2014. **289**(39): p. 27065-79.

263. Tsai, W.W., et al., *ATF3 mediates inhibitory effects of ethanol on hepatic gluconeogenesis.* Proc Natl Acad Sci U S A, 2015. **112**(9): p. 2699-704.

264. Wang, A., et al., *The transcription factor ATF3 acts as an oncogene in mouse mammary tumorigenesis.* BMC Cancer, 2008. **8**: p. 268.

265. Lu, D., C.D. Wolfgang, and T. Hai, *Activating transcription factor 3, a stress-inducible gene, suppresses Ras-stimulated tumorigenesis.* J Biol Chem, 2006. **281**(15): p. 10473-81.

266. Ling, K.H., et al., *Metabolism of terfenadine associated with CYP3A(4) activity in human hepatic microsomes.* Drug Metab Dispos, 1995. **23**(6): p. 631-6.

267. Woosley, R.L., et al., *Mechanism of the cardiotoxic actions of terfenadine.* JAMA, 1993. **269**(12): p. 1532-6.

268. Odland, T.M., *Azacyclonol (frenquel) hydrochloride in the treatment of chronic schizophrenia; a double-blind, controlled study.* J Am Med Assoc, 1957. **165**(4): p. 333-5.

269. Braun, D.L., B.B. Brown, and R.G. Feldman, *The pharmacologic activity of alpha-(4-piperidyl)-benzhydrol hydrochloride (azacyclonol hydrochloride); an ataractive agent.* J Pharmacol Exp Ther, 1956. **118**(2): p. 153-61.

270. Vilar, S., et al., *Drug-drug interaction through molecular structure similarity analysis.* J Am Med Inform Assoc, 2012. **19**(6): p. 1066-74.

271. OECD, *OECD, 2013. Guidance Document on Developing and Assessing Adverse Outcome Pathways. Series on Testing and Assessment No. 184.* 2013.

272. Becker, R.A., et al., *Increasing Scientific Confidence in Adverse Outcome Pathways: Application of Tailored Bradford-Hill Considerations for Evaluating Weight of Evidence.* Regul Toxicol Pharmacol, 2015. **72**(3): p. 514-537.

273. Fujimoto, K., et al., *Sensitivity of liver injury in heterozygous Sod2 knockout mice treated with troglitazone or acetaminophen.* Toxicol Pathol, 2009. **37**(2): p. 193-200.

274. Hornig-Do, H.T., et al., *Isolation of functional pure mitochondria by superparamagnetic microbeads.* Anal Biochem, 2009. **389**(1): p. 1-5.

275. Garcia-Cazarin, M.L., N.N. Snider, and F.H. Andrade, *Mitochondrial isolation from skeletal muscle.* J Vis Exp, 2011(49).

276. Schmidt-Mende, J., et al., *Early mitochondrial alterations in ATRA-induced cell death.* Cell Death Differ, 2006. **13**(1): p. 119-28.

277. Coelho, A.M., et al., *Hepatic damage during acute pancreatitis in the rat.* Braz J Med Biol Res, 1997. **30**(8): p. 947-53.

278. Mantena, S.K., et al., *High fat diet induces dysregulation of hepatic oxygen gradients and mitochondrial function in vivo.* Biochem J, 2009. **417**(1): p. 183-93.

279. Tirapelli, L.F., et al., *Renal ischemia in rats: mitochondria function and laser autofluorescence.* Transplant Proc, 2008. **40**(5): p. 1679-84.

280. Ruggiero, C., et al., *High-fat diet induces an initial adaptation of mitochondrial bioenergetics in the kidney despite evident oxidative stress and mitochondrial ROS production.* Am J Physiol Endocrinol Metab, 2011. **300**(6): p. E1047-58.

281. Tucci, S., Jr., et al., *Calcium channel blocker and renal mitochondrial function in warm renal ischemia.* Int Braz J Urol, 2005. **31**(4): p. 384-9.

282. Kemp, R., et al., *Evaluation of the mitochondrial respiration of cardiac myocytes in rats submitted to mechanical bile duct obstruction.* Acta Cir Bras, 2008. **23 Suppl 1**: p. 66-71; discussion 71.

283. Labieniec-Watala, M., K. Siewiera, and Z. Jozwiak, *Resorcylidene aminoguanidine (RAG) improves cardiac mitochondrial bioenergetics impaired by hyperglycaemia in a model of experimental diabetes.* Int J Mol Sci, 2011. **12**(11): p. 8013-26.

284. Taylor, D., S. Bhandari, and A.M. Seymour, *Mitochondrial dysfunction in uremic cardiomyopathy.* Am J Physiol Renal Physiol, 2015. **308**(6): p. F579-87.

285. Shen, X., et al., *Protection of cardiac mitochondria by overexpression of MnSOD reduces diabetic cardiomyopathy.* Diabetes, 2006. **55**(3): p. 798-805.

286. Yajid, F., et al., *Effects of 4 wk of hindlimb suspension on skeletal muscle mitochondrial respiration in rats.* J Appl Physiol (1985), 1998. **84**(2): p. 479-85.

287. Crescenzo, R., et al., *Skeletal muscle mitochondrial oxidative capacity and uncoupling protein 3 are differently influenced by semistarvation and refeeding.* FEBS Lett, 2003. **544**(1-3): p. 138-42.

288. Muller, F.L., et al., *Denervation-induced skeletal muscle atrophy is associated with increased mitochondrial ROS production.* Am J Physiol Regul Integr Comp Physiol, 2007. **293**(3): p. R1159-68.

289. Lin, L., et al., *Regulation of skeletal muscle oxidative capacity and muscle mass by SIRT3.* PLoS One, 2014. **9**(1): p. e85636.

290. Stauch, K.L., P.R. Purnell, and H.S. Fox, *Aging synaptic mitochondria exhibit dynamic proteomic changes while maintaining bioenergetic function.* Aging (Albany NY), 2014. **6**(4): p. 320-34.

291. Yan, W. and J. Liu, *Effects of Chinese herbal monomers on oxidative phosphorylation and membrane potential in cerebral mitochondria isolated from hypoxia-exposed rats in vitro.* Neural Regen Res, 2012. **7**(27): p. 2099-106.

292. Cormier, A., et al., *Nicotine protects rat brain mitochondria against experimental injuries.* Neuropharmacology, 2003. **44**(5): p. 642-52.

293. Pandya, J.D., V.N. Nukala, and P.G. Sullivan, *Concentration dependent effect of calcium on brain mitochondrial bioenergetics and oxidative stress parameters.* Front Neuroenergetics, 2013. **5**: p. 10.

294. Singh, I.N., et al., *Phenelzine mitochondrial functional preservation and neuroprotection after traumatic brain injury related to scavenging of the lipid peroxidation-derived aldehyde 4-hydroxy-2-nonenal.* J Cereb Blood Flow Metab, 2013. **33**(4): p. 593-9.

295. Papkovsky, D.B., et al, *Phosphorescent Oxygen Sensitive Probes.*SpringerBriefs in Biochem and Mol Bio, 2012. DOI: 10.1007/978-3-0348-0525-4_2

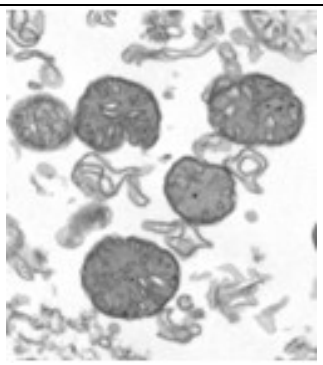
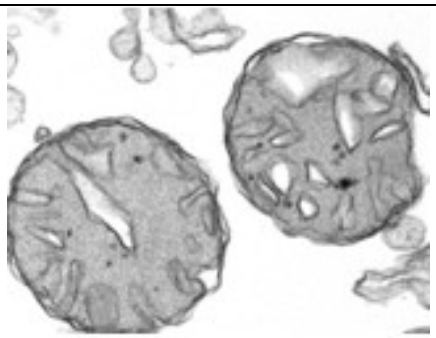
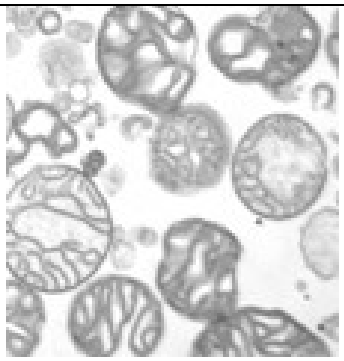
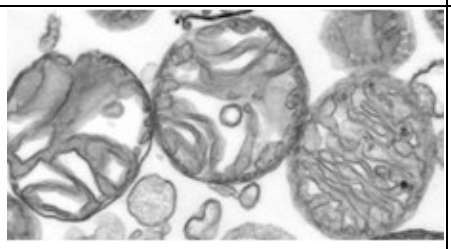
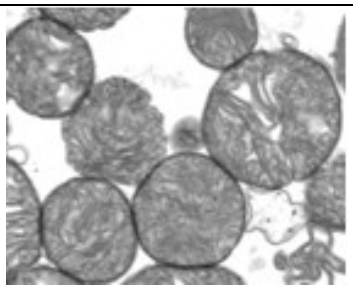
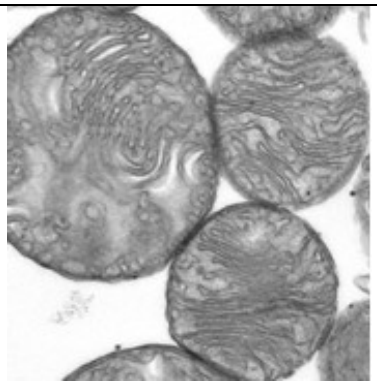
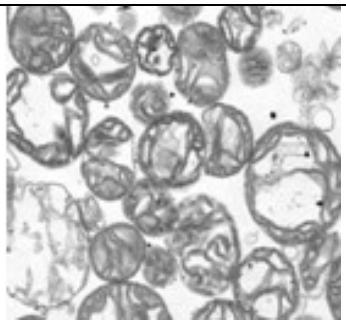
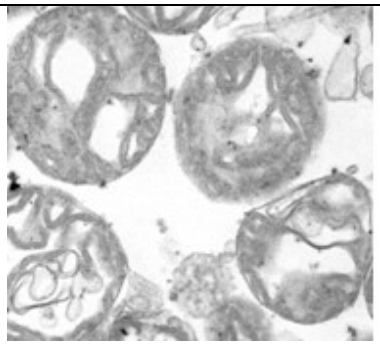
296. Dranka, D.P., et al., *Assessing bioenergetic function in response to oxidative stress by metabolic profiling*. Free Radic Biol Med, 2011. **51**(9): 1621-1635.

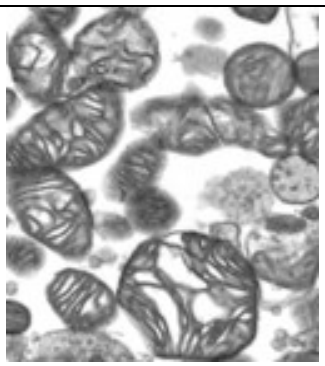
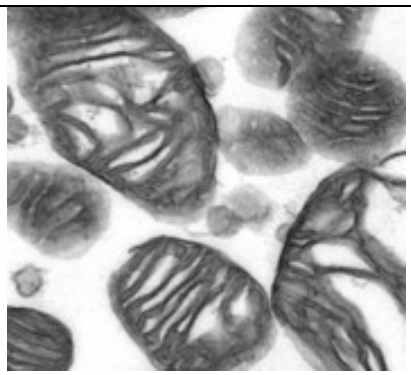
APPENDIX I – STRUCTURAL ASSESSMENT OF ISOLATED MITOCHONDRIAL FRACTIONS

Following optimisation of mitochondrial isolation procedures for the five tissues of highest metabolic load (i.e. the liver, kidney, heart, skeletal muscle and brain) it was important to assess the structural integrity of the obtained fractions. Although the use of isolated mitochondria have proved to be a very powerful tool in the study of the OXPHOS system, biogenesis, substrate oxidation etc., compromises remain regarding their utility as tools to study DIMT. One of the primary compromises relates to the effect of mitochondrial isolation on the structural integrity of the obtained fraction and as a result, the "likeness" of the isolated mitochondria to those in the *in vivo* milieu. The isolation of mitochondria from animal tissues is a stressful procedure, typically relying on Dounce, Potter-Elvehjem and rotor/stator shearing homogenisers [102]. This causes structural damage to the mitochondria, disruption of the heterogeneous bioenergetic network and disturbance to dynamic mitochondrial processes (e.g. fission and fusion). It was therefore decided to use electron microscopy and Western blots to assess the structural integrity of the mitochondria isolated from each tissue in an attempt to determine the suitability of these isolates for the study of DIMT.

APPENDIX 1.1: Transmission Electron Microscopy

TEM imaging was performed on isolated mitochondrial pellets (from all five tissues) as described in section 2.10.1. TEM images and a description of the main findings are presented in Appendix Table 1.1 below.

Organ	Low magnification (12000x)	High magnification (30000x)	Details
Liver			The mitochondria were generally of typical appearance with intact cristae and medium electron dense matrices. The cristae showed a degree of swelling and the occasional pale swollen mitochondrion was seen. A large amount of heterogeneous material (tubular, vesicular and amorphous material) was present between the mitochondria.
Kidney			Little heterogeneous material and no presence of other organelles. Large swelling of cristae was observed with low electron density matrices
Heart			The mitochondria were generally of normal appearance although a small proportion had swollen cristae. They show a high density of tightly packed cristae. There was little heterogeneous material observed between the mitochondria with no other organelles present.
Skeletal Muscle			Many of the mitochondria were swollen or showed quite marked dilation of the cristae. The mitochondria obtained from this tissue were considered to be the most altered. Other organelles were not present but fragments of myofibrils were seen among the mitochondria.

Brain			The mitochondria were generally of normal appearance but a proportion contained swollen cristae. The mitochondrial membranes appeared densely organised.

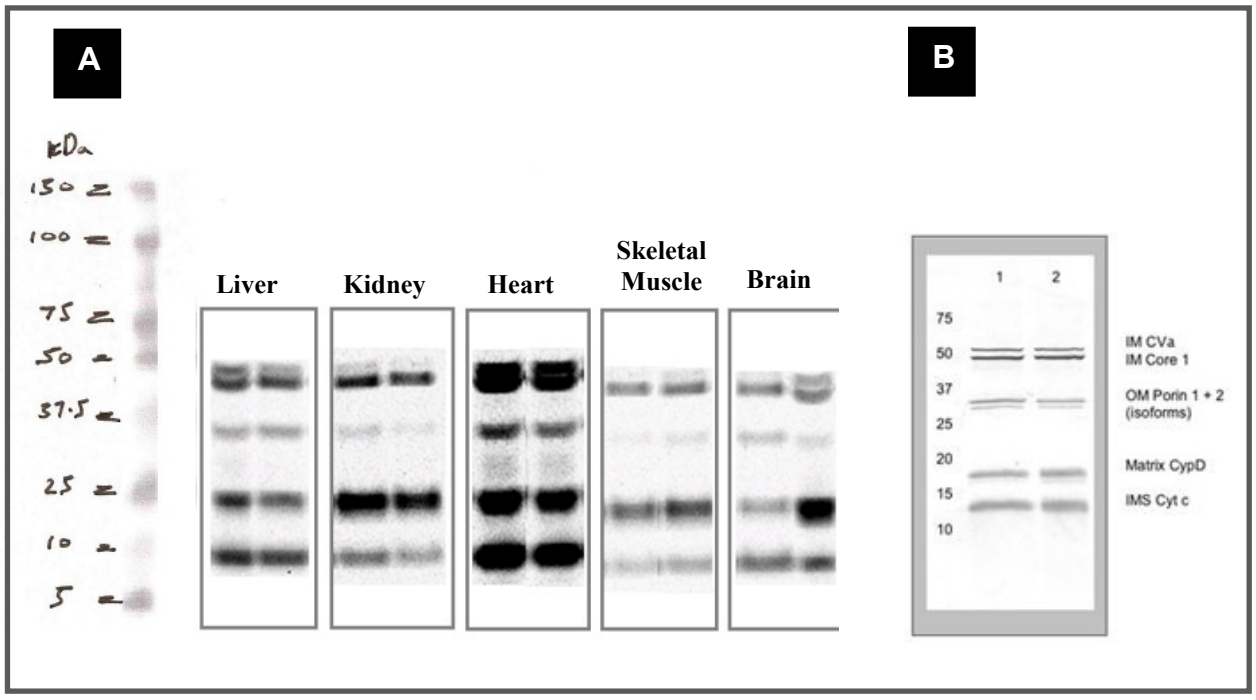
APPENDIX TABLE 1.1: TEM Analysis of crude mitochondrial pellets isolated from five tissues of high metabolic load. Isolated mitochondria from liver, kidney, heart, skeletal muscle and brain were processed for TEM as described in section 2.10.2. Images are shown at 12,000x and 30,000x magnification.

In addition to observations made in appendix table 1.1 above, brain mitochondria were often observed within membrane bound vacuoles. It is believed that these vacuoles are synaptosomes which are formed when pre-synaptic membranes re-seal enclosing the contents of the nerve terminals (not shown). Furthermore a number of liver mitochondria were observed undergoing fission/fusion events although it remains unclear whether this is physiological (e.g. repair mechanisms, natural replication) or simply an idiosyncratic observation with little relevance to the population of mitochondria (not shown).

APPENDIX 1.2: Western Blot

The Western blot data presented in Fig.Appendix1 below generally supports observations from the TEM investigations described above. Mitochondrial protein was analysed by Western blot according to the method outlined in section 2.11. Mitochondria were also probed for detection of proliferating cell nuclear antigen (anti-PCNA) and alpha-tubulin (Anti-α-tubulin) as markers of both the nuclear and cytoplasmic fractions respectively. This was performed to ensure purity of the mitochondrial fractions from other cellular compartments. Despite observations of cellular debris in the TEM images, no PCNA or α-tubulin was detectable via Western blot (data not shown), suggesting that mitochondrial preparations from all tissues are relatively pure and lacking in contamination.

The molecular weights of the structural subunit proteins are generally consistent with those suggested by the manufacturer (outlined in Appendix-Fig.1.1B) although a slight discrepancy is seen with the cyclophilin D and cytochrome c proteins. Western blot data supports the TEM observations which show mitochondria isolated from the heart with prominent banding and protein abundance especially in terms of the inner membrane respiratory complexes, the mitochondrial matrix and the IMS. The dense banding also suggests larger quantities of protein at all mitochondrial levels per mg of mitochondria analysed. Likewise mitochondria from the skeletal muscle were suggested to be the most altered in terms of structure following TEM analysis and this is confirmed via Western blot where banding appears faint and only very minor levels of the OMM porin proteins were detected.



APPENDIX FIGURE 1.1: Assessment of mitochondria isolated from 5 rodent tissues via Western blot.(A) Mitochondria isolated from the liver, kidney, heart, skeletal muscle and brain were examined via Western blot using a multiplexed Antibody cocktail containing proteins essential to the IMM (complex V), OMM (porin), matrix (cyclophilin D) and IMS (cytochrome C). (B) Image lifted from Mitosciences protocol booklet (Abcam #ab110414) detailing the expected molecular weights of each protein and the identification of corresponding bands [http://www.abcam.com/membrane-integrity-wb-antibody-cocktail-ab110414.html] – Accessed 10 July 2015.

Western blot data with liver, kidney and brain suggests that the integrity of the mitochondria isolated from these tissues is generally fair although all have relatively faint banding of the OMM porin protein. This was to be expected as it suggests that the isolation procedure affects the outer membrane structure more severely than the IMM, IMS and matrix. Despite general accordance with the manufacturer's expected banding (see Fig.Appendix 1B) no separation of the two OMM porin isoforms was observed in any mitochondrial preparation. It remains unknown whether this is due to structural damage to the outer membrane or due to poor resolution/contrast in the Western blot images. Following analysis of both TEM images and Western blot data, the rank order of structural integrity following mitochondrial isolation is shown below.

Heart > Liver > Brain > Kidney > Skeletal Muscle

The structural data presented in this appendix does however suggest that all mitochondrial isolates are relatively fit for purpose. The isolation protocols are all selective for the mitochondrial population (i.e. no obvious presence of other organelles) and all isolate mitochondria which remain structurally sound (although to varying degrees of success). Future work should focus on the continued improvement of isolation protocols and should assess the utility of methods, either not involving the manual homogenisation of tissue (i.e. tissue shredders [102] or nitrogen cavitation [130]), or which rely less on stressful homogenisation steps (i.e. the magnetic bead capture methods [274]).

APPENDIX II – FUNTIONAL ASSESSMENT OF ISOLATED MITOCHONDRIAL FRACTIONS

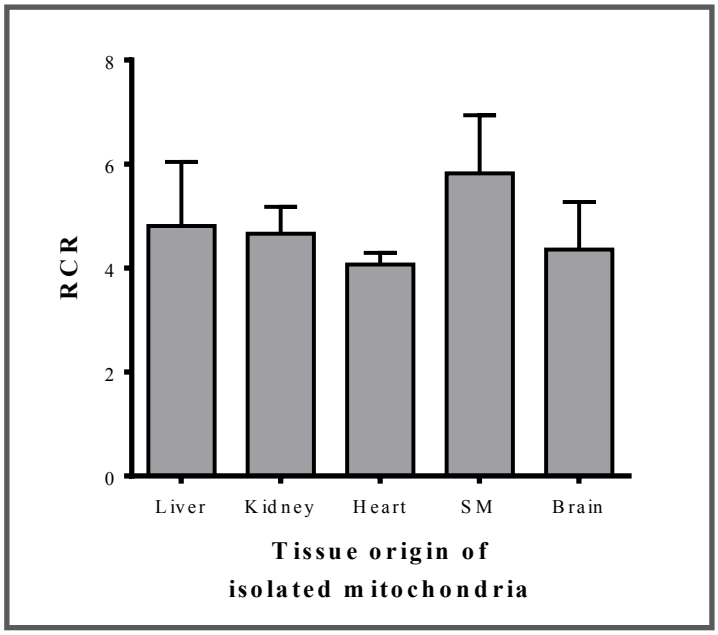
Following optimisation of mitochondrial isolation procedures, it was important to ensure the obtained fractions were functional in a number of key assays. A sustained period of time was spent optimising the parameters for mitochondria isolated from all five tissues in the CRC, OCR and mitochondrial ΔΨ assays. It does however remain inherently challenging to compare mitochondria isolated from each tissue. This is a result of the vastly different isolation protocols which produce fractions which vary widely with regard to the following…

- Mitochondrial number (i.e. per mg of tissue).
- The degree of structural damage caused by the isolation procedure, particularly the tissue homogenisation step.
- The resulting buffer which the mitochondria are stored in.

As a result of the above factors, the optimisation of each assay with each mitochondrial fraction required individual tailoring. This optimisation created a functional battery of assays with mitochondria from these five tissues. Key optimisation variables included the mitochondrial substrate (i.e. complex I or complex II driven substrates) and the concentration of mitochondria. The resulting assay kinetics therefore reflect artefacts of both the isolation protocol and optimisation parameters in combination with the biology and metabolic activity of the mitochondria from each tissue. As a result and due to the fact that the assay conditions of mitochondria from each tissue are so non-standardised, directly comparing the functionality of mitochondria from each tissue is fundamentally problematic.

A functional assessment which was made however was the respiratory control ratio (RCR) of mitochondria from all five tissues. The RCR is calculated by dividing the respiration in state 3 (ADP-driven respiration) by that in state 4. As a result, the RCR represents the degree of coupling between ETC function and OXPHOS with high RCR values implying that mitochondria have a high capacity for substrate utilisation and ATP turnover and a low proton leak [75]. Although there is no benchmark RCR to define functional/dysfunctional mitochondria (as RCR is substrate and tissue dependent), Garcia-

Cazarin and colleagues in 2011 suggested that an RCR of above 4 is considered as evidence of a viable mitochondrial population [275]. This was therefore the arbitrary RCR-number which was deemed acceptable for mitochondria isolated from each tissue. In order to validate the viability and functionality of the obtained RCR values, comparisons were drawn to others reported in the literature with mitochondria isolated from each tissue. RCR values obtained from isolated mitochondrial fractions are shown in Appendix Fig.2.1 below. These RCR values have been calculated as an average (±SD) of a number of control animals used in multiple studies at GlaxoSmithKline over the course of the PhD (n-numbers stated below).



APPENDIX FIGURE 2.1: RCR values obtained for mitochondria isolated from liver, kidney, heart, skeletal muscle and brain rat tissues. Data represents RCR values (state 3/state 4) for mitochondria isolated from rat liver (n=37), kidney (n=8), heart (n=37), skeletal muscle (n=24) and brain (n=17). Data shown is mean ± SD.

RCR values shown in appendix Fig.2.1 above correlate well with published values obtained in other laboratories as shown in appendix table 2.1 below. It is however important to acknowledge that measurement of mitochondrial respiration is performed using multiple different techniques (i.e. Seahorse Bioanalysers, Luxcel oxygen sensing probes, Clarke-type electrode) and, as a result, RCR values are likely to differ greatly making the drawing of valid comparisons challenging. The technique used to generate the reported RCR's is also detailed in appendix table 2.1.

Tissue Origin	Achieved RCR	Published RCR (including method used for respiratory analyses)
Liver	4.81	RCR = 4 (Hanastech Instruments, Oxygen electrode) [276]. RCR = 5.86 (Clark-type electrode)[104]. RCR = 4.45 (Gilson oxygraph) [277] RCR = 4.4 - 4.5 (Clark-type electrode) [278].
Kidney	4.66	RCR = 3.6-4.1 (Oroboros oxygraph system) [102] RCR = 3 – 3.5 (Clark-type electrode) [279] RCR = ~3.2 (Seahorse XF24) [280]. RCR = 5.21 (Gilson oxygraph) [281].
Heart	4.06	RCR = 4.3 (Clark-type electrode) [282]. RCR = 2.4 – 3.5 (Clark-type electrode)[283] RCR = 5 – 12 depending on substrate utilised (Clark-type electrode) [284]. RCR = 6 – 8.5 (Clark-type electrode) [285].
Skeletal Muscle	5.82	RCR = ~2 – 6 depending on substrate utilised (Clark-type electrode) [286] RCR = 3.4 – 10 depending on substrate utilised (Clark-type electrode)[287] RCR = 6-10 (Clark-type electrode)[288] RCR = ~3.9 (Oroboros oxygraph)[289] .
Brain	4.36	RCR = 3 – 3.25 (Seahorse XF24) [290]. RCR = 5.5 (Clark-type electrode) [291]. RCR = 3 – 3.5 (Clark-type electrode) [292] RCR = 6.6 (Clark-type electrode)[293] RCR = ~7 (Seahorse XF24) [294].

APPENDIX TABLE 2.1: Non-quantitative comparison between obtained RCR values for mitochondria isolated from five tissues of high metabolic load and published RCR values.

The obtained RCR values are comparable with those reported in the literature although, with all tissues, higher RCR values can be found in the literature. Any future attempts to improve isolation protocols should use RCR values as the gold-standard measure of mitochondrial viability and isolation protocols should only be changed if higher RCR values are consistently obtained.

APPENDIX III – CONCENTRATION OF GSK932121A IN ISOLATED LIVER MITOCHONDRIA OF RATS TREATED WITH A 50MG/KG DOSE (CHAPTER 3)

Rat ID	GSK932121A level in mitochondrial fraction (µg/mg)	GSK932121A concentration (µM)
i	1.79	4.2
ii	1.71	4.02
iii	0.92	2.16
iv	0.81	1.9
v	0.74	1.74
vi	0.0016	0.0038
vii	0.381	0.89
viii	0.831	1.95
ix	0.706	1.66
x	0.127	0.3

Appendix Table 3.1: Levels of GSK932121A in the mitochondrial fraction. GSK932121A levels were assessed in the mitochondrial fraction to determine if GSK932121A had been washed out during the isolation procedure. An average concentration of 1.9µM (± 1.4µM sd) GSK932121A was detected in the mitochondrial fraction which is above the IC_{50} for mammalian cytochrome bc1 inhibition as described in reference [12], i.e.IC_{50} = 0.4µM (human Hek293 cells) and 0.6µM (rat H9C2 cells).

APPENDIX IV: METABOLOMICS RAW DATA

Liver Data

	Control						12.5mg/kg GSK932121A							50mg/kg GSK932121A						
	1	**2**	**3**	**4**	**5**	**6**	**7**	**8**	**9**	**10**	**11**	**12**	**13**	**14**	**15**	**16**	**17**	**18**	**19**	**20**
Maltohexaose	1.196	1.026	0.675	0.974	1.100	1.306	1.056	1.652	0.889	0.165	0.165	0.165	0.228	2.576	0.165	0.165	0.165	0.535	0.165	0.165
Maltotriose	12.954	13.252	10.160	10.838	13.005	15.368	11.461	10.745	11.877	7.635	1.531	4.209	7.905	16.607	0.459	0.057	0.091	8.940	1.000	0.345
Maltose	3.090	3.325	2.489	2.934	3.200	3.727	2.885	2.280	3.283	2.694	1.169	1.678	2.597	3.831	0.693	0.086	0.154	2.513	0.555	0.548
Glucose	1.393	1.485	1.176	1.543	1.152	1.427	1.259	1.116	1.484	1.411	0.806	1.098	1.328	1.250	0.696	0.247	0.306	1.199	0.499	0.615
Glucose 6 Phosphate	0.797	0.796	0.727	1.522	0.752	0.797	0.790	0.963	0.777	1.526	1.004	1.000	1.183	1.139	1.116	1.349	0.931	1.045	1.239	1.582
2-Phosphoglycerate	0.426	0.603	0.870	1.000	0.465	0.694	0.544	0.644	0.575	0.970	1.277	1.004	0.805	1.159	1.089	0.893	1.055	0.750	1.261	1.145
Phosphoenolpyruvate	0.547	0.684	0.676	1.000	0.424	0.624	0.666	0.636	0.602	0.906	1.113	1.208	0.932	0.986	1.113	1.212	0.972	0.705	1.278	1.267
Pyruvate	1.773	3.074	3.946	2.612	1.733	4.343	0.301	2.246	0.840	1.727	1.000	1.528	2.179	4.701	0.605	0.217	0.012	0.690	1.567	0.332
Lactate	1.207	1.270	1.215	1.451	1.164	1.245	1.005	1.106	1.080	1.492	0.909	1.167	1.177	1.000	0.843	0.379	0.456	0.971	0.675	0.758
3-hydroxybutyrate (BHBA)	0.968	0.689	0.954	0.569	0.933	0.529	1.274	0.456	1.029	0.635	1.000	1.029	1.302	0.552	1.438	1.326	1.985	1.127	1.532	1.543
Serine	0.853	0.975	0.732	0.690	0.879	0.888	1.109	1.049	0.940	1.200	0.967	1.059	1.074	1.170	1.305	1.389	1.328	0.996	1.341	1.075
Threonine	0.899	0.942	0.724	0.620	0.917	0.898	0.874	0.788	0.979	1.203	1.025	1.209	1.071	0.913	1.617	1.602	1.763	0.810	1.514	1.297
Valine	0.893	0.899	0.942	0.786	0.908	1.000	0.970	0.916	1.121	1.173	0.977	0.962	1.001	0.981	1.197	0.972	1.242	0.870	1.154	1.289
Leucine	0.871	0.947	1.020	0.776	0.980	1.097	0.970	0.967	1.170	1.179	0.920	0.874	0.961	1.037	1.147	0.889	1.187	0.871	1.069	1.252
Isoleucine	0.934	0.989	1.006	0.850	0.948	1.086	0.989	0.935	1.186	1.181	0.970	0.887	1.000	1.053	1.205	0.934	1.223	0.889	1.169	1.311
Sedoheptulose-7-phosphate	0.679	0.980	0.758	1.016	0.585	0.831	1.331	0.767	0.726	1.898	1.428	1.191	1.120	0.544	4.001	4.368	1.467	2.804	2.979	3.892
Cysteine-glutathione disulfide	0.606	0.446	1.417	0.652	0.566	0.545	1.704	0.896	0.726	1.208	0.841	0.940	1.000	0.873	0.939	1.080	0.982	0.767	1.328	0.666
Opthalmate	1.504	0.665	0.909	0.359	0.641	0.397	1.000	0.987	0.783	0.938	1.693	1.625	1.802	0.720	0.166	0.319	0.082	0.225	0.708	0.633
Glutathione Reduced (GSH)	1.558	1.502	1.124	1.578	1.505	1.415	1.260	1.376	1.717	1.367	1.187	1.590	1.057	1.258	0.600	0.564	0.789	1.282	0.608	0.980
Glutathione Oxidized (GSSG)	0.676	0.980	1.396	0.753	0.760	0.900	0.938	0.762	0.753	1.152	0.908	0.884	1.065	0.910	1.250	1.000	0.869	1.011	1.497	1.146

Appendix Table 4.1: Liver metabolomics raw data: The table shown details the raw (scaled intensity) liver metabolomics data for the biochemicals reported in chapter 4. Raw metabolomics data is assigned to the rat ID (numbered 1-20) showing the differential effect of GSK932121A (12.5mg/kg and 50mg/kg) and vehicle control.

Plasma Data

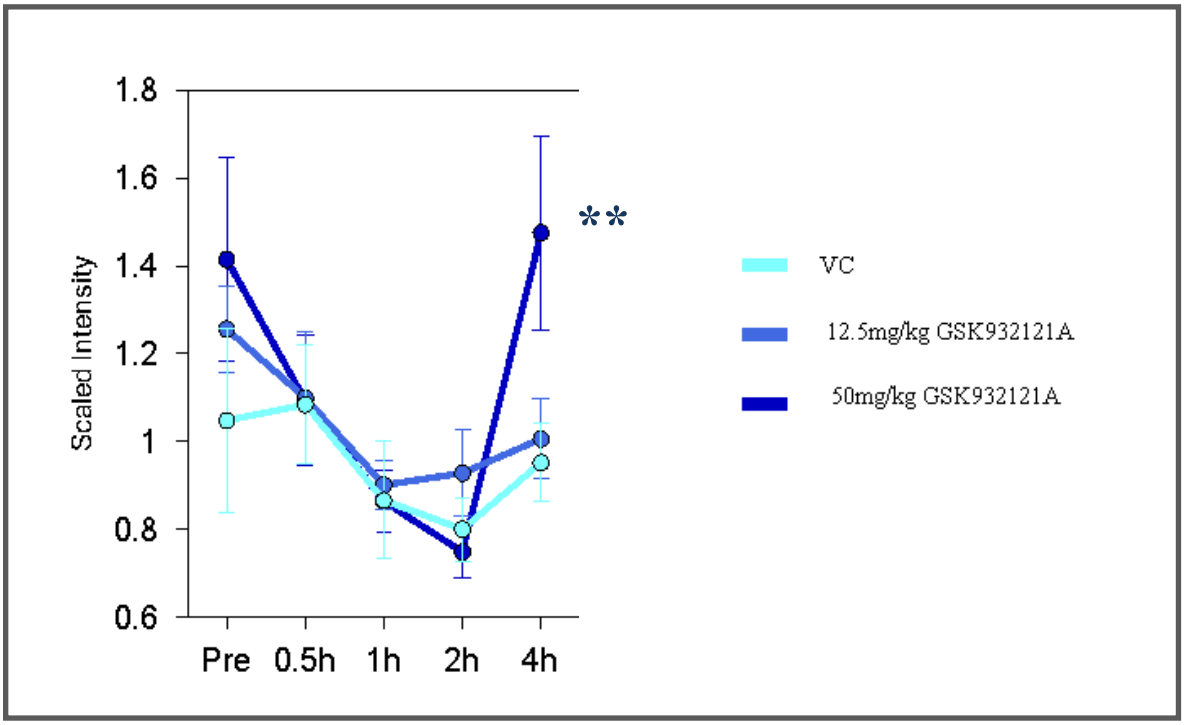
Animal	Time	Dose (mg/kg)	citrate	α-ketoglutarate	succinate	fumarate	malate	carnitine	BHBA	Palmitoyl Carnitine (C16)	Oleoyl carnitine (C18)	Stearoyl Carnitine (C18)	valine	leucine	isoleucine	AHB	AKB
1	Predose		0.642	0.375	0.863	0.594	0.495	1.045	0.386	0.630	0.595	0.542	0.664	0.700	0.623	0.470	0.206
2	Predose		0.867	0.745	1.111	0.804	0.835	0.939	0.554	0.879	0.678	0.849	1.047	1.126	1.010	0.655	0.048
3	Predose	**VC**	1.162	0.956	1.100	0.953	1.151	0.961	1.000	0.712	0.745	0.978	1.088	1.095	1.019	0.671	0.268
4	Predose		0.990	1.522	1.378	1.554	1.683	0.917	0.711	0.750	0.609	0.785	1.099	1.084	1.012	0.850	1.048
5	Predose		1.118	0.846	0.945	0.896	0.956	0.812	0.665	0.441	0.338	0.612	1.050	1.035	0.967	0.428	0.786
7	Predose		1.085	1.184	0.885	0.755	0.912	0.884	0.702	0.630	0.593	0.698	0.792	0.916	0.788	1.000	0.209
8	Predose		1.097	0.714	0.986	0.721	0.718	0.786	0.608	0.643	0.599	0.770	1.023	1.149	0.996	0.430	0.048
9	Predose		1.132	1.189	1.943	1.906	2.016	0.776	0.821	0.707	0.663	0.744	1.009	1.020	0.996	1.012	0.401
10	Predose	**12.5**	0.914	0.821	0.992	1.044	1.233	0.998	0.587	0.873	0.712	0.901	0.922	0.959	0.859	0.822	2.163
11	Predose		1.250	2.023	2.093	2.015	2.078	0.994	1.007	1.146	1.190	1.114	1.043	1.000	1.000	0.911	0.220
12	Predose		1.224	1.031	1.786	1.306	1.195	1.007	0.847	1.002	1.168	1.100	0.900	0.881	0.773	0.972	0.209
13	Predose		1.046	0.679	1.023	0.711	0.651	0.784	0.996	1.095	1.497	1.116	0.923	0.891	0.864	0.538	0.048
14	Predose		1.110	0.581	0.855	0.753	0.740	0.831	0.529	0.835	0.760	0.999	0.932	1.023	0.921	0.833	0.332
15	Predose		0.968	0.955	1.213	0.951	0.878	1.037	0.662	0.778	0.569	0.739	1.070	1.063	1.005	0.631	0.478
16	Predose		0.968	0.970	1.000	0.982	1.000	0.861	1.414	1.298	1.518	1.126	1.000	0.962	0.940	1.032	1.410
17	Predose	**50**	1.412	1.512	2.353	2.330	3.037	0.928	0.839	0.837	0.724	0.868	1.116	1.132	1.045	0.876	0.048
18	Predose		0.940	0.779	1.046	1.035	0.929	0.977	0.878	0.631	0.514	0.718	1.137	1.174	1.087	0.508	1.066
19	Predose		1.205	2.257	4.726	2.656	3.171	1.044	1.003	1.078	0.929	1.067	1.064	1.074	1.019	0.981	0.151
20	Predose		1.026	1.305	2.208	1.454	1.488	0.945	0.876	0.980	0.993	0.983	0.993	1.072	0.909	0.691	0.240
1	0.5h		1.011	1.454	1.266	1.000	0.902	1.257	0.583	0.971	1.000	0.763	0.958	1.033	0.958	0.599	0.245
2	0.5h		1.176	1.054	0.849	0.577	0.725	0.983	0.668	0.760	0.767	0.785	0.992	1.000	0.974	0.644	0.048
3	0.5h		1.013	0.746	0.891	0.607	0.605	1.099	0.711	0.878	0.918	0.981	0.965	1.062	0.988	0.336	0.048
4	0.5h	**VC**	1.332	1.981	2.289	2.114	2.407	1.068	0.946	0.879	0.708	0.791	1.061	1.031	1.051	1.051	0.296
5	0.5h		1.321	1.608	1.093	1.009	0.803	1.004	0.931	0.509	0.484	0.692	1.002	1.097	1.014	0.765	0.328
6	0.5h		1.565	1.351	1.215	0.828	0.860	0.948	0.443	0.603	0.524	0.650	0.816	0.872	0.796	0.315	0.402
7	0.5h		0.879	0.892	0.682	0.600	0.467	0.824	0.589	0.894	0.868	1.001	0.865	0.934	0.825	0.775	0.288
9	0.5h		0.970	1.167	1.093	0.850	0.760	0.774	0.824	0.883	0.970	0.864	0.977	1.008	0.977	0.820	0.048
10	0.5h	**12.5**	0.998	0.932	0.894	1.051	1.117	1.043	0.649	0.998	0.899	1.132	0.902	0.998	0.920	0.875	0.048
11	0.5h		1.637	2.135	2.218	2.297	2.592	1.035	2.407	1.957	2.569	1.374	0.921	0.910	0.946	2.241	2.066
12	0.5h		1.235	1.756	1.884	1.622	1.827	1.140	1.201	1.220	1.296	1.000	0.806	0.809	0.782	3.331	1.052
13	0.5h		1.306	0.883	1.321	1.454	1.451	0.819	0.857	1.024	1.000	1.120	0.986	1.010	1.006	1.319	0.609
14	0.5h		1.079	0.877	0.744	0.694	0.599	0.955	0.632	0.896	0.881	0.957	0.872	0.908	0.896	0.739	0.412
15	0.5h	**50**	1.104	0.649	1.857	1.112	1.413	1.184	1.019	1.136	1.007	1.072	0.973	0.979	0.989	1.138	0.281
16	0.5h		1.202	0.631	1.529	1.663	1.789	0.914	1.393	1.352	1.507	1.263	0.960	0.985	0.973	2.220	2.188

17	0.5h		1.531	0.853	1.224	1.021	1.000	1.006	1.252	1.012	1.053	0.939	1.008	1.034	0.994	0.912	0.048
18	0.5h		1.000	1.080	1.035	1.021	1.008	1.000	1.306	0.685	0.733	0.761	0.905	0.940	0.882	0.365	0.048
19	0.5h		1.201	0.797	2.388	1.877	1.921	1.276	1.497	1.288	1.457	1.046	0.842	0.921	0.903	2.835	1.063
20	0.5h		0.981	1.029	1.657	1.367	1.211	0.958	1.003	1.374	1.413	1.275	0.994	1.008	0.999	2.064	1.305
1	1h		1.212	1.066	0.872	0.638	0.686	1.288	0.738	0.909	0.961	0.730	1.061	1.081	1.051	0.956	0.502
2	1h		0.982	0.507	1.525	1.013	1.059	0.999	0.703	1.089	1.000	1.062	1.060	1.046	1.059	0.832	0.048
3	1h		1.097	1.194	1.000	0.723	0.741	1.064	1.656	0.717	0.902	0.762	1.006	0.964	0.975	0.362	0.563
4	1h	**VC**	1.282	1.750	3.780	2.201	2.158	1.168	1.011	1.073	0.859	0.941	0.962	1.009	1.016	1.020	0.048
5	1h		1.308	1.140	1.077	1.161	1.245	0.946	0.792	0.455	0.369	0.527	1.022	1.002	0.974	0.702	0.048
6	1h		1.000	0.286	0.746	0.535	0.320	0.928	0.319	0.601	0.501	0.614	0.858	0.931	0.822	0.244	0.207
7	1h		0.860	0.851	0.823	0.740	0.646	0.855	0.709	0.792	0.753	0.844	0.893	0.987	0.880	0.822	0.308
8	1h		0.867	0.546	1.276	0.827	0.639	0.728	0.406	0.435	0.497	0.497	0.719	0.793	0.705	0.271	0.048
9	1h		1.059	0.979	0.858	0.791	0.744	0.872	0.559	0.856	0.908	0.961	0.991	0.980	0.990	0.672	0.048
10	1h	**12.5**	0.949	0.816	0.995	0.982	0.980	1.059	0.780	1.002	0.921	1.007	0.900	0.964	0.963	0.673	0.465
11	1h		1.348	2.162	1.024	1.381	1.444	1.000	1.756	1.681	2.051	1.270	0.887	0.859	0.883	1.947	1.777
12	1h		1.115	0.980	1.000	0.859	0.782	1.098	1.591	1.500	1.477	1.277	0.944	0.916	0.924	2.593	1.400
13	1h		1.412	1.200	2.624	1.359	1.327	0.776	1.966	0.969	1.284	1.106	1.043	1.001	1.091	1.052	0.685
14	1h		0.923	0.735	0.624	0.758	0.544	1.006	0.668	0.883	0.903	1.001	0.898	0.895	0.895	0.690	0.048
15	1h		1.068	0.662	0.799	0.603	0.672	1.053	0.758	0.997	0.932	0.993	0.998	0.965	1.016	0.960	0.048
16	1h		1.487	2.629	1.447	1.710	1.946	0.891	1.922	1.621	1.688	1.281	0.937	0.888	0.908	3.149	2.083
17	1h	**50**	1.532	1.112	1.165	0.989	1.104	0.976	1.486	0.867	0.874	0.795	0.984	0.977	1.032	1.314	0.353
18	1h		1.162	1.014	0.909	1.000	0.884	1.000	1.341	0.725	0.746	0.718	0.813	0.813	0.796	0.405	0.048
19	1h		1.350	1.777	1.172	1.406	1.302	1.129	1.900	1.103	1.359	1.021	0.860	0.814	0.851	2.834	1.788
20	1h		1.115	0.717	1.076	0.991	1.280	0.933	1.049	0.934	1.043	0.953	1.004	0.961	1.001	2.153	1.326
1	2h		0.974	0.293	0.657	0.431	0.657	1.234	0.970	0.888	0.876	0.780	1.147	1.125	1.143	1.000	1.470
2	2h		0.868	0.720	0.689	0.529	0.476	1.000	0.552	0.815	0.799	0.994	1.026	1.000	0.983	0.652	0.316
3	2h		0.965	1.046	1.129	0.792	0.778	0.937	0.914	1.032	0.988	1.137	0.861	0.873	0.862	0.481	0.302
4	2h	**VC**	1.017	0.904	1.109	1.029	0.928	0.994	0.476	0.882	0.720	0.929	0.919	0.980	0.939	0.733	0.335
5	2h		1.081	0.971	1.156	0.870	0.848	1.002	0.800	0.628	0.496	0.694	0.902	0.897	0.863	0.734	0.048
6	2h		0.977	1.000	1.223	0.746	0.522	0.956	0.409	0.788	0.623	0.821	0.825	0.905	0.840	0.322	0.048
7	2h		0.962	0.803	0.578	0.672	0.606	0.811	1.214	0.947	0.878	0.861	0.817	0.857	0.818	0.900	0.257
8	2h		1.432	0.992	1.518	0.970	1.136	0.813	0.756	0.710	0.808	0.890	0.957	1.019	0.958	0.365	0.188
9	2h		0.879	0.691	1.118	0.828	0.709	0.902	0.718	0.979	1.124	1.001	0.900	0.900	0.919	0.524	0.048
10	2h	**12.5**	1.148	1.492	1.171	1.218	1.446	0.980	1.394	1.078	1.106	0.975	1.019	1.014	1.127	2.372	1.306
11	2h		1.206	0.740	0.782	0.804	0.951	0.952	2.272	2.332	2.224	1.463	0.963	0.946	1.026	2.544	3.611
12	2h		1.295	1.049	1.393	1.000	1.183	0.959	2.868	1.767	1.985	1.244	0.903	0.908	1.000	4.946	1.846
13	2h		1.096	0.960	0.603	0.657	0.565	0.692	2.248	1.665	2.118	1.276	0.908	0.848	0.947	2.194	2.508

14	2h		1.010	0.483	0.485	0.584	0.636	0.903	0.662	1.021	1.030	1.054	0.833	0.868	0.902	0.562	0.048
15	2h		0.988	0.690	0.699	0.627	0.623	0.984	0.925	1.347	1.368	1.048	1.021	0.931	1.074	1.365	1.020
16	2h		1.346	1.485	0.723	0.979	0.935	0.707	2.619	1.682	1.883	1.130	0.949	0.863	0.949	3.582	3.332
17	2h	**50**	1.253	0.539	0.807	0.708	0.715	0.790	1.039	0.781	0.891	0.776	1.000	0.905	1.067	1.352	0.944
18	2h		1.113	0.515	0.714	0.813	0.608	0.865	2.514	1.249	1.388	1.113	0.925	0.913	1.061	0.623	0.560
19	2h		1.349	1.136	0.813	1.129	1.165	0.979	3.839	2.267	2.798	1.166	0.911	0.847	0.970	7.664	5.104
20	2h		1.002	1.295	0.690	0.665	0.681	0.908	1.579	1.322	1.782	1.151	1.055	1.005	1.104	3.677	6.051
1	4h		1.066	0.800	0.658	1.911	2.498	1.139	0.911	0.989	0.803	0.817	1.309	1.273	1.352	2.288	2.475
2	4h		0.853	0.455	0.423	0.738	0.799	0.992	0.709	0.934	0.800	0.926	1.179	1.196	1.239	1.256	1.188
3	4h	**VC**	0.965	1.239	0.490	0.880	0.862	1.031	1.196	0.898	0.783	0.929	0.954	0.907	0.938	1.000	1.252
4	4h		0.934	1.688	0.907	1.979	1.963	1.057	0.997	0.755	0.625	0.813	0.956	1.089	1.056	1.258	0.411
5	4h		0.968	1.134	0.597	1.443	1.530	0.981	1.035	0.605	0.598	0.538	0.883	0.862	0.913	0.941	0.710
6	4h		0.857	0.644	0.622	1.020	1.031	0.915	0.624	0.768	0.690	0.768	1.033	1.094	1.089	0.499	0.939
7	4h		1.364	1.472	0.559	1.398	1.906	0.734	1.591	1.169	1.036	1.053	0.917	0.931	0.995	3.694	2.193
8	4h		1.118	1.115	0.674	1.359	1.450	0.744	0.739	0.721	0.826	0.816	1.008	1.078	1.166	1.156	1.246
9	4h		0.974	0.490	0.379	0.748	0.724	0.763	1.016	0.964	1.045	0.896	1.022	1.001	1.192	0.988	0.408
10	4h	**12.5**	1.031	1.034	0.581	1.211	0.939	0.867	0.997	1.181	1.020	0.893	0.979	0.920	1.095	7.376	6.091
11	4h		1.093	1.690	1.256	3.221	3.098	0.943	1.722	2.498	2.036	1.339	1.018	0.951	1.074	4.020	3.203
12	4h		1.053	1.457	0.605	1.871	1.760	0.942	1.768	2.003	1.738	1.406	1.143	1.074	1.250	6.856	3.618
13	4h		1.044	1.000	0.783	1.440	1.528	0.712	4.050	2.610	2.862	1.442	1.000	0.986	1.140	6.380	8.154
14	4h		0.954	0.774	0.509	0.916	1.025	0.840	1.591	1.248	1.287	1.047	1.166	1.191	1.366	1.691	1.933
15	4h		1.430	1.675	1.227	5.937	8.771	0.695	1.928	1.864	1.752	1.262	1.482	1.493	1.756	8.013	2.910
16	4h		1.269	4.528	2.627	10.358	11.156	0.682	1.801	2.134	1.925	1.464	1.356	1.470	1.527	7.429	5.848
17	4h	**50**	2.152	4.178	4.709	15.840	22.674	0.662	3.914	2.190	2.351	1.149	1.856	1.969	2.051	10.990	3.112
18	4h		1.030	1.487	0.735	1.948	1.737	0.850	1.737	1.279	1.330	0.884	1.196	1.168	1.358	1.193	0.833
19	4h		1.136	2.763	1.416	4.004	4.335	0.926	1.949	2.181	2.228	1.431	1.170	1.166	1.387	13.343	5.806
20	4h		1.156	1.775	0.602	1.481	1.527	0.746	3.120	1.883	2.312	1.248	1.108	1.008	1.237	11.351	10.924

Appendix Table 4.2: Plasma metabolomics raw data: The table details the raw (scaled intensity) plasma metabolomics data for the biochemicals reported in chapter 4. Raw metabolomics data is assigned to the rat ID (numbered 1-20) showing the differential effect of GSK932121A (12.5mg/kg and 50mg/kg) and vehicle control. Data is ordered according to 5 sample collection times (pre-dose, 0.5hr, 1hr, 2hr and 4hr post dose).

APPENDIX V: METABOLON PLASMA LACTATE ANALYSIS



Appendix Fig.5.1: Plasma lactate measured by Metabolon following treatment of rats with 12.5mg/kg and 50mg/kg GSK932121A. Data shows the effect of GSK932121A (12.5mg/kg light blue line and 50mg/kg dark blue line) on plasma lactate levels compared to VC (turquoise line). Plasma samples were assessed pre-dose and then 0.5, 1, 2 and 4 hours post-dose. Data shown represents scaled intensity of the total ion counts for each metabolite whereby the median ion is equal to 1. A significant increase in plasma lactate was observed at 4 hours post-dose with 50mg/kg GSK932121A (n=7) compared to VC (n=6), $p<0.01$**.